REOVIRUS-DRIVEN MYELOID CELLS IN ONCOLYTIC VIRUS THERAPY AND INFECTION

by

Derek R. Clements

Submitted in partial fulfilment of the requirements
for the degree of Doctor of Philosophy

at

Dalhousie University
Halifax, Nova Scotia
March 2018

TABLE OF CONTENTS

LIST OF TABLES

LIST OF FIGURES

ABSTRACT

Cancer-associated immunosuppression represents a major contributor to tumor progression and impairment of spontaneous or therapeutically-induced anti-tumor immunity. Myeloid cells are a key mediator of such immunosuppression. These tumor-associated myeloid cells promote angiogenesis, metastasis, and prevent immune-mediated attack and elimination of cancer cells. Thus, it is not surprising that current cancer immunotherapeutic approaches, which exploit immune cell functions to target cancer, aim to overcome immunosuppression within the tumor microenvironment (TME).

Oncolytic viruses (OVs) represent a novel class of anti-cancer therapeutic agents. OVs, including reovirus, preferentially target and kill cancer cells. Additionally, numerous OVs readily overturn the otherwise suppressed immune system and facilitate the activation of beneficial anti-tumor T cell responses. Contrary to this paradigm, our previous findings illustrated that reovirus transiently augments a myeloid cell population, commonly associated with an immunosuppressive phenotype, following reovirus administration. Thus, this thesis focuses on elucidating the biological and therapeutic impact that these cells have on reovirus-based OV therapy. As such, the broad objectives of this thesis are to 1) phenotypically and functionally characterize reovirus-driven myeloid cells in the context of OV therapy, 2) implement complementary immunological interventions to modulate these cells during therapy, and 3) develop a mass spectrometry-based proteomics platform to understand how these cells respond throughout virus infection *in vivo*.

The following work illustrates that reovirus drives the accumulation of suppressive monocytic myeloid cells (MMCs) within the TME and enhances tumor-associated immunosuppression. Depletion of these MMCs in the TME (using gemcitabine) accelerated the development of anti-tumor T cell immunity and improved therapeutic efficacy. Although the use of gemcitabine hampered MMC accumulation, it also hindered reovirus replication. Hence, an alternative approach to manipulate these MMCs could benefit OV therapy effectiveness.

Lastly, the implementation of our quantitative temporal *in vivo* proteomics platform unveiled that reovirus-driven MMCs, in the context of infection and absence of a TME, naturally possess anti-viral/pro-inflammatory properties and are precursors for antigen-presenting cells. With such environmentally-dependent and contrasting cellular properties, our data suggest that, as an alternative to MMC depletion strategies, future work could harness the pro-inflammatory phenotype of these MMCs to further potentiate the generation of anti-tumor immunity during OV therapy.

LIST OF ABBREVIATIONS AND SYMBOLS USED

5-FU	5-Fluorouracil
7-AAD	7-Aminoactinomycin D
ACK	Ammonium Chloride Potassium
ADAM17	A Disintegrin and Metalloproteinase Domain 17
AIM2	Absent in Melanoma 2
AKT	Protein Kinase B
APC	Antigen-presenting Cell
ARG1	Arginase 1
ATCC	American Type Culture Collection
ATP	Adenosine Triphosphate
ATRA	All Trans Retinoic Acid
BCL	B-cell Lymphoma
BFA	Brefeldin A
BHCRI	Beatrice Hunter Cancer Research Institute
BM	Bone Marrow
BP	Biological Process
BRAF	Serine/Threonine-protein kinase B-raf
CAF	Cancer-associated Fibroblast
CATB	Cathepsin B
CATD	Cathepsin D
CC	Cellular Compartment
CCAC	Canadian Council on Animal Care
CCL2	C-C Motif Chemokine Ligand Type 2
CCL3	C-C Motif Chemokine Ligand Type 3
CCL7	C-C Motif Chemokine Ligand Type 7
CCR2	C-C Motif Chemokine Receptor Type 2
CD	Cluster of Differentiation

CD45RO	Splice Variant of Tyrosine Phosphatase CD45
CDI	Cell Division Index
cDNA	Complementary DNA
CFA	Complete Freund’s Adjuvant
CFSE	Carboxyfluorescein Succinimidyl Ester
CI	Confidence Interval
CIHR	Canadian Institutes of Health Research
CMP	Common Myeloid Progenitor
ConA	Concanavalin A
COX2	Cyclooxygenase 2
CRTP	Cancer Research Training Program
CTLA-4	Cytotoxic T-lymphocyte-associated Antigen 4
CXCR	C-X-C Chemokine Receptor
d.p.f.i.	Days Post First Infection
d.p.i.	Days Post Infection
d.p.l.i.	Days Post Last Infection
DAF	Decay-accelerating Factor
DAF-FM	4-Amino-5-Methylamino-2’,7’-Difluorofluorescein Diacetate
DAMP	Damage-associated Molecular Patterns
DC	Dendritic Cell
DCF	2’,7’-Dichlorofluorescein
DMEM	Dulbecco's Modified Eagle's Medium
dsDNA	Double-stranded Deoxyribonucleic Acid
dsRNA	Double-stranded Ribonucleic Acid
EAE	Experimental Autoimmune Encephalomyelitis
EC	Endothelial Cell
ECAR	Extracellular Acidification Rate
EDTA	Ethylenediaminetetraacetic Acid

ER	Endoplasmic Reticulum
ERK	Extracellular Signal-regulated Kinases
FACS	Fluorescence-activated Cell Sorting
FasL	First Apoptosis Signal Ligand
FAP	Fibroblast Activating Protein-α
FBS	Fetal Bovine Serum
FC	Fragment Crystallizable
FCCP	Carbonyl Cyanide-4-(trifluoromethoxy)phenylhydrazone
FDA	Food and Drug Administration (of the USA)
G	Gauge
g	Grams
xg	times gravity
GAL9	Galectin 9
G-CSF	Granulocyte Colony-stimulating Factor
GEM	Gemcitabine
GFP	Green Fluorescent Protein
GM-CSF	Granulocyte-macrophage Colony-stimulating Factor
G-MDSC	Granulocytic Myeloid-derived Suppressor Cell
HG2A	H-2 Class II Histocompatibility Antigen Gamma Chain
HMGB1	High Mobility Group Box 1
hr	Hour(s)
HRG	Histidine-rich Glycoprotein
HSC	Hematopoietic Stem Cell
HSV	Herpes Simplex Virus
HSV-1	Herpes Simplex Virus-1
HVEM	Herpesvirus Entry Mediator
i.p.	Intraperitoneal
ICAM1	Intercellular Adhesion Molecule 1

ICD	Immunogenic Cell Death
IDO	Indoleamine 2,3-dioxygenase
IFI5A	Interferon-activable Protein 205-A
IFIH1	Interferon-induced Helicase C Domain-containing Protein 1
IFN	Interferon
IGTP	Interferon Gamma-induced GTPase
IL	Interleukin
IMC	Immature Myeloid Cells
iNOS	Inducible Nitric Oxide Synthase
IRF1	Interferon Regulatory Factor 1
IRF3	Interferon Regulatory Factor 3
IRF5	Interferon Regulatory Factor 5
IRF7	Interferon Regulatory Factor 7
IRG1	Immune-responsive Gene 1
ISG20	Interferon-stimulated Gene 20 kda
JAK	Janus Tyrosine Kinase
JMEM	Joklik Modified Minimum Essential Media
Kras	Kirsten Ras Sarcoma Viral Oncogene Homolog
L	Liter
LAK	Lymphokine-activated Killer Cell
LCMV	Lymphocytic Choriomeningitis Virus
LDHA	Lactate Dehydrogenase A
Ly6C	Lymphocyte Antigen 6 Complex, Locus C
Ly6G	Lymphocyte Antigen 6 Complex, Locus G
M	Molar
M.F.I.	Mean Fluorescence Intensity
M1	Classically-activated Macrophage
M2	Alternatively-activated Macrophage

MAPK	Mitogen-activated Protein Kinase
M-CSF	Macrophage Colony-stimulating Factor
M-CSFR	Macrophage Colony-stimulating Factor Receptor
MDSC	Myeloid-derived Suppressor Cell
MDA5	Melanoma Differentiation-associated Gene 5
MEK	MAPK/ERK Kinase
MEM	Minimum Essential Media
MerTK	Tyrosin-protein Kinase Mer
MeV	MultiExperiment Viewer
MF	Molecular Function
MHC	Major Histocompatibility Complex
MHV	Mouse Hepatitis Virus
MIG	Monokine Induced by Gamma Interferon
min	Minute(s)
MIP-1α	Macrophage Inflammatory Protein 1 Alpha
Mito-cluster	Mitochondrial-associated Cluster
mL	Milliliter
mM	Millimolar
MMC	Monocytic Myeloid Cell
M-MDSC	Monocytic Myeloid-derived Suppressor Cell
MMP9	Matrix Metallopeptidase 9
MOI	Multiplicity of Infection
MOSE	Mouse Ovarian Surface Epithelial
MPEG1	Macrophage-expressed Gene 1 Protein Precursor
MRC1	Mannose Receptor C-Type 1
MS	Mass Spectrometry
mTOR	Mechanistic Target of Rapamycin
MUG1	Murinoglobulin 1

NARA	Neutralizing Anti-reovirus Antibodies
NCBI	National Center for Biotechnology Information
NDV	Newcastle Disease Virus
NFκB	Nuclear Factor Kappa-Light-Chain-Enhancer of Activated B cells
ng	Nanograms
NIDDK	National Institute of Diabetes and Digestive and Kidney Disease
NIH	National Institute of Health
NK	Natural Killer
NKT	Natural Killer T
NO	Nitric Oxide
NOD	Nucleotide Oligomerization Domain
NSCLC	Non-small-cell Lung Carcinoma
NSHRF	Nova Scotia Health Research Foundation
OAS1A	2'-5'-Oligoadenylate Synthase 1A
OC	Ovarian Cancer
OCR	Oxygen Consumption Rate
OD	Optical Density
OV	Oncolytic Virus
OVA	Ovalbumin
PAMP	Pathogen-associated Molecular Patterns
PBMC	Peripheral Blood Mononuclear Cell
PBS	Phosphate-buffered Saline
PC	Peritoneal Carcinomatosis
PD-1	Programmed Cell Death Protein 1
PDAC	Pancreatic Adenocarcinoma
pDC	Plasmacytoid Dendritic Cell
PD-L1	Programmed Death-ligand 1
PERF	Perforin-1

PFS	Progression-free Survival
pfu	Plaque Forming Units
PGE2	Prostaglandin E2
PI3K	Phosphoinositide 3-kinase
PIC	Protease Inhibitor Cocktail
PKR	Protein Kinase RNA-activated
PMN-MDSC	Polymorphonuclear Myeloid-derived Suppressor Cell
PRR	Pattern Recognition Receptor
PSGL-1	P-Selectin Glycoprotein Ligand 1
QTiPs	Quantitative Temporal *In Vivo* Proteomics
RANTES	Regulated on Activation, Normal T cell Expressed and Secreted
RBC	Red Blood Cell
Reo	Reovirus
RIG-1	Retinoic Acid Inducible Gene 1
RNA	Ribonucleic Acid
ROS	Reactive Oxygen Species
RPMI	Roswell Park Memorial Institute
RSAD2	Radical S-Adenosyl Methionine Domain-containing Protein 2
SCF	Stem Cell Factor
SCID	Severe Combined Immunodeficiency
SD	Standard Deviation
SDF-1	Stromal Cell-derived Factor 1
SEM	Standard Error of the Mean
SOI	Site of Infection
SP3	Single-pot Solid-phase-enhanced Sample Preparation
SPA3K	Serine Protease Inhibitor A3K
SPS-MS3	Synchronous Precursor Selection with Three-stage Mass Spectrometry
ssRNA	Single-stranded Ribonucleic Acid

STAT	Signal Transducer and Activator of Transcription
STING	Stimulator of Interferon Genes
SV40	Simian Vacuolating Virus 40
TAM	Tumor-associated Macrophage
TAM receptors	Tyro3, Axl, and Mer receptor
TCR	T Cell Receptor
TFRI	Terry Fox Research Institute
TGF-β	Transforming Growth Factor Beta
T_H1	Type 1 T helper
T_H2	Type 2 T helper
TIM3	T Cell Immunoglobulin and Mucin-domain Containing-3
TLR	Toll-like Receptor
TME	Tumor Microenvironment
TMT	Tandem Mass Tag
TNF	Tumor Necrosis Factor
TRAF3	TNF Receptor Associated Factor 3
TRAIL	TNF-related Apoptosis-inducing Ligand
T_{reg}	Regulatory T cell
TRIF	TIR-domain-containing Adapter-inducing Interferon-β
T-VEC	Talimogene Laherparepvec
VCAM1	Vasculature Cell Adhesion Molecule 1
VEGF	Vascular Endothelial Growth Factor
VSV	Vesicular Stomatitis Virus
VV	Vaccinia Virus
WT	Wild Type
ZP1	Zona Pellucida Sperm-binding Protein 1
μL	Microliter
μm	Micromolar

%	Percent
º	Secondary
ºC	Degrees Celsius

ACKNOWLEDGEMENTS

Few things in life, if any, are individually accomplished. Thus, I would like to acknowledge the people who have helped me to get here.

First, I would like to thank my family. My parents, Richard and Annette Clements, and my sisters (Jaclyn Clements and Katherine Clements) have impacted my development and aided me throughout my life. Your support, guidance, and optimism will never be forgotten.

To my supervisors, current and past, I would like to thank Dr. Shashi Gujar for giving me the opportunity, motivation, support, supervision, and friendship throughout the last 10 years. With respect to research, you gave me this opportunity, pushed me, and aided me throughout my PhD. As a friend, you were always there for me and for these reasons I will be forever grateful. I will truly miss you as I move on to the next stage of my life/career. I would also like the thank Dr. Patrick Lee for originally giving me the opportunity to work in the lab, for showing me the excitement of science and inspiring me to pursue a path in research.

Dr. Paola Marcato, not only have been my friend ever since the day you stole my lab coat, but you inspire me in my life and in science. To me, you represent an idol of scientific integrity, a kind and loving friend, and I will greatly miss your guidance and presence as I take the next step of my career.

Lastly, I would like to thank all my friends in aiding me throughout this process. This journey was accomplished due to the help of many and I am thankful that I have been surrounded by so many great friends and colleagues. Thank you.

CHAPTER 1: INTRODUCTION

This work focuses on the use of oncolytic viruses (OVs), "onco" originating from the Greek word onkos meaning mass to describe cancer and "lytic" describing killing, to target and treat cancers. Although the oncolytic properties of viruses have been known or suspected since the early 1900s, it has only been within the last 30 years that our understanding and application of OVs have entered into the clinics. OV research encompasses three major fields of biology: 1) virology, 2) cancer biology, and 3) immunology (particularly cancer immunology). Although many studies attempt to isolate or focus on one or the other, all three fields must be taken into consideration to effectively implement OV therapy in the clinics. To this end, the following sections will introduce anti-viral immunity, OVs, and cancer immunology separately and then amalgamate these topics together. Thus, it is important to understand that unlike a normal homeostatic niche in which common viral infections occur, theses viruses are replicating in an "altered" tumor microenvironment (TME) that can either hinder or aid virus replication. Additionally, the dosage and route of infection does not completely recapitulate how a virus will naturally induce a host immune response. Importantly, the combination of these differences (i.e., high dosage, unnatural route of administration, and the TME) has spawned the following project which focuses on a specific monocytic myeloid cell population that arises within the site of infection immediately following therapeutic injection[1-6]. Monocytic myeloid cells (MMCs) are notorious for their plasticity and effect on both cancer progression and cancer immunotherapies. As will be illustrated in this thesis, we demonstrate that these monocytic myeloid cells have a fundamental role in the efficacy of OV therapy[6]. Moving forward, it is imperative to consider both desirable and undesirable immune aspects of OV therapy and

strategically manipulate these immune aspects to further enhance the therapeutic efficacy of OVs.

1.1 ANTI-VIRAL IMMUNE RESPONSE

Following initial exposure to a virus, the host rapidly prompts the activation of the innate immune system, which effectively recognizes viral components through pattern recognition receptors (PRRs). Although these PRRs are not specific to a sequence or peptide against viruses, they recognize evolutionary conserved features identified as pattern-associated molecular patterns (PAMPs) (e.g., double-stranded (ds)RNA, viral capsids, RNA with 5'-triphosphate ends, viral DNA, or viral proteins), which are molecular structures naturally foreign/unconventional to the host cell. There are several classes of PRRs which have proven to be pivotal in the initial innate immune response of the host: Toll-like receptors (TLRs), retinoic acid-inducible gene I (RIG-I)-like receptors, nucleotide oligomerization domain (NOD)-like receptors, and absent in melanoma 2 (AIM2)-like receptors[7-9]. Viral component recognition by these PRRs and subsequent signaling of downstream host cell factors drive the cascade of innate and adaptive anti-viral immunity. A virus can activate multiple PRRs, which improves anti-viral responsiveness. For example, the dsRNA virus reovirus has been shown to activate RIG-I, melanoma differentiation-associated gene 5 (MDA5) (also known as helicard or IFIH1), and TLR3[10, 11]. RIG-I and MDA5 identify cytoplasmic dsRNA and RNAs with 5'-triphosphate ends, which are normally capped on host RNA. TLR3 binds dsRNA within endosomes, thus providing surveillance in different cellular compartments. Activation of PRRs mediates downstream signaling, which ultimately stimulates nuclear factor kappa-light-chain-enhancer of activated B cells (NFκB), and interferon responsive factors (e.g., IRF3 and IRF7), which drive pro-

inflammatory cytokine release and local interferon (IFN) response[7]. It is important to note that the type of PRR activated additionally impacts the cellular and host responsiveness. For example, a study by Rojas *et al.* demonstrated that the selective activation of TLR3-TIR-domain-containing adapter-inducing interferon-β (TRIF) signaling pathway *versus* the natural vaccinia virus-mediated TLR2 activation skewed the immune response to a more cytolytic T lymphocyte immune response involved in viral clearance as opposed to an antibody-mediated response[12].

Following the primary PRR activation and pro-inflammatory and IFN response, this local anti-viral environment is further heightened by neighbouring cells *via* IFN-mediated autocrine and paracrine signaling through the JAK/STAT pathway. Thus, infected and neighbouring/bystander cells will signal through this pathway leading to the expression of numerous IFN-associated genes, resulting in the upregulation of anti-viral mediators, such as protein kinase R (PKR), oligoadenylate synthesis, and cytokines/chemokines (e.g., tumor necrosis factor-α [TNF-α]; interleukin [IL]-1β, IL-2, IL-6, IL-12; regulated on activation, normal T cell expressed and secreted [RANTES]; CD40L; CC chemokine ligand [CCL]-2, and CCL3) to alert the immune system and mediate increased immune cell infiltration (*via* chemokines and increased intercellular adhesion molecule [ICAM] expression on the endothelium). Recruited innate immune cells (e.g., plasmacytoid dendritic cells [pDCs], DCs, neutrophils, monocytes, macrophages, natural killer [NK] cells, NKT cells) further perpetuate the cytokine and chemokine response, limit infection, and support the antigen presentation process to mediate the development of anti-viral adaptive immunity. In addition to cytokine secretion, NK cells can release cytotoxic granules and directly kill target cells with “altered” or absent class I major

histocompatibility complex (MHC), which is commonly affected by specific viruses[7]. Furthermore, infiltrating neutrophils and monocytes also have their specialized roles by means of phagocytosis and virus degradation through reactive oxygen species (ROS), nitric oxide (NO), and proteolytic enzymes[13, 14].

In this anti-viral environment, DCs and scavenging myeloid cells ingest cellular debris and virus particles, migrate to the peripheral lymphoid tissues, express antigen and costimulatory molecules, mature into antigen-presenting cells (APCs), and activate naïve T cells. The ability of APCs to activate naïve T cells represents the bridge between innate and adaptive immunity and requires three signals: 1) specific antigen presentation in the context of MHC (class I or II), 2) costimulatory molecule interaction (CD28-B7 molecule interaction), and 3) cytokine production mediated by the innate PRR pathways (e.g., IL-6, IL-12, transforming growth factor beta [TGF-β], and IL-4). It is important to note that DCs, macrophages, and B cells are considered as APCs. However, unlike DCs which are notably the superior APCs for naïve $CD4^+$ and $CD8^+$ T cell activation and expansion, macrophages and B cells specialize in processing and presentation of extracellular and soluble antigens, respectively, and interact mainly with effector $CD4^+$ T cells that are already primed.

Following sufficient antigen-specific T cell activation by APCs, these T cells expand into effector cells and following clonal expansion, traffic to the site of infection, where they mediate anti-viral immunity. In particular, $CD4^+$ T cells can differentiate into several subsets of functionally distinct effector cells (e.g., T helper cell type 1 [T_H1], T helper cell type 2 [T_H2], T helper cell type 17 [T_H17], T Follicular Helper cell [T_{FH}], and regulatory T cells [T_{regs}]). Importantly, the type of $CD4^+$ T cell dictates the effector response and is

commonly pathogen-specific. On the one hand, T_H1 cells produce high IFN-γ, IL-2, and IL-12 and are important in cell-mediated responses (activate macrophages and $CD8^+$ T cells), which is common in viral and bacterial infections. On the other hand, T_H2 cells produce IL-4, IL-5, and IL-13 and are commonly associated with parasitic infections and antibody-mediated/B cell-mediated immune responses. Particularly important for virus infections is $CD8^+$ T cell-mediated cytotoxic response. Effector $CD8^+$ T cells recognize specific viral antigens in the context of class I MHC on target cells and release perforin and granzymes to mediate apoptosis of the virus-infected target cell. Notably, immunological memory against virus-associated antigens also develop during this infection process, which enhances virus clearance upon secondary exposure.

1.2 ONCOLYTIC VIRUSES (OVs)

OVs represent a class of naturally occurring or engineered viruses that preferentially kill cancer cells, through a process known as oncolysis, while leaving non-cancerous cells relatively unharmed. This preferential tropism of OVs stems from cellular signaling and anti-viral immune response aberrations within cancer cells. Such an immune-compromised state within cells reduces virus clearance and promotes virus replication/progeny formation simultaneously. The first clinical indications that viruses could be utilized as an anti-cancer agent came from the early twentieth century with reports describing cancer patients who had brief periods of clinical remission following contraction of an infectious disease[15, 16]. Throughout the 1940-80s, numerous viruses (e.g., Egypt 101, measles, mumps, encephalomyelitis, influenza, rabies, herpes simplex virus [HSV], West Nile, and Ilheus virus) were investigated for their oncolytic potential in early clinical trials/case reports and various transplanted tumors in mice[17-26]. For example, the Egypt 101 virus showed no

curative effect but transiently inhibited tumor growth in at least 4, and possibly 9, of 27 patients in whom the infection was established[22]. A clinical trial in 1974 demonstrated the clinical utility of mumps virus in 90 patients with terminal cancer of various kinds[27]. This early clinical trial determined that 37 patients responded well to treatment. Furthermore, patients who retained physical strength showed continuously suppressed tumor growth following the initial effect of treatment[27]. Additionally, early work or incidences using attenuated viruses as anti-cancer agents also surfaced in the 1950-60s with the use of an attenuated Venezuelan equine encephalomyelitis virus[28], and in cases of rabies virus vaccinations[26, 29]. Although these early studies showed promise, many clinicians/researchers dismissed the utility of these novel class of anti-cancer agents due to the inherent safety risks, restricted methods to control virulence, and limited knowledge of the biological mechanisms associated with tumor tropism.

Following these early promising signs of therapy with infectious agents, the link between oncolytic viruses and cancer therapy continued to grow with our increasing knowledge of molecular biology, virology, and tumor immunology/anti-tumor immunity. Ultimately, it was the connection between oncogenes (i.e., Ras) and enhanced virus replication and spread which propelled the field of OV therapy or oncotherapy to where it is today[30]. Subsequently, additional well-studied characteristics of cancer were unveiled and exploited by oncolytic viruses such as common cancer mutations affecting IFN-signaling/anti-viral responsiveness[31-38] and the anti-apoptotic nature of cancer cells[39]. For instance, Stojdl *et al*. illustrated that vesicular stomatitis virus (VSV) selectively killed a variety of human tumor cell lines that were unresponsive to IFN supplementation while normal human primary cell cultures were completely protected[35]. Furthermore, naturally occurring VSV variants,

which are attenuated in IFN-responsive cells due to their defective VSV M protein, retained a highly lytic potential and therapeutic efficacy in multiple tumor models (immunocompromised and competent)[40]. Numerous studies have since confirmed such a link between OV affinity towards cancer cells and cancer-associated aberrant anti-viral immune response with other viruses (e.g., influenza, reovirus, HSV-1, Newcastle disease virus [NDV], and mumps)[41-45]. Subsequently, researchers genetically modified viruses to be IFN-sensitive and therefore preferentially replicate in cancer cells[45, 46]. The anti-viral mediator protein kinase R (PKR) readily binds to dsRNA and mediates translation inhibition through the activation of eukaryotic translation initiation factor eIF2α and thus, prevents viral protein synthesis[47, 48]. Evidently, tumors tend to have aberrant or reduced PKR activity, commonly due to hyperactive Ras pathway signaling. Such impaired anti-viral state provides a selective niche for PKR-sensitive viruses[41, 45]. With this in mind, researchers mutated virus-specific PKR inhibition mechanisms, naturally possessed by HSV-1 and influenza viruses, to render only PKR-defective cancer cells vulnerable to infection[41, 45]. For example, a mutant HSV-1 (designated R3616) with the deleted γ34.5 gene, which normally prevents PKR-mediated translation inhibition, selectively replicates in Ras-induced transformed NIH-3T3 cells[41]. Another study on pancreatic cancer cells illustrated that the Ras activation state was irrelevant, as it was the unregulated PI3-kinase pathway which ultimately allowed R3616 to overcome the PKR-mediated anti-viral response[49]. Such studies allude to the redundancy of how mutations in anti-viral response pathways can differ in various cancer types and how cancer-associated impaired anti-viral immune mechanisms set up a preferential virus replicative niche.

In addition to the aberrations in anti-viral immune mechanisms resulting in OV permissiveness, anti-apoptotic characteristics of cancer cells also contribute to increased susceptibility to OV infections. Wild type (WT) adenovirus possess the E1A gene and E1B genes, which once expressed, induce cellular proliferation and inhibition of E1A-induced apoptosis, respectively. Due to the frequent mutations of p53, tumor suppressor and regulator of apoptosis, in cancer, an engineered adenovirus depleted of the E1B protein, ONYX-015, would preferentially replicate in p53-mutated cells as opposed to normal cells[50]. Furthermore, the B cell lymphoma (BCL) family of cell survival proteins are commonly overexpressed in tumor cells. Thus, oncolytic viruses, like NDV, tend to preferentially replicate in cells overexpressing BCL-XL, which prolongs the incubation time for virus progeny formation and spread[39].

It is now known that numerous OVs also directly target cancer cells as a result of abnormally high expression of virus-specific surface receptors and entry mediators. For instance, intracellular adhesion molecule 1 (ICAM-1/CD54) and decay accelerating factor (DAF) have been shown to be overexpressed in multiple myeloma, melanoma, and breast cancer, and are instrumental in coxsackievirus entry[51-53]. Edmonston strain and wild type isolates of measles viruses use CD46, CDw150 (SLAM), and PVRL4 (Nectin 4), respectively, for cell entry, both of which are cell surface markers that are overexpressed in a variety of cancers[54-61]. The herpesvirus entry mediator (HVEM) receptor, used for HSV-1 attachment/entry, is commonly overexpressed in carcinomas and melanomas. Echovirus has a natural tropism for ovarian cancer cells because it utilizes the often overexpressed I domain of integrin $\alpha 2\beta 1$ for cellular entry[62]. Additionally, researchers have also engineered OVs, such as adenovirus, lentivirus, and measles virus, to directly target

unique cancer-associated markers as cell entry receptors[63-65]. Notably, adenovirus Ad5/3-Δ24 was modified to incorporate an RGD (Arg- Gly- Asp) motif in the outer layer of the adenovirus capsid; such a modification permits virus entry through binding to αvβ3 and αvβ5 integrins, which are overexpressed on ovarian cancer cells[66]. This modified adenovirus is currently undergoing clinical trials[65-67]. Especially with the potential to genetically engineer OVs for cancer-associated markers, OVs represent a novel mean to selectively target and kill cancer cells based on abnormal receptor expression.

Ultimately the natural or engineered tropism of various OVs has prompted their use as a safe anti-cancer therapeutic agent. Currently, numerous viruses (e.g., reovirus[30], NDV[68], measles virus[24, 57, 69-75], VSV[76], vaccinia virus[77], poliovirus[78], HSV[79], adenovirus[80], Sendai virus[81], maraba virus[82, 83], and coxsackievirus[84]) are being tested as a monotherapy and in various combination treatment regimens to optimize their potential. Of the abovementioned OVs, two have been approved for clinical use: 1) H101 (Shanghai Sunway Biotech) and 2) Talimogen laherparepvec (T-VEC). H101 is a genetically modified adenovirus which was approved in China (November 2005) for the treatment of nasopharyngeal carcinoma in combination with chemotherapy and is only regionally used[85]. T-VEC, an attenuated HSV-1-based OV, has been adapted to endogenously express the immunomodulatory cytokine granulocyte macrophage colony-stimulating factor (GM-CSF) and was the first OV to be approved by the U.S. Food and Drug Administration (FDA). While H101 is approved only in China, T-VEC has now been used in North America, Europe, and Australia[86]. An open-label randomized phase III clinical trial (OPTiM) with an enrolment of 295 advanced melanoma patients showed that T-VEC had significant durable response rate of 16.3% and

enhanced overall median survival by 4.1 months. The FDA approval of T-VEC represents the first OV candidate for international clinical practice[87].

1.3 THE 3 MODES OF OV-MEDIATED CANCER CELL KILLING

To date, the mechanisms through which OVs facilitate tumor regression are not completely understood. However, it is accepted that OVs target cancers through at least three major modes: 1) virus-induced oncolysis, 2) immune-mediated cancer cell killing, and 3) disruption of tumor vasculature or anti-angiogenic properties. While the direct oncolytic properties of OVs have previously progressed the field of OV therapy, both immune- and vasculature remodeling-mediated tumor regression are now recognized as critical elements for tumor eradication. Novel approaches that focus on these aspects are further enhancing the efficacy of OV therapy. It is also important to note that the anti-viral immune response against oncolytic viruses provides a beneficial anti-tumor effect while simultaneously hampering both the spread and replication of the viruses itself. Hence, the therapeutic outcome depends on a complex interplay between the opposing forces of anti-viral and anti-tumor immunity, and both forces must be considered when devising an appropriate therapeutic treatment.

The *lytic potential* of OVs stems from their natural ability to usurp the host cells for virus replication, progeny formation, and ultimately spread. Importantly, recent studies have illustrated that how the cell dies with respect to the immune system plays a critical role linking the lytic potential with the anti-tumor immune potential of OV therapy[84, 88, 89]. In addition to driving an anti-viral immune response, an influx of immune cell infiltration, and an inflammatory cytokines production, several OVs induce immunogenic cell death

(ICD)[90]. This newly recognized means of cell death represents a novel pro-inflammatory death profile which releases immunomodulatory molecules and promotes the induction of a potent anti-cancer adaptive immune response[91]. Extensively studied in the context of various chemotherapeutics[91], ICD is characterized by the surface expression of calreticulin, extracellular release of adenosine triphosphate (ATP) and high mobility group box 1 (HMGB1), and involves endoplasmic reticulum (ER) stress and reactive oxygen species. ICD drives both innate and adaptive immunity through the presentation of "danger" signals (e.g., damage-associated molecular pattern (DAMP) and/or PAMP molecules) to DCs, all of which occur following OV administration. Thus, it is not surprising that OVs can mediate ICD. To date, several OVs have been known to induce the release of HMGB1, ATP, and/or uric acid[90]. For instance, CD40-ligand expressing adenovirus [Ad5/3-hTERT-E1A-hCD40L], coxsackievirus B3, and measles virus have shown their direct ability to mediate the key requirements to induce ICD[84, 88, 89]. Other OVs such as vaccinia virus, parvovirus, and HSV mediate the induction of ICD as a monotherapy or in combination with chemotherapeutics[92-95]. It has yet to be determined whether this induction of ICD is due to eventual release of DAMPs during late stage apoptosis, autophagy and/or necrosis, or following virus-mediated immune cytotoxic death[90]. Nonetheless, it is important to consider that cancer cell necrosis has also been associated with the development of advanced cancer and poor prognosis[96]. Specifically, the well-known DAMP IL-1α has been associated with promoting malignant cell transformation and proliferation following necrotic release[97]. Such findings have led to monotherapeutic approaches to inhibit IL-1α, which are currently in phase III clinical trials (see ClinicalTrials.gov identifiers NCT02138422 and NCT01767857). Although it is acknowledged that OVs induce local ICD and promote the presentation of both virus- and tumor-associated antigens, it is

important to consider negative side effects (i.e., IL-1α release and malignant cell transformation) of ICD during OV therapy.

The second mode of OV-mediated cancer cell killing is the induction of *anti-tumor immunity*. As a consequence of being pathogens, OVs naturally drive the development of a robust anti-viral immune response. Due to the preferential targeting and replication of OVs in the tumor niche, this prompts the inadvertent generation of anti-tumor immunity in the process. Although numerous mechanisms have evolved in the TME to limit inflammation (to be discussed in detail in the following sections), OVs have been shown to establish an environment conducive to a functional anti-viral immune response, while simultaneously generating a potent and clinically meaningful anti-tumor immunity[1, 98, 99]. OVs induce the expression of class I MHC pathway-related molecules, thus providing immediate tumor/viral immune recognition in cancer-bearing hosts[1]. OV administration drives a potent pro-inflammatory cytokine and chemokine profile and thus overturns the immunosuppressive nature of the TME and mediates the influx of innate immune cells. Although some OVs have shown negative effects on the immune system, such as vaccinia specifically targeting DC populations[100], numerous OVs (e.g., reovirus, HSV, adenovirus, poxvirus, and measles virus) have been shown to drive both DC cytokine production and maturation[101, 102]. Furthermore, the direct lytic properties of OVs further potentiate the anti-tumor immune response through the induction of ICD. With such a favourable TME and OV-mediated ICD, tumor-associated and viral antigens are readily presented by professional APCs to naïve T cells promoting the generation of a clinically meaningful adaptive immunity (both effector and memory)[99, 103, 104]. Such an adaptive anti-tumor immunity, specifically $CD8^+$ T cell-mediated, is fundamental in tumor regression and the

therapeutic efficacy of treatment, as this adaptive immunity results in the eradication of existing cancer and continual anti-tumor and anti-viral surveillance, even following the discontinuation of therapy. This has been evident in tumor challenge experiments, where tumor growth is prevented in mice that have received an adoptive transfer of lymphocytes from OV-treated tumor-bearing mice[105, 106]. To date, multiple reports have shown, using T cell depletion studies in immunocompetent animals, that the therapeutic efficacy of OV treatment is highly influenced by the anti-tumor immune arm of OV therapy[106-108].

Tumor vasculature destruction and *anti-angiogenic properties* have been recently recognized as a third mode of OV-mediated cancer cell killing. The development of tumor architecture represents a complex network between non-cancerous bystander cells and cancer cells. In many instances, the TME creates an acidic microenvironment and drives the overexpression of immunosuppressive cytokines such as TGF-β and pro-angiogenic factor vascular endothelial growth factor (VEGF). Such an increase in pro-angiogenic factors, especially in the context of solid tumors, mediates the formation of a novel tumor vasculature to support tumor progression through the delivery of oxygen and essential nutrients. In the recent years of OV research, studies have illustrated that some OVs (e.g., adenovirus, HSV, and vaccinia virus) have anti-vascular properties, and thereby inhibit tumor perfusion and progression[109-111]. For instance, the adenovirus protein E1A binds and inhibits angiogenic factor p300. This inhibition regulates the production of VEGF and ultimately impedes tumor angiogenesis[112]. On the other hand, VSV has been shown to naturally elicit the accumulation of neutrophils and promote clot formation, thereby killing cancer cells and mediating tumor vasculature disruption and cellular starvation[113]. In addition, VSV has also been shown to infect tumor-associated vasculature without harming

normal vasculature[114]. Although the exact mechanism has yet to be determined, it is suggested that the tumor-endothelial or tumor-stromal cell interactions promote a pro-virus environment[109, 115]. Ultimately, the use of either natural or engineered OVs with anti-vasculature properties could impede tumor-associated endothelial cell proliferation, prevent oxygen and nutrient supply, and induce cancer cell death. Such approaches with natural/engineered anti-vascular OVs or combination therapies with anti-VEGF antibodies are currently undergoing investigations to enhance OV-based therapy[109, 116]. Of note, anti-angiogenic and vasculature disruption-mediated mechanisms have differing therapeutic efficacy based on the stage of tumor development. On one hand, anti-angiogenic therapy prevents initiation and subsequent development/growth of tumor vasculature, and thus is more effective in early stage tumors. On the other hand, vasculature disruption is beneficial in late stage tumors where the tumors are dependent on established tumor vasculature. Thus, it is imperative that the proper combination or OVs is utilized based on the stage of tumor development.

With our greater understanding of how OVs effectively mediate cancer cell killing, the field of OV therapy is developing novel strategies tailored to enhance therapeutic outcome. To date, numerous combination strategies have been investigated including enhancing OV-mediated oncolysis (e.g., radiation or chemotherapy), tumor vasculature remodeling with anti-angiogenic factors, and skewing or prolonging anti-tumor immunity (e.g., immune checkpoint blockade inhibitors[117, 118], TLR-signaling manipulation[12], cytokine supplementation[87], and heterologous virus prime-boost strategies[119]). One such strategy is the combination of OVs with immune checkpoint blockade inhibitors (i.e., programmed cell death protein 1 [PD-1], programmed death-ligand 1 [PD-L1] or cytotoxic T-

lymphocyte associated protein 4 [CTLA-4]) to prevent T cell exhaustion. To date, numerous OVs (e.g., reovirus, Maraba virus, VSV, vaccinia virus, NDV) have shown clinical benefit with these immunomodulators[119-122]. Altogether, such complementary combination therapies alongside OV therapy have illustrated much promise for the treatment of a multitude of cancers.

1.4 ONCOLYTIC REOVIRUS AS A MONOTHERAPEUTIC AGENT

Respiratory Enteric Orphan virus, commonly known as reovirus, is a human pathogen isolated from the respiratory and gastrointestinal tracts. It is referred to as an "orphan" virus due to its asymptomatic nature, despite the recent discovery that reoviruses can break dietary antigen tolerance, suggesting that reovirus is a possible culprit for the onset of celiac disease[123]. Reovirus consists of a non-enveloped, icosahedral capsid and has a 10-segment dsRNA genome. Commonly studied as a natural model of acute virus infection, reovirus (type 3 Dearing strain) is also a potent OV currently undergoing phase I, II, and III clinical trials internationally[103]. Unlike double-stranded DNA (dsDNA) OVs, such as adenovirus and HSV which can be genetically engineered to enhance tumor tropism, anti-tumor immunity, or oncolytic potency; the decreased genomic stability of dsRNA viruses has made genetic manipulation of reovirus difficult. To date, there are no genetically engineered reovirus variants undergoing clinical trials. However, natural reovirus has been shown to kill a variety of cancer types including cancers of the breast, lung, head and neck, brain, bladder, lymphoma, ovarian, skin, epithelium, spinal, prostate, and colon[124-136]. Early connections with reovirus and its oncolytic attributes were first observed in the paper by

Hashiro *et al.*, where it was shown that certain tumors and spontaneously transformed cell lines (e.g., W-18Va2, HEP-2, HeLa, and L-929 cell-lines, KB, RA) had preferential susceptibility toward oncolysis[137]. Furthermore, simian virus (SV-40)-transformed human embryonic lung cells (WI-38 cells) showed enhanced sensitivity to reovirus cytotoxicity compared to non-transformed WI-38 cells[138]. While these studies provided a glimpse into the oncolytic potential of reovirus, it was the study by Coffey *et al*. that linked the activated Ras pathway to the selective oncolytic effect of reovirus[30]. This report demonstrated that a single intratumoral reovirus injection could mediate the regression of established human U87 glioblastoma or v-erbB–transformed NIH 3T3 tumors in 80% of xenografted severe combined immunodeficient (SCID) mice. Furthermore, reovirus injection, in an immune competent mouse model (C3H mice bearing Ras-transformed C3H-10T1/2 tumors), had effectively mediated complete regression in 65% of treated mice[30]. Subsequent studies aimed to further understand the association of the Ras-transformation and cancer cell permissiveness to reovirus infection/replication. In particular, Marcato *et al.* demonstrated that Ras-transformation mediated selective viral oncolysis by enhancing virus uncoating, particle infectivity, and apoptosis-dependent release of virus progeny[139, 140]. Additionally, it was illustrated that oncogenic Ras was also involved in the regulation of innate anti-viral defence mechanisms, specifically the suppression of IFN-β. Shmulevitz *et al*. extensively demonstrated that the MEK/ERK pathway, downstream of Ras, inhibits IFN-β expression through the regulation of RIG-I[36].

Following the study by Coffey *et al.*, numerous studies focused on elaborating the therapeutic potential of reovirus as a single anti-cancer agent in a range of cancer types: breast, brain, ovarian, lymphoma, spinal, bladder, colon[103, 124, 125, 127, 130, 134, 136, 141]. One

study showed that reovirus killed 100% of *ex vivo* low-passage surgically excised human gliomas from nine patients[130]. Additionally, a study by Hata *et al.* demonstrated the ability of reovirus to selectively kill cancer cells by directly comparing oncolysis of six human breast cancer cell lines (SK-BR-3, CRL1500, KPL4, MCFT, MDA-MB-453, and MDA-MB-231) with the normal mammary gland epithelial cell line (Hs578Bst)[124]. To complement this study, Norman *et al.* utilized a bilateral tumor model of MDA-MB-453 in SCID mice and demonstrated that reovirus could be successfully used for systemic therapy for breast cancer, as the remote non-injected tumor also responded to reovirus treatment[126].

In support of pre-clinical studies, phase I clinical trials with REOLYSIN® (Pelareoprep), hereon referred to as reovirus, as a monotherapy demonstrated the safety, tolerability, and preferential cancer cell killing in humans with a variety of tumor types[142-145]. In particular, six prostate cancer patients were placed in a translational study to assess the therapeutic efficacy of a single reovirus injection followed by prostatectomies three weeks later. Immunohistochemical analysis of resected prostate tissues revealed that reovirus preferentially infected cancerous tissue as opposed to non-cancerous tissue and increased lymphocyte infiltration within the tumor milieu[142]. With such promising results, reovirus progressed on to its first phase II clinical trial in 2008 for the treatment of metastatic melanoma[146]. Although productive reovirus replication was detected in 2 of 13 melanoma metastases after one week of treatment, no patients met the complete or partial response. It was suggested that combination therapy, as opposed to monotherapy, could be more efficacious. In contrast, another phase II clinical trial for the intravenous administration of reovirus in 52 patients with lung metastases of soft tissue sarcomas demonstrated a total clinical benefit rate of 43% (i.e., 19 of 44 evaluable patients experienced stable disease for

2 to 22 months)[147]. These results suggest that reovirus was well tolerated and that reovirus shows promise for intravenous therapy for metastatic sarcomas.

Similar to other OVs, reovirus invokes a chain of immunological events that ultimately drives the development of an anti-tumor immune response even in the presence of various tumor-induced immunosuppressive mechanisms[1, 98, 105, 148-150]. Multiple studies affirm that reovirus treatment/administration mediates increased levels of pro-inflammatory cytokines and chemokines[1, 98, 151], DC maturation, and innate and adaptive anti-tumor immunity[98, 151]. Furthermore, reovirus-stimulated DCs possess the ability to prime tumor antigen-specific T cells (both *in vitro* and *in vivo*)[98] and increase the cytolytic activity of innate immune cells (e.g., neutrophils, monocytes, and NK cells)[3, 151-153]. Importantly, reovirus drives a tumor-specific immunity capable of protecting the host against subsequent tumor challenge even after discontinuation of therapy[98]. These pre-clinical studies have now driven reovirus-based OV therapy into a new realm which takes an advantage of anti-tumor immunity and combination approaches to further potentiate such a response.

1.5 ONCOLYTIC REOVIRUS: COMBINATION TREATMENT

To enhance its treatment efficacy, reovirus was combined with various anti-cancer treatment options such as chemotherapeutic agents or radiotherapy. Pre-clinical studies revealed synergistic effects, both *in vitro* and *in vivo,* with reovirus in combination with chemotherapeutic agents such as cisplatin, gemcitabine, vinblastine, paclitaxel, docetaxel, or cisplatin-paclitaxel doublet chemotherapy or radiotherapy[131-133, 135, 154]. One of such studies investigated the synergistic effect of reovirus combination therapy with various chemotherapeutics against human non-small-cell lung cancer (NSCLC) cells[135].

Interestingly, a synergistic effect was observed in cell lines that were responsive to the chemotherapy compounds alone (cisplatin, gemcitabine, or vinblastine); however, regardless of the cell line sensitivity to paclitaxel, the combination of reovirus and paclitaxel was invariably synergistic in all NSCLC cell lines. The authors speculated that accelerated apoptosis triggered by paclitaxel-mediated mitotic arrest further enhanced treatment effectiveness. In agreement of this hypothesis, several studies have illustrated that the activation or stabilization of apoptotic pathways (*via* p53-dependent NFκB activation) further heightens reovirus-induced apoptosis[128, 129]. These pre-clinical studies suggest that a combination approach further enhances reovirus-mediated cytotoxicity.

The first clinical trial administering reovirus intratumorally in combination with palliative radiotherapy was conducted on patients with melanoma, squamous cell carcinoma of the skin, lung, ovarian, head and neck, esophageal, colorectal, and pancreatic cancers [155]. This study determined that the combination therapy was well tolerated with minimal toxicity profiles. A subsequent phase II trial confirmed the safety and positive clinical outcomes of the combination regimen with low radiotherapy[156]. Future reovirus clinical trials in combination with radical radiotherapy are expected to be designed for a curative intent.

In addition to palliative radiotherapy, combinatorial reovirus and chemotherapy clinical trials have been completed or are ongoing. Recently, results from Phase II clinical trials have shown that reovirus in combination with various chemotherapeutics are well tolerated; however, they have demonstrated no significant progression-free survival (PFS). These trials include the use of reovirus in combination with: paclitaxel/carboplatin (for metastatic pancreatic adenocarcinoma (PDAC)[157], malignant melanoma[158], and NSCLC)[159], paclitaxel (for recurrent ovarian, tubal, or peritoneal cancers)[160], and pemetrexed/docetaxel (for

advanced stage refractory platinum doublet NSCLC)[161]. Of note, the randomized Phase II trial for reovirus with upfront treatment of metastatic PDAC showed no improvement with regards to PFS[157]. However, patient immune phenotypes, specifically decreased levels of IL-6 and IL-10, increased memory T cells, and lowered CTLA-4 expression on $CD8^+$ T cells, were associated with overall positive patient survival regardless of treatment[162]. In addition, reovirus treatment mediated increased fractalkine, IL-10, RANTES, Stromal cell-derived factor 1(SDF-1), and VEGF-A cytokine levels and the frequency of T_{regs}, $CD4^+$ $CTLA4^+$, $CD8^+$ $CTLA4^+$, and $CD8^+$ $TIM3^+$ T cells subsets in comparison to the paclitaxel/carboplatin treatment in patients[157]. These Phase II clinical trials suggest that reovirus is well tolerated but novel approaches are needed to further enhance the efficacy of reovirus-based OV therapy with an emphasis on the therapeutic manipulation of immunosuppressive mediators.

Recently, numerous immunotherapeutic approaches are being combined with standard reovirus therapy to enhance and prolong the effects of anti-tumor immunity. One such approach is the combination of reovirus with immune checkpoint blockade inhibitor, anti-PD-1. This combination of reovirus and PD-1 blockade in the B16 mouse melanoma model enhanced reovirus-mediated pro-inflammatory cytokine secretion and NK cell cytotoxicity, decreased T_{reg} functionality, and significantly prolonged tumor-bearing host survival in comparison to each treatment alone[117]. This study and others further confirm the benefit of immunotherapy complementation with reovirus and pushed such strategies into clinical trials[117, 119, 163]. To date, reovirus is being combined with Pembrolizumab (anti-PD-1) alone or with chemotherapy (gemcitabine, Irinotecan, Leucovorin, or 5-fluorouracil) in PDAC patients (NCT02620423)[164], Lenalidomide or Pomalidomide in multiple myeloma patients

(NCT03015922), and with GM-CSF for skin melanoma (NCT03282188). All of these combinations have immunomodulatory effects such as affecting angiogenesis and/or the immunosuppressive niche (Lenalidomide/Pomalidomide), driving enhanced myeloid cell homing and activity (GM-CSF), or preventing T cell exhaustion (Pembrolizumab/anti-PD-1). Of the indicated clinical trials above, data from the phase I trial using reovirus with pembrolizumab and chemotherapy have shown manageable safety profiles, and 1 of 11 patients had a partial response to treatment. Importantly, the primary objective of this phase I clinical trial was safety and secondary tumor response and reovirus replication/immune analysis. Thus, further evaluation of these combinations is suggested to be studied in both pre-clinical and clinical settings.

1.6 CURRENT OBSTACLES LIMITING THE EFFICACY OF OV THERAPY

With the completion of numerous clinical trials and with continued progress in pre-clinical studies, the use of reovirus as an anti-cancer agent in combination seems like an increasingly favourable alternative to a monotherapeutic approach. Importantly, both pre-clinical and clinical studies have recognized key obstacles that dictate the successful translation of reovirus-based OV therapy. These key obstacles are associated with 1) difficulties in systemic reovirus delivery, 2) anti-viral immunity, and 3) tumor-associated immunosuppressive mechanisms.

First, reovirus delivery to tumor cells through systemic/intravenous administration represents a major obstacle in the optimization of reovirus-based OV therapy. Although intratumoral injections are the best means to deliver the highest dosage of virus particles to the tumor vicinity, a systemic viral administration increases the probability of treating

metastatic or multi-nodular tumors. However, due to various host factors, such as neutralizing anti-reovirus antibodies (NARAs), non-specific organ entrapment (spleen, lung, and liver), scavenging immune cells, and/or vascular dysregulation/collapse[165, 166], the successful delivery of therapeutic virus dosage is significantly reduced in many intravenously administered OVs[167]. Thus, pre-clinical studies with OVs are using means such as cell carriers to not only avoid immune detection but also for their tumor-homing properties to tumor microenviroments[167-171]. For instance, Eisenstein *et al.* engineered a strain of VSV (rVSV(MΔ51)-M3) which binds to myeloid-derived suppressor cells (MDSCs), *via* non-neutralizing VSV antibody and fragment crystallizable (FC) receptor interactions, to use the MDSC's natural tropism to the TME. This approach increased VSV-homing to the TME and improved systemic administration[169]. Interestingly, a reovirus Phase I clinical study demonstrated that intravenously injected reovirus was naturally associated with peripheral blood mononuclear cells (PBMCs) in 14% of patients 10 days post the last reovirus injection. Additional findings suggest that administered reovirus is often taken up by PBMCs and carried systemically while also avoiding circulating NARAs[171]. To enhance systemic reovirus delivery and overcome circulating NARAs, Jennings *et al*. conducted reovirus-loading of lymphokine-activated killer cells co-cultured with DCs. They demonstrated that ascites, associated with peritoneal carcinomatosis in ovarian cancer, inhibits reovirus-induced oncolysis due to the presence of NARAs[170]. Thus, reovirus-loading of these cell carriers enhanced the tumor cell killing, pro-inflammatory cytokine production, and the generation of a specific anti-tumor adaptive immune response. With respect to the prevalence of NARAs in most adults owing to previous exposure to reovirus during their lifetime[142, 146, 155, 171-176], such an approach promises to enhance systemic reovirus delivery.

As one may expect, the host immune system poses a major hurdle for reovirus-based OV therapy as the therapeutic administration of reovirus drives two contrasting immunities: anti-viral and anti-tumor. Whereas anti-tumor immunity is highly desirable as it targets cancer cells, anti-viral immunity curtails the replication and spread of reovirus prematurely before sufficient tumor eradication. A few studies have minimized the humoral anti-viral adaptive immunity by packaging OVs within cell carriers or by hampering NARA production to prevent NARA-virus interactions[12, 167, 170, 174, 177]. Other studies have taken a heterogenous OV boost approach, which primes the tumor microenvironment with one OV followed by a subsequent treatment or "boost" with a different OV[119, 178], thus avoiding the adaptive anti-viral response against a particular virus and generating a more robust anti-tumor immunity. In particular, Ilett *et al*. conducted a study focused on using reovirus to prime followed by a VSV-ASMEL (VSV expressing a cDNA library of melanoma antigens) boost for the treatment of subcutaneous B16 melanoma tumors. This approach significantly improved the survival of B16 tumor-bearing mice[119]. Further, this study additionally incorporated both anti-PD-1 therapy and GM-CSF treatment with this heterogenous boost approach and generated a fully systemic and effective anti-tumor immunotherapy[119]. Such an approach paves the way for future OV-based combination studies to enhance anti-tumor immunity while minimizing the restraining effects of anti-viral adaptive immunity.

The third obstacle, and the most relevant with regards to my thesis, is the appropriate management of tumor-associated immunosuppression during OV therapy. Cancer immunotherapies have shown considerable promise; however, cancer-associated immunosuppression can hamper an anti-tumor immune response. Although reovirus and

other OVs overturn multiple tumor immune evasion mechanisms, a greater understanding of how an immunosuppressive TME responds to treatment and how it can be manipulated must be revealed to enhance the effectiveness of therapy. To this end, the following sections will cover cancer-associated immunosuppression and follow up on how understanding this immunosuppressive component is vital to further enhance the efficacy of OV therapy.

1.7 CANCER-ASSOCIATED IMMUNOSUPPRESSION AND ITS EFFECT ON CANCER IMMUNOTHERAPY

Early efforts to understand tumor biology and progression were conducted solely on transformed cells. Considerable evidence now suggests that non-neoplastic cells play key roles in all stages of cancer progression (initiation, growth, invasion, and metastasis)[179-181]. The cellular constituents of the TME can be composed of a plethora of cell types (e.g., T cells, B cells, NK cells, mast cells, macrophages, DCs, fibroblasts, pericytes, granulocytic cells [neutrophils, basophils, eosinophils], and immature myeloid cells). According to the immunoediting hypothesis[182, 183], the host immune system and tumor cells undergo three stages of complex interaction: *elimination*, *equilibrium,* and *escape*. The tumor *elimination* phase represents a state in which the innate and adaptive immune systems cooperate in the detection and elimination of the transformed cells. This state is commonly accompanied by a T_H1 response, which is indicative of anti-tumor cell-mediated cytotoxicity, and the expression of IL-2, IL-12, IL-15, IL-18, and IFN-γ cytokines. In this model, tumor infiltrating/resident lymphocytes act as sentinels by recognizing and eliminating nascent transformed cells. On one hand, this immune response plays a fundamental role in tumor elimination and progression; however, on the other hand, it pressures tumors to adopt immune evasive mechanisms and avoid such immune assault. Furthermore, in situations of

chronic inflammation, a persistent inflammatory state can act as a driving force for tumorigenesis and even promote an exhaustive TME, leading to a phase of tumor *escape*. The phase of *equilibrium* represents one that has immune-mediated control of tumor progression leading to tumor dormancy but not elimination. Both clinical and pre-clinical studies, in which a host becomes immunocompromised or is immunocompromised following organ transplantation, have proposed such a phase as there is a resurgence of tumor progression once the immune pressure has been lifted[184-186]. Lastly, the *escape* phase is one that tumor cells have persisted through immune pressure and evaded immune-mediated elimination. Such immune evasion mechanisms include the development of T_H2-like TME (i.e., high levels of IL-4, IL-5, IL-10, and IL-13), immune checkpoint blockades, tissue barriers, regulatory/dysfunctional immune cells, and defective antigen presentation[187-194]. To increase the complexity of such Darwinian phenomena, TMEs are heterogenous in nature and develop differently on a case-by-case basis. For instance, Gajewski *et al.* suggest that there are generally two broad groups of immunological profiles in cancer patients: 1) "hot" tumors with T cell infiltration and 2) "cold" non-T cell-infiltrated tumors[187]. The first immunological profile, "hot" tumors, represents an exhaustive TME commonly composed of increased immune checkpoint mediators, impaired DCs, increased frequencies of immunosuppressive immune cells such as T_{regs} and MDSCs. It is postulated that this type of TME has arisen because of a spontaneous anti-tumor immune response[187]. "Cold" tumors are characterized by poor chemokine expression, void of T cell infiltrate, lack of established immune checkpoint mediators, immunosuppressive cytokines, and a tissue/extracellular barrier to prevent effector cell chemotaxis[187]. From a clinical and immunotherapeutic perspective, these immunosuppressive mechanisms are negatively correlated with patient prognosis and are

major obstacles for the therapeutic efficacy of treatment. Such heterogeneity in TME suggests that the most effective cancer treatment is one that is devised based on the individual's immunological profile, which forms the basis of modern personalized immunotherapies.

Cancer-associated immunosuppression is represented in many forms and it is ultimately characterized as mechanisms which prevent the infiltration, activation, survival, and/or function of innate and adaptive effector immune cells. It is important to note that numerous immune cells (e.g., T_{regs}, B cells, mast cells, tumor-associated macrophages [TAMs], immature monocytic myeloid cells/monocytic MDSCs, fibroblast, endothelial cells, pericytes, granulocytic cells/granulocytic MDSCs) have or acquire immunosuppressive functions leading to tumor immune evasion (summarized in Table 1.1). For instance, tumor-associated endothelial cells can establish a "tumor endothelial barrier"[195] which directly affects T cell infiltration, function, and survival. This "tumor endothelial barrier" can affect T cell infiltration through the downregulation and/or declustering of ICAM1 and vasculature cell adhesion molecule 1 (VCAM1)[195, 196]. Furthermore, tumor-associated endothelial cells can selectively upregulate immune checkpoint mediators and immunosuppressive factors (PGE2, IL-10, and TGF-β) and mediate T cell apoptosis by expressing apoptosis-inducing molecules such as TRAIL and FasL[197-199]. Similarly, cancer-associated fibroblasts (CAFs) have been shown to contribute to the downregulation of endothelial adhesion molecules, minimize lymphocyte infiltration, and additionally promote TAM and MDSC recruitment and accumulation[200-202]. Depletion of fibroblast activating protein-α (FAP)-expressing CAFs mediates a shift in balance from a T_H2 to a T_H1-like immune profile and reduced levels of MDSCs, TAMs, and T_{regs} within the

TME[200, 202-204]. In addition to cancer-associated endothelial and fibroblasts which significantly contribute to the TME and architecture of the tumor, infiltrating immune cells such as regulatory B cells (B_{regs}) and T_{regs} also exhibit immunosuppressive potential leading to tumor progression and impaired anti-tumor immunity. One of such mechanisms of immunosuppression by both B_{regs} and T_{regs} is the secretion of IL-10, TGF-β, and IL-35 cytokines, leading to decreased T_H1-type immune response in $CD4^+$ T cells, $CD8^+$ T cells, and monocytes[205-207]. T_{regs} have also been shown to mediate immunosuppression of $CD8^+$ T cells *via* the competitive scavenging of local IL-2[208]. Furthermore, both B_{regs} and T_{regs} can suppress effector T cell function *via* the actions of checkpoint inhibitors (e.g., PD-L1 and cytotoxic T-lymphocyte-associated antigen 4 [CTLA-4]). Lastly, cancer-associated myeloid cells, encompassing both granulocytic myeloid cells and monocytic myeloid cells (MMCs), significantly contribute to both innate and adaptive immunosuppressive mechanisms. Unlike their phagocytic and anti-viral or anti-bacterial counterpart, immunosuppressive G-MDSCs have been shown to promote tumor progression *via* increased angiogenesis, metastasis, and immunosuppression. Immunosuppressive G-MDSC-mediated immunosuppression has been commonly associated with increased secretion of reactive oxygen species (ROS), immunosuppressive cytokine secretion (e.g., TGF-β), and production of arginase 1 (ARG1)[209], which limit the anti-tumor potential by promoting a more immunosuppressive TME or by directly affecting innate and adaptive immune cell function. It is important to note that G-MDSCs and tumor-associated neutrophils (TANs) are indistinguishable with common surface markers. However, TANs have illustrated both anti-tumor and pro-tumor properties. For instance, Eruslanov *et al.* illustrated that TANs acquire a pro-inflammatory phenotype and promote T cell activation in early stage human lung cancer[210]. Similar results were illustrated by Fridlender *et al.*,

who showed that TGF-β blockade mediated an influx of TANs with high levels of pro-inflammatory cytokines and anti-tumor cytotoxic properties[211]. Interestingly, TANs possessed pro-tumor properties prior to TGF-β blockade, suggesting that TANs are environmentally responsive and that TGF-β is a significant contributor to the immunosuppressive nature of TANs[211]. Importantly, tumor cells themselves also have numerous immunosuppressive mechanisms (e.g., nutrient deprivation, PD-L1 expression, high indoleamine 2,3-dioxygenase [IDO] expression, and FasL expression) which both enhance cancer-associated immunosuppression and limit anti-tumor immunity[212-214].

In an era where there is a growing interest in cancer immunotherapies, it is of the utmost importance to understand the TME and manipulate the existing immunosuppressive burdens that hamper the efficacy of therapy. To date, the FDA has approved multiple immunotherapeutic approaches, such as sipuleucel-T (APC 8015, Provenge) vaccine[215], ipilimumab[216], lambrolizumab[217], and T-VEC[218]. Although patients treated with cancer vaccines, OVs, and immune checkpoint blockade inhibitors (anti-PD-1, anti-PD-L1, or anti-CTLA-4 antibodies) develop antigen-specific T cell responses, only a minority of them demonstrate clinical benefits[219-221]. These results suggest that novel approaches must be considered to prime an effective anti-tumor response in the TME while altering/tailoring the immunosuppressive mechanisms in play.

As indicated above, numerous cells encourage the development of cancer-associated immunosuppression and act through various mechanisms. Of such cells, monocytic myeloid cells are now being appreciated as a major influencer of anti-tumor immunity and cancer progression. As such the focus of my project was to study MMCs.

Table 1.1. *TME-associated Immunosuppressive Immune Cellular Constituents.*

Cell Types	Immunosuppressive Mechanisms	Ref
Myeloid-derived suppressor cells (monocytic & granulocytic)	-Deplete T cell-essential nutrients (ARG1- and iNOS-mediated) -secrete immunosuppressive cytokines (i.e., TGF-β, IL-10) -produce oxidative stress which impedes antigen-specific stimulation and responsiveness of T cells -interfere with lymphocyte trafficking (ADAM17) -affect T cell viability and function *via* PD-L1 and TIM3 expression -secrete IDO which upregulates IL-6 production and their recruitment/accumulation. IDO also depletes tryptophan which is an essential nutrient for T cell viability and proliferation	190, 222-227
Tumor-associated macrophages	-secrete immunosuppressive factors (TGF-β, IL-10, ARG1, and PGE2) -recruit T_{regs} (CCL22-mediated) -express PD-L1, B7-H3/H4 which affects T cell viability/function -secrete IDO which affects T cell viability and proliferation	228-234
Plasmacytoid dendritic cells	-secrete immunosuppressive factors such as IDO -express PD-L1 which affects T cell viability and function	235-237
Tumor-associated neutrophils	-deplete arginine (T cell-essential nutrient) -promote oxidative stress (ROS) which impedes antigen-specific stimulation and responsiveness of T cells -secrete VEGF promoting angiogenesis and poor vascularization	238, 239
Regulatory T cells	-secrete immunosuppressive cytokines (IL-10, TGF-β) -deplete IL-2, IL-7, IL-12, and IL-15 -impair antigen-presenting cell costimulatory molecule presentation (CTLA4) -inhibit myeloid cell differentiation (LAG3)	206, 240-243
Regulatory B cells	-secrete immunosuppressive cytokines (IL-10, TGF-β) -express PD-L1, CTLA-4, and FasL	205, 244
Mast cells	-mediate ultraviolet-B-induced immunosuppression through the secretion of histamines and TNF-α -secrete immunosuppressive cytokines (TGF-β and IL-10) -secrete VEGF to decrease cell adhesion molecules	245
Cancer-associated fibroblasts	-secrete SDF-1 and TGF-β which enforce an immunosuppressive niche -stimulate VEGF expression -recruit tumor-associated macrophages and MDSCs -mediate the downregulation of cell adhesion molecules	200, 202, 203, 246
Tumor endothelial cells	-provide a barrier against immune infiltration -secrete immunosuppressive factors (PGE2, IL-10, and TGF-β) -express several checkpoint inhibitors (PD-L1, PD-L2, TIM3, B7-H3/H4) -mediate the selective accumulation of T_{regs} -mediate T cell apoptosis *via* Fas-FasL interaction and TRAIL expression -downregulate cell adhesion molecules to prevent T cell infiltration into the TME	195-199
Pericytes	-secrete immunosuppressive factors such as TGF-β, PGE2, hepatocyte growth factor (HGF), and human leukocyte antigen-G (HLA-G) -increase oxidative stress (NO) thereby hindering effector cell responsiveness	247

1.8 MONOCYTIC MYELOID CELLS (MMCS)

MMCs are essential contributors to tissue homeostasis, anti-pathogenic clearance and defence, immune tolerance, and known for their role in initiating and sustaining adaptive immunity. They have been assigned context-dependent and contrasting phenotypes, ranging from immunostimulatory to immunosuppressive, in response to a plethora of pathological conditions (such as infections[248], autoimmunity[249], and cancer progression[250-252]). MMCs arise in the bone marrow (BM) from hematopoietic stem cells (HSCs) and after a step-wise progression into common progenitor cells, emigrate from the BM to the circulation *via* a CCL2-CCR2 or CX3C-chemokine ligand 1 dependent mechanism. Under normal conditions, monocytes replenish tissue macrophages and dendritic cells in a steady state and represent 2-5% of circulating white blood cells in a healthy mouse. Of note, these are a heterogenous population of cells and are characterized using various markers, which will be described in the following sections. Following infection, pro-inflammatory signals, including pro-inflammatory cytokines and PAMPs, induce the emigration of MMCs from the BM to the site of infection. These MMCs sufficiently mount a rigorous immune response and aid in the clearance of numerous pathogens (e.g., *Listeria monocytogenes*, *Klebsiella pneumoniae*, or influenza virus infection[248, 253, 254]). For example, influenza virus-mediated MMC recruitment is a major contributor to the excessive collateral damage within the lungs; however, the absence of such recruitment impairs viral clearance[254]. In addition to this direct anti-microbial role, these MMCs carry pathogenic antigens to local lymph nodes, where they further differentiate into DCs or transfer antigens to classical dendritic cells[255]. MMC-differentiated DCs can be as effective as classical DCs in priming $CD4^+$ and $CD8^+$ T cells[13, 256]. This suggests that MMCs can contribute to pathogen-specific

T cell responses throughout the development of adaptive immunity[257]. Under pathological conditions (e.g., cancer, sepsis, autoimmunity), the common myeloid progenitor cells (CMPs) have impaired or altered differentiation and possess an immunosuppressive phenotype, identified as either monocytic myeloid-derived suppressor cells (M-MDSCs) or granulocytic/polymorphonuclear myeloid-derived suppressor cells (G-MDSCs). M-MDSCs are not terminally differentiated as they have been shown to further differentiate into alternatively-activated macrophages (M2-macrophages)[251], which further supports tumor progression. Ultimately, these immunosuppressive MMCs predominantly have a negative correlation with patient survival and promote both cancer-associated immunosuppression and progression.

To this end, the following sections will focus on the role of suppressive MMCs/monocytic MDSCs (in relation to their G-MDSC counterparts), tumor-associated macrophages (TAMs), and impaired DCs. These populations/cellular states (highlighted in Figure 1.1) will be described in the context of cancer and with respect to their immunosuppressive functions, functional impairments, pro-tumor properties, and their role with regards to the efficacy of cancer immunotherapies.

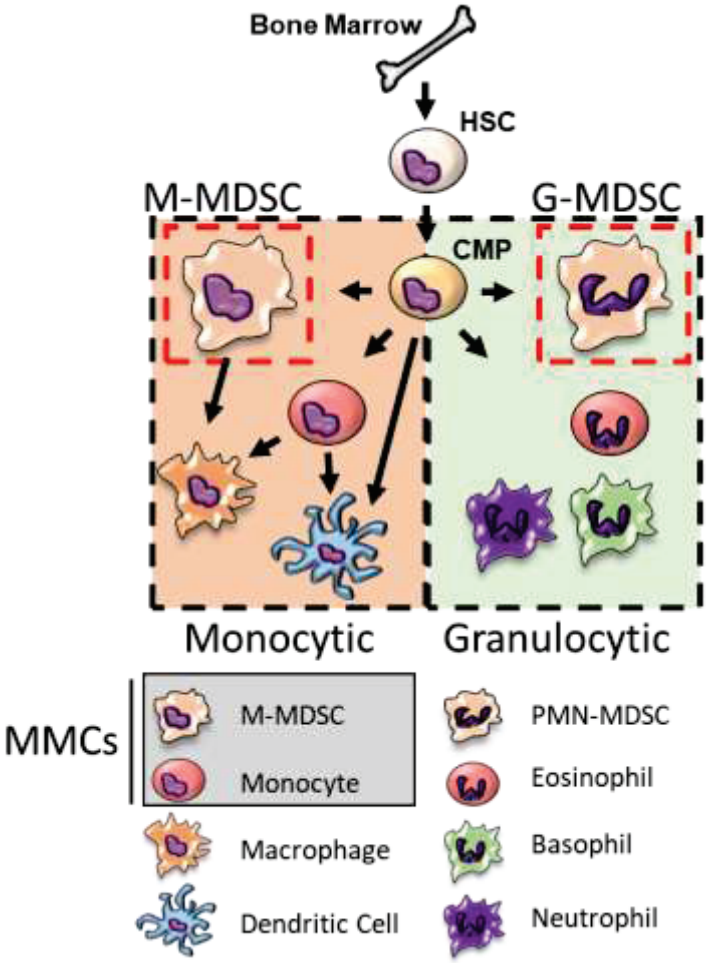

Figure 1.1. *Myeloid Cell Differentiation Under Normal and Pathological Conditions.* Myeloid cells arise from the bone marrow as hematopoietic stem cells (HSCs) and subsequently differentiate into common myeloid progenitor cells (CMPs). During normal myelopoiesis, CMPs can differentiate into granulocytic cells (eosinophils, basophils, and neutrophils) or monocytic cells (monocytes, macrophages, and dendritic cells). Under pathological conditions, such as tumor development or sepsis, CMPs have impaired differentiation and maturation and thus, the immunosuppressive phenotypes/states of granulocytic and monocytic myeloid cells (G-MDSCs and M-MDSCs, respectively) accumulate. M-MDSCs have also been shown to further differentiate into terminally differentiated macrophages (specifically M2-like macrophages; tumor-associated macrophage [TAM]) in tumor models. The term monocytic myeloid cell (MMC), in the context of this thesis, is represented as both monocytes and M-MDSCs regardless of functional discrepancies.

1.8.1 Myeloid-derived Suppressor Cells (MDSCs)

Extensive evidence, thus far, indicates that MDSCs are key players in the regulation of tumor progression because they suppress host immunity and promote both angiogenesis and metastasis[222]. Thus, it is not surprising that elevated frequencies of MDSCs are often associated with advanced cancer stage, decreased disease-free survival, and correlate with poor clinical outcome[209, 258]. Initially termed to capture the functionality and not a novel population of myeloid cells, MDSCs represent a heterogeneous group of myeloid progenitor cells. They are currently characterized as being both monocytic (M-MDSCs) and granulocytic/polymorphonuclear (G-MDSCs/PMN-MDSCs) in nature. Mouse MDSCs are commonly characterized by the expression of myeloid lineage markers (myeloid differentiation antigen [Gr-1]) and integrin alpha M (CD11b). Gr-1 can be further dichotomized into lymphocyte antigen 6 complex, locus G (Ly6G) and locus C (Ly6C) to separate monocytic *versus* granulocytic lineages. In mice, M-MDSCs are identified as $CD11b^{+}$ $Ly6G^{-}$ $Ly6C^{high}$ or $CD11b^{+}$ $Gr\text{-}1^{low}$ $Ly6C^{high}$ cells while G-MDSCs are recognized as $CD11b^{+}$ $Ly6G^{+}$ $Ly6C^{low}$ or $CD11b^{+}$ $Gr\text{-}1^{high}$ $Ly6C^{low}$ cells. Human MDSCs are commonly characterized by the expression of $CD11b^{+}$ $CD14^{+}$ $HLA\text{-}DR^{-/low}$ $CD15^{-}$ for M-MDSCs and $CD11b^{+}$ $CD14^{-}$ $CD15^{+}$ or $CD11b^{+}$ $CD14^{-}$ $CD66b^{+}$ for G-MDSCs. Since few $CD15^{+}$ cells are $CD11b^{-}$, the CD33 myeloid marker can also be used in place of CD11b and thus, displays as $CD33^{+}$ and $CD33^{dim}$ in M-MDSCs and G-MDSCs, respectively[259, 260]. MDSCs represent a broad and transient state of immature myeloid progenitors and are termed as suppressor cells based on their ability to suppress innate and adaptive immune cells. As the surface marker phenotype of MDSCs overlaps with the markers used to

phenotype monocytes, neutrophils, and macrophages, functional assays are often conducted to classify these immature myeloid cells as "suppressive" MDSCs[251].

In healthy individuals, myeloid progenitor cells are generated in the BM and subsequently differentiate into monocytes, granulocytes (neutrophils, basophils, eosinophils), macrophages, or dendritic cells. However, under pathological conditions such as cancer, infections, trauma, or sepsis, the complete differentiation and maturation of myeloid progenitor cells are impaired, resulting in the accumulation of MDSCs[222]. Numerous tumor-derived cytokines such as granulocyte-macrophage colony-stimulating factor (GM-CSF), granulocyte-CSF (G-CSF), and macrophage-CSF (M-CSF), stem cell factor (SCF), VEGF, and IL-3 promote myelopoiesis and contribute to impaired myeloid cell maturation[222, 261]. Furthermore, pro-inflammatory cytokines such as IFN-γ, IL-4, IL-6, IL-10, and IL-13 also initiate a feedback response that mediates the expansion of MDSCs[262]. MDSC accumulation contributes to the immunosuppressive nature of TMEs and has been documented in various cancer types including those of breast, ovarian, colon, kidney, and prostate[223, 263-265].

MDSCs mediate immunosuppression *via* a plethora of mechanisms, which are further dependent on their phenotypic heterogeneity. For instance, G-MDSCs predominantly suppress antigen-specific T cells through the production of ROS. In contrast, M-MDSCs suppress mainly effector T cells *via* high expression of enzymes ARG1, inducible nitric oxide synthase (iNOS), and reactive nitrogen species. In general, the immunomodulatory functions of MDSCs can be broadly categorized into five main classes. The first is through the depletion of T cell-essential nutrients, primarily L-arginine and L-cysteine, resulting in the downregulation of the T cell receptor (TCR) ζ-chain and subsequent proliferation arrest

of activated T cells. MDSC-mediated depletion of L-arginine is induced by the overexpression of ARG1 and iNOS[224]. L-cysteine depletion is mediated by the increased consumption and sequestration by MDSCs[266]. The second MDSC suppression mechanism is the secretion of immunosuppressive factors (e.g., TGF-β and IL-10) which can inhibit NK cells[225], promote T_{reg} expansion, impair DC function, and modulate the cytokine production of macrophages to favour tumor progression (T_H2-like macrophage). Oxidative stress represents the third mechanism of immunosuppression as increased ROS and reactive nitrogen species (peroxynitrite) mediate the loss of TCR ζ-chain and affect TCR and IL-2 signaling *via* nitration or nitrosylation, respectively[190, 222]. Finally, MDSCs also interfere with lymphocyte trafficking and viability. Surface expression of the metalloproteinase ADAM17 cleaves T cell surface expressed-CD62L, which is required for T cell migration to draining lymph nodes[267]. MDSCs also express PD-L1 and galectin-9 (GAL9), which when bound to their respective molecules (PD-1 and T cell membrane protein 3 [TIM3], respectively) mediate T cell apoptosis and/or anergy[226, 227]. To this end, MDSCs represent crucial orchestrators of tumor-associated immunosuppression using numerous direct and indirect mechanisms.

In line with their immunosuppressive activities, MDSCs hamper the successful implementation of numerous cancer immunotherapeutic approaches, including cancer vaccines, immune checkpoint blockade inhibitors, adoptive T cell therapy, and OVs[2, 4-6, 268-274]. Such therapeutic hindrance was evident in a study by De Henau *et al.* which demonstrated that targeting PI3Kγ in myeloid cells overcomes resistance to checkpoint blockade therapy[268]. Interestingly, pharmacological inhibition of PI3Kγ, which signals *via* Akt and mTOR and thereby inhibits NFκB activation[275], drove a more pro-inflammatory

tumor-associated myeloid cell phenotype, increased PD-1 and CTLA-4 expression on T cells, and ultimately overcame checkpoint inhibitor blockade therapy resistance[268]. To this end, various approaches are currently targeting MDSCs through the 1) promotion of MDSC differentiation and maturation, 2) depletion of MDSC populations utilizing chemotherapeutics, and 3) the functional inhibition of MDSCs. The use of all-trans-retinoic acid (ATRA) during combination therapy is currently under clinical trials to promote MDSC differentiation and maturation[276]. ATRA is a necessary factor for the maturation of myeloid cells and alleviates MDSC-mediated immunosuppression[273, 277]. It is important to note that ATRA can also promote the accumulation and function of T_{regs}[278]. Thus, the strategic management of each population must be considered when using such an approach. The depletion of MDSCs using chemotherapeutics (e.g., gemcitabine and 5-fluorouracil [5-FU]) has been utilized in numerous combination therapies as they have been shown to selectively deplete MDSCs[279-281]. The fact that gemcitabine and 5-FU are commonly used chemotherapeutic agents makes them promising candidates for combination therapy in clinical trials. In addition to chemotherapeutics, small molecule inhibitors such as sunitinib and verumurafenib reduce both MDSC and T_{reg} levels within cancers of multiple origins[282-284]. The functional inhibition of MDSCs is also being pursued with the use of multiple factors such as PI3Kγ, phosphodiesterase type 5 (PDE-5)[285] or cyclooxygenase-2 (COX-2) inhibitors[286]. In particular, COX-2 inhibitors alter the TME by reducing MDSC-chemotactic factor CCL2 and upregulating T cell associated chemokine CXCL10[286]. Altogether, the selective depletion or inhibition of MDSCs has generally been associated with enhanced therapeutic outcome for cancer patients.

1.8.2 Tumor-associated Macrophages (TAMs)

Although much of the focus on the suppressive capacity of myeloid cells is directed towards MDSCs, TAMs have a major role in the development of the TME, inhibition of chemotherapy-induced apoptosis, promotion of angiogenesis and tumor metastasis[261, 287-289]. Macrophages are a group of terminally differentiated myeloid cells that are necessary to eliminate infectious agents, promote wound healing, and regulate adaptive immunity in healthy individuals. This varied array of functionality is due to the plastic nature of these cells, as their function is dictated by environmental stimuli. Macrophages lie on a gradient of two spectrums, one being the "classically-activated" or M1 macrophages and the other being the "alternatively-activated" or M2 macrophages. The generation of M1-like macrophages is stimulated by IFN-γ and PAMPs and they express high levels of immunostimulatory cytokines (such as IL-12, IL-1β, and TNF-α) and little to no IL-10. Furthermore, M1-like macrophages have high surface expression of CCR2, low expression of scavenging receptors (e.g., CD206 and CD163), and are highly glycolytic with lower oxidative phosphorylation metabolic potential. In contrast, M2-like macrophages are commonly triggered by IL-4, IL-10, VEGF, and IL-13 and glucocorticoid hormones, have reduced expression of pro-stimulatory cytokines and heightened expression of IL-10. M2-like macrophages are commonly associated with low CCR2 expression, high scavenger receptor surface expression, increased oxidative phosphorylation, and decreased glycolysis metabolism[290]. In the context of cancer, the heightened frequency of TAMs is commonly attributed to increased circulating precursor ($CCR2^{high}$, $CD11b^{+}$ cells) recruitment and differentiation in the tumor niche[291, 292]. This accumulation perpetuates an immunosuppressive TME through the production of multiple immunosuppressive factors (TGF-β, IL-10, ARG1, and prostaglandin E2 [PGE2]). TAMs are ineffective APCs that can interact extensively with other immune cells and enhance MDSC function, support T_{reg}

recruitment through the secretion of chemokine (C-C motif) ligand 22 (CCL22)[293], and suppress T cell function *via* the expression of PD-L1[228]. Animal studies which hindered TAM recruitment and accumulation, *via* genetic ablation of the crucial maintenance regulator M-CSF, showed delayed tumor progression and malignancy[294, 295]. Furthermore, human studies revealed positive associations between CCL2 and/or M-CSF overexpression and poor prognosis in numerous types of cancers (e.g., breast, colorectal, endometrial, pancreatic, and hepatocellular tumors[296-301]). Such accumulation of pro-tumor mediators promotes a self-propagating and impenetrable environment that impedes the development of an anti-tumor immune response.

In addition to the generally negative connotation that TAMs (M2-like phenotype) have on cancer progression, they can also hamper the responsiveness of cancer therapies. For instance, TAMs have been shown to limit chemotherapy efficacy (e.g., doxorubicin, melphalan, or dexamethasone) *via* PSGL-1/selectin and ICAM-1/CD18 interactions in multiple myeloma and prevent cancer cell apoptosis[302]. M2-like macrophages were also found to accumulate in perivascular areas and promote tumor revascularization and relapse following chemotherapy with cyclophosphamide in a Lewis lung carcinoma model[303]. Additionally, Arlauckas *et al*. illustrated that TAMs significantly limit the effectiveness of anti-PD-1 therapy by accruing the anti-PD-1 antibodies through the Fc domain glycan and the Fcg receptors expressed by TAMs. Disrupting Fc binding enhances immunotherapy-mediated tumor regression and prolongs anti-PD-1 antibody binding to TME-infiltrating $CD8^+$ T cells[304]. Thus, TAMs represent an important cellular population with potential to negatively skew therapeutic efficacy. Hence, current approaches are attempting to deplete TAM populations through different means such as targeting M-CSF-M-CSFR signaling

with monoclonal antibodies[201, 305, 306], small molecule inhibitors[305, 307, 308], and nanoparticle-based gene expression silencing[309, 310]. Additionally, approaches tailored to reprogram TAMs and harness potential pro-inflammatory or anti-tumor properties (M1-phenotype) are currently being utilized to enhance therapeutic outcomes. For instance, the use of receptor tyrosine kinase MerTK triggers a pro-inflammatory phenotype in TAMs, enhances T cell infiltration, and improves tumor progression in pre-clinical mouse models[311, 312]. Furthermore, studies have suggested that chromatin remodelling with either histone deacetylase inhibitors[313, 314] or bromodomain/extra-terminal motif proteins[315, 316] affect M1-like polarization. These studies suggest the TAM "reprogramming" can impede tumor progression and ameliorate therapeutic effectiveness.

1.8.3 Functionally Impaired DCs

DCs are major professional APCs and bridge the gap between innate and adaptive immunity. Although DCs are not generally viewed as "pro-tumor" immune cells, the functional impairment of DCs tolerates the development of tumors and encourages immunosuppression within the TME. Functionally impaired DCs tend to be immature DCs that express lower levels of costimulatory molecules, such as CD40, CD80, and CD86, and are defective in antigen presentation in the context of MHC class I and II molecules. Furthermore, several tumor-derived mediators such as VEGF, M-CSF, GM-CSF, IL-6, and IL-10 contribute to this altered differentiation state[317]. The accumulation of immunosuppressive cells (MDSCs and T_{regs}) hampers DC differentiation[222] and mediates the downregulation of costimulatory molecule expression[242], ultimately impairing DC-antigen presentation and activation potential. Certain subsets of DCs also further promote immunosuppression. For example, pDCs, commonly associated with a robust type 1 IFN

response following viral infections, tend to be tolerogenic, defective in IFN production, and can express indoleamine 2,3-dioxygenase (IDO) and PD-L1 within the TME[235-237]. Such impairment of adaptive immune priming represents a major obstacle in the effort to effectively generate an anti-tumor immune response in a clinical setting.

Interestingly, due to the plastic nature of DCs, impaired DCs can regain costimulatory molecular expression, antigen presentation capabilities, and cytokine production following therapeutic interventions[98, 151]. Recent studies also revealed a specific subset of $CD8^+$ DCs that may induce type I IFN production, mediated *via* the STING pathway[318], and is postulated to be key mediators in the spontaneous generation of anti-tumor immunity observed in immune-infiltrating tumors. These studies strive to find a means to alter DC impairment to enhance immunotherapeutic anti-tumor T cell priming.

1.9 CANCER-ASSOCIATED IMMUNOSUPPRESSION AND OV THERAPY

In consideration of both the immunological and oncolytic properties associated with the use of OVs, it is possible that overcoming cancer-associated immunosuppression could enhance the effectiveness of anti-tumor immunity. Pre-clinical and clinical studies have combined various OVs with immunotherapeutic strategies (e.g., checkpoint blockade inhibitors [anti-PD-1 and anti-CTLA-4], GM-CSF supplementation, and immunosuppressive cell [MDSCs or T_{regs}] depletion), which have been shown to significantly aid the therapeutic effectiveness of OV therapy. For example, combination treatment of OVs with MDSC-depleting drugs increased therapeutic responsiveness[319-325]. Furthermore, Walker *et al.* found that targeting PGE2, a major mediator in MDSC and T_{reg} development and activity, using an HSV-1 constitutively expressing 15-prostaglandin

dehydrogenase (targets PGE2 degradation) significantly decreased splenic MDSCs, alleviated immunosuppression, and reduced tumor burden in primary and metastatic murine breast cancer models[326]. Such studies suggest that TME immunosuppression limits OV therapy and that the manipulation of such mechanisms could further enhance the effectiveness of treatment.

As indicated above, reovirus has been shown to hijack myeloid cells for tumor trafficking, overturn immunosuppressive mechanisms, and promote anti-tumor immunity[1, 101, 104, 170, 171, 327]. However, our previous work has also shown that reovirus administration mediates an early recruitment and accumulation of MDSCs within the TME[1]. At the time, the detailed characteristics, the pathophysiological implications, and significance of such virus-driven myeloid cell population in the context of reovirus-based OV therapy were unknown. Thus, the following research was designed to focus on the evaluation of such a population with respect to its role in infection and reovirus-based OV therapy, and whether the therapeutic manipulation of such a population could enhance the efficacy of OV therapy.

CHAPTER 2: MATERIALS AND METHODS

2.1 CELL LINES & REAGENTS

Mouse ovarian surface epithelial (MOSE) ID8 and ID8-ova cells were obtained from Edith Lord (University of Rochester, Rochester, NY)[328] and cultured in complete Dulbecco's Modified Eagle Medium (DMEM) which included: 5% (vol/vol) Glutamax, 10% fetal bovine serum (FBS), 1X sodium pyruvate, 1X nonessential amino acids, and 1X Antibiotic-Antimycotic (Anti-Anti) (all from Invitrogen, Carlsbad, CA). Mouse fibroblast L929 cells were purchased from American Type Culture Collection (ATCC) (Manassas, VA) and complete minimum essential media (MEM) containing 5 % FBS, 1X sodium pyruvate, 1X nonessential amino acids, and 1X Anti-Anti (all from Invitrogen, Carlsbad, CA). The following reagents (antibodies, peptides, and cellular stains) were used for single cell flow cytometry analysis. DAF-FM Diacetate (4-Amino-5-Methylamino-2',7'-Difluorofluorescein Diacetate) (D23844), CM-H2DCFDA (C6827), and Alexa Fluor® 488-Annexin V, and 5- (and -6)-carboxyfluorescein diacetate succinimidyl ester (CFSE) were purchased from Molecular Probes (Thermo-Fisher Scientific, Rochford, IL, USA). Cell viability staining 7-Amino-Actinomycin D (7-AAD) was purchased from BD Biosciences (Mississauga, Ontario, Canada). Ovalbumin peptide- SIINFEKL ($ova_{257-264}$) was purchased from GenScript (Piscataway, NJ). A full list of antibodies including primary conjugated fluorochrome, clone, and distributor can be found in Table 2.1.

Table 2.1. *Antibodies Utilized for Flow Cytometry or Western Blot Analysis.* Unless the reactivity is indicated, the following antibodies react to mouse proteins.

Target	*Clone*	*Fluorescence*	*Company*
β-Actin	C4	non-conjugated	Santa Cruz (California, USA)
CCR2	Cat#FAB5538a	APC	R&D systems (Minneapolis, MN)
CD115	T38-320	PE	BD Bioscience (San Jose, CA)
CD11b	M1/70	PerCP-Cy™5.5	BioLegend (San Diego, CA)
CD11b	M1/70	FITC	BD Bioscience (San Jose, CA)
CD11c	HL3	BV786	BD Bioscience (San Jose, CA)
CD14	rmC5-3	PE-CF594	BD Bioscience (San Jose, CA)
CD206	C068C2	APC	BioLegend (San Diego, CA)
CD273	TY25	BV421	BD Bioscience (San Jose, CA)
CD274	MIH5	PE	BD Bioscience (San Jose, CA)
CD28	37.51	non-conjugated	eBioscience (San Diego, CA)
CD3	eBio500A2	PE	eBioscience (San Diego, CA)
CD3	145-2C11	non-conjugated	eBioscience (San Diego, CA)
CD4	RM4-5	FITC	eBioscience (San Diego, CA)
CD45	30-F11	APC-Cy™7	BD Bioscience (San Jose, CA)
CD69	H1.2F3	APC	eBioscience (San Diego, CA)
CD71	R17217	PE	eBioscience (San Diego, CA)
CD8	53-6.7	PerCP	eBioscience (San Diego, CA)
CD86	GL1	BV605	BD Bioscience (San Jose, CA)
F4/80	6F12	BV510	BD Bioscience (San Jose, CA)
F4/80	BM8	APC	eBioscience (San Diego, CA)
Gr1.1	RB6-8C5	APC	eBioscience (San Diego, CA)
Gr1.1	RB6-8C5	Alexa Fluor® 488	eBioscience (San Diego, CA)
H2.kb (SIINFEKL)	25-D1.16	PE	
IFNγ	eBiol7-7311	APC	eBioscience (San Diego, CA)
Ly6C	AL-21	PE-Cy™7	BD Bioscience (San Jose, CA)
Ly6C	HK1.4	APC	BioLegend (San Diego, CA)
Ly6C	HK1.4	PE	BioLegend (San Diego, CA)
Ly6G	1A8	APC/Cy7™	BioLegend (San Diego, CA)
Ly6G	1A8	BV711	BD Bioscience (San Jose, CA)
Ly6G	1A8	Alexa Fluor® 647	BioLegend (San Diego, CA)
Ly6G	1A8	FITC	BioLegend (San Diego, CA)
MHC-11(I-A/I-E)	M5/114.15.2	Alexa Fluor® 647	BioLegend (San Diego, CA)
MHC-I	AF6-88.5.5.3	APC	BioLegend (San Diego, CA)
NK-1.1	PK136	PE	BD Bioscience (San Jose, CA)
Reovirus (Rabbit)	Poly clonal	non-conjugated	In house
Anti-Rabbit 2º ab	Poly clonal	Cy™2	Jackson ImmunoResearch Laboratories (West Grove, PA)
Anti-Rabbit 2º ab	Poly clonal	Alexa Fluor® 488	Thermo-Fisher Scientific, Rochford, IL, USA

2.2 ANIMALS

In vivo experimental procedures were approved by the Dalhousie University Animal Ethics Committee in accordance with the regulations/guidelines from the Canadian Council on Animal Care (CCAC). C57BL/6 mice were purchased from Charles River Laboratory (Montreal, Quebec, Canada), while CCR2 KO and C57BL/6-green fluorescent protein (GFP) mice were purchased from Jackson Laboratory (Bar Harbor, ME).

2.3 REOVIRUS PLAQUE PICKING AND TITERING

Reovirus was titered on L929 cells by standard plaque assay. L929 cells were seeded in 12-well plates and grown until they were 80-90% confluent in complete MEM. Original virus stock was serially diluted (1/10) in MEM incomplete. Growth medium for the L929 cells was removed, cells were washed with phosphate-buffered saline (PBS), and reovirus dilutions were added to the 12-well plates at a total volume of 100 µL per well. Cells were infected with reovirus for 1 hr and shook every 10 mins to prevent cells from drying out. Subsequently, reovirus dilutions were removed from the wells and agar plugs were added (equal volume of 2X MEM complete and 2% agar). Plates were then incubated at 37ºC, at 5% CO_2, for 96 hrs to allow visible virus plaque formation. Individual virus plaques were either collected with a glass pipette and bulb for reovirus expansion/collection or titers were performed using standard crystal violet staining procedures to identify the concentration of the virus in plaque forming units (pfu)/mL.

Standard crystal violet staining was conducted by the process of formaldehyde fixation (30-40% formaldehyde in PBS), manual agar plug removal, methanol wash, and crystal violet stain (1% crystal violet in 50% ethanol) for ~1 min. Crystal violet stain was removed and

the cells were rinsed with water. Plates were allowed to dry prior to manually counting plaques.

Individual plaques from the reovirus standard plaque assay were collected, incubated in 1 mL of incomplete MEM for 24 hrs at 4°C, and then added to a T75 flask of ~80-90% confluent L929 cells. The cells and individual virus plaques were incubated at 37°C at 5% CO_2 until all cells were dead (approximately 72 hrs). Dead cells and supernatant were collected as reovirus stocks for expansion/collection and stored at -20°C until needed.

2.4 REOVIRUS EXPANSION AND COLLECTION

Reovirus expansion was performed in L929 cells in a spin culture round-bottom flask. L929 cells were grown in a spin culture with complete Joklik modified minimum essential media (JMEM; 11.05 g/L JMEM powder, 2.2 g/L $NaHCO_3$, 1.2 g/L, 1 g/L glucose, pH 7.2) at 37°C until they reached a concentration of $1x10^6$ cells/mL. Then, an individual reovirus stock was thawed, where half of the stock was used per liter of cells, and the spin culture temperature was reduced to 32.5°C. The infection proceeded for ~3 days and the culturing temperature was maintained at 30.5-32.5°C, depending on the percentage of cell death to control the virus replication rate and to expand the collection window. Once the percentage of cell death reached 50-60%, the flasks were placed at 4°C overnight. The following day, cells were collected, by centrifugation at 500xg for 15 mins, and placed at -80°C for short term (1-7 days) prior to reovirus extraction.

2.5 REOVIRUS EXTRACTION AND DIALYSIS

The collected cell pellet was resuspended in 15 mL of resuspension buffer (0.25 M NaCl, 10 mM Tris-HCl [pH 8.0]) per 1L of L929 cells cultured from the reovirus expansion.

Reovirus was extracted using Vertrel (Dymar Chemicals Ltd., Mississauga, ON), followed by a repetitive sequence of sonication/homogenization, centrifugation, supernatant collections, and a final ultra centrifugation of 107,000 xg for 1 hr at 4ºC (a detailed schematic is illustrated in Figure 2.1). Following ultra centrifugation, the supernatant was removed, and the pellet was kept at 4ºC overnight. The following day, the virus/debris pellet was resuspended in 1 mL of SSC buffer (0.15 M NaCl, 0.015 M sodium citrate, pH 7.0), homogenized *via* glass homogenizer, gently pipetted on a CsCl gradient ranging from 1.2-1.4 g/ml in 20 mM Tris-HCl (pH 7.4), and spun at 107,000 xg for 2 hrs at 4ºC. Following centrifugation, the whole and empty reovirus particles were separated within the gradient. The whole reovirus fraction was collected with a 21G needle and placed in dialysis tubing for a 3-day dialysis process. Importantly, the dialysis buffer (0.15 M NaCl, 15 mM $MgCl_2$, 10 mM Tris-HCl [pH 7.4]) was changed a total of three times with fresh dialysis buffer. Following dialysis, reovirus was titered *via* a standard plaque assay and stored at 4ºC. The particle to pfu ratio was calculated based on the optical density $(OD)_{260}$ using the following formula: 1 $OD_{260} = 2.1x10^{12}$ reovirus particles.

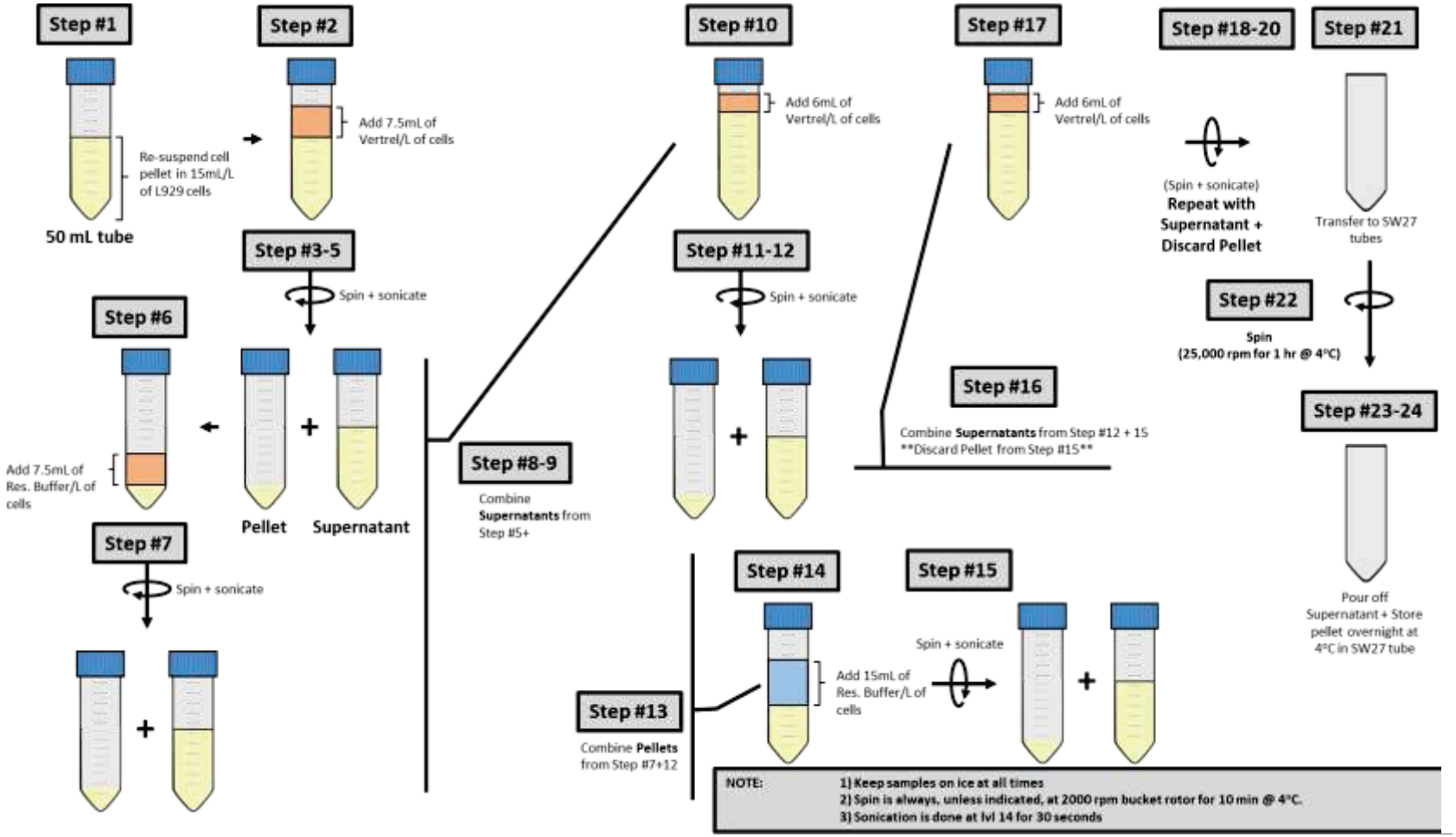

Figure 2.1. ***Schematic Representation of the Steps in the Reovirus Extraction Protocol.*** Reovirus extraction was conducted in the indicated step-by-step procedure starting at the resuspension of the cellular pellet from the reovirus expansion and collection protocol (step #1).

2.6 BONE MARROW AND MDSC ISOLATION

BM cells were harvested from the femurs and tibias of sacrificed 6-8-week-old C57BL/6 mice and flushed using a 26G needle attached to a syringe containing complete RPMI 1640 media. Peritoneal cavity (PC)-derived myeloid cells were harvested *via* flushing the PC with 5 mL of PBS with 10 mM ethylenediaminetetraacetic acid (EDTA), PBS-EDTA, or separated from the ascitic fluid of tumor-bearing C57BL/6 mice *via* Ficoll gradient (95021-205L, GE Healthcare, Quebec, Canada) and centrifugation at 400 xg for 40 mins. Harvested single cell suspensions were strained through 40-70 μm cell strainers and treated with red blood cell (RBC)-lysing ammonium-chloride-potassium (ACK) buffer. Cells were washed with PBS-EDTA, pelleted *via* centrifugation, and isolated following the manufacturer's instructions for the mouse myeloid-derived suppressor cell isolation kit (Miltenyi Biotec, Auburn, CA). The purity of these isolated MDSCs exceeded 90%. PC- and BM-derived myeloid cells were cultured in complete RPMI 1640 medium supplemented with 1X GlutaMax™. Cell-free ascitic fluid was collected from reovirus-treated or non-treated ovarian cancer-bearing hosts *via* centrifugation prior to ACK treatment and washing. Cell-free ascitic fluid was stored at -80^{o}C until further use for the indicated assays.

2.7 M1- AND M2-LIKE MACROPHAGE GENERATION

BM cells were collected from femurs and tibias as described above and cultured for 6-8 days in RPMI complete media supplemented with granulocyte macrophage colony-stimulating factor (20 ng/mL, for M1-like macrophages) or macrophage colony-stimulating factor (100 ng/mL, for M2-like macrophages). Adherent cells were used for the indicated experiments after 6-8 days in culture.

2.8 FLOW CYTOMETRY AND FLUORESCENCE-ACTIVATED CELL SORTING

Following single cell suspension isolation of cells through flushing (BM or PC) or tissue homogenization (spleen, tumor, liver, lung, and mesenteric lymph node), cells were strained through a 40-70 μm cell strainer, washed with flow cytometry running buffer (FACs buffer [PBS-EDTA with 1% FBS]), and treated with ACK. Flow cytometry for MHC-ova (SIINFEKL) was conducted by first pulsing unlabelled immune cells harvested from the PC with SIINFEKL peptide (5 μg/mL) for 2 hrs at 37^{o}C in RPMI complete medium. Harvested cells (PC, tumor, ascites, spleen, and BM) were washed with FACs buffer and blocked with anti-CD16/32 antibody prior to primary-conjugated antibody. For metabolic stains, cells were incubated with 2.5 μM DAF-FM Diacetate or 2.5 μM CM-H2DCFDA (DCF) for 30 mins at 37°C, in combination with other antibodies, in FACs buffer. The eBioscience^{TM} mouse regulatory T cell staining kit #3 (San Diego, CA) was used for the intracellular staining of IFN-γ following the extracellular staining of cell surface markers. Cells harvested for flow cytometry, with the exception of DAF-FM or DCF stained cells, were fixed with 4 % paraformaldehyde, washed, and re-suspended in FACs buffer prior to analysis. Cells harvested for cellular sorting were sorted live with the FACSariaIII (BD Biosciences, San Jose, CA) to obtain individual cell populations (greater than 93% purity).

Flow cytometry data were collected using a BD FACSCalibur, BD FACS Canto II, or the BD LSR Fortessa SORP flow cytometer (BD Bioscience, San Jose, CA). Data acquisition was performed with the use of CellQuest Pro or BD FACSDiva™ Software (BD

Bioscience, San Jose, CA). Flow cytometry analysis was analyzed with FCS Express V3 or V6 software (DeNovo Software, Los Angeles, CA).

2.9 CHEMOTAXIS ASSAY

Chemotaxis of MDSCs was measured using 24-well transwell plates with an 8 μm pore size (Corning, cat#: 3422). The test supernatant or medium was added to the bottom chamber and $1x10^6$ harvested BM cells were added to the top chamber. Samples were incubated at 37°C, for 2 hrs, in 5% CO_2 incubator. Cells from the bottom chamber were harvested, stained and then analyzed using flow cytometry. The chemotaxis of myeloid cells was represented as the fold change of migrating myeloid cell subpopulation over control (complete medium alone).

2.10 ANTIBODY-BASED QUANTITATIVE CYTOKINE ARRAY

Cell-free ascites and blood collected from reovirus treated or non-treated tumor-bearing animals were evaluated with antibody-based Quantibody Cytokine Arrays (Raybiotech, Inc., Norcross, GA). For this evaluation, a custom array containing antibodies against GM-CSF, G-CSF, M-CSF, VEGF, SCF, MCP-1, SDF-1α, IL-10, IL-12p70, IL-13, IL-6, IFN-γ, IL-1β, TNF-α, RANTES, MIP-1α, IL-8 and MIG was designed and implemented.

2.11 T CELL FUNCTIONAL ASSAYS

The suppressive nature of myeloid cells and the tumor microenvironment were quantified by monitoring their ability to suppress T cell proliferation and IFN-γ production. T cell proliferation was examined using a carboxyfluorescein succinimidyl ester (CFSE)-based cell proliferation assay as previously described[329]. For this, CFSE-labelled T cells were cultured in the presence of the indicated splenocyte to MDSC cell number ratio and

simultaneously activated using anti-CD3 and anti-CD28 antibodies for 96 hrs and analyzed for the halving of CFSE fluorescence. The cell division index (CDI) is defined as the percentage of cells with halved CFSE fluorescence after stimulation divided by halved CFSE fluorescence cultured in medium only. T cell suppression is defined as the percentage of T cell proliferation subtracted from 100% (controls being 100% proliferation) for the respective treatment. To monitor the MDSC-mediated suppression of IFN-γ production, T cells from naïve mice were activated by anti-CD3 and anti-CD28 antibodies in the presence of the indicated ratio of isolated myeloid cell populations. Eighteen hours following T cell stimulation, the cells were treated with 2 μg/mL Brefeldin A (BFA) (Sigma, B7651) and incubated for an additional 6 hrs prior to intracellular and extracellular staining for IFN-γ and T cell markers (CD3 and CD8), respectively. The percentage of $CD3^+$, $CD8^+$, IFN-γ^+ cells was analyzed *via* flow cytometry, and the IFN-γ response was calculated as a fold change compared to the respective controls. As a positive control, concanavalin A (ConA) was also used where indicated at 1.25-2.5 μg/mL.

2.12 QUANTITATIVE REAL-TIME POLYMERASE CHAIN REACTION (QPCR)

RNA extractions were conducted using TRIzol™ methodology. RNA was quantified and 1-2 μg of RNA was used to synthesize cDNA using Superscript II (Invitrogen, Burlington, ON). qPCR was performed using GoTaq qPCR Master mix (Promega, Madison, WI) or SsoAdvanced Universal SYBR Green Supermix (BioRad, Hercules, CA) and analyzed on CFX Manager Software (BioRad, Hercules, CA). All primers used, as described in Table 2.2, were purchased from Invitrogen. Primers were designed using NCBI Primer Blast Tool and tested for primer efficiency and primer dimers prior to use. qPCR results were analyzed

Table 3.2. *Gene-specific Mouse Primer Sequences Utilized for qPCR.*

Primer	*Forward Sequence (5'-3')*	*Reverse Sequence (5'-3')*
B2m	ATGGGAAGCCGAACATACTG	CAGTCTCAGTGGGGGTGAAT
Cd3	TCTCGGAAGTCGAGGACAGT	TTGAGGCTGGTGTGTAGCA
Cd4	AGGAAGTGAACCTGGTGGTG	CTCCTGCTTCAGGGTCAGTC
Cd8	ACTGCAAGGAAGCAAGTGGT	CACCGCTAAAGGCAGTTCTC
Cox2	AGAAGGAAATGGCTGCAGAA	GCTCGGCTTCCAGTATTGAG
Gapdh	TGGCAAAGTGGAGATTGTTG	AAGATGGTGATGGGCTTCCC
Gm-csf	ATGCCTGTCACGTTGAATGA	CCGTAGACCCTGCTCGAATA
H2d	GAGTGAGCCTGAGGAACCTG	AGCCAGACATCTGCTGGAGT
Ido1	GGGGGTCAGTGGAGTAGACA	TGGGCAGCTTTTCAACTTCT
Ifn-β	CCCTATGGAGATGACGGAGA	ACTTGAGGTGGTCGTCTGTC
Ifn-γ	GCGTCATTGAATCACACCTG	TGAGCTCATTGAATGCTTGG
Il-1β	GCCCATCCTCTGTGACTCAT	AGGCCACAGGTATTTTGTCG
Il-4	CCTCACAGCAACGAAGAACA	AAATATGCGAAGCACCTTGG
Il-6	CCGGAGAGGAGACTTCACAG	TCCACGATTTCCCAGAGAAC
Il-10	CCAGGGAGATCCTTTGATGA	AACTGGCCACAGTTTTCAGG
Tap1	CTGTTCAGGTCCTGCTCTCC	CCACAAGGCCTTTCATGTTT
Tap2	GCTGTGGGGACTGCTAAAAG	GCAGAAGCCACTCGGACTAC
Tgf-β	GGACTCTCCACCTGCAAGAC	GACTGGCGAGCCTTAGTTTG
Arg-1	TTAGGCCAAGGTGCTTGCTGCC	TACCATGGCCCTGAGGAGGTTC
Ccl2	GTTAACGCCCCACTCACCTG	GCTTCTTTGGGACACCTGCT
Cxcr1	CCAGGTATCGGTCCACACTG	AATGCTGCCCACTGGAGATT
Cxcr2	CCTGTTCTTTGCCCTGACCT	GCACAGGGTTGAGCCAAAAG
iNos	TCCTGGACATTACGACCCCT	AGGCCTCCAATCTCTGCCTA
S100a8	TGGAGAAGGCCTTGAGCAAC	AGTCATTCTTGTAGAGGGCATGG
S100a9	GCCAACAAAGCACCTTCTCAG	TTCCTTCTTGCTCAGGGTGTC
Sdf-1	GCTCTGCATCAGTGACGGTA	TCAGATGCTTGACGTTGGCT
Cd40	AAGGATAATGAGATGTTACCCCTG	AAAGGTCAGGAAGCAGCCATC
Igtp	AGCCGTCTTTTCACGACTT	TGTACTCCGAGCTACCTGCT
Serpina3k	CTGCTGCCACAGGGGTTATT	AGCCAACTTTGGAACAGCCA
Ccl7	AAGTGGGTCGAGGAGGCTAT	CCATTCCTTAGGCGTGACCA
Ifit3	TGTGGAGTGCTGCTTATGGG	TCAAAAGGTGCTCTGTCTGCT
Irgm1	ATGACAACATGGGCGAGTG	GATCTGCGGAGGGAAGATGG
Ifi205a	AGCAGGCCACTTCTGTTGTT	GCAGGACTTGCTTCTTGCCT
Irf4	CCATGCATGCTGATGCCTTC	CAGAAAGCACCCGTGAGACT
Ccl17	AATGTAGGCCGAGAGTGCTG	TGCCCTGGACAGTCAGAAAC
Cd86	ACGATGGACCCCAGATGCACCA	GCGTCTCCACGGAAACAGCA
Cd68	CCACAGGCAGCACAGTGGACA	TCCACAGCAGAAGCTTTGGCCC
Socs1	CAACGGAACTGCTTCTTCGC	AGCTCGAAAAGGCAGTCGAA
Mrc1	TCAGAACAGACTGCGTGGA	AGGGATCGCCTGTTTTCCAG
Pepd	CTATTCGCCCTGAACAGGCA	CAGGTGGCGTAGCTATCAGG
H2-ab1	CCCTCAACCACCACAACACT	ACATCTTGCTCCAGGCAGAC
Cd74	TCATACCCCACTTCCCGTCT	GGGCCTTTATAGCGGTAGCC
Tpp1	GCCGCACTATCTGATGGCTA	GCGGCCATTGAGGATTCTGT
Lip1	TCCCACCAAGTAGGTGTAGG	CATCTTCCGGGAGTGGTCCT
Ym1	ACCCCTGCCTGTGTACTCACCT	CACTGAACGGGGCAGGTCCAAA
Cd206	TCAGCTATTGGACGCGAGGCA	TCCGGGTTGCAAGTTGCCGT
Il4	TGGGTCTCAACCCCCAGCTAGT	TGCATGGCGTCCCTTCTCCTGT

using the Livak and Schmittgen's $2^{-\Delta\Delta CT}$ method[330]. To calculate fold change, signals were first normalized against GAPDH and then compared against the respective controls.

2.13 WESTERN BLOTS

Whole cell lysates were harvested and lysed using RIPA buffer (50 mM Tris-HCl pH 7.4, 1% NP-40, 0.5% Na-deoxycholate, 150 mM NaCl, 1 mM EDTA, 2 mM NaF, 2 mM NaVO4 and 1X protease inhibitor cocktail [PIC] [Sigma, US]). Protein samples were boiled for 5 mins in protein sample buffer (50 mM Tris pH 6.8, 1% SDS, 10% glycerol, 0.01% Bromophenol Blue, 5% β-mercaptoethanol) and loaded on a 12% SDS-PAGE gel. Following electrophoresis, proteins were transferred onto a nitrocellulose membrane (BioRad, Hercules, CA). Odyssey® blocking buffer (Li-Cor, Lincoln, NE) was used to block the membrane for 1 hr at room temperature after protein transfer. Primary antibodies were added to the membrane and incubated overnight at 4°C. Secondary antibody (Li-Cor, Lincoln, NE) was added at a 1:10,000 dilution for 1 hr at room temperature. Blots were scanned with the Odyssey Infrared Imaging System (Li-Cor, Lincoln, NE) to visualize protein signals and intensities.

2.14 MASS SPECTROMETRY SAMPLE PREPARATION, LABELLING, AND DATA ACQUISITION/ANALYSIS

Isolated cells (*via* fluorescent cell-sorting) were washed with PBS, pelleted, and lysed in 6 M guanidine-HCl, 50 mM HEPES, pH 8.5, containing Roche complete mini protease inhibitor mixture (1 tablet per 10 ml) (Roche, Madison, WI). Lysis was performed by sonication and cleared by centrifugation. Cysteine residues were reduced using 5 mM dithiothreitol and then alkylated with 14 mM iodoacetamide. Aliquots containing 50 µg of

protein were diluted to 1.5 M guanidine-HCl, 50 mM HEPES (pH 8.5) and digested with trypsin (Promega, Madison, WI). Digested peptides were desalted using 60 mg solid-phase C18-extraction cartridges (Waters, Milford, MA), lyophilized, and were labelled using tandem mass tag (TMT) 10-plex reagents as described previously[331]. Samples were then mixed equally, desalted using solid-phase C18 extraction cartridges (Waters, Milford, MA), and lyophilized.

TMT10-labelled samples were fractionated using high-pH reversed phase chromatography performed with an Onyx monolithic 100 x 4.6 mm C18 column (Phenomenex, Torrance, CA). The flow rate was 800 μL/min and a gradient of 5-40% acetonitrile (10 mM ammonium formate, pH 8) was applied over 60 mins using an Agilent 1100 pump (Agilent) from which 12 fractions were collected. Fractions were desalted using homemade Stage Tips[332], lyophilized, and analyzed with an Orbitrap Fusion mass spectrometer (Thermo-Fisher Scientific, Rochford, IL) using the SPS-MS3 method as described previously[331, 332]. Protein identification was performed using a database search against a mouse proteome database (downloaded from UniProtKB September 2014) concatenated to a mammalian orthoreovirus 3 (Dearing strain) database (downloaded from UniProtKB September 2014). All false discovery rate (FDR) filtering and protein quantitation was performed as previously described[331]. Data for heat maps and individual protein profiles are represented by relative intensity, which is based on the summed signal to noise.

GO-annotation analysis was originally conducted on the whole dataset using the open access Gene Ontology Consortium[333, 334]. The dataset was subsequently analyzed *via* k-means clustering with Euclidean distance using MultiExperiment Viewer (MeV)[335], followed by DAVID Bioinformatics Resources (https://david.ncifcrf.gov/) to conduct GO-

term analysis for biological processes (BPs), molecular functions (MFs), and cellular compartment (CC) on specific clusters. Our total dataset was utilized as the background for the data analysis searches. The mass spectrometry proteomics data have been deposited into ProteomeXchange Consortium[336] *via* the PRIDE[337] partner repository.

2.15 EXTRACELLULAR FLUX ANALYSIS

Flow cytometry-sorted myeloid cells ($5x10^5$ cells) were re-suspended in XF medium and plated onto X24 Seahorse cell plates coated with Cell-Tak (Corning). Oxygen consumption rate (OCR) and extracellular acidification rate (ECAR) were measured in XF assay medium under basal conditions and in response to 1 μM oligomycin, 1.5 μM carbonyl cyanide 4-(trifluoromethoxy)-phenylhydrazone (FCCP), 1 μM rotenone, and 1 μM antimycin A (all purchased from Sigma-Aldrich, ON, Canada) on the XF24 extracellular flux analyzer (Seahorse Bioscience, Billerica, MA, USA). Basal OCR was calculated by subtraction of the residual rate after antimycin A treatment. Maximal rate was calculated by subtraction of the residual rate after antimycin A treatment from FCCP-induced OCR. Proton leak was calculated as the difference between OCR after oligomycin treatment and OCR after antimycin A treatment. ATP production was calculated by subtraction of OCR after oligomycin treatment from basal OCR. Spare respiratory capacity was calculated by the difference between maximal OCR and basal OCR. Spare respiratory capacity coupling efficiency was calculated by the dividend of basal OCR and ATP production. Glycolytic capacity was calculated as the ECAR after oligomycin treatment. Glycolytic reserve was calculated by the difference between glycolytic capacity and ECAR. Glycolytic reserve percentage was calculated by dividing the glycolytic capacity from the basal ECAR.

2.16 STATISTICAL ANALYSIS

Depending on the indicated experiment, one-way ANOVA with Bonferroni post-test or a two-tailed Student's t-test with 95% confidence interval was used for statistical analysis using GraphPad Prism software version 6. Probability (p) values of <0.05 were considered significant. Asterisks were used to signify p values as follows: not significant (ns) = $p > 0.05$; *$p \leq 0.05$; **$p \leq 0.01$; ***$p \leq 0.001$.

CHAPTER 3: NEWLY RECRUITED CD11B^{+} GR-1^{+} LY6C^{HIGH} MYELOID CELLS AUGMENT TUMOR-ASSOCIATED IMMUNOSUPPRESSION IMMEDIATELY FOLLOWING THE THERAPEUTIC ADMINISTRATION OF ONCOLYTIC REOVIRUS

This work appears in part in the publication:

Clements D, Sterea A, Kim Y, Helson E, Dean C, Nunokawa A, Coyle K, Sharif T, Marcato P, Gujar SA and Lee PWK. 2015. Newly recruited CD11b^{+}, GR-1^{+}, Ly6C^{high} myeloid cells augment tumor-associated immunosuppression immediately following the therapeutic administration of oncolytic reovirus. J Immunol. 194 (9): 4397-412.

Contribution:

DC – designed the study, carried out the experimentation, collected and analyzed data, and prepared the manuscript

AS, YK, EH, CD, AN, KC, TS – assisted with experimentation and data collection

PM, SG, and PL – assisted with study design and critical review of the manuscript

3.1 ABSTRACT

Tumor-associated immunosuppression aids cancer cells to escape immune-mediated attack and subsequent elimination. Recently, however, many oncolytic viruses, including reovirus, have been reported to overturn such immunosuppression and promote the development of a clinically desired anti-tumor immunity, which is known to promote favourable patient outcomes. Contrary to this existing paradigm, we demonstrate that reovirus augments tumor-associated immunosuppression immediately following its therapeutic administration. Our data show that reovirus induces preferential differentiation of highly suppressive $CD11b^{+}$ $Gr\text{-}1^{+}$ $Ly6C^{high}$ myeloid cells from bone marrow hematopoietic progenitor cells. Furthermore, reovirus administration in tumor-bearing hosts drives a time-dependent recruitment of $CD11b^{+}$ $Gr\text{-}1^{+}$ $Ly6C^{high}$ myeloid cells in the tumor milieu, which is further supported by virus-induced increased expression of numerous immune factors involved in myeloid-derived suppressor cell (MDSC) survival and trafficking. Most importantly, $CD11b^{+}$ $Gr\text{-}1^{+}$ $Ly6C^{high}$ myeloid cells specifically potentiate the suppression of T cell proliferation and are associated with the absence of IFN-γ response in the tumor microenvironment early during oncotherapy. Considering that the qualitative traits of a specific anti-tumor immunity are largely dictated by the immunological events that precede its development, our findings are of critical importance and must be considered while devising complementary interventions aimed at promoting the optimum efficacy of oncolytic virus-based anti-cancer immunotherapies.

3.2 INTRODUCTION

Anti-cancer immunotherapies target cancer cells by exploiting the beneficial functions of the immune system and represent one of the most promising modern-age therapeutic interventions for the treatment of cancers[338]. These immunotherapies usually focus on establishing anti-cancer immune responses by stimulating the otherwise suppressed immune system of cancer-bearing hosts. Evidence thus far clearly demonstrates that a robust anti-tumor immune response can eliminate existing cancer cells, establish protection against possible relapse, and is associated with favourable patient outcomes[339-341]. Cancers of almost every origin including prostate, colon, breast, ovarian, and advanced melanoma have been successfully targeted with various immune-based interventions[189, 342, 343]. However, the tumor-associated immune microenvironment usually contains various suppressive mechanisms that resist the successful development of anti-cancer immune responses. Thus, the efficacy of anti-cancer immunotherapeutic options is dictated by the immunological niche present in and around the tumor microenvironment. Hence, the successful implementation of anti-cancer immunotherapies demands a thorough understanding and management of tumor-associated immunosuppression.

Reovirus, a naturally occurring benign human pathogen, preferentially targets and kills cancerous cells[30], and is currently being evaluated as an anti-cancer agent in phase I, II, and III clinical trials internationally[103, 344]. Similar to other oncolytic viruses (OVs)[30, 68, 76, 80, 83], the use of reovirus as an anti-cancer therapeutic was based on its capacity to preferentially kill cancer cells (in a process known as oncolysis) while leaving normal cells relatively unharmed. However, recent discoveries have shown that, in addition to its direct oncolytic activities, reovirus also stimulates the immune system of cancer-bearing hosts and induces

a clinically relevant anti-cancer immunity. These reovirus-induced anti-tumor immunotherapeutic activities target existing cancer cells and can protect the host against subsequent tumor relapse even after discontinuation of the therapy[98]. Following its therapeutic administration, reovirus invokes a sequence of immunological events that ultimately overturns numerous tumor-associated immune evasion mechanisms and facilitates the development of innate and adaptive anti-tumor immune responses[1, 5, 98, 105, 148, 150, 151]. Thus, comprehensive characterization and subsequent therapeutic management of the virus-induced immunological events are absolutely necessary to harness the beneficial effects of reovirus-driven anti-cancer therapy.

Recently, tumor-associated myeloid-derived suppressor cells (MDSCs) have been identified as one of the key mediators of tumor-associated immunosuppression. Apart from their immunosuppressive functions, MDSCs also influence angiogenesis and metastasis[222], and thus represent a major therapeutic target that could be manipulated to facilitate anti-tumor immunity. In mice, MDSCs were originally defined as cells expressing CD11b (αM-integrin) and Gr-1 markers, while in humans these cells were mainly defined as $CD11b^{+}$ $CD14^{-}$ $CD33^{+}$ or LIN^{-} $HLA\text{-}DR^{-}$ $CD33^{+}$ cells. However, it is now clear that MDSCs represent a heterogeneous population of cells that consists of progenitor as well as immature myeloid cells (IMCs)[222, 345]. These subpopulations of MDSCs are shown to have differential biological roles and require further phenotypical characterization to enable precise therapeutic targeting. Considering this gap in existing knowledge, recent efforts have been focused on further dissecting various subpopulations within MDSCs.

In healthy individuals, MDSCs are generated in the bone marrow (BM), subsequently differentiated into mature granulocytes, macrophages or dendritic cells, and are believed to

be involved in regulating hyperactive or unnecessary immune responses[346, 347]. With respect to cancer progression and treatment, MDSCs have a remarkable ability to inhibit tumor surveillance and killing[224, 266, 348-350] by directly suppressing anti-cancer T cells or indirectly through the recruitment of regulatory T cells (T_{regs}) and squelching of essential nutrients for T cell activity[222, 224, 348]. Furthermore, MDSCs have also been reported to regulate innate immune responses of natural killer (NK) cells[274] and modulate cytokine production by macrophages[349]. These myeloid cells have also been studied in the context of parasitic[351], bacterial[352], and viral infections[353-355]. Although the exact role of MDSCs in such processes is still obscure, increasing evidence thus far suggests that pathogen-mediated accumulation of MDSCs postpones pathogen clearance and contributes to the critical balance between pathogen eradication and pathogenicity[351, 355].

Recently, we reported that intraperitoneal therapeutic injections of reovirus drive the accumulation of $CD11b^+$ $Gr\text{-}1^+$ myeloid cells in the tumor microenvironment of the hosts with peritoneal carcinomatosis (PC)[1, 5]. However, the detailed characteristics, the pathophysiological significance of such virus-driven MDSCs, and possible subpopulations in the context of a tumor microenvironment are presently unknown. Hence, this study was focused on dissecting the phenotypic heterogeneity, kinetics, differentiation, chemotactic trafficking, and functional capacities of OV-driven myeloid cells. Contrary to the existing dogma, we demonstrate that oncolytic reovirus promotes the generation and recruitment of highly suppressive $CD11b^+$ $Gr\text{-}1^+$ $Ly6C^{high}$ myeloid cells into the tumor microenvironment and transiently potentiates tumor-associated immunosuppression during the early phase of oncotherapy. In light of the ongoing phase III clinical trials, these findings bear crucial

significance and must be considered while designing complementary approaches aimed at enhancing the efficacy of OV-based oncotherapies to promote better cancer outcomes.

3.3 RESULTS

3.3.1 Phenotypically Distinct Heterogeneous Subpopulations of CD11b$^+$ Myeloid Cells Accumulate in the Tumor Microenvironment During the Early Phase of Reovirus Oncotherapy

Our recent studies have demonstrated that the therapeutic administration of reovirus in ovarian cancer-bearing hosts with PC causes a transient accumulation of CD11b$^+$ cells within the ascites and spleen at 3 days post first infection (d.p.f.i.)[1, 5]. Considering the fact that such myeloid cells could consist of a heterogeneous population of cells with differential suppressive capacities, we first characterized the phenotypic heterogeneity of reovirus-induced myeloid cells in cancer-bearing hosts. To perform this study, immuno-competent C57BL/6 mice were intraperitoneally (i.p.) injected with ID8 cells and allowed to develop PC (approximately 4-6 weeks). Once PC was visible, mice were either treated with a therapeutic regimen of reovirus (reo-treated group) or left untreated (non-treated group) as per the schematic shown in Figure 3.1A. Next, single cell suspensions from the ascites, solid tumors spread in the peritoneum, and spleen were prepared from respective groups and analyzed for the surface expression of CD11b, GR1.1 (Gr-1) and Ly6C at 1 d.p.f.i., 3 d.p.f.i., and 7 d.p.f.i.. Therapeutic injection of reovirus in PC-bearing hosts induced significantly higher frequencies of CD11b$^+$ Gr-1$^+$ cells as early as 1 d.p.f.i., which persisted further at 3 d.p.f.i. within ascites and spleen (Fig 3.1B and 3.1C) as compared to those seen in non-treated animals. Interestingly, a statistically significant increase in the

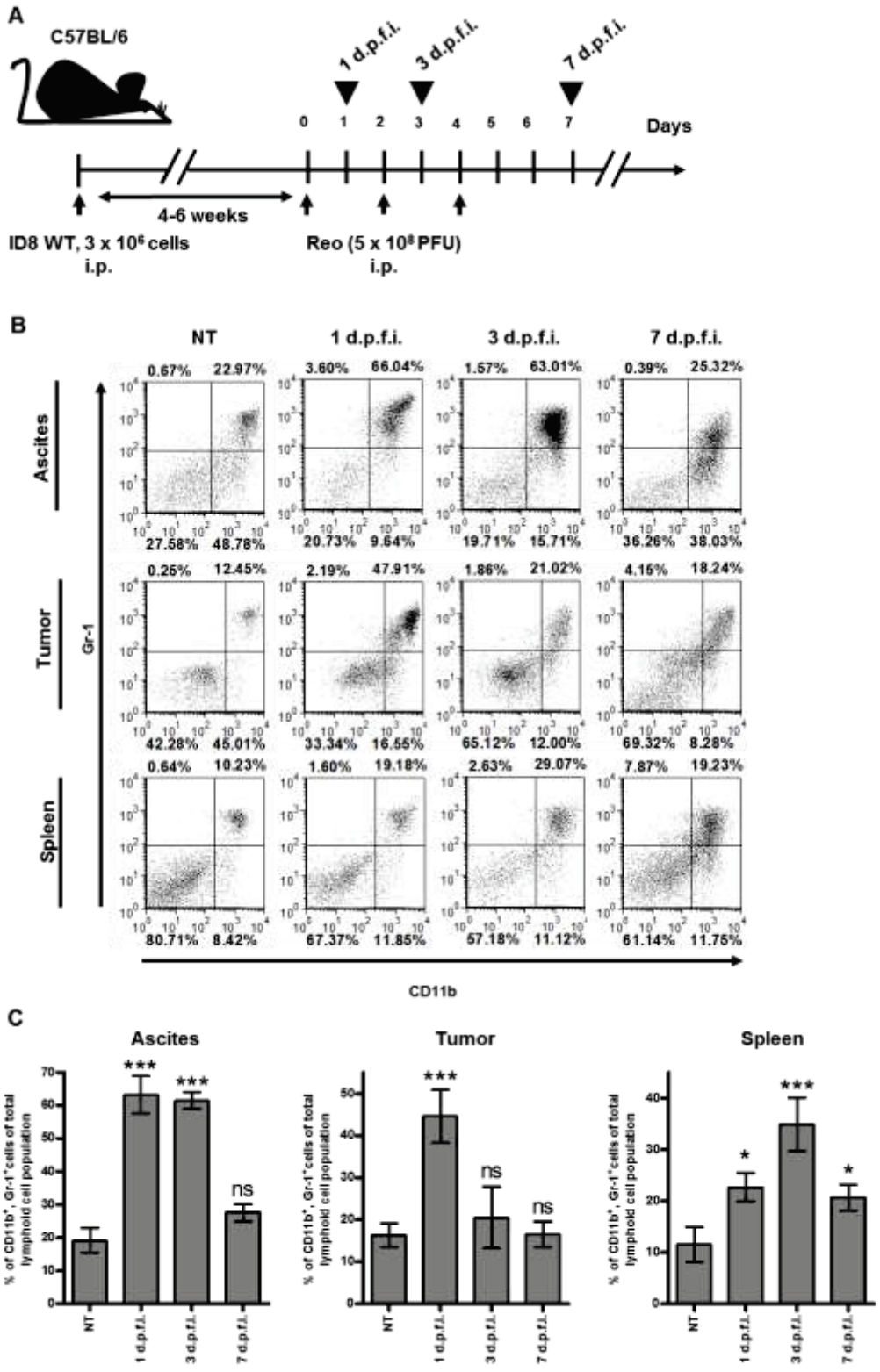

Figure 3.1. *Oncolytic Reovirus Promotes Local and Systemic Accumulation of CD11b$^+$ Gr-1$^+$ Cells as Early as 1 Day Post Therapeutic Administration.* (A) C57BL/6 mice were

first injected with 3 x 10^6 ID8 cells, allowed to develop peritoneal carcinomatosis, and then treated with a therapeutic regimen of reovirus (5 x 10^8 PFU/injection) at indicated time points. The frequency of total $CD11b^+$ $Gr\text{-}1^+$ cells (B and C) in the single cell suspensions collected from the ascites, tumor, and spleen were evaluated over the course of therapy (non-treated [NT], 1 d.p.f.i., 3 d.p.f.i., and 7 d.p.f.i.) using flow cytometry analysis. Statistical analysis was performed with one-way ANOVA with Bonferroni post-test; ns = $p > 0.05$; *$p \leq 0.05$; **$p \leq 0.01$; ***$p \leq 0.001$. Asterisks shown immediately on top of the bars signify the p values obtained by comparing the respective data against the non-treated control group. Each column is the mean +/- SD of n = 5. Data are representative of more than 8 independent experiments.

numbers of $CD11b^+$ $Gr\text{-}1^+$ cells were also observed in the solid tumor masses spread through the peritoneum at 1 d.p.f.i.. These elevated levels of $CD11b^+$ $Gr\text{-}1^+$ cells subsequently subsided at 7 d.p.f.i. in all of the three tissues tested. These data showed that the injection of oncolytic reovirus induces an accumulation of putative $CD11b^+$ $Gr\text{-}1^+$ MDSCs in local tumor microenvironment, as well as in systemic immune organs, as early as 1 day post injection.

Next, we dissected the phenotypic heterogeneity of the $CD11b^+$ $Gr\text{-}1^+$ population. Considering that a simultaneous analysis of Ly6C on $CD11b^+$ $Gr\text{-}1^+$ cells allows further sub-fractionation of the putative MDSC populations, a panel of anti-CD11b, anti-Gr-1 and anti-Ly6C antibodies was employed to delineate the lineage and phenotypic diversity of reovirus-driven myeloid cells. As illustrated in Figure 3.2A and Supplementary Figure 3.1C and summarized in Figure 3.2B, single cell suspensions from the ascites, tumor, and spleen collected from reovirus-treated or non-treated animals were first gated on $CD11b^+$ cells and then analyzed for the expression of Gr-1 and Ly6C markers. Interestingly, most of the myeloid cells present in non-treated, control tumor-bearing animals bear a distinct $CD11b^+$ $Gr\text{-}1^+$ $Ly6C^{low}$ cell phenotype (denoted as R1). However, immediately following the injection of reovirus, especially at 1 d.p.f.i. and 3 d.p.f.i., myeloid cells from the ascites, tumor, and spleen displayed a predominant population of $CD11b^+$ $Gr\text{-}1^+$ $Ly6C^{high}$ cell phenotype (denoted as R2), which was almost absent in non-treated, tumor-bearing animals. While the levels of this R2 population gradually declined around 7 d.p.f.i., especially in the ascites and spleen, an additional population with a $CD11b^+$ $Gr\text{-}1^-$ $Ly6C^+$ phenotype (denoted as R3) became apparent at 7 d.p.f.i. in all of the tested tissues. It should

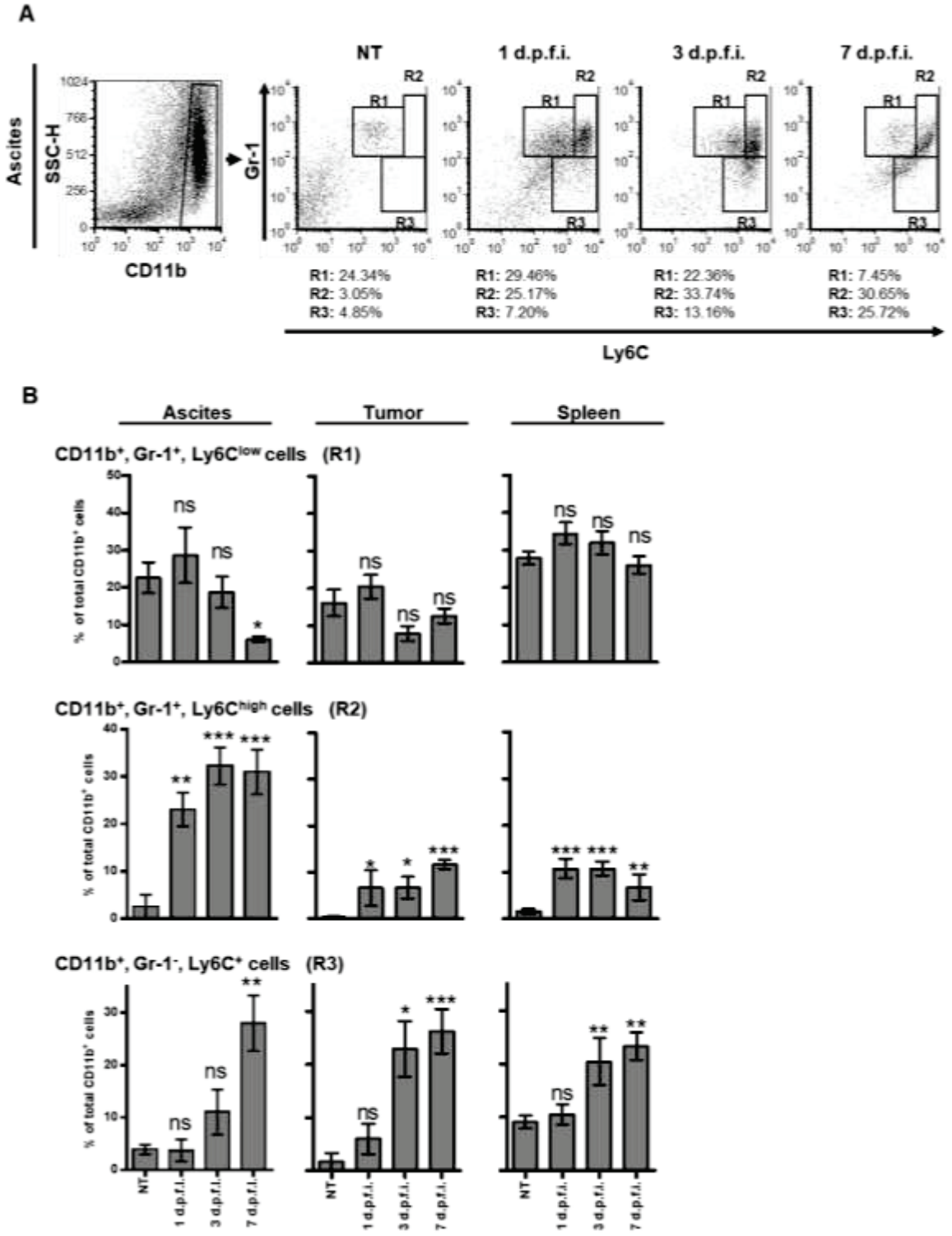

Figure 3.2. *Phenotypically Distinct Heterogeneous Subpopulations of CD11b$^+$ Myeloid Cells Accumulate in the Tumor Microenvironment During the Early Phase of Reovirus Oncotherapy.* (A) C57BL/6 mice were treated according to the schematic illustrated in

Figure 3.1A, and $CD11b^+$, $Gr\text{-}1^+$ myeloid cells in single cell suspensions collected from the ascites, tumor, and spleen (A and B; also see Supplementary Fig 3.1C) were further analyzed for the expression of Ly6C markers throughout the early phase of therapy (non-treated [NT], 1 d.p.f.i., 3 d.p.f.i., and 7 d.p.f.i.) *via* flow cytometry analysis. Statistical analysis was conducted using one-way ANOVA followed by a Bonferroni post-test; ns = $p > 0.05$; *$p \leq 0.05$; **$p \leq 0.01$; ***$p \leq 0.001$. Asterisks shown immediately on top of the bars signify the p values obtained by comparing the respective data against non-treated control group. Each column represents the mean +/- SD of n = 5. Data are representative of more than 8 independent experiments.

be noted that the levels of $CD11b^{+}$ $Gr\text{-}1^{+}$ $Ly6C^{low}$ (R1) cells remain relatively constant throughout the course of oncotherapy as compared to those observed in non-treated animals (except for 7 d.p.f.i., when a slight decrease in the number of the R1 population was observed in the ascites).

Due to the fact that the Gr-1 antigen contains not only the Ly6C epitope but also the epitope for Ly6G, we also considered a staining combination aimed at the simultaneous analysis of CD11b, Gr-1 and Ly6G (and Ly6C) markers on the myeloid cells. In line with previous reports[356], we found that the anti-Gr-1 monoclonal antibody (clone RB6-8C5) blocks the binding of the anti-Ly6G antibody (clone 1A8) (Supplementary Fig 3.2A). This observation restricted the use of anti-Ly6G antibody (clone 1A8) in combination with anti-Gr-1 antibody (clone RB6-8C5) in this study. Although it should be noted that when anti-Ly6G antibody is combined with anti-CD11b and anti-Ly6C antibodies, the predominant tumor-associated myeloid cells from the non-treated tumor-bearing animals is positive for Ly6G ($CD11b^{+}$ $Ly6G^{+}$ $Ly6C^{low}$; referred as S1) (Supplementary Fig 3.2B). On the other hand, reovirus treatment in these tumor-bearing animals induces the accumulation of $CD11b^{+}$ $Ly6G^{-}$ $Ly6C^{high}$ myeloid cells (indicated as S3) at 1 d.p.f.i., which persists throughout the observation period. However, owing to the incompatibility between the anti-Gr-1 and anti-Ly6G antibodies, the Ly6C+Ly6G staining combination fails to concretely differentiate between the R2 and R3 subpopulations achieved through the Gr-1 and Ly6C combination. Hence, this study employed mainly the combination of anti-CD11b, anti-Gr-1 and anti-Ly6C antibodies to characterize various subpopulations of myeloid cells. Thus, the reovirus-driven myeloid cells in systemic and localized tissues consist of a phenotypically

heterogeneous population of cells which is comprised of mostly newly occurring $CD11b^+$ $Gr\text{-}1^+$ $Ly6C^{high}$ (R2) and $CD11b^+$ $Gr\text{-}1^-$ $Ly6C^+$ (R3) cells.

3.3.2 Independent of the Oncolysis of Cancer Cells, Reovirus Drives the Selective Differentiation of Bone Marrow Progenitors into $CD11b^+$ $Ly6G^+$ $Ly6C^{high}$ (R2) Myeloid Cells

Various subpopulations of myeloid cells demonstrate a plastic phenotype and are known to differentiate from the common progenitors present in the BM. Hence, we next wanted to dissect the effect of reovirus on the differentiation of various subpopulations of myeloid cells from hematopoietic progenitor cells in the context of a tumor microenvironment. For this purpose, cell-free ascitic fluid from either reovirus-treated or non-treated tumor bearing mice was collected throughout the course of the *in vivo* experiment (performed as per Fig 3.1A) and cultured with BM progenitor cells collected from naïve syngeneic mice. As illustrated in Figure 3.3A and summarized in Figure 3.3B, we observed that the BM progenitor cells cultured in the presence of the ascitic fluid collected from non-treated tumor-bearing animals displayed a significantly higher frequency of $CD11b^+$ $Gr\text{-}1^+$ $Ly6C^{low}$ (R1 in Fig 3.3A) and lower frequency of $CD11b^+$ $Gr\text{-}1^-$ $Ly6C^+$ cells (R3 in Fig 3.3A) as compared to those cultured without any ascites (non-treated control). More importantly, and in correlation with our *in vivo* data, the ascites from non-treated PC-bearing animals did not promote the generation of $CD11b^+$ $Gr\text{-}1^+$ $Ly6C^{high}$ cells (R2 in Fig 3.3A). These data show that ascites from ovarian cancer-bearing animals can selectively promote or support the differentiation of $CD11b^+$ $Gr\text{-}1^+$ $Ly6C^{low}$ (R1), but not of $CD11b^+$ $Gr\text{-}1^+$ $Ly6C^{high}$ (R2) or $CD11b^+$ $Gr\text{-}1^-$ $Ly6C^+$ (R3), myeloid cell subpopulations. In contrast, the incubation of BM cells with the ascites from reovirus-treated PC-bearing animals

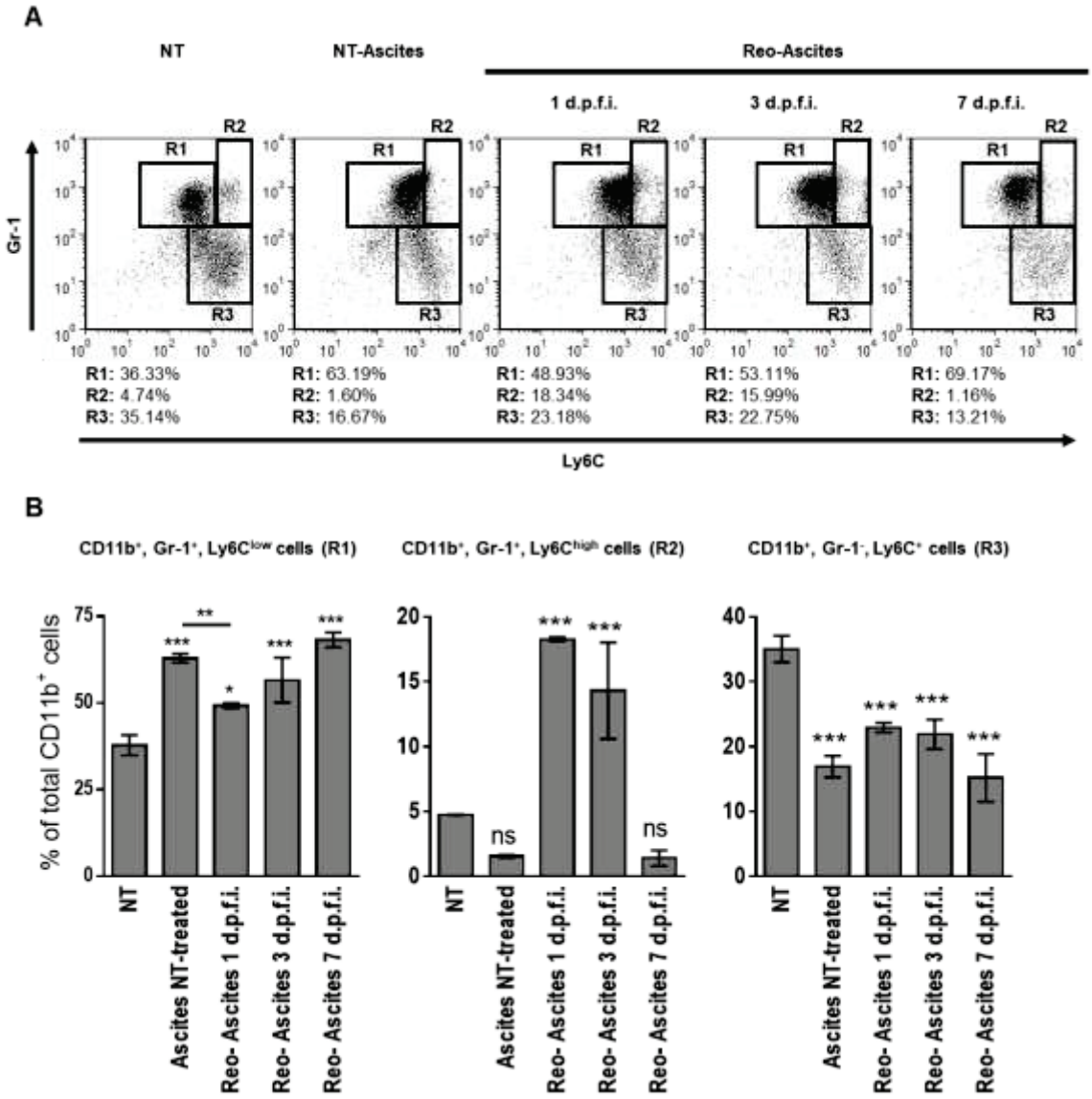

Figure 3.3. *Reovirus-modulated Tumor Microenvironment Selectively Promotes the Differentiation of CD11b$^+$ Gr-1$^+$ Ly6C^{high} (R2) Myeloid Cells from Bone Marrow Progenitors.* (A and B) Bone marrow cells collected from naïve C57BL/6 were incubated with the cell-free ascitic fluid that was collected at the indicated collection points from PC-bearing, reovirus-treated or non-treated animals. After 24 hrs, cells were analyzed for the frequency of each of the three CD11b$^+$ cell subsets, CD11b$^+$ Gr-1$^+$ Ly6C^{low} (R1), CD11b$^+$ Gr-1$^+$ Ly6C^{high} (R2), and CD11b$^+$ Gr-1$^-$ Ly6C$^+$ (R3), by flow cytometry. One-way ANOVA with Bonferroni post-test was conducted for statistical analysis; ns = $p > 0.05$; *$p \leq 0.05$; **$p \leq 0.01$; ***$p \leq 0.001$. Asterisks immediately above bars signify the p values obtained by comparing the respective data against the non-treated control group, while asterisks shown above the horizontal lines display the p values obtained through comparison of the groups containing individual time-points. The data are represented as the mean +/- SD of n = 3-5.

collected at 1 and 3 d.p.f.i. induced a significant increase in the frequency of $CD11b^+$ $Gr\text{-}1^+$ $Ly6C^{high}$ (R2) cells. Interestingly, BM cells treated with the ascitic fluid from non-treated as well as reovirus-treated (collected at 1, 3, and 7 d.p.f.i.) animals were unable to recover the loss in $CD11b^+$ $Gr\text{-}1^-$ $Ly6C^+$ (R3) cells which was evident when the numbers were compared to those observed in non-treated ascites-treated BM. Collectively, these data illustrate that the tumor microenvironment of non-treated PC-bearing animals promotes the differentiation of $CD11b^+$ $Gr\text{-}1^+$ $Ly6C^{low}$ (R1) cells and reduces the frequencies of $CD11b^+$ $Gr\text{-}1^-$ $Ly6C^+$ (R3) cells. The most remarkable observation, however, is that reovirus-modulated tumor microenvironment selectively promotes the generation of $CD11b^+$ $Gr\text{-}1^+$ $Ly6C^{high}$ (R2) cells, especially during early phases of oncotherapy (at 1 and 3 d.p.f.i.). Taking this into consideration, our subsequent investigations were focused on the $CD11b^+$ $Gr\text{-}1^+$ $Ly6C^{high}$ (R2) cell subpopulation.

Reovirus is known to affect the functions and phenotype of various immune cells *via* direct interaction or through the products of oncolytic activities on cancer cells[98, 101, 105]. Therefore, we next asked whether reovirus itself or reovirus-mediated oncolysis can affect the differentiation of BM cells in various myeloid subpopulations. To this end, BM hematopoietic progenitors co-cultured in the presence or absence of ID8 cells were either treated with reovirus (10 multiplicity of infection [MOI]) or left untreated for 24 hrs, and then analyzed for the expression of CD11b, Gr-1, and Ly6C. As illustrated in Figure 3.4A and summarized in Figure 3.4B, BM cells cultured without ID8 cells and then exposed to reovirus displayed increased frequencies of $CD11b^+$ $Gr\text{-}1^+$ $Ly6C^{high}$ (R2) cells with no significant increase in the percentages of $CD11b^+$ $Gr\text{-}1^+$ $Ly6C^{low}$ (R1) or $CD11b^+$ $Gr\text{-}1^-$ $Ly6C^+$ (R3) cells as compared to those cultured in the absence of reovirus. These data

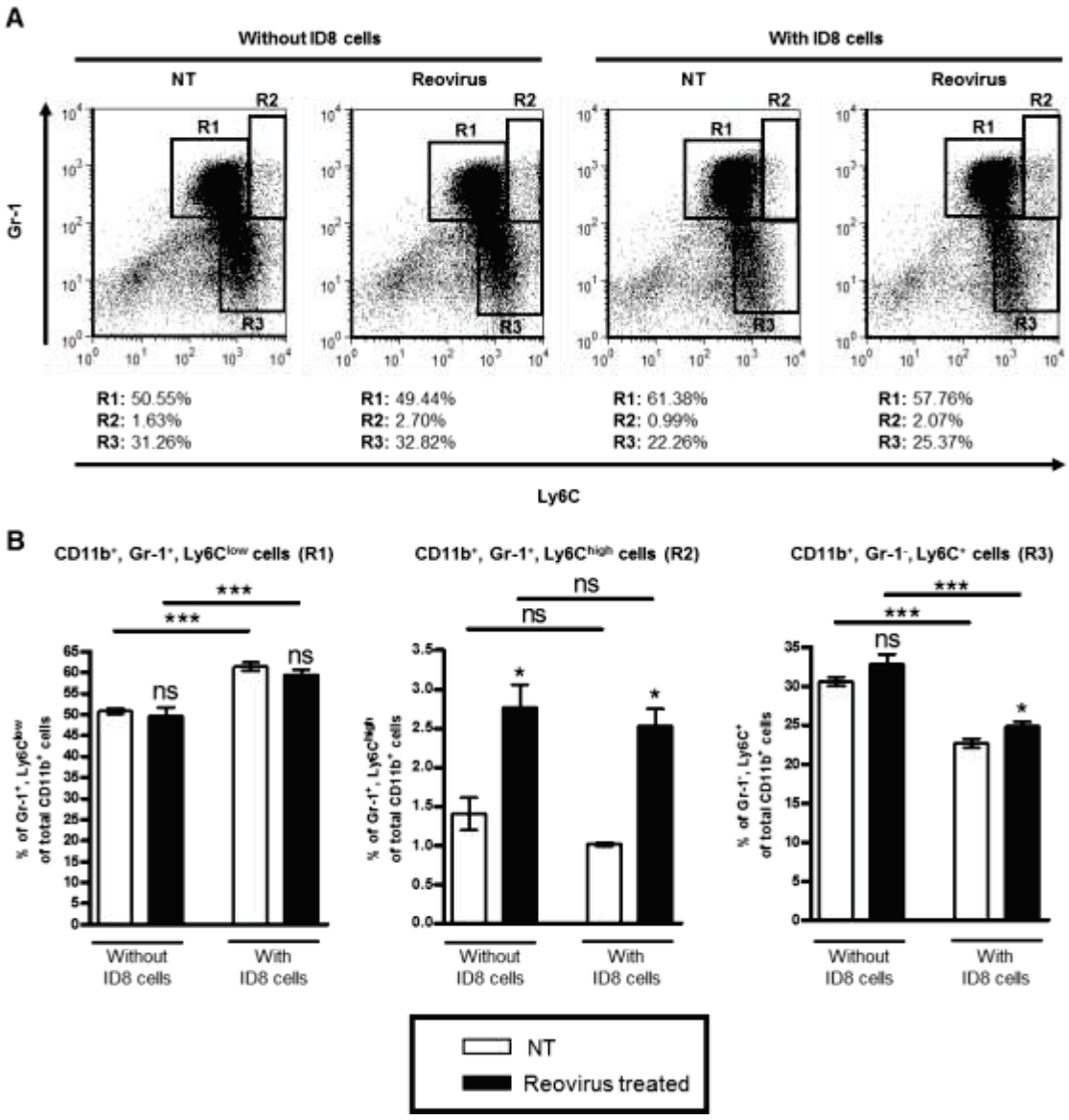

Figure 3.4. *Reovirus Selectively Drives the Differentiation of CD11b^{+} Gr-1^{+} Ly6C^{high} (R2) Myeloid Cells from Bone Marrow Progenitors Independent of Oncolysis.* (A and B) ID8 tumor cells were treated with reovirus (10 MOI) for 24 hrs and then co-cultured with bone marrow cells collected from naïve C57BL/6 mice for an additional 24 hrs. Next, cultures were harvested and analyzed for the frequencies of respective myeloid cell subsets using flow cytometry. Statistical analysis was performed with one-way ANOVA with Bonferroni post-test; ns = $p > 0.05$; *$p \leq 0.05$; **$p \leq 0.01$; ***$p \leq 0.001$. Asterisks shown immediately on top of the bars represent the p values obtained by comparing the respective data against the non-treated control group. Asterisks above the horizontal lines display the p values obtained from the comparison of the groups containing individual time-points. The data are represented as the mean +/- SD of n = 3-5.

demonstrate that reovirus itself can drive the differentiation of CD11b^{+} Gr-1^{+} Ly6C^{high} (R2) myeloid cells, and that this process does not require the products of oncolysis. In contrast, the addition of ID8 cells cultured in the presence of BM cells and in the absence of reovirus showed higher frequencies of CD11b^{+} Gr-1^{+} Ly6C^{low} (R1) cells, lower numbers of CD11b^{+} Gr-1^{-} Ly6C^{+} (R3) cells, and unchanged frequencies of CD11b^{+} Gr-1^{+} Ly6C^{high} (R2) cells. In line with our *in vivo* data (Fig 3.3), these data further suggest that cancer cells promote the preferential differentiation of the CD11b^{+} Gr-1^{+} Ly6C^{low} (R1) subpopulation from BM progenitors. Interestingly, when BM cells were co-cultured with reovirus-infected ID8 cells, significantly higher frequencies of CD11b^{+} Gr-1^{+} Ly6C^{high} (R2) and, to a lesser extent, of CD11b^{+} Gr-1^{-} Ly6C^{+} (R3) and lowered frequencies of CD11b^{+} Gr-1^{+} Ly6C^{low} (R1) cell populations were evident as compared to those co-cultured with non-treated ID8 cells. Collectively, these findings demonstrate that reovirus, either on its own or through the modulation of the tumor microenvironment, promotes a selective differentiation of CD11b^{+} Ly6G^{+} Ly6C^{high} (R2) myeloid cells from bone marrow hematopoietic progenitors independent of oncolysis.

3.3.3 Elevated Levels of Pro-MDSC Factors in Systemic as well as Local Milieu Accompany the Reovirus-driven Accumulation of CD11b^{+} Gr-1^{+} Ly6C^{high} (R2) Cells and is Contributed by Both Cancer and Immune Cells

The dynamics of myeloid cell differentiation, survival, recruitment, and accumulation are dictated by various immune mediators, commonly known as pro-MDSC factors. Therefore, we next conducted a protein and gene expression analysis of well-known pro-MDSC factors in systemic (blood and spleen) as well as local (ascites and tumor) microenvironments. For this purpose, cell-free ascitic fluid and blood from reovirus-treated or non-treated PC-bearing hosts were collected at 1, 3 and 7 d.p.f.i., and analyzed using the

antibody-based quantitative cytokine array to determine the levels of soluble pro-MDSC factors[190, 222, 357] (as listed in Supplementary Table 3.2). As shown in Figure 3.5, ascitic fluid from reovirus-treated animals contained significantly higher amounts of IL-6, G-CSF, MCP-1 (CCL2), MCP-5 (CCL12), and RANTES (CCL5) at 1 and 3 d.p.f.i. as compared to those observed in the ascites from non-treated PC-bearing animals. Similar trends were also observed for the expression of IL-6, MCP-1 (CCL2) and MCP-5 (CCL12) in the blood samples. These elevated levels of MCP-1, MCP-5 (for both ascites and blood), and G-CSF (for ascites only) were also maintained at 7 d.p.f.i., while significantly higher levels of TNF-α were evident on 1 and 7 d.p.f.i. in the ascitic fluid. Interestingly, the levels of VEGF, a known growth factor for MDSCs, were elevated at 1 and 7 d.p.f.i. in the blood and decreased in the ascites at 7 d.p.f.i.. Unlike the abovementioned pro-MDSC factors, there was no significant change in the levels of CXCL16, GM-CSF, IL-10, IL-1β, M-CSF, SCF, or SDF-1α (Supplementary Table 3.1). These data suggest that the recruitment and accumulation of $CD11b^{+}$ $Gr\text{-}1^{+}$ $Ly6C^{high}$ (R2) myeloid cells are concomitant with the elevated levels of numerous pro-MDSC factors in the local and systemic milieu of reovirus-treated cancer-bearing hosts.

To further pinpoint the source of these pro-MDSC factors, gene expression analysis by quantitative PCR (qPCR) was conducted on the cells collected from the ascites, tumor, and spleen of reovirus-treated or non-treated PC-bearing animals (Fig 3.6). In correlation with the cytokine array data, the overall expression levels of IL-6 and MCP-1 (CCL2) as well as TGF-β, which was not covered in the cytokine array, were significantly upregulated in the cellular constituents of the ascitic fluid collected early during reovirus oncotherapy as

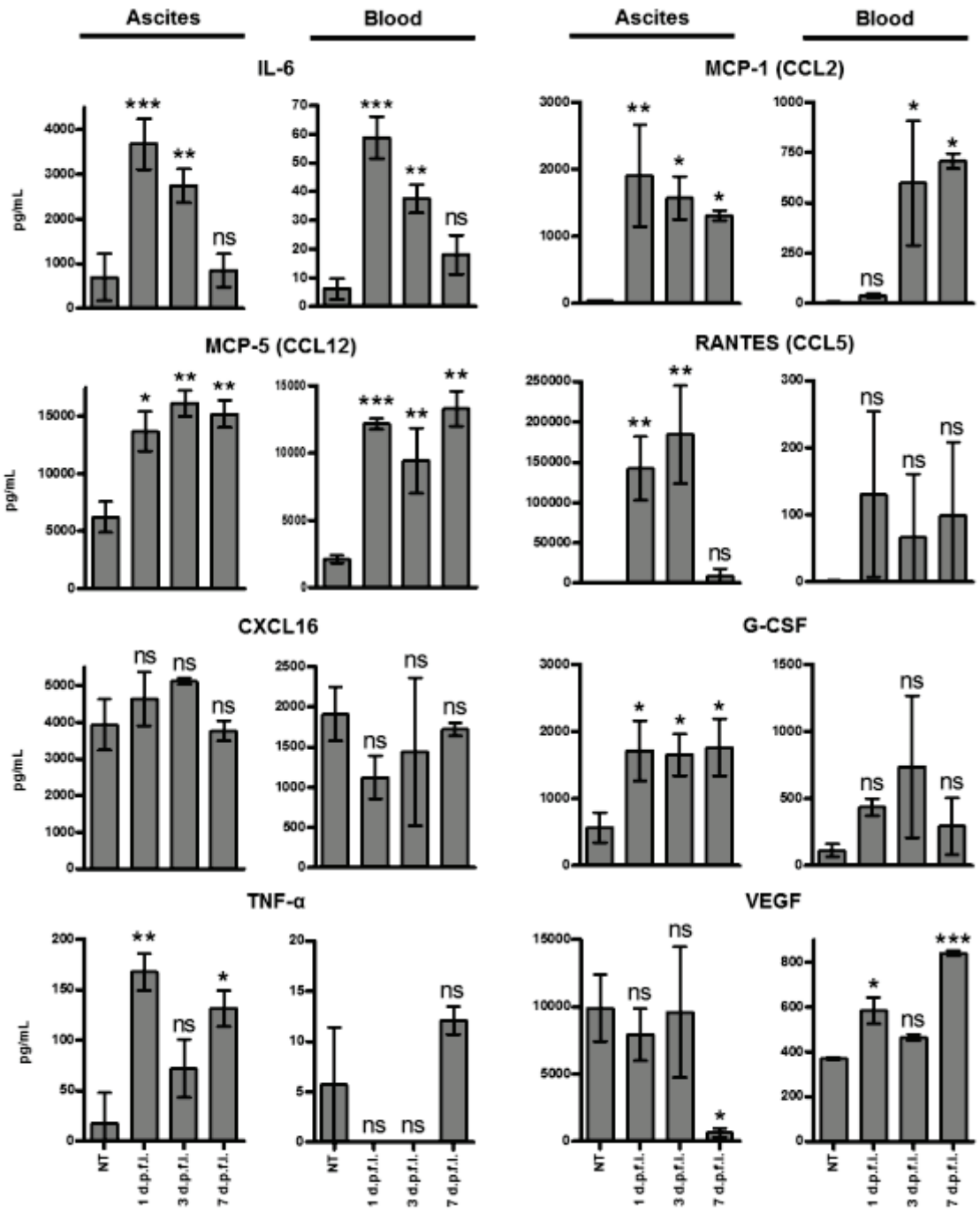

Figure 3.5. *Preferential Recruitment of CD11b^{+} Gr-1^{+} Ly6C^{high} (R2) Cells in the Tumor Milieu is Accompanied by Enhanced Quantities of Pro-MDSC Proteins in the Ascites and Blood.* PC-bearing C57BL/6 mice were treated according to Figure 3.1A and cell-free ascitic fluid and blood, collected at the indicated time points, were analyzed using an antibody-based quantitative cytokine array to measure the concentrations of selected mouse cytokines. Statistical analysis was performed with one-way ANOVA coupled with Bonferroni post-test; ns = $p > 0.05$; *$p \leq 0.05$; **$p \leq 0.01$; ***$p \leq 0.001$. Asterisks shown

immediately on top of the bars signify the *p* values obtained by comparing the respective data against the non-treated control group. Data are representative of 3 independent experiments.

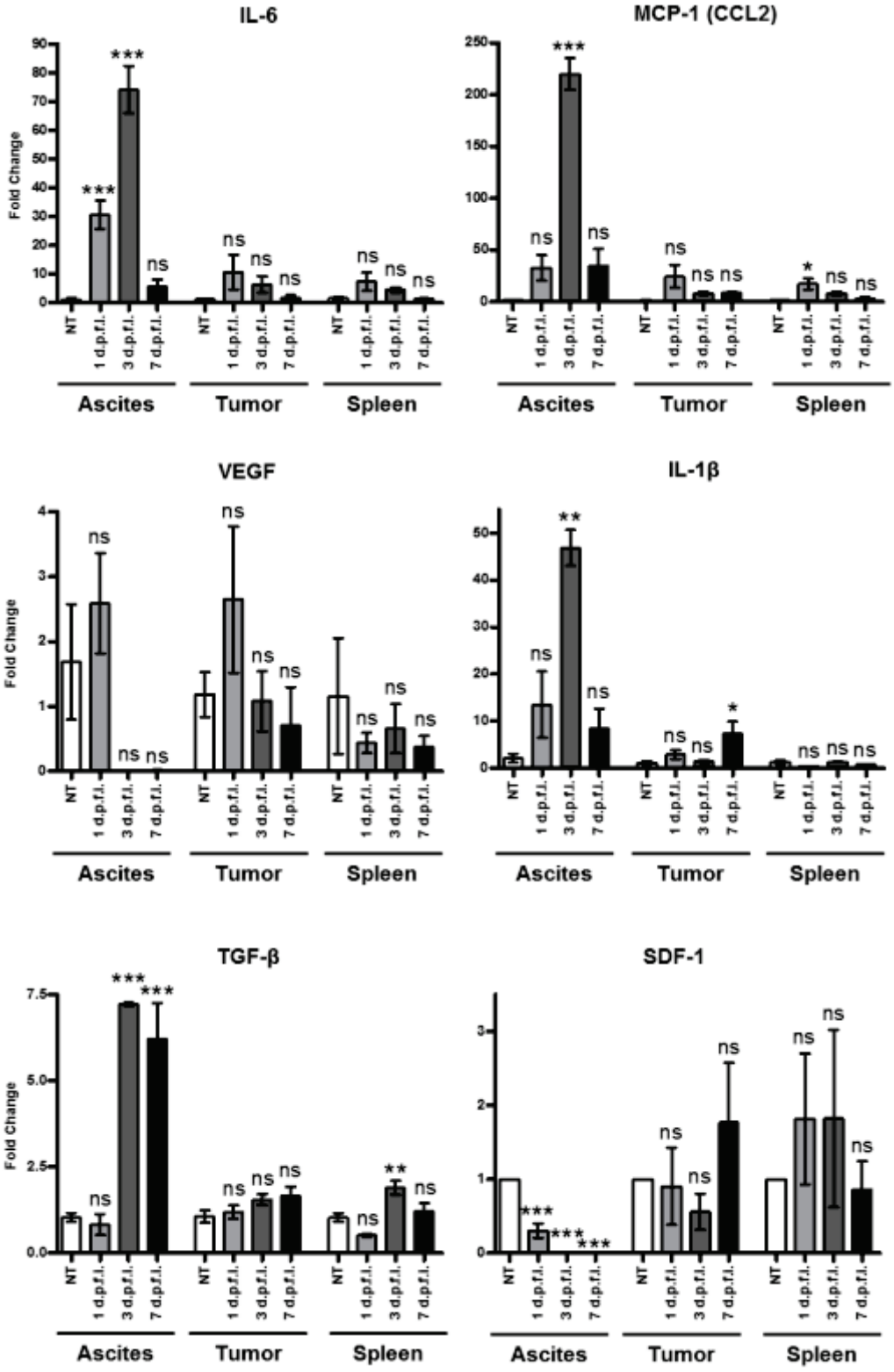

Figure 3.6. *Reovirus-driven Accumulation of CD11b^{+} Gr-1^{+} Ly6C^{high} (R2) Cells is Concurrent with Increased Gene Expression of Pro-MDSC Factors.* Cells from the ascites,

tumor, and spleen of the control or reovirus-treated PC-bearing C57BL/6 mice (injected as per the schematic in Figure 3.1A) were collected at the indicated time points and were analyzed using qPCR to measure the expression of various immune markers known to be involved in MDSC pathophysiology (as denoted on the top of each bar graph). Data were analyzed following the Livak and Schmittgen's $2^{-\Delta\Delta CT}$ methodology[330]. Graphs illustrate the fold change normalized to its own GAPDH and compared against the respective non-treated control. One-way ANOVA coupled with Bonferroni post-test was performed; ns = $p > 0.05$; *$p \leq 0.05$; **$p \leq 0.01$; ***$p \leq 0.001$. Asterisks shown immediately on top of the bars signify the p values obtained by comparing the respective data against non-treated control group. Data are representative of 3-5 independent experiments.

compared to those collected from the non-treated PC-bearing animals. Contrary to the cytokine array data, qPCR analysis of IL-1β showed a significant increased expression within the ascites and the tumor at 3 and 7 d.p.f.i., respectively. Surprisingly, the elevated expression of these pro-MDSC factors was observed in mostly the samples collected from the ascites and not from tumor or spleen, suggesting that the likely source of these immune mediators is the cells of the ascites.

The ascites of PC-bearing hosts is known to contain a mixture of cancer cells and infiltrating immune cells[358]. Thus, to dissect the contribution of each subset in question, tumor (ID8) cells, BM progenitors, and lymphoid cells from the spleen were separately cultured in the presence or absence of reovirus *in vitro* for 24 hrs, and then analyzed for the gene expression of various pro-MDSC factors using qPCR (Fig 3.7). In accordance with our *in vivo* and *ex vivo* data, ID8 cells, BM, and spleen cells treated with reovirus showed significantly higher expression of IL-6 and MCP-1 as compared to that observed in non-treated cells. Analysis of other pro-MDSC factors, such as VEGF and SDF-1, showed no significant change in expression following reovirus treatment. As compared to the respective non-treated controls, a significant increase in TGF-β and IL-1β expression was observed only in reovirus-treated ID8 and BM cells, respectively. Collectively, these data suggest that ID8, BM, and splenocytes are all potentially responsible for the increased expression of multiple pro-MDSC factors following reovirus exposure. However, the expression of certain pro-MDSC factors such as IL-1β or TGF-β could be generated from the infiltrating BM originating cells or cancer cells, respectively. Taken together, these data demonstrate that reovirus can act on either cancer or immune cells and induce the

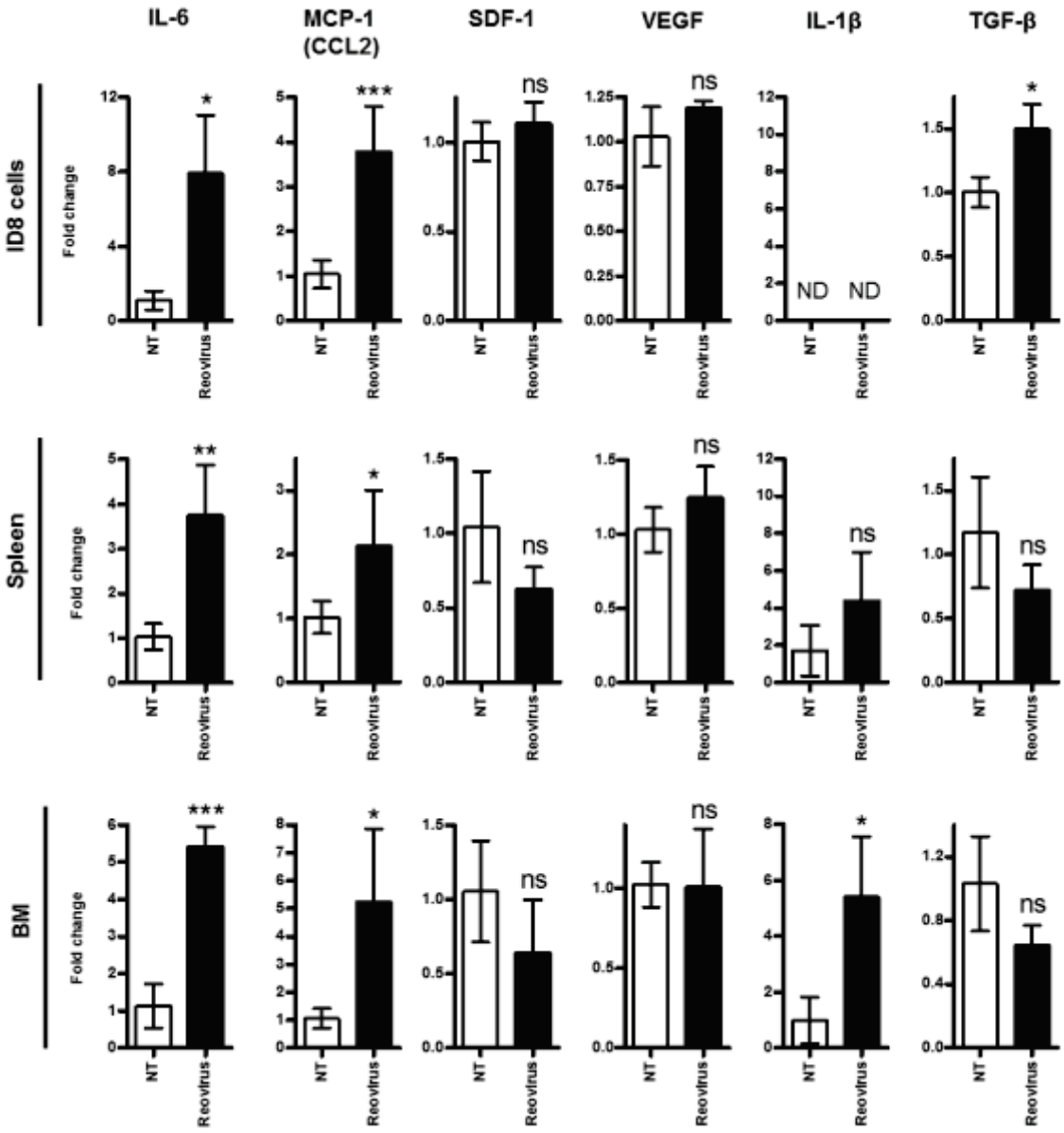

Figure 3.7. *Reovirus Can Mediate the Production of Pro-MDSC Factors from Cancer Cells, as well as Immune Cells. In vitro* cultured ID8 cells, harvested spleen, or bone marrow (BM) cells were cultured with or without reovirus (10 MOI) for 24 hrs and then analyzed by qPCR for the expression of IL-6, MCP-1, SDF-1, VEGF, IL-1β, and TGF-β coupled with data analysis as explained in Figure 3.6. Statistical analysis was conducted using a two-tailed Student's t-test with 95% confidence interval; ns = $p > 0.05$; *$p \leq 0.05$; **$p \leq 0.01$; ***$p \leq 0.001$. Asterisks immediately on top of the bars signify the p values obtained by comparing the respective data against the non-treated control group. Data are representative of 3 independent experiments.

production of pro-MDSC factors, in local and systemic milieu, that are capable of supporting growth, differentiation, and recruitment of myeloid cells.

3.3.4 Exclusively During the Early Phase of Oncotherapy, Reovirus Drives the Selective Chemotaxis of CD11b^{+} Gr-1^{+} Ly6C^{high} Cells

To further understand the mechanism through which myeloid cells accumulate in the tumor microenvironment, we asked whether reovirus promotes selective chemotaxis of any of the myeloid subpopulations, CD11b^{+} Gr-1^{+} Ly6C^{low} (R1), CD11b^{+} Gr-1^{+} Ly6C^{high} (R2) or CD11b^{+} Gr-1^{-} Ly6C^{+} cells (R3), in question. To answer this, a standard transwell chemotaxis assay was performed. BM cells from naïve C57BL/6 mice were added in the top chamber, while cell-free ascites from either reovirus-treated or non-treated PC-bearing mice collected at indicated time points were placed in the bottom chamber of the transwell system. Following a 2-hr incubation, the cells that had migrated into the bottom chamber were evaluated for their respective myeloid subpopulation phenotype. As shown in Figure 3.8A, the migration of either CD11b^{+} Gr-1^{+} Ly6C^{low} (R1) or CD11b^{+} Gr-1^{-} Ly6C^{+} (R3) cells remains unchanged in the presence of ascitic fluid collected from either reovirus-treated or non-treated animals. It should, however, be noted that the CD11b^{+} Gr-1^{+} Ly6C^{low} (R1) population migrates at a significantly higher rate in the presence of ascites as compared to when cultured in media alone. Most importantly, ascitic fluid collected at 1 d.p.f.i. from reovirus treated PC-bearing animals exclusively promotes significantly greater chemotaxis of the CD11b^{+} Gr-1^{+} Ly6C^{high} (R2) subpopulation as compared to ascitic fluid from non-treated animals or media alone. To further investigate this selective migratory potential, the expression of chemotactic receptors (CXCR1, CXCR2, and CCR2) in isolated CD11b^{+} Gr-1^{+} Ly6C^{low} (R1) and CD11b^{+} Gr-1^{+} Ly6C^{high} (R2) subpopulations was assessed

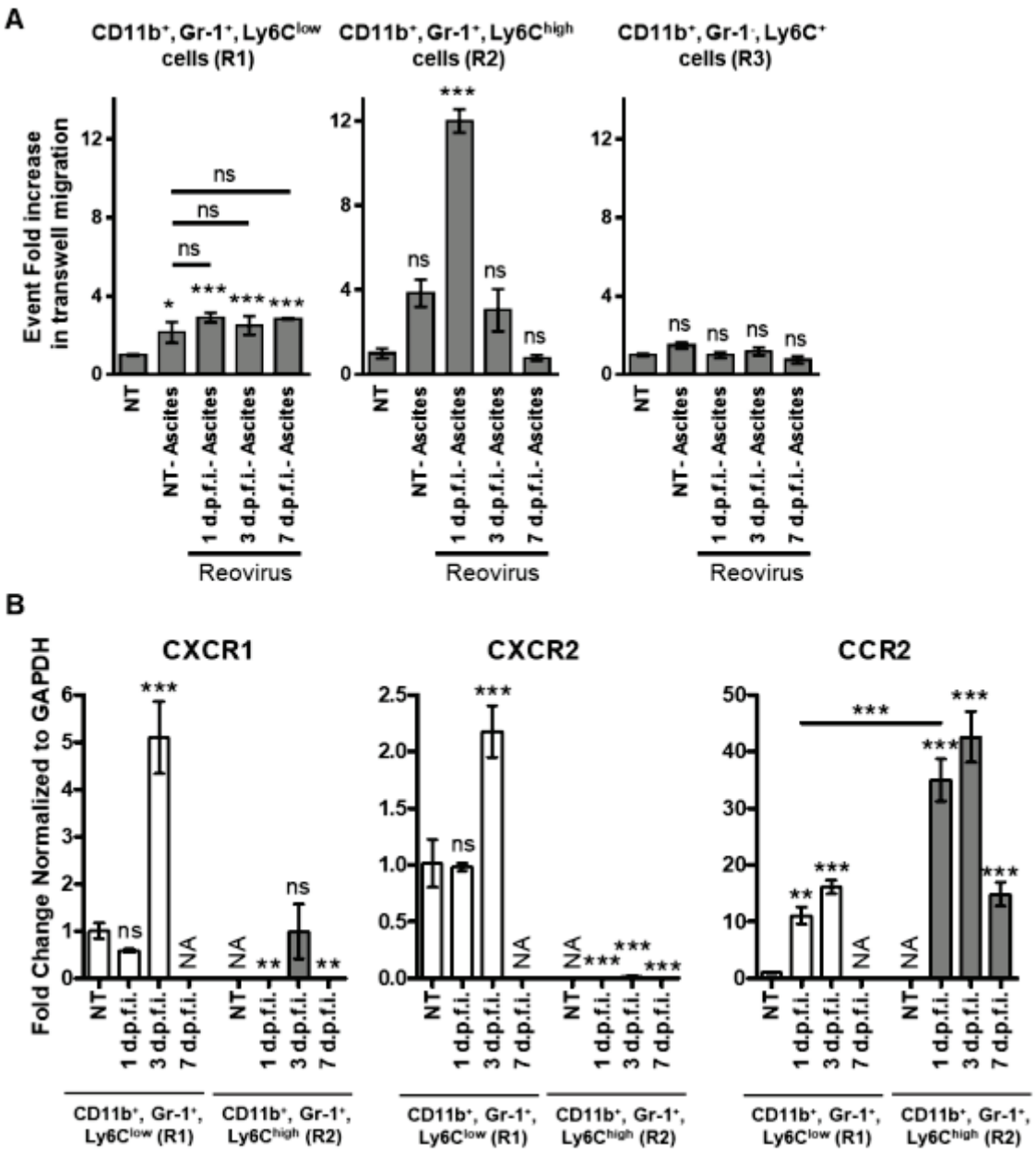

Figure 3.8. *Reovirus-modulated Tumor Milieu Promotes Selective Migration of CD11b$^+$ Gr-1$^+$ Ly6C^{high} (R2) Cells.* (A) Cell-free ascitic fluid was collected from non-treated or reovirus-treated PC-bearing C57BL/6 mice (treated as per Fig 3.1A) and was placed in the bottom chamber of an 8 μm transwell plate. Bone marrow cells (1x10^6 cells) from naïve C57BL/6 were seeded in the upper chamber of the same transwell plate and allowed to migrate to the bottom chamber. After 2 hrs, flow cytometry analysis was used to measure the frequencies of CD11b$^+$ Gr-1$^+$ Ly6C^{low} (R1), CD11b$^+$ Gr-1$^+$ Ly6C^{high} (R2), and CD11b$^+$ Gr-1$^-$ Ly6C$^+$ (R3) cells that migrated into the bottom chamber. (B) C57BL/6 mice were

injected as per the schematic in Figure 3.1A and the $CD11b^+$ $Gr\text{-}1^+$ $Ly6C^{low}$ (R1) and $CD11b^+$ $Gr\text{-}1^+$ $Ly6C^{high}$ (R2) cell populations were isolated *via* fluorescent cell sorting. qPCR was conducted on cDNA synthesized from the RNA extracted from isolated $CD11b^+$ $Gr\text{-}1^+$ $Ly6C^{low}$ (R1) and $CD11b^+$ $Gr\text{-}1^+$ $Ly6C^{high}$ (R2) populations to measure the expression of known myeloid cell chemotactic receptors (CXCR1, CXCR2, CCR2). NA indicates that sufficient sample could not be recovered for qPCR. One-way ANOVA coupled with Bonferroni post-test was performed; ns = $p > 0.05$; *$p \leq 0.05$; **$p \leq 0.01$; ***$p \leq 0.001$. Asterisks shown immediately on top of the bars signify the p values obtained by comparing the respective data against the non-treated $CD11b^+$ $Gr\text{-}1^+$ $Ly6C^{low}$ (R1) control group. Data are representative of 4-5 mice and qPCR samples were run in duplicate experiments.

throughout the course of therapy (Fig 3.8B). Such comparative analysis illustrated that the R1 population had significantly greater expression of CXCR1 and CXCR2 whereas the R2 population contained greater expression of CCR2. Of note, the cytokine array data (Fig 3.5) show significantly elevated expression of chemotactic MCP-1 (CCL2), known to support such trafficking, at 1 d.p.f.i.. Additionally, we also found heightened gene expression of S100A8 and S100A9 proteins, known to drive the chemotaxis of $CD11b^+$ cells, in the cells collected from the ascites of reovirus-treated PC-bearing animals (Supplementary Fig 3.3). These data clearly demonstrate that reovirus modulates the tumor microenvironment and drives the selective chemotaxis of $CD11b^+$ $Gr\text{-}1^+$ $Ly6C^{high}$ (R2) cells exclusively during the early phase of oncotherapy, and explain the mechanism by which these cells accumulate in the tumor microenvironment.

3.3.5 Augmented Tumor-associated Immunosuppression During the Early Phase of Reovirus Oncotherapy is Mediated by Newly Recruited $CD11b^+$ $Gr\text{-}1^+$ $Ly6C^{high}$ (R2) Myeloid Cells

Tumor-associated myeloid cells are known to inhibit various immune responses, especially those mediated by T cells. Considering the critical role of T cell responses in OV-driven anti-cancer immunotherapy, we investigated the T cell suppression capacities of the reovirus-driven heterogeneous myeloid cell populations. For this purpose, C57BL/6 mice were injected with ID8 tumor cells and subsequently treated with the therapeutic regimen of reovirus as per the schematic shown in Figure 3.1A. At the indicated time points, cells from the ascitic fluid were collected and then passed through an antibody-based myeloid cell isolation column to obtain purified $CD11b^+$ $Gr\text{-}1^+$ cells (a purity of greater than 90%; Supplementary Fig 3.1A), containing both the $CD11b^+$ $Gr\text{-}1^+$ $Ly6C^{low}$ (R1) and $CD11b^+$ $Gr\text{-}1^+$ $Ly6C^{high}$ (R2) populations. These cells were then analyzed for their capacity to

suppress T cell proliferation. As shown in Figure 3.9A, $CD11b^+$ $Gr\text{-}1^+$ cells collected at 1 and 3 d.p.f.i. showed significantly higher potency to inhibit T cell proliferation at 1:4 effector-to-target ratio than the cells collected at 7 d.p.f.i or those collected from non-treated PC-bearing animals. Of note, $CD11b^+$ $Gr\text{-}1^+$ cells collected at 7 d.p.f.i. displayed comparable suppressive capacities as those displayed by the cells from non-treated animals. These data demonstrate that $CD11b^+$ $Gr\text{-}1^+$ cells present in the tumor microenvironment of reovirus-treated PC-bearing animals have a higher capacity to suppress T cell activation than those collected from the non-treated PC-bearing animals, especially at 1 and 3 d.p.f.i. during oncotherapy.

To pinpoint the contribution of each constituent subpopulation, we sub-fractioned the $CD11b^+$ $Gr\text{-}1^+$ cells into $CD11b^+$ $Gr\text{-}1^+$ $Ly6C^{low}$ (R1) or $CD11b^+$ $Gr\text{-}1^+$ $Ly6C^{high}$ (R2) subpopulations (a purity between 91-96%; Supplementary Fig 3.1B), and analyzed their respective T cell suppressive capabilities to hamper proliferation and cytotoxicity (i.e., IFN-γ response). As shown in Figure 3.9B, newly recruited $CD11b^+$ $Gr\text{-}1^+$ $Ly6C^{high}$ (R2) cells displayed enhanced suppression capacity that was significantly higher than that observed with $CD11b^+$ $Gr\text{-}1^+$ $Ly6C^{low}$ (R1) cell population collected from non-treated PC-bearing animals. Interestingly, both $CD11b^+$ $Gr\text{-}1^+$ $Ly6C^{low}$ (R1) and $CD11b^+$ $Gr\text{-}1^+$ $Ly6C^{high}$ (R2) cell populations from reovirus-treated mice contained comparable suppressive capacities. Similar to the proliferation data, both the $CD11b^+$ $Gr\text{-}1^+$ $Ly6C^{low}$ (R1) and $CD11b^+$ $Gr\text{-}1^+$ $Ly6C^{high}$ (R2) subpopulations rom reovirus treated mice had enhanced capability to suppress IFN-γ production from $CD8^+$ T cells at 1 and 3 d.p.f.i., whereas the $CD11b^+$ $Gr\text{-}1^+$ $Ly6C^{low}$ (R1) myeloid cell population collected from the non-treated animals or isolated at 7 d.p.f.i. had no effect on the IFN-γ production. Interestingly,

CD11b^{+} Gr-1^{+} Ly6C^{high} (R2) population promoted the IFN-γ production at 7 d.p.f.i.. To complement such increase in immunosuppression at 1 and 3 d.p.f.i., qPCR analysis of isolated CD11b^{+} Gr-1^{+} Ly6C^{low} (R1) and CD11b^{+} Gr-1^{+} Ly6C^{high} (R2) myeloid cell populations illustrated that both CD11b^{+} Gr-1^{+} Ly6C^{low} (R1) and CD11b^{+} Gr-1^{+} Ly6C^{high} (R2) populations have significantly higher expression of iNOS at 1 d.p.f.i. (although this does decrease in the CD11b^{+} Gr-1^{+} Ly6C^{high} (R2) population at 3 and 7 d.p.f.i.) and IL-10 at 3 d.p.f.i. as compared to the non-treated CD11b^{+} Gr-1^{+} Ly6C^{low} (R1) population (Fig 3.9D). In addition, there is also a significant increase in ARG1 and TGF-β in the CD11b^{+} Gr-1^{+} Ly6C^{high} (R2) population at 3 d.p.f.i (Fig 3.9D). Such factors play a key role in tumor progression but most importantly to suppress T cell function and proliferation.

It should be noted that following reovirus injection, significantly higher numbers of CD11b^{+} Gr-1^{+} Ly6C^{high} (R2) cells are selectively recruited to the tumor microenvironment (Fig 3.8) and comprise the major portion of tumor-associated myeloid cells (Fig 3.2A, Fig 3.2B, and Supplementary Fig 3.1C). Especially, the ratio of CD11b^{+} Gr-1^{+} Ly6C^{high} (R2): CD11b^{+} Gr-1^{+} Ly6C^{low} (R1) cells during the early phase of oncotherapy is significantly greater than that observed in non-treated animals (as illustrated in Fig 3.10). Thus, even though both CD11b^{+} Gr-1^{+} Ly6C^{low} (R1) and CD11b^{+} Gr-1^{+} Ly6C^{high} (R2) populations bear comparable suppressive capacities, the augmentation of the tumor-associated suppression happens only following the recruitment of CD11b^{+} Gr-1^{+} Ly6C^{high} (R2) cells. Together, these data suggest that the newly recruited CD11b^{+} Gr-1^{+} Ly6C^{high} (R2) cells further enhance the tumor-associated immunosuppression at 1 and 3 d.p.f.i. that eventually subsides at 7 d.p.f.i.. This conclusion is further supported by the fact that the ascitic fluid from reovirus-treated PC-bearing animals showed significantly higher

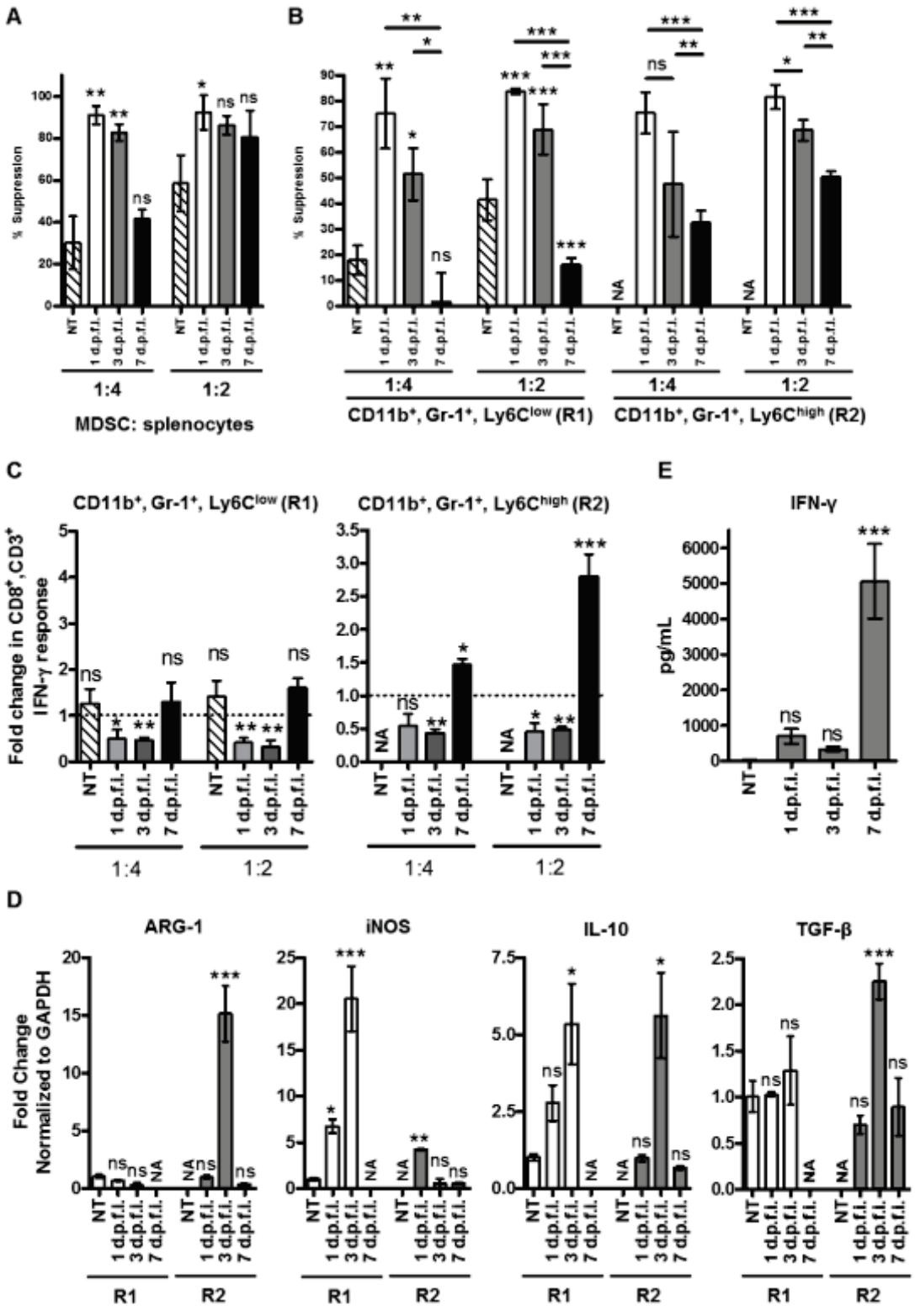

Figure 3.9. *Augmented Tumor-associated Immunosuppression During the Early Phase of Reovirus Oncotherapy Is Mediated by Newly Recruited CD11b^{+} Gr-1^{+} Ly6C^{high} (R2)*

Myeloid Cells. PC-bearing C57BL/6 mice were treated according to Figure 3.1A. Total $CD11b^+$ $Gr\text{-}1^+$ cells (A) or isolated subpopulations of $CD11b^+$ $Gr\text{-}1^+$ $Ly6C^{low}$ (R1) and $CD11b^+$ $Gr\text{-}1^+$ $Ly6C^{high}$ (R2) cells (B) were incubated with T cells activated *via* CD3 and CD28 antibodies at the indicated MDSC: splenocyte ratio. Activated T cells were harvested from syngeneic naïve mice and stained with CFSE or monitored for IFN-γ response from $CD8^+$ T cells. (A and B) After 96 hrs, cells were stained with anti-CD3 antibodies and then analyzed by flow cytometry for halving of CFSE fluorescence in $CD3^+$ cells to determine the percentage of T cell suppression. (C) After 18 hrs, brefeldin A was added to the co-culture and incubated for 6 additional hours. Flow cytometry was conducted to monitor IFN-γ response *via* extracellular and intracellular staining for T cell markers (CD3 and CD8) and IFN-γ, respectively. (D) C57BL/6 mice were treated according to Figure 3.1A, and $CD11b^+$ $Gr\text{-}1^+$ $Ly6C^{low}$ (R1) and $CD11b^+$ $Gr\text{-}1^+$ $Ly6C^{high}$ (R2) cell populations were isolated *via* fluorescent cell sorting. QPCR was conducted using the cDNA synthesized from the RNA extracted from the isolated $CD11b^+$ $Gr\text{-}1^+$ $Ly6C^{low}$ (R1) and $CD11b^+$ $Gr\text{-}1^+$ $Ly6C^{high}$ (R2) populations to measure the expression of ARG1, iNOS, IL-10, and TGF-β using gene specific primers. All values were normalized to the internal control (GAPDH). NA indicates that sufficient sample could not be recovered for qPCR. (E) Cell-free ascitic fluid from non-treated or reovirus-treated animals was analyzed using the antibody-based quantitative cytokine array to measure mouse cytokine concentrations of IFN-γ. Statistical analysis was performed with one-way ANOVA with Bonferroni post-test; ns = $p > 0.05$; *$p \leq 0.05$; **$p \leq 0.01$; ***$p \leq 0.001$. Asterisks shown immediately alongside the horizontal bars signify the p values obtained by comparing the respective data while asterisks above the bars are representative of the p values obtained by comparing against the respective control. Data are representative of the mean +/- the SD at n=4-6.

levels of IFN-γ protein, a signature marker of T_H1 activation, only at 7 d.p.f.i. (Fig 3.9E). Taken together, our data show that reovirus transiently augments tumor-associated immunosuppression during the early phase of oncotherapy, and that this suppression is mediated by newly recruited $CD11b^+$ $Gr\text{-}1^+$ $Ly6C^{high}$ (R2) cells.

3.4 DISCUSSION

Anti-cancer immunotherapies promote the development of anti-cancer immune responses that are capable of eradicating existing or possibly relapsing cancer cells. However, tumor-associated immunosuppression, present either locally or systemically, hampers the development of such beneficial anti-cancer immune responses and poses a major impediment towards the successful implementation of anti-cancer immunotherapies. It is now clear that detailed knowledge about the biology and subsequent functional consequences of tumor-associated immunosuppression is essential for achieving the optimum efficacy of any anti-cancer immunotherapy. In this report, we demonstrate that the therapeutic administration of oncolytic reovirus, which is known to promote beneficial anti-tumor immunity, transiently augments tumor-associated immunosuppression during the early phase of oncotherapy (Fig 3.10). In the context of the highly sought-after anti-cancer immunotherapeutic activities of OVs, this discovery unearths a biological phenomenon that will further assist the development of strategies aimed at achieving the best possible outcome from OV-based cancer therapies.

Immunological events induced following reovirus administration in cancer-bearing hosts concern both anti-viral and anti-tumor immune responses. In the context of reovirus-based oncotherapy, anti-tumor immune responses are beneficial while anti-viral immune responses are detrimental. Thus, to achieve the optimum efficacy of OV-based

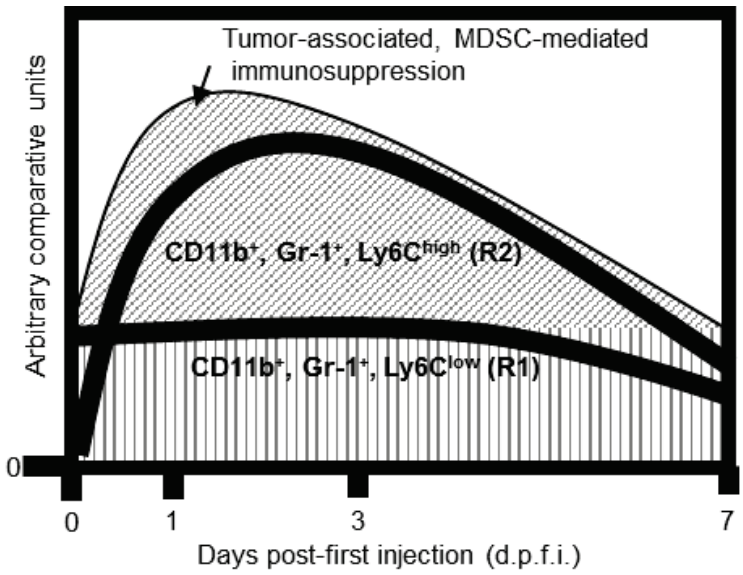

Figure 3.10. *Relationship Between the Kinetics of Tumor-associated, MDSC-mediated Suppressive Activities and the Frequencies of Myeloid Cell Subpopulations.* In this schematic, x-axis represents the timeline following reovirus injections while y-axis represents the levels of either MDSC-mediated immunosuppressive capacities or the frequencies of $CD11b^+$ $Gr\text{-}1^+$ $Ly6C^{low}$ (R1) and $CD11b^+$ $Gr\text{-}1^+$ $Ly6C^{high}$ (R2) populations. At the beginning of the oncotherapy (time 0 days post first infection [d.p.f.i.]), tumor-associated, MDSC-mediated suppression (represented by the shaded area) and $CD11b^+$ $Gr\text{-}1^+$ $Ly6C^{low}$ (R1) cells both exist at substantial levels and hence are represented to start at a higher level than "0" on the y-axis. On the other hand, $CD11b^+$ $Gr\text{-}1^+$ $Ly6C^{high}$ (R2) cells are present in minute quantities and are thus represented to start at a lower point than that of $CD11b^+$ $Gr\text{-}1^+$ $Ly6C^{low}$ (R1) cells. Following reovirus injection, the level of MDSC-mediated suppressive activities first gets potentiated at 1 and 3 d.p.f.i., which then return to the pre-treatment levels at 7 d.p.f.i.. Similar kinetic of appearance is also followed by the $CD11b^+$ $Gr\text{-}1^+$ $Ly6C^{high}$ (R2) cells. On the contrary, the numbers of $CD11b^+$ $Gr\text{-}1^+$ $Ly6C^{low}$ (R1) cells remain comparatively constant, especially at 1 and 3 d.p.f.i.. Collectively, this kinetic analysis shows that MDSC-mediated suppressive capacities follow the kinetics of $CD11b^+$ $Gr\text{-}1^+$ $Ly6C^{high}$ (R2) cells and further supports a role of $CD11b^+$ $Gr\text{-}1^+$ $Ly6C^{high}$ (R2) cells in potentiating tumor-associated immunosuppression.

oncotherapies, therapeutic strategies that can simultaneously promote anti-tumor immunity while suppressing anti-viral immunity are desired. In view of the complex interplay between anti-tumor and anti-viral immunity, oncolytic virus-driven immunomodulation requires comprehensive dissection in order to understand its anti-cancer immunotherapeutic implications.

Recent studies have illustrated that reovirus-mediated immunomodulation overturns tumor-associated immune evasion mechanisms and subsequently initiates a clinically meaningful anti-tumor immunity[1, 105]. Interestingly, some of these studies also reported that reovirus drives an accumulation of suppressive cells, such as MDSCs and T_{regs}, following its therapeutic administration[1]. Considering the capacity of reovirus to initiate functional and clinically relevant anti-tumor immune responses, the accumulation of suppressive cells following its administration is counterintuitive. Similar accumulation of myeloid cells has been reported in other acute infections including vaccinia virus, adenovirus, and the acute lymphocytic choriomeningitis virus (LCMV)[274, 355, 359, 360]. It is hypothesized that these suppressive cells either protect the infected host against excessive collateral damage by limiting the attack of immune cells on virally infected cells or are recruited by the virus as an immune evasion mechanism to thwart the immune-mediated attack aimed at eliminating the replication niche. In the context of oncotherapy, the presence of these OV-driven suppressive cells, especially during the early phase of oncotherapy when the anti-tumor immune responses are primed, is considered to be detrimental. Therefore, this study was focused on understanding the biology, phenotypic heterogeneity, biodiversity, and pathophysiology of reovirus-induced suppressive myeloid cells. Of note, the heterogeneity of MDSCs or immature myeloid cells (IMCs) is still obscure partially due to the fact that

the myeloid cells of different phenotypes are addressed as a singular "MDSC" population. Considering these facts, and in an effort to avoid further confusion, in this article we have defined such putative "MDSCs" simply by their phenotype (for example, $CD11b^+$ $Gr\text{-}1^+$ $Ly6C^{high/low}$ myeloid cells).

The accumulation of myeloid cells in the tumor microenvironment following exposure to oncolytic reovirus could result from either selective survival or trafficking of a specific subpopulation. Survival of myeloid cells is orchestrated by various survival factors including IL-6, G-CSF, TNF-α, TGF-β, and IL-1β that are present in their microenvironment. Thus, *in vitro* studies aimed at investigating the survival/apoptosis of MDSCs are hampered by the fact that these cells are less amenable to long-term culture conditions, most likely owing to the absence of the growth factors in the culture media. Similar to other publications[280, 281], we have found that the harvesting of tumor-associated myeloid cells in standard culture medium causes a large majority of the $CD11b^+$ $Gr\text{-}1^+$ cells to spontaneously die within 24 hrs. However, as suggested by Suzuki *et al.*, the supplementation of culture medium with tumor-bearing mouse plasma, or in our case with cell-free ascitic fluid, reduces the spontaneous apoptosis of tumor-associated MDSCs[281]. This phenomenon has been observed in various mouse cancer models including those initiated with lung epithelial cells (TC-1 cells[281]), mammary tumor cells (4T1 cells[280]) and our ovarian cancer cells (MOSE ID8 cells), suggesting that this is rather a generalized and not cancer model-specific phenomenon. We have previously identified that tumor-associated $CD11b^+$ $Gr\text{-}1^+$ myeloid cells, now known as $CD11b^+$ $Gr\text{-}1^+$ $Ly6C^{low}$ (R1) myeloid cells, cultured in medium supplemented by ascitic fluid from a non-treated ovarian cancer-bearing mouse, show a greater amount of annexin V^+ cells following exposure to

reovirus *in vitro*[5]. In this report, we demonstrate that only $CD11b^+$ $Gr\text{-}1^+$ $Ly6C^{high}$ (R2) myeloid cells, and not $CD11b^+$ $Gr\text{-}1^+$ $Ly6C^{low}$ (R1) myeloid cells, display enhanced chemotactic potential immediately following reovirus therapy. Thus, these results collectively suggest that the reovirus-induced accumulation of myeloid cells in the tumor microenvironment is associated with lower survival of $CD11b^+$ $Gr\text{-}1^+$ $Ly6C^{low}$ (R1) myeloid cells and higher chemotactic potential of $CD11b^+$ $Gr\text{-}1^+$ $Ly6C^{high}$ (R2) myeloid cells.

Many pathological conditions, including infections and immunization protocols employing complete Freund's adjuvant (CFA), are known to promote a transient expansion of the IMCs that fail to fully develop into mature MDSCs but still possess immunosuppressive capacities[222, 361]. In line with this evidence, we recently discovered that reovirus drives the expansion and accumulation of myeloid cells co-expressing CD11b (detected by clone M1/70) and Gr-1 (detected by clone RB6-8C5) markers following its therapeutic administration in ovarian PC-bearing C57BL/6 mice. However, whether this reovirus-driven putative MDSC population contains a phenotypically and functionally heterogeneous population of myeloid cells or IMCs remained unknown. Such sub-fractionation of MDSCs is usually done by using a combination of antibodies against CD11b, Gr-1, Ly6G, and Ly6C markers. However, the use of the Ly6G marker in this study was avoided based on the conflicting reports which suggest that the monoclonal antibody Gr-1 (clone RB6-8C5) blocks the binding of the Ly6G antibody (clone 1A8)[356]. Therefore, to be consistent with our previous findings, we subdivided myeloid cells into various subgroups based on their CD11b, Gr-1, and Ly6C expression, and focused on $CD11b^+$ $Gr\text{-}1^+$ $Ly6C^{low}$ (R1), $CD11b^+$ $Gr\text{-}1^+$ $Ly6C^{high}$ (R2), and $CD11b^+$ $Gr\text{-}1^-$ $Ly6C^+$ (R3) cells.

Biological functions of MDSCs are mediated through a multitude of mechanisms and often have contrasting physiological implications. Although MDSCs were first characterized in tumor-bearing mice and humans[362-364], they were also found to exist in healthy hosts and reported in other pathological conditions including viral, bacterial, and parasitic infections[351, 360, 361, 365-368]. Not surprisingly, the implications of MDSC-driven suppressive activities are dictated by the health or disease conditions in which they occur. For example, MDSCs found in tumor-bearing hosts or those suffering from chronic viral infections profoundly suppress the functions of immune cells and contribute towards the aggravation of the disease condition[365, 366]. In contrast, MDSCs developed during autoimmune conditions (e.g., experimental autoimmune encephalomyelitis [EAE][369]) and acute infections[274] are postulated to protect the hosts against self-damaging immune assault by inhibiting the functions of hyperactive immune cells. Hence, the specific role of MDSC-driven suppressive immune activities must be evaluated in the context of the specific health condition. In the context of oncotherapy, it must be kept in mind that the virus-driven myeloid cell accumulation occurs in the simultaneous presence of the two entities that are known to endow MDSCs with contrasting pathophysiological attributes: cancer microenvironment and acute viral infection. Considering that the characterization of MDSCs within the abovementioned unique, but clinically important, scenario has remained undiscovered, this study was focused on the functional attributes of oncotherapy-driven myeloid cell subpopulations. Only through such special consideration, the pathophysiological importance and a possible immunotherapeutic potential of these cells during OV-based oncotherapy would be realized.

Reovirus-based oncotherapy, similar to other OV-based therapies, is being recognized for its anti-cancer immunotherapeutic properties. It is now clear that to achieve the optimum efficacy of OV-based therapy, direct oncolytic properties of OVs must be complemented with immune interventions that can promote OV-driven immunotherapeutic benefits. While most of the efforts to date have been focused on understanding the beneficial immunological effects of OV-based therapy, very little attention has been paid to the immunological events that have a capacity to either compromise or negatively affect the efficacy of such therapies. In this report, we illustrate that, in addition to the immunostimulatory properties, reovirus oncotherapy also promotes a transient phase of immunosuppression that is mediated through the selective recruitment and accumulation of highly suppressive $CD11b^{+}$ $Gr\text{-}1^{+}$ $Ly6C^{high}$ (R2) cells. In the context of ongoing efforts to supplement OV-based therapies with complementary interventions aimed at synergistically enhancing its anti-cancer benefits, identification of such therapeutic targets is extremely advantageous. Strategic management of such immunosuppressive entities can further potentiate OV-driven immunotherapeutic effects and enhance the efficacy of reovirus oncotherapy. Thus, the findings reported here are of critical importance and can be directly translated in clinical settings to achieve better patient outcomes, especially in the context of ongoing phase III clinical trials.

3.5 CONFLICT OF INTEREST

None to declare

3.6 SUMMARY OF CHAPTER 3 AND TRANSITION TO CHAPTER 4

Contrary to the beneficial anti-tumor responsiveness of reovirus-based OV therapy, this chapter illustrates that reovirus transiently augments cancer-associated immunosuppression through the recruitment and accumulation of the immunosuppressive $CD11b^{+}$ $Gr\text{-}1^{+}$ $Ly6C^{high}$ MMC population. The data suggest that not all therapy-mediated infiltrating immune cells are beneficial in the context of OV therapy. These results propose that approaches which curtail cancer-associated immunosuppression and enforce a potent anti-tumor immunity are of the upmost importance to optimize the therapeutic effectiveness of OV therapies.

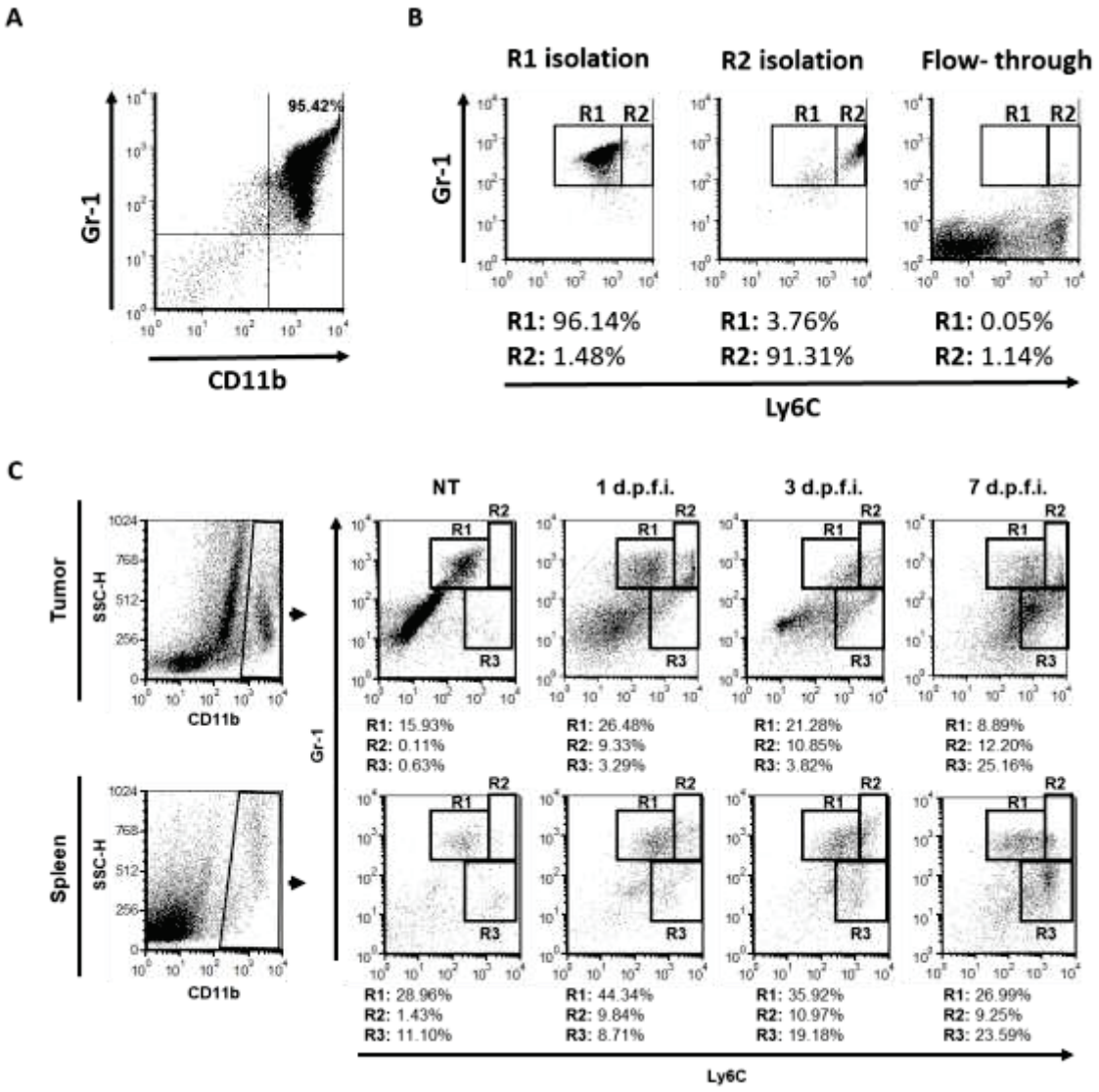

Supplementary Figure 3.1. *Purification Check of CD11b$^+$ Gr-1$^+$ Ly6C^{low} (R1) and CD11b$^+$ Gr-1$^+$ Ly6C^{high} (R2) Cell Isolation and Their Accumulation in the Tumor and Spleen Tissue Throughout the Course of Reovirus Oncotherapy.* C57BL/6 mice were treated according to the schematic in Figure 3.1A. The ascites was collected at 1 d.p.f.i. and the CD11b$^+$ Gr-1$^+$ cells (A) were isolated. (B) represents the specific isolation of CD11b$^+$ Gr-1$^+$ Ly6C^{low} (R1) and CD11b$^+$ Gr-1$^+$ Ly6C^{high} (R2) cells following the manufacturer's instructions at 1 d.p.f.i. of reovirus administration. (C) C57BL/6 mice were treated according to the schematic in Figure 3.1A and flow cytometry analysis was conducted to evaluate the frequency of CD11b$^+$ myeloid cell subsets collected from the tumor and spleen. The above dot-plots are representative images of CD11b$^+$ cell subsets in the tumor and spleen cells harvested during reovirus therapeutic administration.

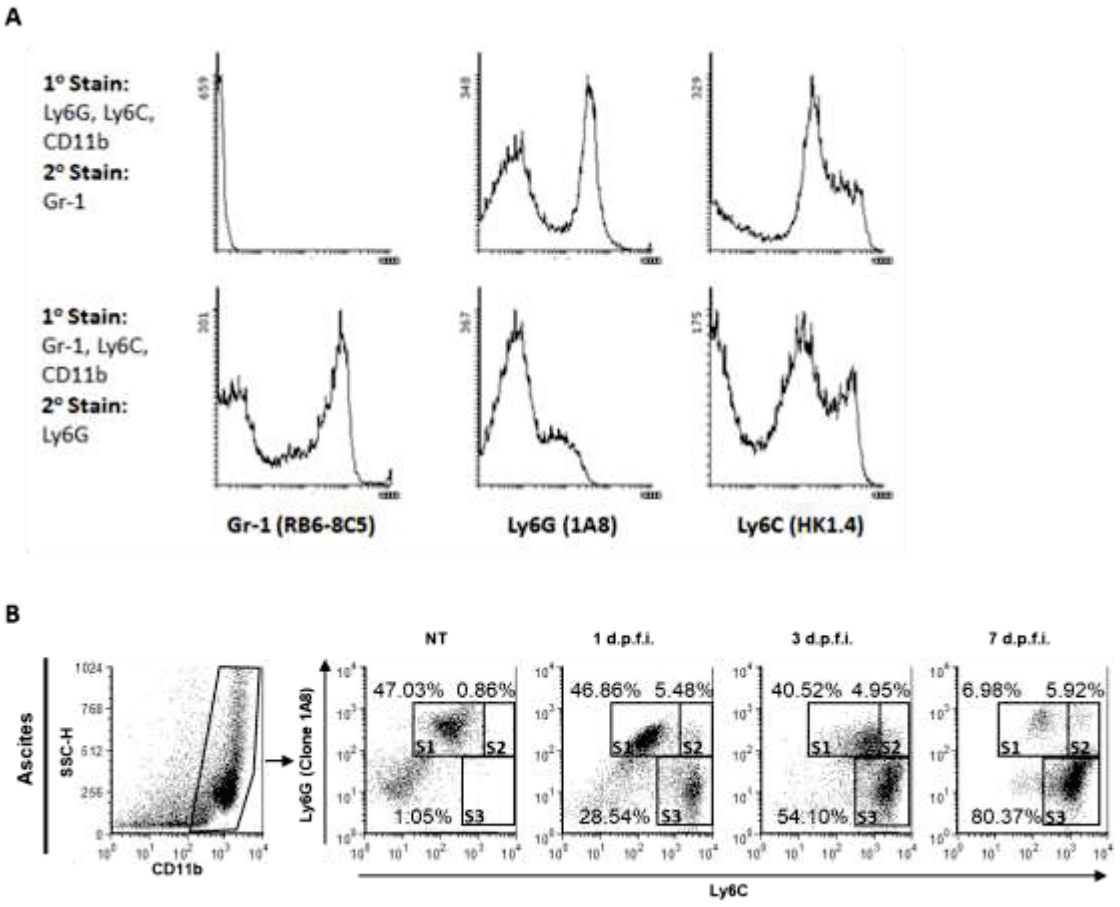

Supplementary Figure 3.2. *Antibody Staining Interference Between Ly6G (1A8) and Gr-1 (RB6-8C5) and the CD11b, Ly6G, and Ly6C Status of Ascites-harvested Myeloid Cells Over the Course of Reovirus Oncotherapy*. (A) Isolated bone marrow cells from naïve animals were stained with the indicated primary fluorescent-conjugated antibody (1° Stain). To confirm the blocking interference, a secondary stain (2° Stain) following 1° Stain and washing of excess antibody was conducted and the fluorescent intensity was analyzed by flow cytometry. (B) C57BL/6 mice were treated according to the schematic in Figure 3.1A and flow cytometry analysis was conducted to evaluate the frequency of $CD11b^+$ myeloid cell subsets collected from the ascites and stained with CD11b, Ly6G (1A8), and Ly6C (HK1.4). The indicated sections are S1 ($CD11b^+$ $Ly6G^+$ $Ly6C^{low}$), S2 ($CD11b^+$ $Ly6G^+$ $Ly6C^{high}$), and S3 ($CD11b^+$ $Ly6G^-$ $Ly6C^{high}$). The above dot-plots are representative images of ascites-harvested $CD11b^+$ cell subsets during reovirus therapeutic administration and representative images of n=3.

Supplementary Table 3.1. *Antibody-Based Quantitative Cytokine Array Analysis of Pro-MDSC Soluble Factors in the Blood and Ascites.*

Cytokine	Source	Treatment	Change relative to non-treated	Below LOD	Above MAX	LOD (pg/mL)	MAX (pg/mL)
CXCL16	Ascites	NT	-	N	N		
		1d.p.f.i.	-	N	N		
		3d.p.f.i.	-	N	N		
		7d.p.f.i.	-	N	N	14.9	6,000
	Blood	NT	-	N	N		
		1d.p.f.i.	-	N	N		
		3d.p.f.i.	-	N	N		
		7d.p.f.i.	-	N	N		
G-CSF	Ascites	NT	-	N	N		
		1d.p.f.i.	↑	N	N		
		3d.p.f.i.	↑	N	N		
		7d.p.f.i.	↑	N	N	18.3	30,000
	Blood	NT	-	N	N		
		1d.p.f.i.	-	N	N		
		3d.p.f.i.	-	N	N		
		7d.p.f.i.	-	N	N		
IFN-γ	Ascites	NT	-	Y	N		
		1d.p.f.i.	-	N	N		
		3d.p.f.i.	-	N	N		
		7d.p.f.i.	↑↑↑	N	N	54.7	30,000
	Blood	NT	-	Y	N		
		1d.p.f.i.	-	Y	N		
		3d.p.f.i.	-	Y	N		
		7d.p.f.i.	-	N	N		
IL-10	Ascites	NT	-	N	N		
		1d.p.f.i.	-	N	N		
		3d.p.f.i.	-	N	N		
		7d.p.f.i.	-	N	N	114.9	30,000
	Blood	NT	-	N	N		
		1d.p.f.i.	-	N	N		
		3d.p.f.i.	-	N	N		
		7d.p.f.i.	-	N	N		
IL-1β	Ascites	NT	-	Y	N		
		1d.p.f.i.	-	Y	N		
		3d.p.f.i.	-	Y	N		
		7d.p.f.i.	-	N	N	31.4	30,000
	Blood	NT	-	Y	N		
		1d.p.f.i.	-	Y	N		
		3d.p.f.i.	-	Y	N		
		7d.p.f.i.	-	Y	N		
IL-6	Ascites	NT	-	N	N		
		1d.p.f.i.	↑↑↑	N	Y		
		3d.p.f.i.	↑↑	N	N		
		7d.p.f.i.	-	N	N	1.2	3,000
	Blood	NT	-	N	N		
		1d.p.f.i.	↑↑↑	N	N		
		3d.p.f.i.	↑↑	N	N		
		7d.p.f.i.	-	N	N		
MCP-1 (CCL2)	Ascites	NT	-	N	N		
		1d.p.f.i.	↑↑	N	N		
		3d.p.f.i.	↑	N	N		
		7d.p.f.i.	↑	N	N	10.8	3,000
	Blood	NT	-	Y	N		
		1d.p.f.i.	-	N	N		
		3d.p.f.i.	↑	N	N		
		7d.p.f.i.	↑	N	N		
MCP-5 (CCL12)	Ascites	NT	-	N	N		
		1d.p.f.i.	↑	N	N		
		3d.p.f.i.	↑↑	N	N		
		7d.p.f.i.	↑↑	N	N	19.7	30,000
	Blood	NT	-	N	N		
		1d.p.f.i.	↑↑↑	N	N		
		3d.p.f.i.	↑↑	N	N		
		7d.p.f.i.	↑↑	N	N		
M-CSF	Ascites	NT	-	Y	N		
		1d.p.f.i.	-	N	N		
		3d.p.f.i.	-	Y	N		
		7d.p.f.i.	-	Y	N	54	30,000
	Blood	NT	-	Y	N		
		1d.p.f.i.	-	Y	N		
		3d.p.f.i.	-	Y	N		
		7d.p.f.i.	-	Y	N		
MIG (CXCL9)	Ascites	NT	-	N	N		
		1d.p.f.i.	-	N	N		
		3d.p.f.i.	↑	N	N		
		7d.p.f.i.	↑	N	N	2.7	3,000
	Blood	NT	-	N	N		
		1d.p.f.i.	-	N	N		
		3d.p.f.i.	-	N	N		
		7d.p.f.i.	↑↑	N	N		
MIP-1α	Ascites	NT	-	Y	N		
		1d.p.f.i.	-	N	N		
		3d.p.f.i.	-	N	N		
		7d.p.f.i.	-	N	N	18.6	30,000
	Blood	NT	-	Y	N		
		1d.p.f.i.	↑	N	N		
		3d.p.f.i.	-	N	N		
		7d.p.f.i.	↑↑	N	N		
RANTES	Ascites	NT	-	Y	N		
		1d.p.f.i.	↑↑	N	Y		
		3d.p.f.i.	↑↑	N	Y		
		7d.p.f.i.	-	N	N	62.6	30,000
	Blood	NT	-	Y	N		
		1d.p.f.i.	-	N	N		
		3d.p.f.i.	-	N	N		
		7d.p.f.i.	-	N	N		
SCF	Ascites	NT	-	N	N		
		1d.p.f.i.	-	N	N		
		3d.p.f.i.	-	N	N		
		7d.p.f.i.	-	N	N	264.3	150,000
	Blood	NT	-	N	N		
		1d.p.f.i.	-	N	N		
		3d.p.f.i.	-	N	N		
		7d.p.f.i.	-	N	N		
SDF-1α	Ascites	NT	-	N	N		
		1d.p.f.i.	-	N	N		
		3d.p.f.i.	-	N	N		
		7d.p.f.i.	-	N	N	26.9	60,000
	Blood	NT	-	N	N		
		1d.p.f.i.	-	N	N		
		3d.p.f.i.	-	N	N		
		7d.p.f.i.	-	N	N		
TNF-α	Ascites	NT	-	N	N		
		1d.p.f.i.	↑↑	N	N		
		3d.p.f.i.	-	N	N		
		7d.p.f.i.	↑	N	N	70	60,000
	Blood	NT	-	N	N		
		1d.p.f.i.	-	Y	N		
		3d.p.f.i.	-	Y	N		
		7d.p.f.i.	-	Y	N		
VEGF	Ascites	NT	-	N	N		
		1d.p.f.i.	-	N	N		
		3d.p.f.i.	-	N	N		
		7d.p.f.i.	↓	N	N	51.5	30,000
	Blood	NT	-	N	N		
		1d.p.f.i.	↑	N	N		
		3d.p.f.i.	-	N	N		
		7d.p.f.i.	↑↑	N	N		

Abbreviations and symbols: Arrows (↑ or ↓) denote a significant change (Arrows were used to signify p values as follows: not significant (-) = $p > 0.05$; ↑ $p \leq 0.05$; ↑↑ $p \leq 0.01$;

↑↑↑ $p \leq 0.001$). LOD represents the limit of detection and the above MAX denotes that the concentrations are greater than the levels of the standards.

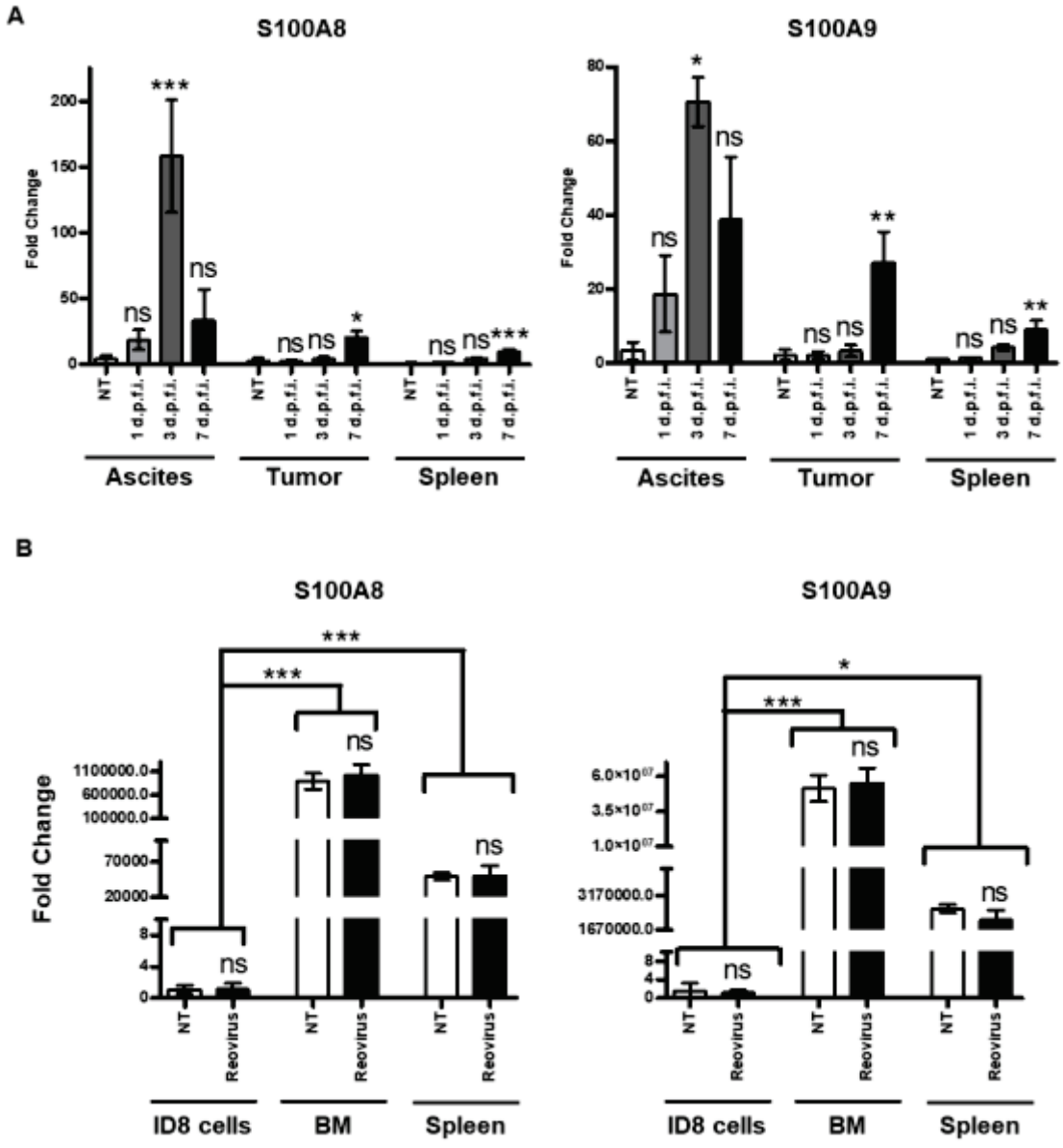

Supplementary Figure 3.3. *Reovirus Induces an Increased Expression of the Pro-inflammatory S100A8/A9 Markers Within the Tumor Milieu.* (A) Samples from the ascites, tumor, and spleen of non-treated or reovirus-treated PC-bearing C57BL/6 mice (treated as per Figure 3.1A) were collected at the indicated time points and analyzed for the expression of S100A8 and S100A9 using qPCR. (B) Samples from cultured ID8 cells, splenocytes, and bone marrow (BM) cells were treated with reovirus (10 MOI) for 24 hrs followed by qPCR analysis for the expression of S100A8 and S100A9 from cDNA reversed transcribed from RNA extracts. Both qPCR analysis was coupled with data analysis as explained in Figure 3.6. One-way ANOVA with Bonferroni post-test was performed; ns = $p > 0.05$; *$p \leq 0.05$; ***$p \leq 0.001$. Asterisks shown immediately on top of the bars signify p values obtained by comparing the respective data against non-treated control group. Asterisks above horizontal bars signify p values obtained from the comparison between the indicated groups. Data are representative of 4 independent experiments.

CHAPTER 4: GEMCITABINE ENHANCES THE EFFICACY OF REOVIRUS-BASED ONCOTHERAPY THROUGH ANTI-TUMOR IMMUNOLOGICAL MECHANISMS

This work appears in part in the publication:

Gujar S, Clements D (co-first author), Dielschneider R, Helson E, Marcato P, Lee PWK. 2014. Gemcitabine Enhances the Efficacy of Reovirus-based Oncotherapy Through Anti-tumor Immunological Mechanisms. British Journal of Cancer. 110 (1): 83-93.

DC and SG – designed the study and prepared the manuscript

DC – carried out the experimentation, collected and analyzed data

RD, EH – assisted with experimentation and data collection

PM and PL – assisted with study design and critical review of the manuscript

4.1 ABSTRACT

Background: Reovirus preferentially infects and kills cancer cells and is currently undergoing clinical trials internationally. While oncolysis is the primary mode of tumor elimination, increasing evidence illustrates that reovirus additionally stimulates anti-tumor immunity with a capacity to target existing and possibly relapsing cancer cells. These virus-induced anti-tumor immune activities largely determine the efficacy of oncotherapy. On the other hand, anti-viral immune responses can negatively affect oncotherapy. Hence, the strategic management of anti-tumor and anti-viral immune responses through complementary therapeutics is crucial to achieving the maximum anti-cancer benefits of oncotherapy.

Methods: Wild type C57BL/6 mice intraperitoneally injected with mouse ovarian surface epithelial cells (ID8 cells) were treated with a therapeutic regimen of reovirus and/or gemcitabine and then analyzed for prolonged survival, disease pathology, and various immunological parameters. Furthermore, *in vitro* analyses were conducted to assess apoptosis, viral spread, and viral production during reovirus and/or gemcitabine treatment.

Results: We demonstrate that reovirus and gemcitabine combination treatment postpones peritoneal carcinomatosis development and prolongs the survival of cancer-bearing hosts. Importantly, these anti-cancer benefits are generated through various immunological mechanisms, including: 1) inhibition of myeloid-derived suppressor cell recruitment to the tumor microenvironment, 2) down-modulation of pro-MDSC factors, and 3) accelerated development of anti-tumor T cell responses.

Conclusions: The complementation of reovirus with gemcitabine further potentiates virus-initiated anti-cancer immunity and enhances the efficacy of oncotherapy. In the context of ongoing clinical trials, our findings represent clinically relevant information capable of enhancing cancer outcomes.

4.2 INTRODUCTION

Reovirus, a double-stranded benign human RNA virus, preferentially infects and kills transformed, cancerous cells as compared to healthy normal cells[30]. This selective oncolytic ability of reovirus has advocated its use as a novel anti-cancer agent for the treatment of various cancers[140]. While the primary mode of action for reovirus oncotherapy is oncolysis (i.e., direct destruction of cancer cells), increasing evidence suggests that reovirus further invokes a chain of anti-tumor immunological events that ultimately culminate in the development of tumor-specific immune responses[1, 98, 105, 150]. Such reovirus-induced anti-tumor immunity attacks existing cancer cells and further protects the host against subsequent tumor challenge even after discontinuation of the therapy[98], and thus bears the potential to govern long-term cancer-free health. Therefore, reovirus oncotherapy can simultaneously target cancer cells through two distinct anti-cancer mechanisms: 1) direct oncolysis, and 2) anti-cancer immunity. Currently, reovirus is undergoing phase I, II, and III clinical trials in Belgium, the UK, and the United States.

Exhaustive evidence thus far documents that the presence of anti-tumor immunity strongly correlates with positive cancer outcomes and better survival[339, 340]. However, in the context of the tumor microenvironment, the induction of anti-tumor T cell responses is faced with many challenges. Tumors employ various immune evasion strategies and thus establish a milieu that prohibits the activation of anti-tumor immune activities. For example, tumors

escape immune-mediated elimination through impaired antigen presentation[370, 371] or processing[372], enhanced expression of immunosuppressive molecules[373, 374], and recruitment of immunosuppressive cells such as regulatory T cells and myeloid-derived suppressor cells (MDSCs). Indeed, the desired anti-cancer immunity can be enhanced by using interventions that challenge the tumor-associated suppressive microenvironment[375, 376]. In this regard, reovirus is known to overturn various tumor-associated immune evasion mechanisms before invoking protective anti-tumor immunity[1, 98, 105].

It should be noted, however, that oncolytic virus-driven immune responses have both positive and negative effects on the efficacy of oncotherapy. The anti-viral immune responses produced after therapeutic injections of reovirus have proven to be detrimental for the oncolytic capabilities of the virus. Hence, although reovirus has shown tremendous potential in *in vitro* studies and in immuno-compromised animals, its efficacy is compromised when implemented in hosts with an intact immune system. It is now acknowledged that the optimum efficacy of reovirus-based therapy can be achieved only after strategic management of both oncotherapy-initiated anti-tumor and anti-viral immune responses. In this context, complementary interventions that can potentiate anti-tumor and/or dampen anti-viral immunity are considered to be the key partners in achieving the maximum benefits of oncolytic virus-based therapies.

Gemcitabine (GEM) is an FDA-approved chemotherapeutic agent that is now used for the treatment of a variety of cancers including pancreatic cancer, bladder cancer, lung cancer, and ovarian cancer (OC)[377-382]. Apart from its direct cancer killing activity, GEM also induces anti-tumor immune responses in cancer-bearing hosts in pre-clinical studies[383]. Thus, we hypothesized that GEM may complement reovirus therapy to achieve enhanced

direct oncolysis and to further potentiate reovirus-induced anti-tumor immunological activities. Using an immuno-competent murine model of OC, we demonstrate that the reovirus+GEM combination therapy produces better cancer outcomes and that these therapeutic benefits result primarily from the augmentation of anti-tumor immune responses through the modulation of the tumor-associated immunosuppressive microenvironment.

4.3 RESULTS

4.3.1 Reovirus and Gemcitabine Combination Treatment Significantly Increases the Survival of OC-bearing Mice as Compared to Either Treatment Alone

Currently, live reovirus (Reo) and GEM combination treatment (Reo+ GEM) is undergoing clinical trials[174]. To understand any possible benefits of this combination therapy, we first evaluated the kinetics of the disease pathology and survival in OC-bearing animals. To perform this study, ID8 tumor-bearing C57BL/6 animals were treated with Reo and GEM alone or in combination as per the schematic shown in Figure 4.1A and then monitored for ascites development and survival. In accordance with our previous observations[1], the animals treated with Reo showed delayed development of peritoneal carcinomatosis (PC), as evidenced by ascites development (Fig 4.1B), and statistically greater survival (Fig 4.1C) as compared to PBS-treated animals (median survival: PBS control- 34 days vs. Reo-treated- 47 days). Interestingly, when GEM was added to the Reo regimen, ascites development was further delayed, and even higher survival was promoted (median survival: GEM-treated- 39.5 days; Reo+ GEM-treated- 67 days). These results demonstrate that Reo+ GEM combination can further delay the development of the disease pathology and enhance survival in OC-bearing hosts, as compared to Reo (or GEM) treatment alone.

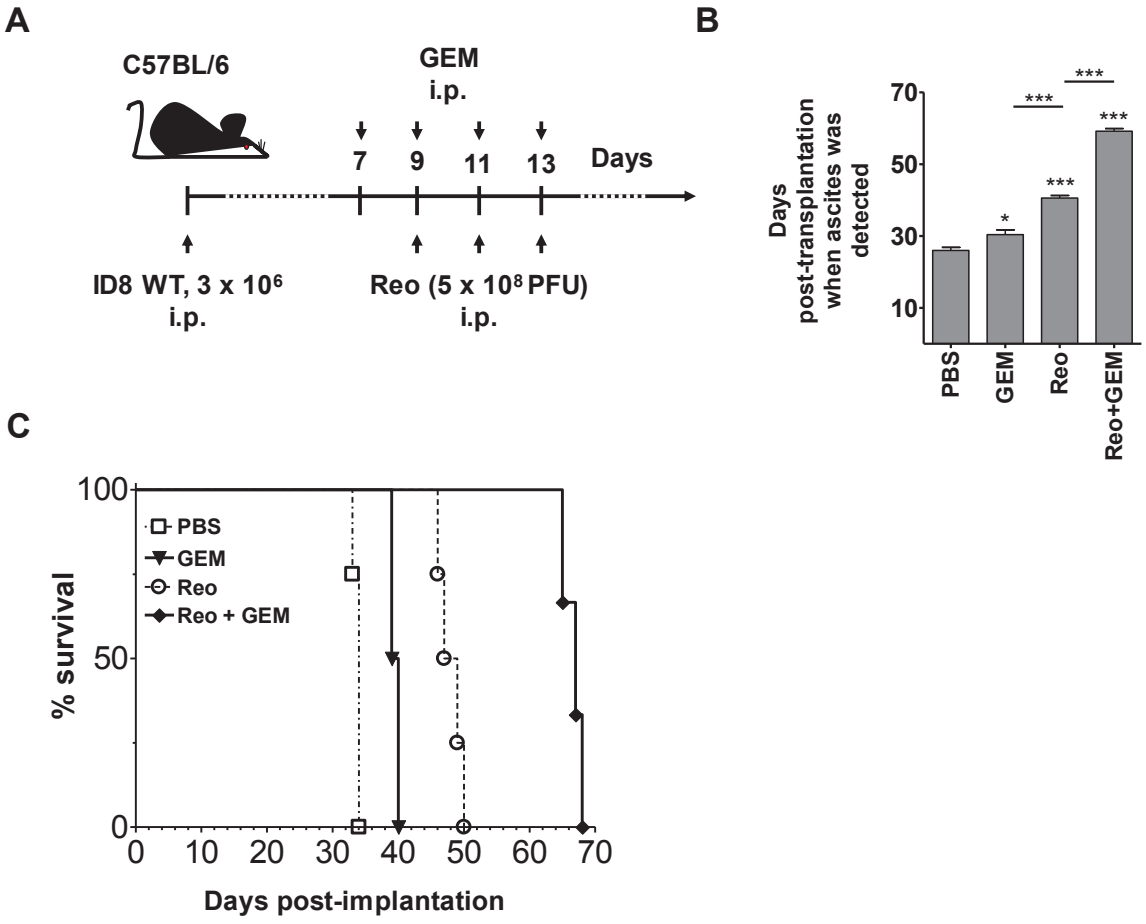

Figure 4.1. *Reovirus and Gemcitabine Combination Treatment Significantly Increases the Survival of Ovarian Cancer-bearing Mice.* (A) Female C57BL/6 mice were implanted i.p. with $3x10^6$ MOSE ID8 cells, injected with a regimen of PBS/GEM/Reo alone or in combination, and then monitored for the development of ascites (B) and survival (C). Survival in respective experimental groups was calculated with the Kaplan-Meier survival method. Results were analyzed with two-tailed, Statistical analysis was performed with one-way ANOVA with Bonferroni post-test; ns = $p > 0.05$; *$p \leq 0.05$; **$p \leq 0.01$; ***$p \leq 0.001$. Asterisks shown immediately on top of the bars represent p values obtained by comparing the respective data against PBS control, while asterisks shown above the horizontal lines display p values obtained through comparison between the indicated groups. Error bars are defined as mean + SD and data are representative of 3 independent experiments.

4.3.2 Gemcitabine Hampers Reovirus Spread and Replication

Since both GEM and reovirus target cancer cells, we first investigated whether the prolonged survival seen in animals described in Figure 4.1 was due to increased cell death. For this purpose, ID8 cells were exposed to either a 0.1 or 1 multiplicity of infection (MOI) of Reo or PBS with or without GEM (1μM, EC_{50} concentration of ID8 cells [Supplementary Fig 4.1]) for 24, 48, and 72 hr. The cultures were monitored for cell death with annexin V and 7-AAD staining using flow cytometry. The results (Fig 4.2A) showed that in general, GEM exhibited significantly greater killing capacity than that induced by Reo alone. At 24 hr post treatment, the Reo+ GEM combination induced more cell death than did either agent alone. However, at or beyond 48 hr post treatment, the levels of cell death induced by the combination were comparable to those caused by GEM alone (approaching 100%).

We next examined whether GEM had a negative or positive effect on reovirus replication, in both total virus production as well as virus released into the medium. As shown in Figure 4.2B, GEM treatment significantly decreased the viral titers of both total virus produced and virus released in a dose dependent manner. Next, utilizing intracellular staining with an anti-reovirus antibody, we carried out flow cytometry analysis to determine if GEM also negatively affects reovirus infection and spread. A comparable number of cells stained positive for reovirus for both Reo (1 MOI) alone or Reo (1 MOI) + GEM treated cultures at 24 hr, suggesting that GEM did not affect initial virus entry or replication at this time point (Fig 4.2C and Supplementary Fig 4.2). Similar observations were also obtained with Reo (10 MOI) alone or Reo (10 MOI) + GEM treated cultures at 24 hr. However, at both 48 and 72 hr time points, cells treated with the Reo+ GEM combination showed significantly reduced reovirus infectivity compared to those treated with Reo alone (for

both 1 and 10 MOI concentrations). The lower percentage of reovirus-infected cells at the 48 and 72 hr time points compared to the 24 hr time point (particularly for the 1 MOI cultures) likely reflects the higher number of dead cells at these later times. In congruence with the flow cytometry data, western blot analysis showed reduced abundance of reovirus proteins in Reo+ GEM treated cells as compared to cells infected with Reo alone at 24, 48, and 72 hr (Fig 4.2D). Collectively, we conclude that GEM negatively affects the spread and replication of reovirus.

4.3.3 Reovirus and Gemcitabine Combination Blocks the Early Recruitment of MDSCs

Since GEM has a negative effect on reovirus replication and release *in vitro*, we speculated that its ability to enhance reovirus efficacy *in vivo* is likely due to its capacity to modulate anti-tumor immune activities. From a mechanistic point of view, GEM is known to affect immune functions through the inhibition of $CD11b^+$ $Gr\text{-}1^+$ cells (MDSCs)[280, 281]. Recently, we have demonstrated that reovirus administration alone in OC-bearing animals induces a significant accumulation of MDSCs in the cancer microenvironment at 3 days post first injection (d.p.f.i.), which eventually subsides at 3 and 10 days post last injection (d.p.l.i.)[1]. Hence, we next determined whether GEM can alter this kinetics of reovirus-induced accumulation of MDSCs. To this end, C57BL/6 mice with ID8-induced ascites were injected with a therapeutic regimen of reovirus and GEM as per the schematic shown in Figure 4.3A and then analyzed for the frequencies of $CD11b^+$ $Gr\text{-}1^+$ cells at 3 d.p.f.i. and 3 d.p.l.i..

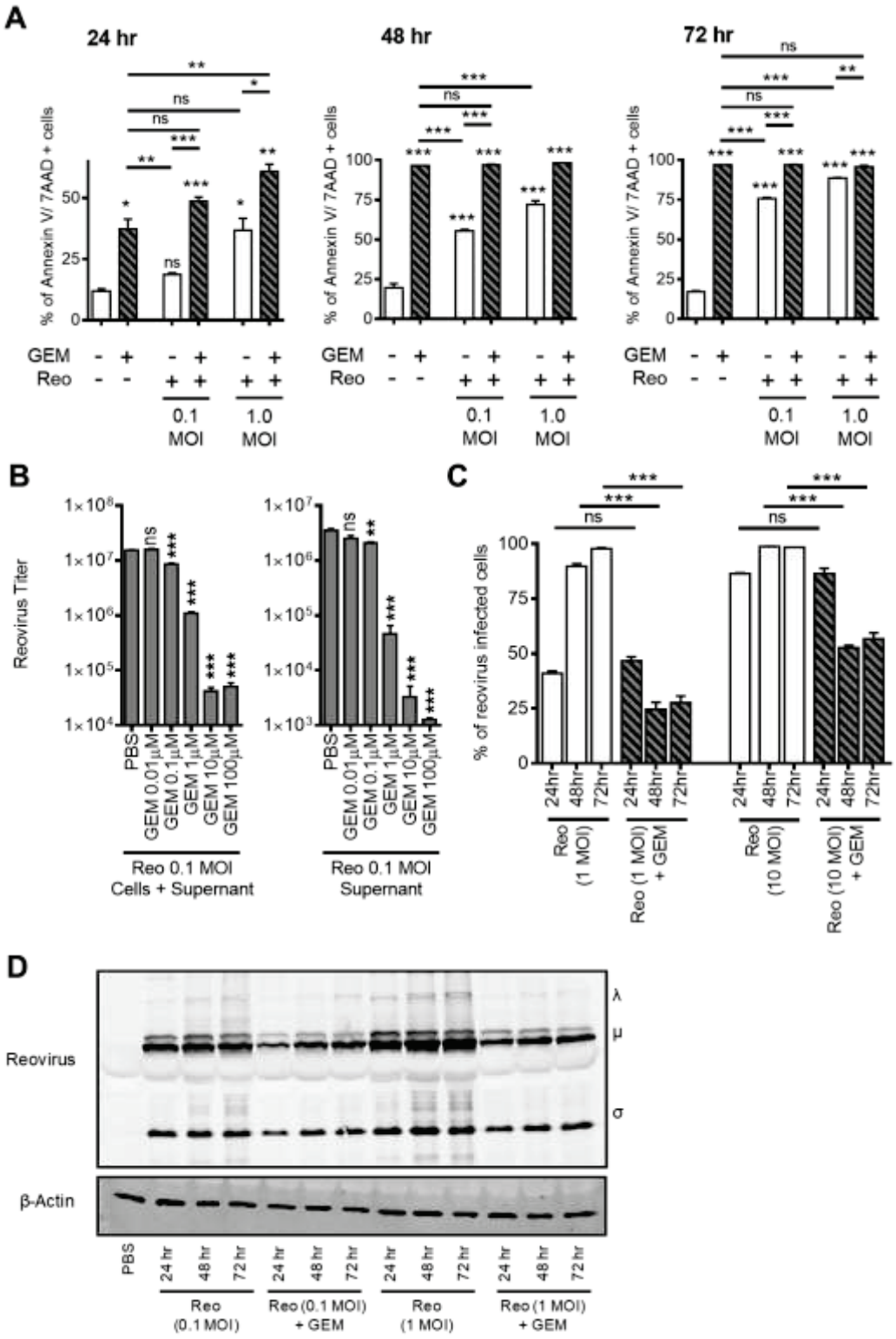

Figure 4.2. *Increased Gemcitabine-induced Cell Death Negatively Affects the Spread and Propagation of Reovirus In Vitro.* (A) MOSE ID8 cells were infected *in vitro* with 1 or 10

MOI of Reo in the presence or absence of 1 μM of gemcitabine and then harvested at 24, 48, and 72 hr and stained with annexin V and 7-AAD (detection of apoptotic cells). (B) ID8 cells were infected with reovirus (0.1 MOI) and treated with various GEM concentrations (0.01, 0.1, 1, 10, or 100 μM). Intracellular and extracellular fractions were collected after 24 hr and assessed by standard plaque assay to quantify viral titers (pfu/mL). (C) illustrates cumulative data on intracellular staining of MOSE ID8 cells with anti-reovirus antibodies to visualize reovirus-infected cells. The cumulative data for all conditions tested as noted. The asterisks shown above the horizontal lines display the *p* values obtained through comparison between Reo and Reo+ GEM groups at the respective time points. Asterisks shown immediately on top of the bars represent the *p* values obtained by comparing the respective GEM-treated group against PBS control. Statistical analysis was performed with one-way ANOVA with Bonferroni post-test; ns = $p > 0.05$; *$p \leq 0.05$; **$p \leq 0.01$; ***$p \leq 0.001$. Error bars are defined as mean + SD. (D) Abundance of reovirus protein in ID8 cells collected after 24, 48, and 72 hr were analyzed by western blot. Data are representative of 3 independent experiments.

As shown in Figure 4.3B, animals injected with Reo alone showed a prompt increase in Gr-1$^+$ CD11b$^+$ cell numbers at 3 d.p.f.i.. However, the Reo+ GEM combination failed to induce this increase. As summarized in Figure 4.3C, Reo+ GEM-treated mice showed significantly lower frequencies of Gr-1$^+$ CD11b$^+$ cells in both the ascites and spleen as compared to animals treated with Reo alone at both 3 d.p.f.i. and 3 d.p.l.i.. GEM alone treatment also caused similarly reduced Gr-1$^+$ CD11b$^+$ cell frequencies at respective time points. Collectively, these results demonstrate that GEM inhibits the early recruitment of reovirus-induced Gr-1$^+$ CD11b$^+$ cells to the tumor microenvironment.

To rule out the possibility that GEM suppresses MDSC recruitment by direct killing of these cells, we isolated MDSCs from the ID8-induced ascites and cultured them in the presence or absence of GEM and Reo, each alone or in combination. Similar to other publications[280, 281], we have found that harvesting tumor-associated MDSCs in standard *ex vivo* culture media resulted the spontaneously death of the majority of the tumor-associated MDSCs within 24 hrs. However, with the supplementation of cell-free ascitic fluid, we were able to significantly reduce the spontaneous apoptosis of tumor-associated MDSCs in a dose dependent manner (Supplementary Fig 4.3). Thus, MDSCs collected from the ascites were cultured in 50% cell-free ascitic fluid and treated with the indicated treatments. GEM alone showed similar rates of survival as those cultured in medium only control (Fig 4.3D). Interestingly, MDSCs were effectively killed by either Reo alone or Reo+ GEM treatment. In contrast, MDSCs isolated from the bone marrow of naïve C57BL/6 mice were not significantly affected by Reo alone, GEM alone, or Reo+ GEM treatments (Fig 4.3E). Collectively, our data demonstrate that GEM does not kill tumor-associated MDSCs

directly but rather impedes the recruitment of these cells following therapeutic administration of reovirus in OC-bearing hosts.

4.3.4 Gemcitabine Impairs the Expression of Reovirus-induced Pro-MDSC Factors In Vivo

The survival and pathophysiology of MDSCs is dictated by various immune factors such as TGF-β, IL-1β, IDO-1, GM-CSF, and COX2. Hence, we next analyzed whether GEM can modulate the expression of these pro-MDSC factors during reovirus therapy. For this purpose, the ascites and tumor samples from ID8 cancer-bearing mice (injected as per the schematic shown in Figure 4.3A) were collected at various indicated time points, and then analyzed for the expression of TGF-β, IL-1β, IDO-1, GM-CSF, and COX2 using quantitative PCR (qPCR). As shown in Figure 4.4, the therapeutic administration of reovirus induced significantly greater expression of TGF-β, IL-1β, IDO-1, GM-CSF, and COX2 in the ascites (especially at 3 d.p.f.i.) compared to the levels PBS-treated ID8-tumor bearing animals. In comparison, when similar ascites-bearing animals were treated with Reo+ GEM combination, there was a significant reduction in the expression of all pro-MDSC factors (TGF-β, IL-1β, IDO-1 and COX2) except GM-CSF in ascites. Similarly, significantly lower expression of IDO-1 and IL-1β was observed in the tumor samples collected from Reo+GEM combination treated animals as compared to Reo alone treated animals at 3 d.p.l.i.. Such expression of pro-MDSC factors remained unchanged following GEM alone treatment in both ascites and tumor, except for increased expression of IDO-1 in ascites at both 3 d.p.fi. and 3 d.p.l.i., and GM-CSF in tumor at 3 d.p.f.i.. Collectively, these results show that GEM impairs the expression of pro-MDSC immune factors during reovirus oncotherapy.

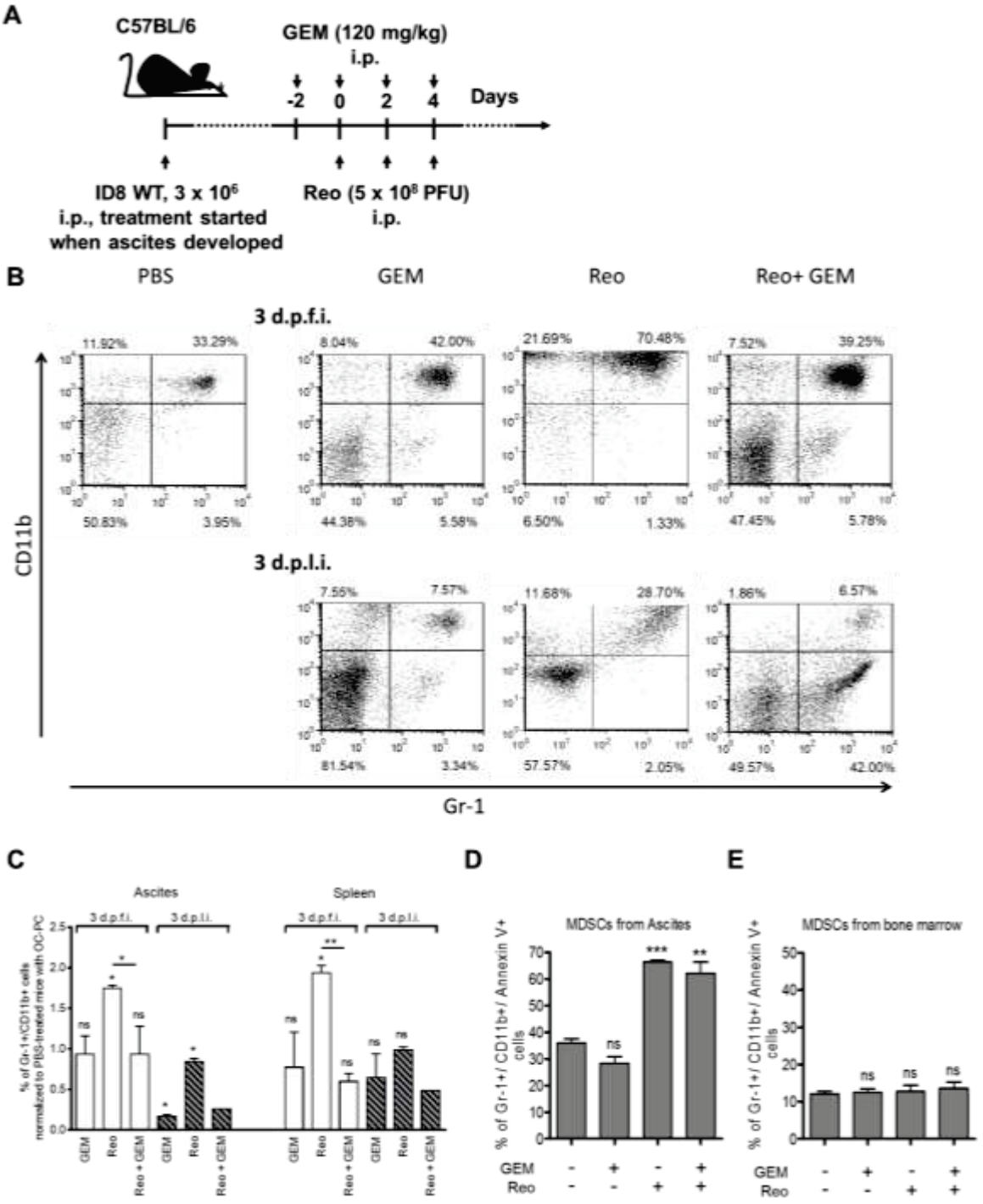

Figure 4.3. *Gemcitabine Blocks Reovirus-induced Early Recruitment of Cancer-associated MDSCs in the Cancer Environment Through Means other than Direct Oncolysis.* (A) Female C57BL/6 mice were implanted i.p. with ID8 cells and then monitored for the development of PC. Then, these mice were injected with a regimen of PBS/GEM/Reo alone or in combination as shown in the schematic. (B) Ascites were harvested and stained to

detect the percentage of MDSCs (Gr-1$^+$/CD11b$^+$ cells) by flow cytometry at the respective time points and as shown in a representative example. The events were collected with the same settings of the acquisition mode in FACSCalibur, demonstrating the gradient of CD11b expression between various samples; however, the statistical data include all relevant events in the analysis. The cumulative data from both the ascites and spleen shown in (C) represent the fold increase/decrease in the percentages of MDSCs after normalizing against PBS-treated control at the respective day post first injection (d.p.f.i.) or day post last injection (d.p.l.i.). The data are representative of n=3 except for Reo+ GEM 3 d.p.l.i. which is n=1. MDSCs were isolated from the ascites of OC-bearing mice and cultured in 50% cell-free ascitic fluid and complete RPMI 1640 media (D), while those isolated from the bone marrow of naïve mice were cultured in complete RPMI 1640 media (E). Isolated MDSCs were then treated with Reo (1 MOI) and GEM (1 μM) alone or in combination as indicated. Cells were harvested at 24 hr and stained with anti-Gr-1 and anti-CD11b antibodies along with the apoptosis marker annexin-V followed by flow cytometry. Data are representative of 3 independent experiments. Asterisks shown immediately on top of the bars represent *p* values obtained by comparing the respective Reo + PBS, GEM+PBS, and Reo+ GEM-treated groups against PBS control. Statistical analysis was performed with one-way ANOVA with Bonferroni post-test; ns = $p > 0.05$; *$p \leq 0.05$; **$p \leq 0.01$; ***$p \leq 0.001$. Error bars are defined as mean + SD.

4.3.5 Lymphocyte Survival and Functionalities Remain Intact During Reo+ GEM Treatment

Most chemotherapeutic agents are known to cause immunosuppression through adverse effects on lymphocytes. However, our data thus far indicate the beneficial contribution of immunological components in promoting greater survival following Reo+ GEM combination administration in cancer-bearing animals. Hence, we further investigated the effect of GEM and Reo, alone or in combination, on the survival and functionalities of T lymphocytes. To this end, splenocytes from naïve C57BL/6 mice were isolated and incubated in the presence of Reo and/or GEM for 24 hr, and then stained for annexin V along with CD3, CD4, and CD8 T cell markers. As shown in Figure 5A, all analyzed T cell subsets displayed similar rates of survival in the presence of Reo and GEM, either alone or in combination.

Similarly, to monitor the functional competencies of T cells, splenocytes from naïve C57BL/6 mice were isolated and then stimulated with a mitogen (concanavalin A [ConA]) for 24 hr in the presence of Reo and GEM, alone or in combination, and then analyzed for the expression of activation markers (CD69 and CD71) on T cell populations. As shown in Figures 4.5B and 4.5C and summarized in Figure 4.5D, both $CD4^+$ and $CD8^+$ cells displayed comparable frequencies and magnitude of activation in the presence of GEM and Reo, alone or in combination, as compared to those treated with PBS control. Collectively, these data demonstrate that the survival and functionalities of T cells remain unaffected in the presence of Reo+ GEM combination. In the context of our previously published results[1, 98], we have additionally observed that tumor cells treated with Reo+ GEM combination preserve reovirus-induced elevated expression of the molecules involved in antigen processing and presentation (Supplementary Fig 4.4).

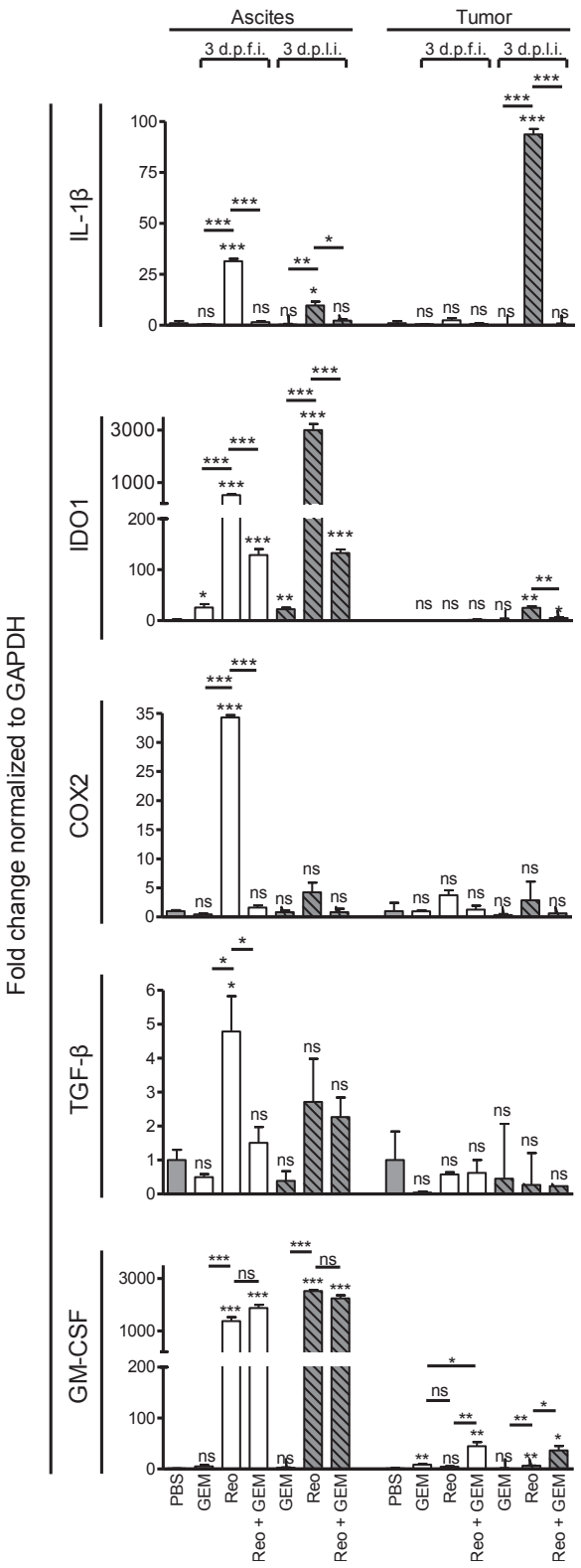

Figure 4.4. *Gemcitabine Impairs the Expression of Reovirus-induced Pro-MDSC Factors in Ovarian Tumors In vivo.* Female C57BL/6 mice were injected as per the protocol shown

in Figure 4.3A, and then sacrificed at the indicated time points to obtain respective tissues. The samples for "ascites" were collected from the cellular contents of the ascitic fluid, while the samples for "tumor" were collected from the solid tumor masses attached to the vasculature in the peritoneum. These samples were processed, RNA was extracted, purified, and reverse transcribed using random primers. QPCR was conducted with gene-specific primers for IL-1β, IDO1, COX2, TGF-β, and GM-CSF followed by analysis using the Livak and Schmittgen's $2^{-\Delta\Delta CT}$ method[330]. Bar graphs illustrate the linear fold change of the indicated mRNA replicates normalized to GAPDH and compared against PBS control. Gene expression data are representative of 3 independent experiments. Statistical analysis was performed with one-way ANOVA with Bonferroni post-test; ns = $p > 0.05$; *$p \leq 0.05$; **$p \leq 0.01$; ***$p \leq 0.001$. Asterisks shown immediately on top of the bars represent the p values obtained by comparing the respective data against PBS control, while asterisks shown above the horizontal lines display the p values obtained through comparison between Reo alone-treated animals and GEM alone or Reo+ GEM-treated animals at the respective time points. Error bars are defined as mean + SD and data are representative of 3-5 mice in each group and the qPCR was completed in duplicates.

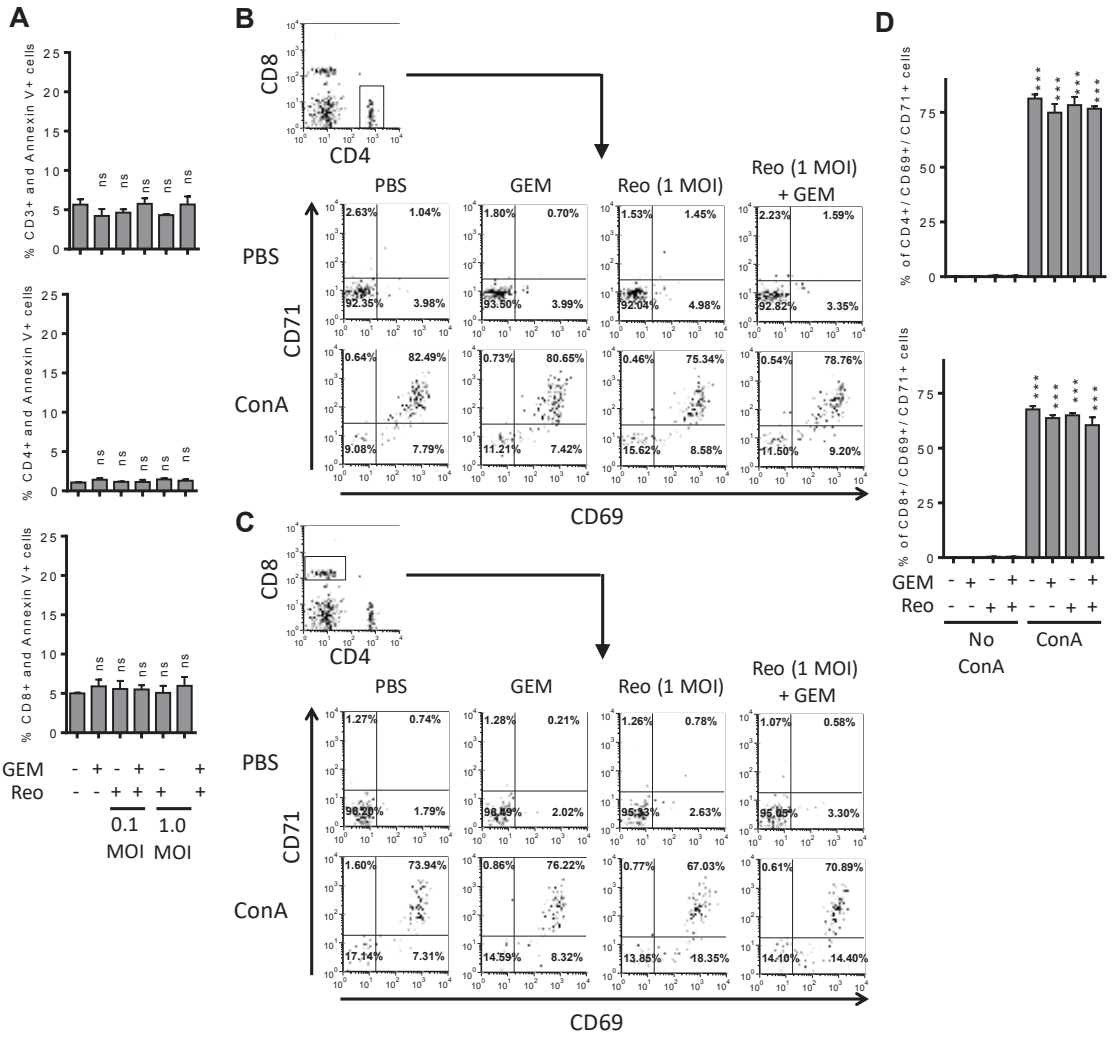

Figure 4.5. *Effect of Reo+ GEM Combination on T Cell Functionality and Survival, and Tumor Antigen Presentation Capacity.* Splenocytes isolated from naïve C57BL/6 mice were stimulated with ConA (2.5 μg/mL) and treated with Reo (1 MOI) and GEM (1 μM) alone or in combination for 24 hr. (A) Splenocytes were harvested and stained with anti-CD3, anti-CD4 and anti-CD8 antibodies along with annexin V and analyzed by flow cytometry. Alternatively, cells were stained with anti-CD4 (B) and anti-CD8 (C) antibodies along with anti-CD69 and anti-CD71 antibodies and analyzed by flow cytometry. (D) Bar graph represents representative data from 1 of 4 independent experiments. Asterisks shown immediately on top of the bars signify the *p* values obtained by comparing the ConA-stimulated groups against their respective ConA-stimulated counterparts, while asterisks shown above the horizontal lines display the *p* values obtained through comparison between ConA-stimulated PBS control and other ConA-stimulated experimental groups as indicated. Asterisks represent the *p* values obtained by comparing the PBS control groups at indicated time points with that of various experimental conditions at respective time points. Statistical analysis was performed with one-way ANOVA with Bonferroni post-

test; ns = $p > 0.05$; *$p \leq 0.05$; **$p \leq 0.01$; ***$p \leq 0.001$. Error bars are defined as mean + SD and data are representative of 4 independent experiments.

4.3.6 Gemcitabine Accelerates the Development of Reovirus-induced Anti-tumor Immunity

Recently, we have demonstrated that the therapeutic administration of reovirus in tumor-bearing animals induces tumor-specific immune responses[1, 105]. Hence, we characterized the status, quality, and magnitude of such reovirus-initiated anti-tumor immunity in the presence of concomitant GEM treatment. To investigate this, ID8 tumor cells expressing a surrogate tumor antigen OVA (ID8-ova) were used. In this model, the capacity of T cells to be stimulated specifically by the immunodominant epitope-containing OVA-peptide (SIINFEKL peptide) indirectly illustrates a quantifiable measurement of an anti-tumor immune response. To this end, lymphocytes were obtained from the ID8-ova-tumor bearing C57BL/6 mice that were injected with a therapeutic regimen of Reo and GEM, alone or in combination (as per Fig 4.3A), and then stimulated *in vitro* with the SIINFEKL peptide to monitor proliferation in $CD3^+$ cells and IFN-γ production in $CD3^+$, $CD8^+$ T cells. As shown in Figure 4.6A and in accordance with our recent observation, lymphocytes from the tumor-bearing animals injected with Reo alone displayed a measurable T cell proliferative response on 3 d.p.l.i., but not on 3 d.p.f.i.. Importantly, tumor-bearing animals injected with Reo+ GEM combination displayed significantly higher magnitudes of proliferation on 3 d.p.l.i as compared to Reo only-treated or untreated animals. A similar pattern was also observed in IFN-γ production capacities of SIINFEKL-stimulated $CD3^+$, $CD8^+$ T lymphocytes (Fig 4.6B). Collectively, these results demonstrate that the addition of GEM to the reovirus therapeutic regimen significantly accelerates the development of a reovirus-induced anti-tumor T cell response of a higher magnitude in cancer-bearing hosts.

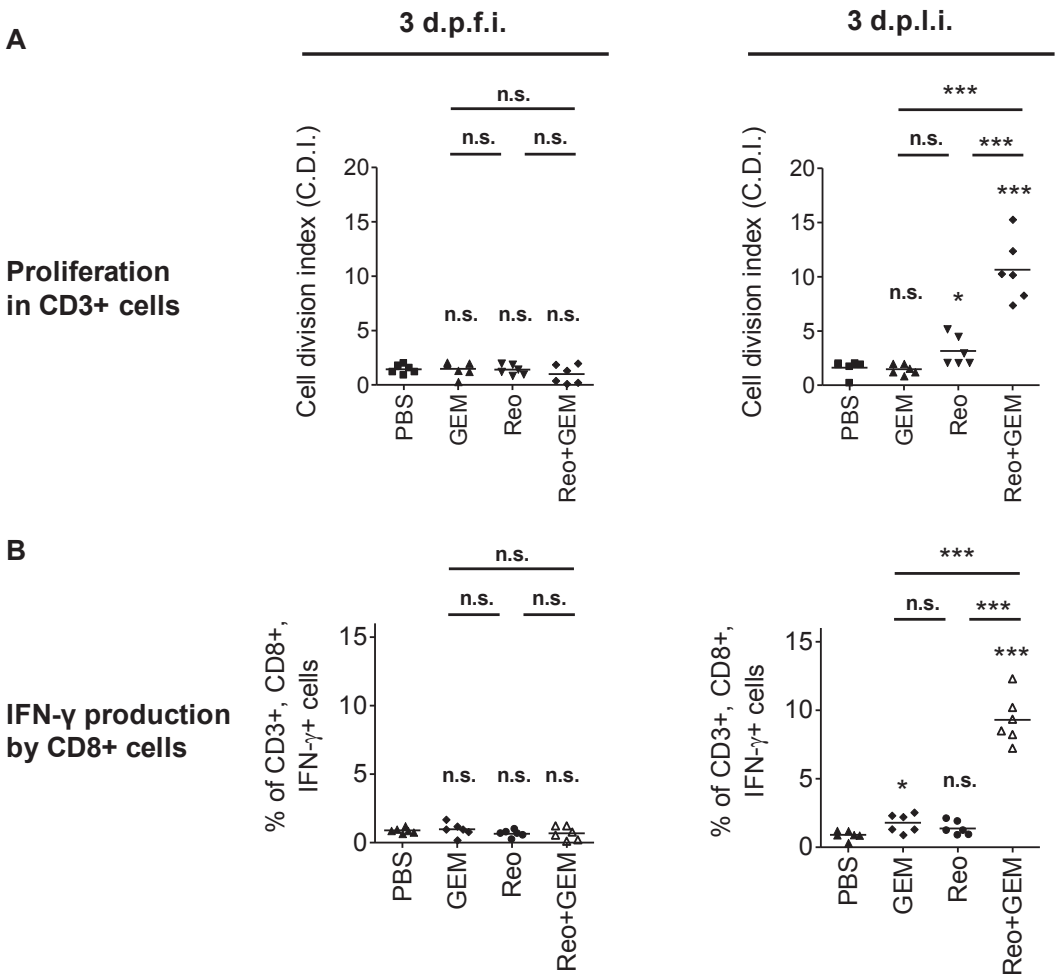

Figure 4.6. *Gemcitabine Potentiates Reovirus-induced Anti-tumor Immune Responses.* C57BL/6 mice were implanted with MOSE ID8-ova cells and then treated with a therapeutic regimen of Reo and GEM, alone or in combination as per the protocol shown in Figure 4.3A. (A) Splenocytes were obtained on 3 d.p.f.i and 3 d.p.l.i., stained with CFSE and then stimulated with SIINFEKL peptide. After 72 hr, cells were stained with anti-CD3 antibodies and then analyzed by flow cytometry for the CFSE fluorescence halving in $CD3^+$ cells to define cell division index. (B) Alternatively, splenocytes were stimulated with SIINFEKL for 18 hr, incubated with brefeldin A for an addition 6 hr, then stained with anti-CD3, anti-CD8 and anti-IFN-γ antibodies and analyzed by flow cytometry. Statistical analysis was performed with one-way ANOVA with Bonferroni post-test; ns = $p > 0.05$; *$p \leq 0.05$; **$p \leq 0.01$; ***$p \leq 0.001$. Asterisks shown immediately on top of the bars signify the p values obtained by comparing the respective data against PBS-treated control group, while asterisks shown above the horizontal lines display the p values obtained through comparison between Reo alone-treated animals and GEM alone or Reo+ GEM-treated animals at respective time points.

4.4 DISCUSSION

It is now acknowledged that the optimum anti-cancer benefits of oncotherapies can be harvested only after managing the effects of the accompanying immunological events. Hence, current scientific efforts have focused on complementing the direct oncolytic properties of these viruses with supplementary interventions that can further potentiate such virus-induced anti-tumor immune activities. Gemcitabine, an FDA-approved anti-OC chemotherapeutic agent known to produce beneficial anti-tumor responses, presents an ideal candidate to fulfill these requirements. We hypothesized that gemcitabine and reovirus can kill cancer cells through their direct oncolytic activities, and further complement each other's capacity to induce anti-cancer immune activities. Gemcitabine was therefore strategically employed in this study to evaluate its potential in promoting the anti-cancer benefits of reovirus therapy.

Our recent report[1] demonstrated that the therapeutic administration of reovirus in ovarian cancer-bearing hosts initiates the accumulation of MDSCs in the ascites as well as spleens during the innate phase of infection (specifically at 3 d.p.f.i.). Interestingly, the elevated levels of MDSCs subsided during the late phase of infection (especially after 3 d.p.l.i-7 d.p.f.i.) and coincided with the appearance of anti-tumor T cell immune activities. Considering the fact that decreased levels of MDSCs correlate with the development of anti-tumor T cell responses, we questioned the functional attributes of MDSC accumulation in the early innate phase. We hypothesized that down-modulation of MDSCs and associated immune effects during the innate phase could accelerate the development of anti-tumor immune activities. Gemcitabine was injected two days prior to, as well as during, reovirus injection regimen. Indeed, gemcitabine efficiently reduced the reovirus-induced

recruitment of MDSCs in the cancer microenvironment. More importantly, this early inhibition of MDSC recruitment was further associated with the development of accelerated tumor-specific T cell response. These data conclusively demonstrate that gemcitabine inhibits reovirus-driven accumulation of cancer-associated MDSCs and accelerates the development of beneficial anti-tumor immune responses.

The pathophysiology of MDSCs is orchestrated by various immune factors, especially those present in the tumor microenvironment[357, 384]. These tumor-derived immune factors drive survival, accumulation, and functionalities of MDSCs and include molecules such as IL-1β, IL-6, IDO-1, TGF-β, GM-CSF, M-CSF, VEGF, COX2 and others (reviewed in Ostrand-Rosenberg *et al.* and Vanneman *et al.*[357, 385]). For example, IL-1β is necessary for the induction, accumulation, and survival of MDSCs in the tumor milieu[386], IDO-1 aids MDSC-mediated depletion of tryptophan that subsequently kills effector T cells[385], and TGF-β promotes the inactivation of T and NK cells[357, 386]. Similarly, tumor cells overexpressing IL-1β, IL-6, and COX-2 are known to induce higher frequencies of MDSCs in the cancer milieu[384]. We observed that during therapeutic reovirus infection, expression of these pro-MDSC factors was first elevated during the early phase (at 3 d.p.f.i.) and then subsided during the late phase (at 3 d.p.l.i.) in the tumor microenvironment. This kinetic was similar to that of the tumor-associated MDSC frequencies. It is hypothesized that reovirus induces MDSCs and pro-MDSC factors during the early phase of infection as an evolutionarily developed mechanism that protects the host against excessive tissue damage driven by virus-induced immunopathology. In the context of oncotherapy, however, these pro-MDSC factors also thwart any immune-mediated attack on tumor cells. Interestingly, GEM restricts the expression of reovirus-induced pro-MDSC factors and establishes

conditions more favourable for the initiation of anti-tumor immunity. As is evident from our data, animals injected with Reo+ GEM developed stronger anti-tumor responses at 3 d.p.l.i., while this event was previously shown to be delayed until 10 d.p.l.i. in Reo alone-treated animals[1]. Collectively, our data suggest that while both reovirus and GEM can kill cancer cells directly, GEM also inhibits reovirus-induced MDSCs, allowing for the accelerated development of anti-tumor immunity and hence, enhanced survival from OC (Fig 4.7).

It would be of great interest to further test our model by carrying out experiments in which one or more components of the immune system (e.g., MDSCs or T cells) is depleted. However, such an approach is impractical as any interventions that down-modulate the immune response would also affect reovirus-mediated oncolysis. We have previously demonstrated that inhibition of T cell responses using anti-CD8 or anti-CD4 depletion antibodies enhances reovirus spread and direct tumor oncolysis[387]. Similarly, the depletion of MDSCs is known to affect viral replication and associated immunopathology[274, 355]. This confounding effect of immune-modulation on reovirus-mediated oncolysis prohibits the use of the "immune cell depletion" approach to delineate the exact contribution of the immune system in anti-tumor response.

In summary, the present study demonstrates the suitability of gemcitabine chemotherapy in conjunction with reovirus-based oncotherapy. We have comprehensively dissected various mechanisms that endow the Reo+ GEM combination with a capacity to induce better outcomes from OC. In the context of current reovirus clinical trials that

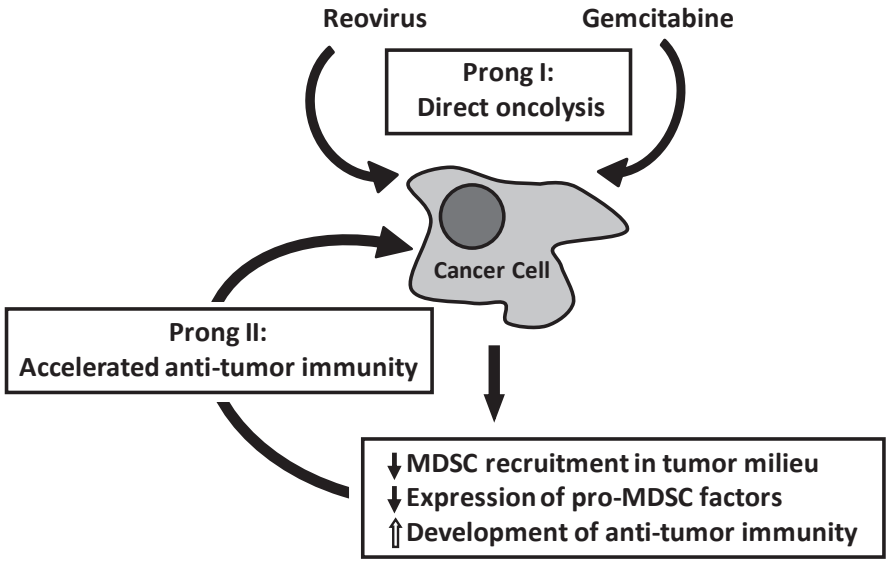

Figure 4.7. *An Illustration of the Various Mechanisms Through which Gemcitabine Enhances the Efficacy of Reovirus-based Oncotherapy*. Reovirus oncotherapy is known to target cancer through two distinct prongs: direct oncolysis (prong I) and virus-induced anti-tumor immune response (prong II). Gemcitabine not only directly kills cancer cells but also enhances the efficacy of reovirus-based therapy through immunological mechanisms, including: 1) inhibition of reovirus-induced MDSC recruitment to the tumor microenvironment, 2) down-modulation of pro-MDSC factors, and 3) accelerated development of anti-tumor immunity.

involve combination therapy with gemcitabine, our findings have important bearings on treatment regimen, efficacy, and patient outcomes.

4.5 CONFLICT OF INTEREST

The authors declared no conflict of interest.

4.6 ACKNOWLEDGEMENTS

This work was supported by an operating grant from the Canadian Institutes of Health Research (CIHR) to P.W.K.L.. S.G. is currently funded by a CIHR Postdoctoral Fellowship, and was funded through Cancer Research Training Program (CRTP) in the past. E.H. received a Norah Stephen Summer Studentship from Beatrice Hunter Cancer Research Institute.

4.7 SUMMARY OF CHAPTER 4 AND TRANSITION TO CHAPTER 5

This chapter illustrates that complementing reovirus-based OV therapy with the MDSC-depleting agent gemcitabine accentuates the immunostimulatory effects of OV therapy and results in enhanced treatment efficacy. Our findings further illustrated that gemcitabine directly impairs reovirus replication and thus, an alternative approach that manipulates reovirus-driven MMCs without affecting reovirus concentration could further enhance therapeutic outcome. Although, the above findings illustrate the immunosuppressive potential of these reovirus-driven MMCs it does not indicate particular signaling pathways which contribute to such immunosuppression. To this end, we felt that such pathways could be identified through the development of a global analytical platform. Thus, the following chapter focuses on the development and application of a novel global mass spectrometry-based platform which can monitor the temporal *in vivo* total proteomic changes of a

particular immune cell population. In particular, we elucidated the function of reovirus-driven MMCs in the context of infection with the ultimate goal to conduct such proteomic investigation of reovirus-driven and tumor-infiltrating MMCs in the future.

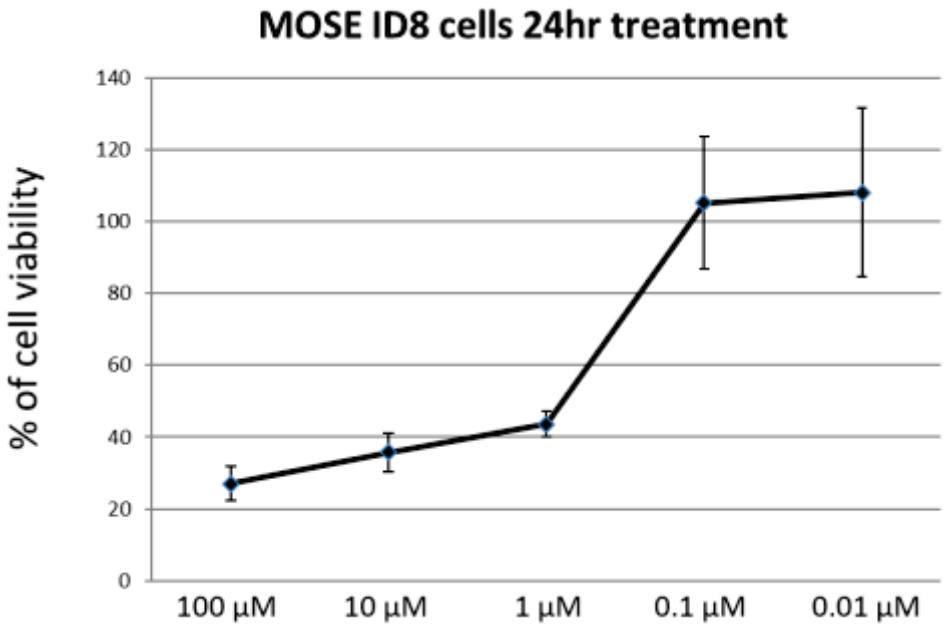

Supplementary Figure 4.1. *MOSE ID8 Cells Have an EC50 of 1 µM of Gemcitabine for the First 24 Hours of Treatment.* ID8 cells were treated with various concentrations of GEM (0.01, 0.1, 1, 10, 100 µM). An MTS assay from Promega (Madison, WI) was performed following the manufacture's instructions. The data illustrate the results of 4 independent experiments.

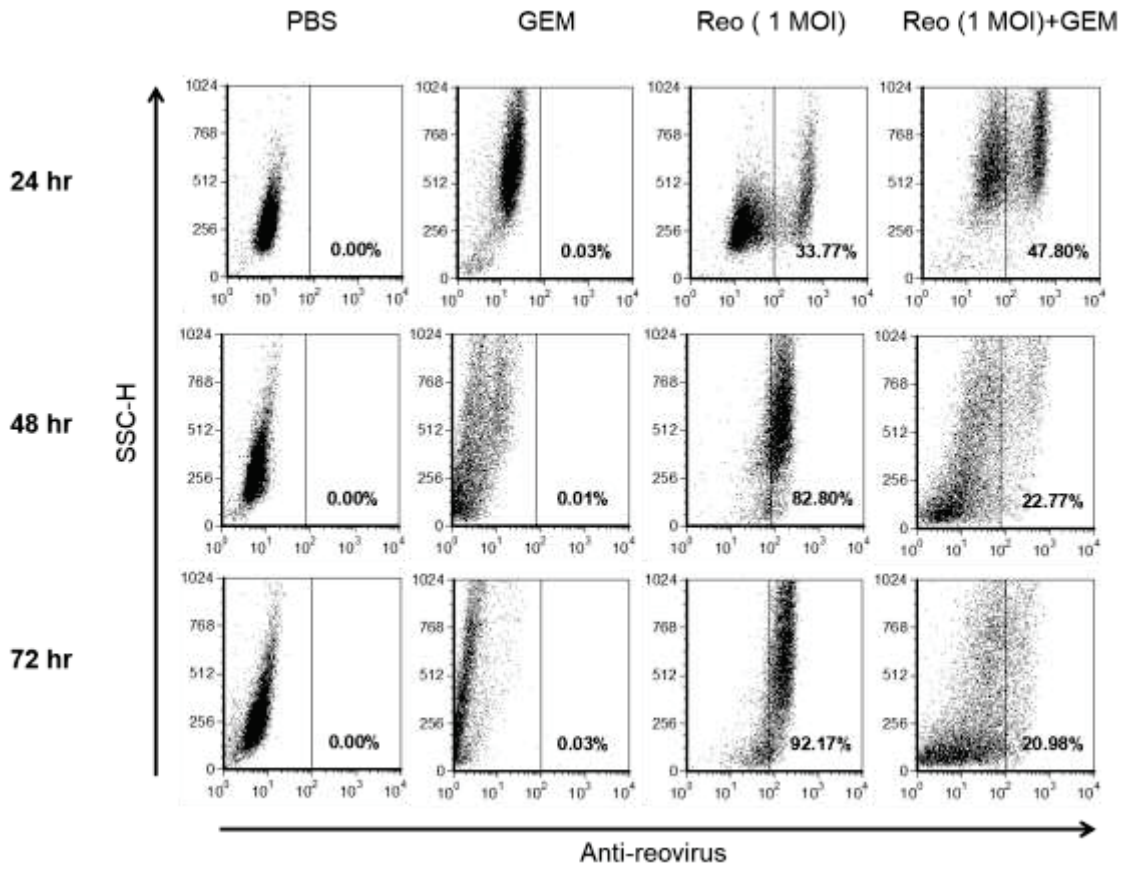

Supplementary Figure 4.2. *Gemcitabine Negatively Affects the Spread of Reovirus In Vitro.* ID8 cells were infected with reovirus (1 MOI) and treated with 1 μM of GEM for 24, 48, and 72 hrs. At the indicated time points, intracellular staining for reovirus positive MOSE ID8 cells was conducted using an anti-reovirus antibody for flow cytometry analysis. The dot-plots illustrated are representative of 3 independent experiments.

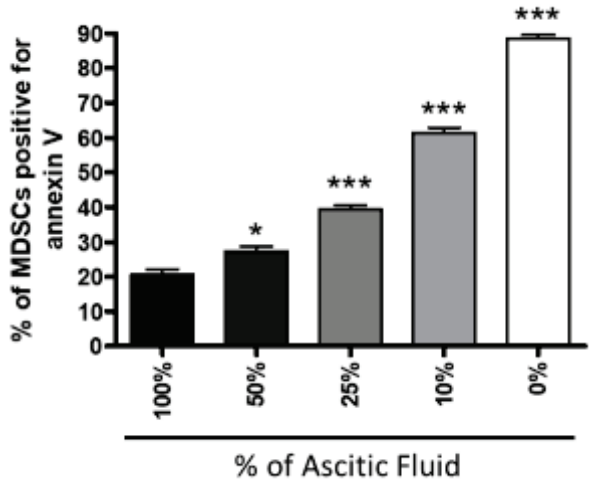

Supplementary Figure 4.3. *Spontaneous Apoptosis of Isolated Tumor-associated MDSCs Can Be Reduced with Increased Percentage of Cell-free Ascitic Fluid.* MDSCs were harvested from the ascitic fluid of late-stage tumor-bearing C57BL/6 mice and isolated using the MDSC isolation kit (Miltenyi Biotec, Auburn, CA) following the manufacturer's instructions. Isolated MDSCs were then plated with increasing percentages of cell-free ascitic fluid. After 24 hr of incubation, the samples were stained with anti-Gr-1, anti-CD11b antibodies and annexin V to monitor spontaneous apoptosis of the isolated MDSCs. Asterisks shown immediately on top of the bars represent the p values obtained by comparing the respective percentage of ascitic fluid to the 100% ascitic fluid control. Statistical analysis was performed with two-tailed, Student's t-test with 95% CI; ns = $p > 0.05$; *$p \leq 0.05$; **$p \leq 0.01$; ***$p \leq 0.001$. Error bars are defined as mean + SD.

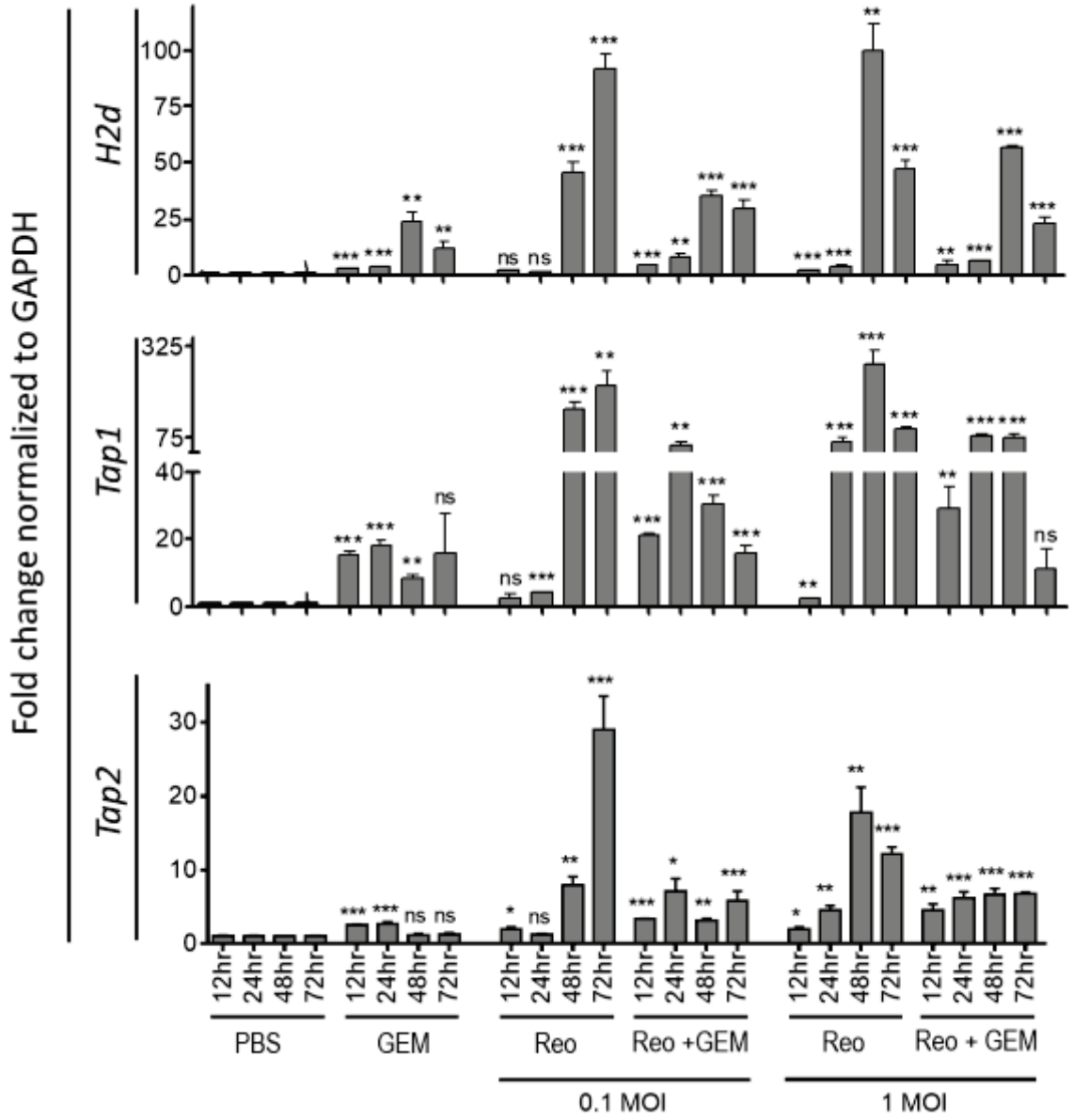

Supplementary Figure 4.4. *Reo+ GEM Combination Preserves Reovirus-induced Expression of Molecules Involved in Antigen Processing and Presentation.* ID8 cells were incubated in the presence or absence of reovirus and GEM, alone or in combination, for 12, 24, 48, or 72 hr, harvested and the analyzed in quantitative real time PCR for the expression of *H2d*, *Tap1* and *Tap2*. Asterisks represent the *p* values obtained by comparing the PBS control groups at indicated time points with that of various experimental conditions at respective time points. Statistical analysis was performed with two-tailed, Student's t-test; ns = $p > 0.05$; *$p \leq 0.05$; **$p \leq 0.01$; ***$p \leq 0.001$. Error bars are defined as mean + SD and data are representative of 4 independent experiments.

CHAPTER 5: QUANTITATIVE TEMPORAL IN VIVO PROTEOMICS (QTIPS) DECIPHERS THE TRANSITION OF VIRUS-DRIVEN MYELOID CELLS INTO M2 MACROPHAGES

This work appears in part in the publication:

Clements DR, Murphy JP, Sterea A, Kennedy BE, Kim Y, Helson E, Almasi S, Holay N, Konda P, Paulo JA, Sharif T, Lee PWK, Weekes MP, Gygi SP, and Gujar SA. 2017. Quantitative Temporal in Vivo Proteomics Deciphers the Transition of Virus-Driven Myeloid Cells into M2 Macrophages. Journal of Proteome Research. DOI: 10.1021/acs.jproteome.7b00425

DC – designed the study, carried out the experimentation, collected and analyzed data, and prepared the manuscript

JPM, AS, BK, YK, EH, SA, NH, PK, JP, and TS – assisted with experimentation and data collection

JPM, MW, PL, SPG, SAG, and PL – assisted with study design and critical review of the manuscript

5.1 ABSTRACT

Myeloid cells play a central role in virus eradication, yet how these cells precisely differentiate throughout the course of acute infections is poorly understood. In this study, we developed a novel quantitative temporal *in vivo* proteomics (QTiPs) platform to capture proteomic signatures of temporally transitioning virus-driven myeloid cells directly *in situ*, thus taking into consideration host-virus interactions throughout the course of an infection. QTiPs, in combination with phenotypic, functional and metabolic analyses, elucidated a pivotal role for inflammatory CD11b^{+} Ly6G^{-} Ly6C$^{high\text{-}low}$ cells in the anti-viral immune response and viral clearance. Most importantly, the time-resolved QTiPs dataset showed the transition of CD11b^{+} Ly6G^{-} Ly6C$^{high\text{-}low}$ cells into M2-like macrophages which displayed increased antigen presentation capacities and bioenergetic demands late in infection. We elucidate a pivotal role of myeloid cells in virus clearance and show how these cells phenotypically, functionally, and metabolically undergo a timely transition from inflammatory to M2-like macrophages *in vivo*. With respect to the growing appreciation for *in vivo* examination of viral-host interactions and for the role of myeloid cells, this study elucidates the use of quantitative proteomics to reveal the role and response of distinct immune cell populations throughout the course of virus infection.

5.2 INTRODUCTION

Myeloid immune cell populations are phenotypically dynamic and arise from a common pluripotent hematopoietic stem cell lineage. Following infection, bone marrow (BM)-emigrating immature monocytic myeloid cells, identified in mice as CD11b^{+} Ly6G^{-} Ly6C^{+} cells, are recruited to the site of infection and mediate anti-microbial, as well as inflammatory, functions. Importantly, site-specific environmental cues dictate the

functionality and cellular phenotype of these myeloid cells, ranging from pro-inflammatory to immunosuppressive. It is hypothesized that through temporal transition, these inflammatory immature myeloid cells differentiate into monocytes and macrophages which acquire specific phenotypes, functionalities, and metabolic profiles throughout infection. Such plasticity permits these myeloid cells to be associated with a plethora of pathological conditions including pathogenic infections[248, 253, 388], inflammatory diseases/responses[249, 389], cancer progression[251, 252, 390, 391], and anti-tumor immune responses[250].

Following infection, recruitment and transition of inflammatory $CD11b^+$ $Ly6C^+$ cells are instrumental in *L. monocytogenes*[253], *K. pneumoniae*[248], and influenza virus clearance[254]. Although the exact mechanism of how inflammatory $CD11b^+$ $Ly6G^-$ $Ly6C^+$ cells contribute to pathogen clearance is unclear, it is apparent that these cells are pivotal in both innate immunity as well as adaptive immunity[248, 392]. Thus, an in-depth examination of their transitory, temporal and stage-specific phenotype is necessary to understand the role and function of virus-driven inflammatory myeloid cells.

Changes in immune cell functions during infections are dependent on dynamic proteomic changes over time. Notwithstanding previous technological challenges, comprehensive and temporal characterization of proteomes to understand cellular function is now possible due to recent advancements in multiplex quantitative proteomics[393, 394]. Combined with novel synchronous precursor selection with three-stage mass spectrometry (SPS-MS3) acquisition methods, extremely precise measurements of cellular proteomes are now possible[395, 396]. Although proteomic analysis has previously captured single time-point "snapshots" of *in vivo* cell populations, *in vivo* dynamics of immune cell populations have not been explored. Here, we report a quantitative temporal *in vivo* proteomics (QTiPs)

approach, which combines SPS-MS3-based 10-plex quantitative proteomics with flow cytometry-based cell sorting to precisely capture temporospatial proteomic changes of newly recruited, transitory CD11b^{+} Ly6G^{-} Ly6C$^{high-low}$ cells during reovirus infection.

Reovirus is a benign, enteric, human dsRNA virus that drives an acute viral infection and is readily cleared by an immuno-competent host[123]. In addition to its use as a model of acute infection, reovirus is known for its potent preferential cancer-killing (also known as oncolytic) activities, and is being tested as a therapeutic oncolytic virus in phase I, II, and III clinical trials internationally for the treatment of a variety of tumors[103, 124, 126, 132, 135, 397]. In this context, it is now clear that immunological events initiated following the administration of reovirus in immuno-competent hosts are an indispensable part of reovirus-based cancer therapy. Thus, a detailed understanding of immunological events initiated following viral infection is pertinent to the therapeutic effectiveness of oncolytic virus-based cancer immunotherapy[6, 101]. Using QTiPs combined with phenotypic, transcriptional, functional, and metabolic validations, we illustrate a temporal transition of reovirus-driven CD11b^{+} Ly6G^{-} Ly6C^{+} cells from their role in innate anti-viral immune response (CD11b^{+} Ly6G^{-} Ly6C^{high} cells) to their acquisition of M2-like macrophage phenotype (CD11b^{+} Ly6G^{-} Ly6C^{low} cells) during viral infection. Our QTiPs approach reports a novel platform to elucidate in-depth, quantitative, temporospatial cellular transitions in the context of various patho-physiological conditions *in situ*.

5.3 RESULTS

5.3.1 QTiPs of Virus-induced CD11b^{+} Ly6G^{-} Ly6C^{high} Myeloid Cells

Exposure to pathogens, especially viruses, drives the recruitment of $CD11b^{+}$ $Ly6G^{-}$ $Ly6C^{high}$ myeloid cells that undergo a functional transition at the site of infection. To directly visualize this transition of newly recruited, virus-induced myeloid cells *in situ*, we performed 10-plex quantitative mass spectrometry (MS) on temporally collected, cell-sorted, reovirus-driven myeloid cells. Reovirus induces the accumulation of otherwise absent $CD11b^{+}$ $Ly6G^{-}$ $Ly6C^{high}$ cells at the site of infection as early as 1 day post injection (d.p.i.), which subsequently exhibit a gradual loss of Ly6C expression over time (hence the reference to these cells as $CD11b^{+}$ $Ly6G^{-}$ $Ly6C^{high-low}$ (Fig 5.1A, Supplementary Fig 5.1A, and Supplementary Fig 5.1B). These $CD11b^{+}$ $Ly6G^{-}$ $Ly6C^{high-low}$ cells were sorted from the site of infection (SOI, inflammatory) and the BM (resident) from ten C57BL/6 mice per collection point. QTiPs analysis identified 6634 proteins and quantified 5019 proteins from the *in vivo* harvested and cell-sorted myeloid cell population spanning the course of 10 days in both the SOI and BM (Fig 5.1B, Supplementary Data 5.1). Comparing 10 d.p.i. to 1 d.p.i., SOI-isolated cells contained more proteomic changes (> or < 2-fold) than in the BM myeloid cells (12.69% vs. 5.46%, respectively) (Fig 5.1C). Since the QTiPs dataset provides rich temporal proteomic data, it can be interrogated further to reveal temporally-distinct virus-driven myeloid cell changes over the course of acute infection.

Due to the limited knowledge of the overall proteomic signature of $CD11b^{+}$ $Ly6G^{-}$ $Ly6C^{high-low}$ cells, we first conducted a GO-annotation analysis[333, 334] of all identified proteins in our dataset. The most represented biological processes (BPs) were cellular (including cell cycle, proliferation, recognition, and growth) and metabolic (including catabolic, biosynthetic, and coenzyme) processes pertaining to 33.6% and 20.7% of the overall annotation analysis, respectively (Fig 5.1D and Supplementary Fig 5.1C). As

anticipated, we observed immune system-associated BPs (Fig 5.1D), which encompassed antigen processing/presentation, immune response, and macrophage activation BPs (Supplementary Fig 5.1C). An investigation of BP-associated proteins identified temporal differences between the SOI and BM. For example, immune-associated proteins (complement C4-B, IFN-inducible GTPase 1, and activated macrophage/microglia WAP domain protein [WFDC17]) were predominantly higher in the SOI-isolated cells. Interestingly, unlike complement C4-B and IFN-inducible GTPase which peak in relative abundance at 1 and 5 d.p.i., respectively, WFDC17 increased ~10-fold from 1-10 d.p.i., suggesting a time-dependent discrepancy in immune function (Fig 5.1E). Additionally, numerous cell cycle-associated proteins (e.g., Retinoblastoma-like protein 1) were more abundant in BM-isolated fractions, proposing that cellular proliferation of these myeloid cells is greater in the BM. Since metabolic alterations can contribute to immune cell function/differentiation, we inspected the dataset for metabolic proteins and observed a 2.1- and 8.4-fold induction of lactate dehydrogenase and glutamine synthetase, respectively, from 1-10 d.p.i. in SOI-isolated cells; however, no change was observed within the BM-isolated collections (Fig 5.1E). These changes suggest that SOI-isolated cells develop a more Warburg-like metabolism at 7 and 10 d.p.i.. Collectively, our QTiPs approach successfully captured temporal, quantitative, and spatially comparable proteomes of transitory myeloid cells directly from their *in situ* microenvironment.

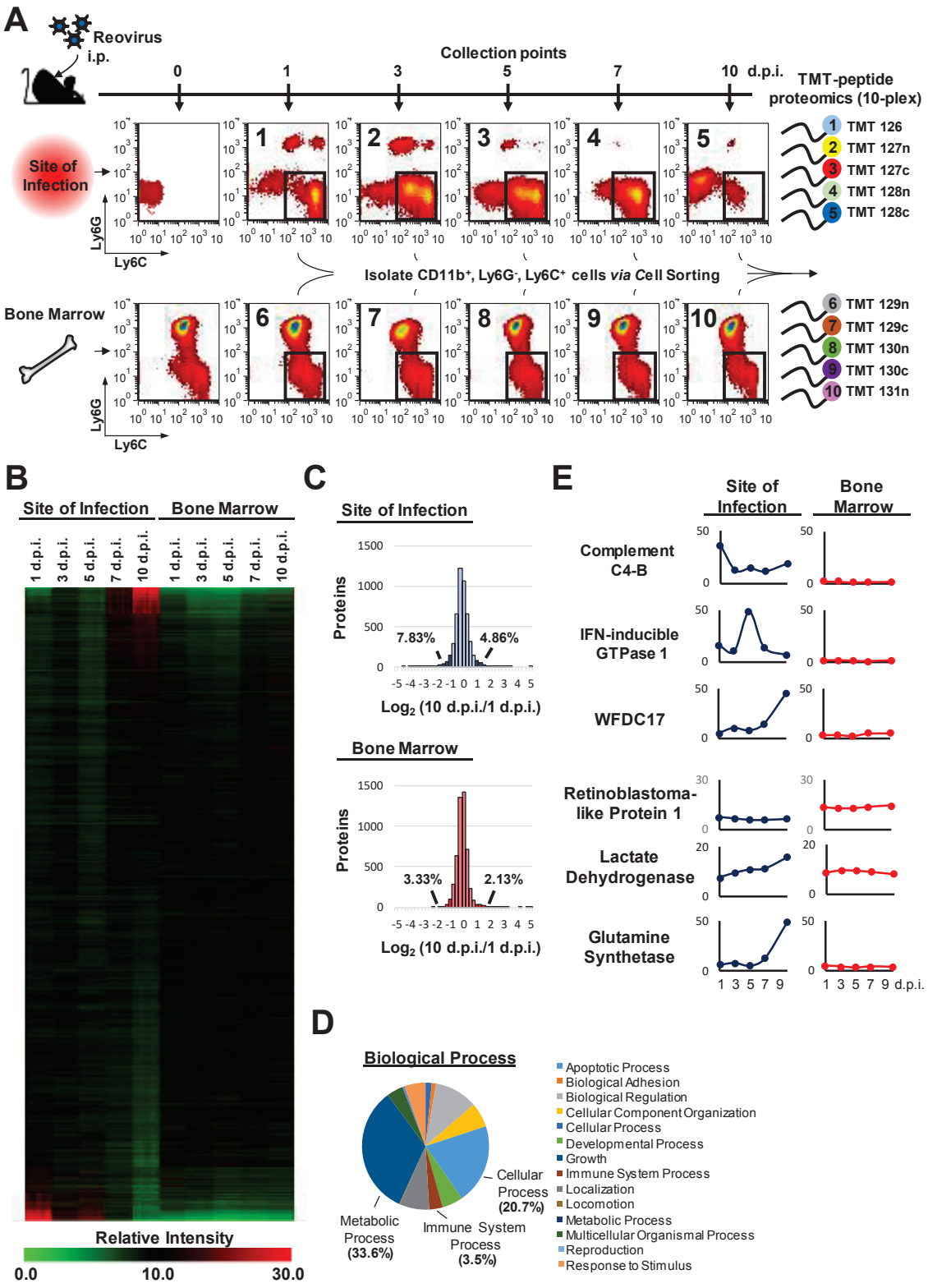

Figure 5.1. *QTiPs Analysis of CD11b^{+} Ly6G^{-} Ly6C$^{high-low}$ Cells Following Reovirus Infection.* (A) Schematic representation of the flow-through for the temporospatial

proteomic approach combining fluorescence-activated cell sorting with TMT-mass spectrometry-based proteomics throughout viral infection (intraperitoneal injection [i.p.]). Dot-plots represent sequential gating strategy and isolated population ($CD11b^{+}$ $Ly6G^{-}$ $Ly6C^{high\text{-}low}$ cells, conserved within the black box) from each collection point from the SOI and BM. A pooled population of $CD11b^{+}$ $Ly6G^{-}$ $Ly6C^{high\text{-}low}$ myeloid cells were isolated from 10 C57BL/6 mice at 1, 3, 5, 7, and 10 d.p.i.. (B) Relative intensity of total quantitative proteomic analysis of $CD11b^{+}$ $Ly6G^{-}$ $Ly6C^{high\text{-}low}$ cells throughout infection in both the SOI and BM. (C) Comparison between total protein levels at 10 d.p.i. to 1 d.p.i. ($\log_2$[10 d.p.i./1 d.p.i.]) of SOI- and BM-isolated cells (D) GO-term enrichment analysis of the biological process terms of total proteomic analysis. (E) Representative protein intensity profiles of selective targets from the highlighted biological process terms (cellular process, immune system process, and metabolic process).

5.3.2 Temporal Transition of Inflammatory CD11b^{+} Ly6G^{-} Ly6C^{high} Cells Aids in Viral Clearance

To understand distinct functions of virus-driven CD11b^{+} Ly6G^{-} Ly6C^{high} cells, we clustered the dataset using k-means clustering, revealing temporally distinct patterns of protein expression. Three of ten clusters contained proteins repressed over the period of 1-10 d.p.i. (Supplementary Fig 5.2). GO-annotation analysis using DAVID bioinformatics[398, 399] of cluster #1 (decreased expression patterns from 1-3 d.p.i.) showed an over-representation of BPs corresponding to response to cytokine stimulus, humoral immune response, defense response (e.g., IFIH1 and CCL2), and steroid metabolic processes (Fig 5.2A-B). Alongside these BPs, serine-type peptidase and endopeptidase inhibitor activity molecular functions (MFs) were over-represented within this cluster (e.g., ZP1 and HRG). In cluster #2 (expression peak at 5 d.p.i.), we observed an over-representation of response to wounding, response to stimulus (hormone and positive regulation) (e.g., CCL7 and CCL12), and endopeptidase inhibitor activity (e.g., SPA3K and MUG1) (Fig 5.2C-D). These data suggest that SOI-isolated cells are early responders to viral infection. Furthermore, cluster #3 represented proteins with a general elevated relative intensity within SOI- vs. BM-isolated cells. GO-annotation of cluster #3 showed an over-representation of BP-associated categories for the response to virus (e.g., RSAD2 and TLR3), response to wounding, endocytosis, and antigen processing/presentation (e.g., ICAM1 and HA11) (Fig 5.2E-F). Specifically, cluster #3 contained hallmark viral infection-associated immunological targets, such as 2'-5'-oligoadenylate synthase 1A (OAS1A),

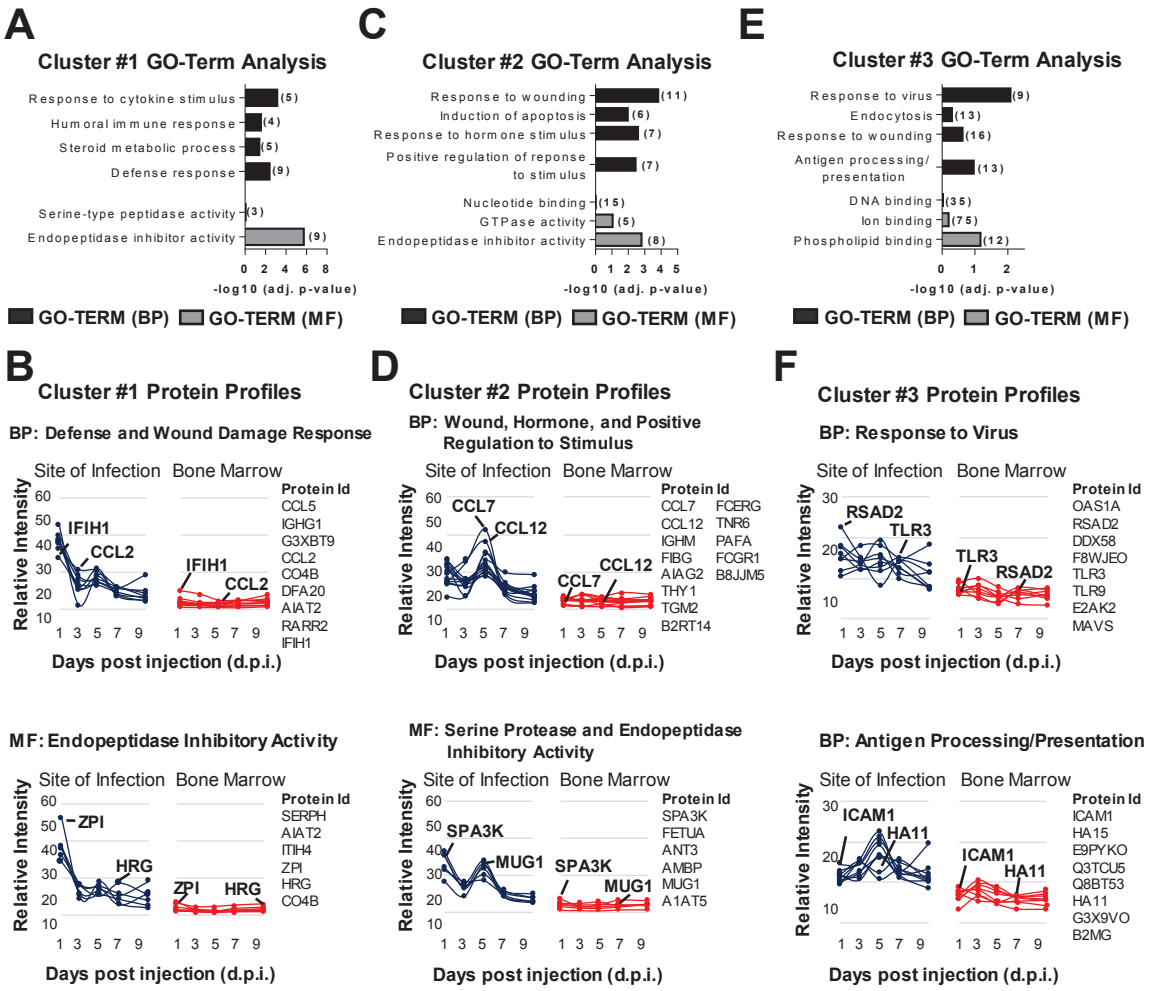

Figure 5.2. *CD11b^{+} Ly6G^{-} Ly6C^{+} Cells Mount an Anti-viral Immune Response Early Following Reovirus Infection.* Cluster #1, 2, and 3 were generated *via* k-means cluster analyses using the Euclidean distance metric and are representative of three of ten clusters of the total proteomic analysis. GO-annotation analysis of biological process (BP) and molecular function (MF) for cluster #1 (A, B), cluster #2 (C, D), and cluster #3 (E, F) using DAVID bioinformatics, summarized in bar graph and represented as individual protein profiles for the indicated GO-Terms. Bar graphs illustrate the -log10 (adjusted [adj.] *p*-value) and number of identified targets per GO-Term (in brackets). The above data are representative of a pooled cell-sorted population from 10 C57BL/6 mice per collection time point.

TLR3, TLR9, H-2 Class-I histocompatibility antigen, beta-2-microglobulin, and ICAM1. Collectively, this analysis reveals a time-dependent transition of inflammatory CD11b^{+} Ly6G^{-} Ly6C$^{high\text{-}low}$ cells and suggests a role for inflammatory CD11b^{+} Ly6G^{-} Ly6C$^{high\text{-}low}$ cells in anti-viral immunity.

Considering that reovirus exposure stimulates pattern recognition receptors (PRRs), especially toll-like receptor 3 (TLR-3), and produces a type I IFN response, clusters #1-3 were additionally analyzed using an Interferome database[400]. This analysis revealed profiles for numerous IFN-associated proteins (e.g., ISG20, MPEG1, IFI5A, Q9DCE9, and IRG1) (Fig 5.3A-C). Gene-specific RT-PCR amplification of *Isg56, Cd40, Igtp, Serpina3k, Ccl7, Ifit3, Irgm1, Trafd1,* and *Ifi205a* showed compatible mRNA expression trends with that of their respective protein expression profile from clusters #1-3 (Fig 5.3D). Importantly, temporal changes in IFN-associated protein expression were mostly within SOI-isolated cells as opposed to their BM-isolated counterparts. Categorizing these IFN-associated proteins into type I and II responses emphasizes a predominant type I IFN response from SOI-isolated cells early following infection, in addition to a secondary elevation in type II IFN-associated proteins (shown in cluster #2) (Fig 5.3E). Together, these results suggest that CD11b^{+} Ly6G^{-} Ly6C$^{high\text{-}low}$ cells contribute to a type I and II IFN response following infection.

Based on the temporal IFN response associated with CD11b^{+} Ly6G^{-} Ly6C$^{high\text{-}low}$ cells, we next sought to determine if they affect viral replication. First, we investigated reovirus titers within CD11b^{+} Ly6G^{-} Ly6C$^{high\text{-}low}$ cells (intracellular), as well as those present within the SOI (extracellular). In congruence with the reoviral lambda protein

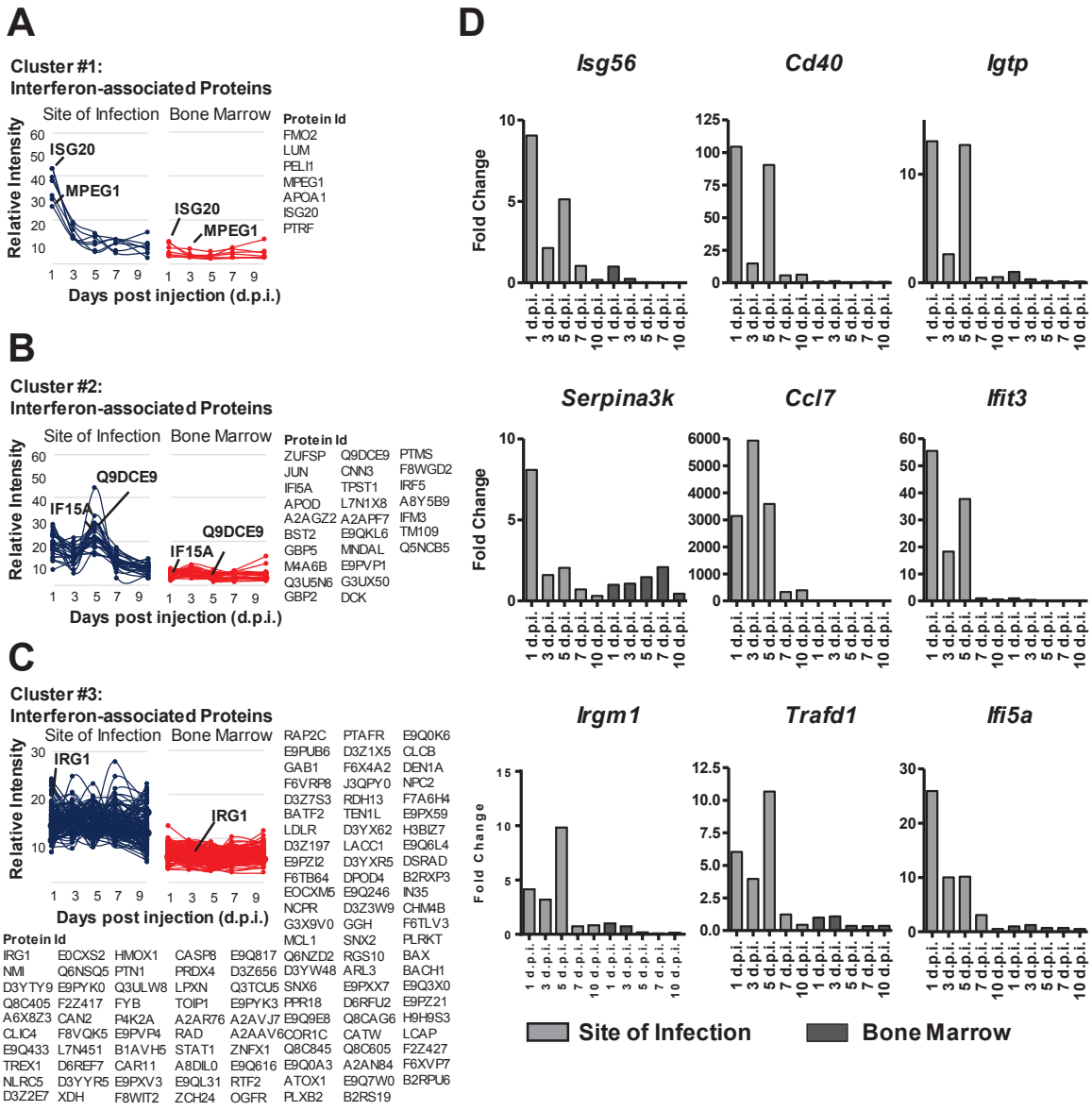

Figure 5.3. *Reovirus-driven CD11b^{+} Ly6G^{-} Ly6C^{high} Cells Display a Predominant Type I IFN Response During the Early Stages of Infection.* Individual protein profiles of selective IFN-associated proteins of cluster #1 (A), cluster #2 (B), and cluster #3 (C) using the Interferome database of annotated IFN-associated proteins. (D) QPCR validation of the indicated genes on isolated CD11b^{+} Ly6G^{-} Ly6C$^{high-low}$ cells. Bars are the representative

mean of n=2 of pooled populations of 5-10 mice per collection time point for both SOI- and BM-isolated cells, ran in duplicate and normalized to GAPDH and compared to 1 d.p.i. BM sample to obtain the fold change. (E) Interferome database of annotated IFN-associated genes from cluster #1-3 were represented in Venn diagram categorized with respect to type I and II IFN.

expression profile captured within the QTiPs data (Fig 5.4A), plaque assay-based analysis for the intracellular and extracellular virus showed the highest viral titers at 1 d.p.i. that steadily declined over the course of 10 days (Fig 5.4B-C). These data demonstrated the ability of inflammatory CD11b^{+} Ly6G^{-} Ly6C$^{high\text{-}low}$ cells to harbor reovirus in a time-dependent manner. In the context of the proposed role for such myeloid cells as oncolytic virus carriers[167, 401, 402], these findings bear clinical relevance.

Since the SOI contains a diverse mixture of immune cells, we wanted to delineate whether the CD11b^{+} Ly6G^{-} Ly6C$^{high\text{-}low}$ cells specifically affect viral persistence. For this purpose, we used a well-documented CCR2 KO mouse model in which the trafficking of inflammatory myeloid cells from the BM to the SOI is defective[253]. Importantly, this characteristic impaired trafficking of inflammatory myeloid cells in CCR2 KO mice is routinely used to identify the contribution of myeloid cells during viral, bacterial, and parasitic infections[254, 392]. Thus, we first conducted comparative frequency/kinetic analysis of reovirus-driven CD11b^{+} Ly6G^{-} Ly6C$^{high\text{-}low}$ cells in wild type (WT) C57BL/6 versus CCR2 KO mice and showed a near absence of CD11b^{+} Ly6G^{-} Ly6C$^{high\text{-}low}$ cell accumulation within the SOI of CCR2 KO mice (Fig 5.4D), confirming the requirement of CCR2 for the recruitment of CD11b^{+} Ly6G^{-} Ly6C$^{high\text{-}low}$ cells at the SOI. No significant frequency/kinetics differences for these cells were observed within the spleen and BM of WT vs. CCR2 KO mice (Supplementary Fig 5.3A). Furthermore, a comparative intracellular virus load analysis on total SOI-collected immune cells illustrated significantly higher titer of replication-competent reovirus in CCR2 KO mice (which contain a lower number of CD11b^{+} Ly6G^{-} Ly6C$^{high\text{-}low}$ cells) as compared to the WT mice (Fig 5.4E) and suggested an anti-viral role for inflammatory myeloid cells. It should

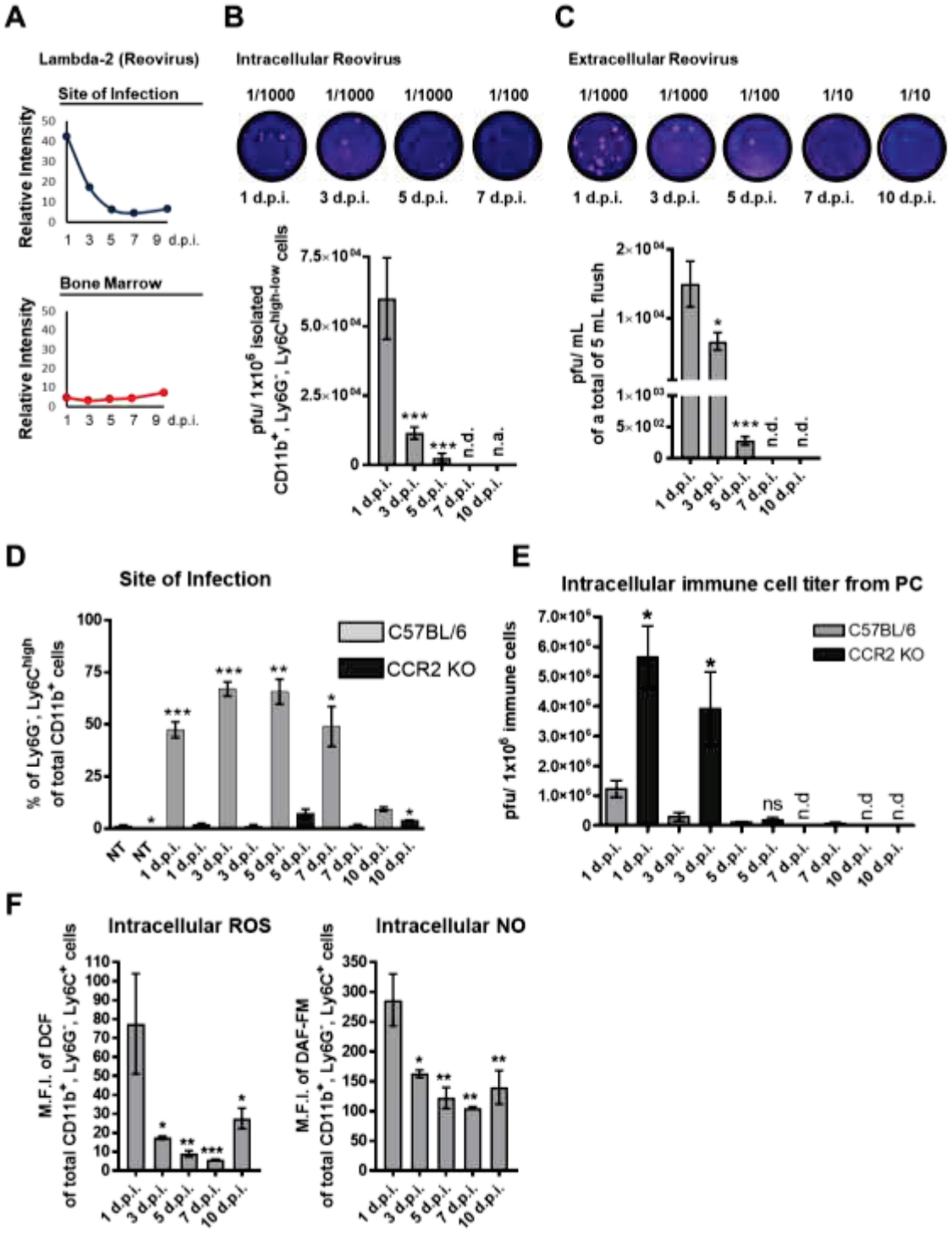

Figure 5.4. *Reovirus-driven, CCR2-dependent Recruitment/Accumulation of CD11b^{+} Ly6G^{-} Ly6C$^{high\text{-}low}$ Cells Hinder Viral Persistence.* (A) Proteomic identification and temporospatial quantitation of reovirus (lambda-2) protein. Temporal reovirus titers from intracellular reovirus (B) in isolated CD11b^{+} Ly6G^{-} Ly6C$^{high\text{-}low}$ cells (pfu/1x10^{6} cells) and

extracellular reovirus (C) collected from the SOI of reovirus-infected animals at the indicated time points. (D) Flow cytometry analysis of $CD11b^{+}$ $Ly6G^{-}$ $Ly6C^{high-low}$ cell frequency/kinetics from the SOI of wild type C57BL/6 mice and CCR2 KO mice. (E) Intracellular reovirus titers (pfu/$1x10^{6}$ immune cells) collected from the SOI of wild type C57BL/6 mice and CCR2 KO mice at the indicated time points post injection. (F) Intracellular staining of ROS (DCF) and NO (DAF-FM) in $CD11b^{+}$ $Ly6G^{-}$ $Ly6C^{high-low}$ cells and shown as mean fluorescent intensity (M.F.I.). Graphs in B-C and E-F are representative of mean +/- SEM with n=5-6 mice per collection. The graph in D is mean +/- SEM and representative of n=30 wild type C57BL/6 mice and n=3-8 CCR2 KO mice per collection point post injection. One-way ANOVA with Bonferroni post-test (B, C, D, and F) or a two-tailed Student's t-test (E) with 95% confidence interval were used for statistical analysis, and p values of <0.05 were considered significant. Asterisks were used to signify p values as follows: *$p \leq 0.05$; **$p \leq 0.01$; ***$p \leq 0.001$.

also be noted that these inflammatory cells also contain the known anti-viral mediators including reactive oxygen species (ROS) and nitric oxide (NO), especially at 1 d.p.i. (Fig 5.4F). Together, these analyses validate the QTiPs-revealed role for CD11b^{+} Ly6G^{-} Ly6C$^{high\text{-}low}$ cells in viral clearance.

5.3.3 Virus-driven CD11b^{+} Ly6G^{-} Ly6C^{high} Cells Acquire Enhanced Antigen Presentation Characteristics

A particularly interesting cluster of proteins showed delayed (7-10 d.p.i.) increased abundance in SOI- but not BM-isolated CD11b^{+} Ly6G^{-} Ly6C$^{high\text{-}low}$ cells (Fig 5.5A, cluster #4). GO-annotation of cluster #4 illustrated an increased peptidase activity (MF) within these cells during the later stages of infection, which included antigen processing/presentation-associated proteins, such as Cathepsin B (CATB) and Cathepsin D (CATD), that are essential to drive an effective adaptive immune response (Fig 5.5B-C)[403]. Go-annotation also revealed an over-representation of MFs of immune effector process, response to wounding (e.g., PERF and ARGI1), homeostatic process, endocytosis, and major histocompatibility complex (MHC)-II antigen processing/presentation (e.g., MRC1 and HG2A) in SOI-isolated cells (Fig 5.5B, D). QPCR-based validation of many of these targets showed consistent temporal gene expression patterns for genes *Mrc1, Pepd, H2-ab1, Cd74, Tpp1,* and *Lip1* (Supplementary Fig 5.3B). Together, our QTiPs data suggested the acquisition of antigen presentation capabilities by inflammatory CD11b^{+} Ly6G^{-} Ly6C$^{high\text{-}low}$ cells late during infection.

To validate this increased antigen presentation capability, we examined MHC-II surface expression on CD11b^{+} Ly6G^{-} Ly6C$^{high\text{-}low}$ cells during infection. Congruent with our proteomics data, these cells demonstrated higher surface expression of MHC-II at 7-10 d.p.i. compared to 3 and 5 d.p.i.; however, it was interesting to note that these cells were

initially recruited with elevated MHC-II expression at 1 d.p.i. (Fig 5.5E). Finally, to demonstrate the antigen presentation capacity, we monitored the ability of virus-driven CD11b^{+} Ly6G^{-} Ly6C$^{high-low}$ cells to present the immunodominant epitope of ovalbumin (OVA; peptide SIINFEKL) in the context of MHC-I. Importantly, CD11b^{+} Ly6G^{-} Ly6C$^{high-low}$ cells showed the highest capacity to present SIINFEKL at 7 d.p.i. (Fig 5.5F). Altogether, our data suggest that inflammatory CD11b^{+} Ly6G^{-} Ly6C$^{high-low}$ cells undergo a phenotypic and functional transition to acquire enhanced antigen processing/presentation abilities during the later stage of infection.

5.3.4 Metabolic Reprogramming Accompanies Inflammatory CD11b^{+} Ly6G^{-} Ly6C$^{high-low}$ Cell Transition/Differentiation

Due to the connection between distinct metabolic pathways and myeloid cell functional capacities and based on the QTiPs-identified induction of proteins regulating metabolism (e.g., LDHA), we also assessed metabolic profiles of transitory CD11b^{+} Ly6G^{-} Ly6C$^{high-low}$ cells. Metabolic-associated proteins (indicated by BPs and cellular compartment GO-annotation analysis) were evident in cluster #5 with an increasing trend from 1-10 d.p.i. in SOI-isolated cells (Supplementary Fig 5.4A-C). We compared our QTiPs dataset to the mouse MitoCarta2.0 dataset[404, 405] to exclusively examine known mitochondrial proteins. Using k-means clustering, we subdivided the total mitochondria-associated proteomic data into various clusters (Mito-clusters #1-10; Fig 5.6A and Supplementary Fig 5.5). GO-annotation analysis of Mito-clusters #1-2 showed an over-representation of proteins involved in cellular response to ROS, fatty acid metabolic process, response to oxidative stress, and generation of precursor metabolites and energy (Supplementary Fig 5.6A).

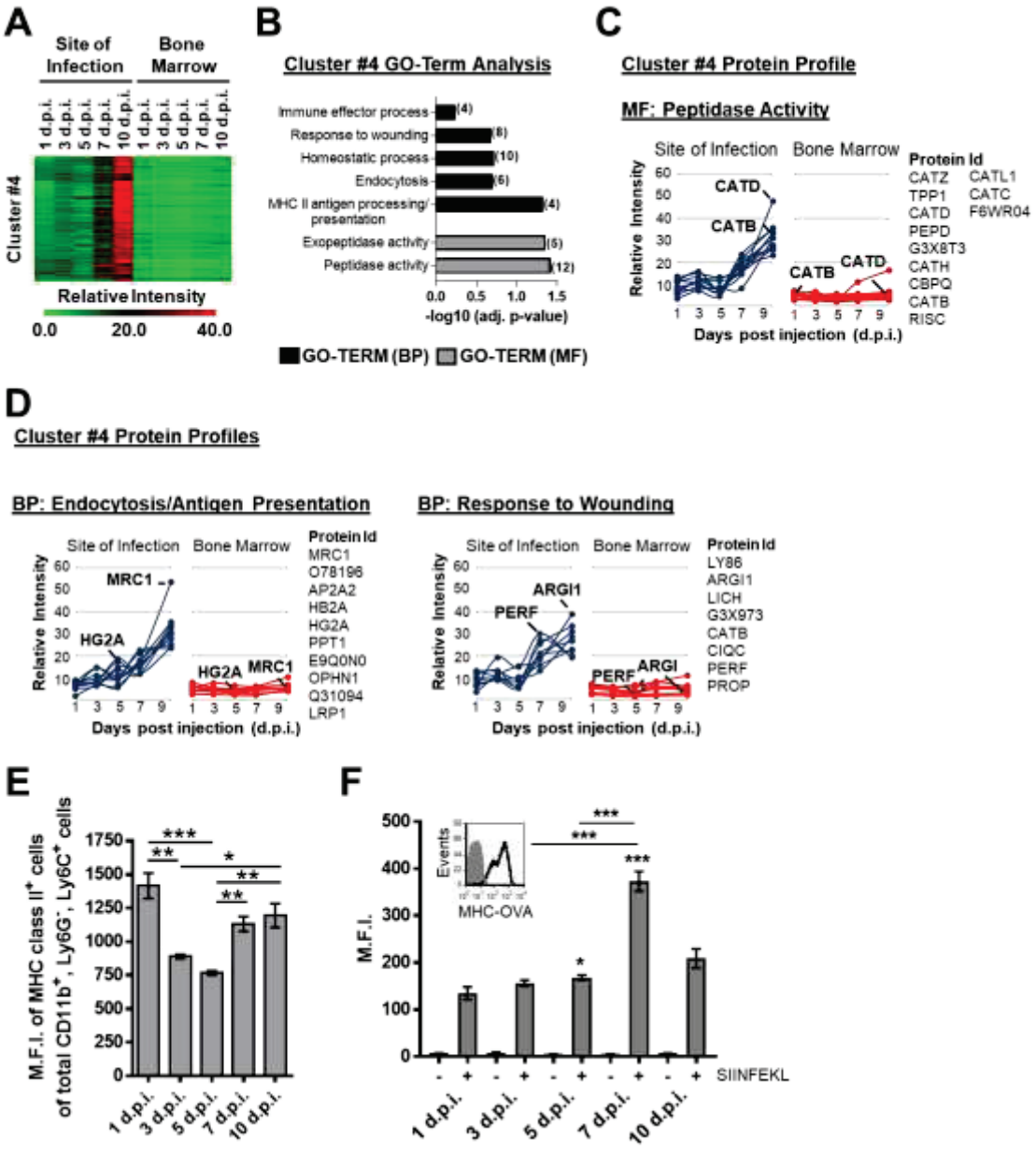

Figure 5.5. *Reovirus-driven CD11b^{+} Ly6G^{-} Ly6C$^{high\text{-}low}$ Cells Acquire Increased Antigen Processing/Presentation Properties at Later Stages of Infection.* (A) K-means cluster analyses with Euclidean distance represented by relative intensity heat map of cluster #4 (1 of 10 clusters) of the total proteomic analysis of CD11b^{+} Ly6G^{-} Ly6C$^{high\text{-}low}$ cells (illustrated in Figure 5.1B). (B) GO-annotation analysis of BP and MF for cluster #4, using DAVID bioinformatics, summarized in bar graph, illustrating the -log10 (adjusted [adj.] p-value), and number of identified targets per GO-Term (in brackets). Individual protein profiles of the indicated MF (C) and BP (D). Flow cytometry analysis of MHC class II (E) and MHC class I-OVA (F) surface expression (represented in mean fluorescence intensity [M.F.I.]) of CD11b^{+} Ly6G^{-} Ly6C$^{high\text{-}low}$ myeloid cells throughout the course of infection.

$CD11b^{+}$ $Ly6G^{-}$ $Ly6C^{high\text{-}low}$ myeloid cells pulsed with OVA peptide (SIINFEKL) were analyzed for MHC class I-OVA at the indicated collection time points. Above experiments (E and F) are the representative bar graphs of mean +/- SEM with n=3-5. One-way ANOVA with Bonferroni post-test (E and F) with 95% confidence interval were used for statistical analysis, and *p* values of <0.05 were considered significant. Asterisks were used to signify *p* values as follows: $*p \leq 0.05$; $**p \leq 0.01$; $***p \leq 0.001$.

KEGG pathway analysis[398, 399] of Mito-clusters #1-2 showed an over-representation of fatty acid metabolism, oxidative phosphorylation, and the citric acid cycle (Supplementary Fig 5.6A); while STRING network analysis[406] further illustrated the interaction of these pathways amongst all metabolic pathway-associated proteins (shown in red) within these clusters (Fig 5.6B). Individual protein profile analysis from Mito-clusters #1-2 of the citrate acid cycle, fatty acid metabolism, and oxidative phosphorylation revealed a general increasing trend from 1-10 d.p.i. (Fig 5.6C). These analyses highlight the metabolic reprogramming of inflammatory $CD11b^{+}$ $Ly6G^{-}$ $Ly6C^{high\text{-}low}$ cells following viral infection.

Since the proteomic data suggested metabolic switch in SOI-isolated $CD11b^{+}$ $Ly6G^{-}$ $Ly6C^{high\text{-}low}$ cells, especially at 7-10 d.p.i., we examined time-dependent cellular bioenergetics (mitochondrial respiration and glycolysis) (Fig 5.6D and Supplementary Fig 5.6B) in isolated $CD11b^{+}$ $Ly6G^{-}$ $Ly6C^{high\text{-}low}$ cells. As shown in Figure 5.6E and Supplementary Figure 5.6C, SOI-isolated cells displayed the highest basal oxygen consumption rate (OCR), ATP production (Supplementary Fig 5.6D), and proton leak (Supplementary Fig 5.6E) at 7 d.p.i., suggesting higher bioenergetic demand at 7 d.p.i.. Concurrently, basal extracellular acidification rate (ECAR) (Fig 5.6E and Supplementary Fig 5.6F) of isolated $CD11b^{+}$ $Ly6G^{-}$ $Ly6C^{high\text{-}low}$ cells were also greatest at 7-10 d.p.i.. Importantly, the opposing trend was observed with spare respiratory capacity (Fig 5.6F), maximal OCR (Supplementary Fig 5.6G), and glycolytic reserve (Fig 5.6G and Supplementary Fig 5.6H), indicating that these cells utilize glycolysis close to their theoretical maximum at 7-10 d.p.i.. These data show that inflammatory $CD11b^{+}$ $Ly6G^{-}$ $Ly6C^{high\text{-}low}$ cells undergo metabolic reprogramming at the SOI and increase both glycolytic and respiratory capacities during the later stages of infection.

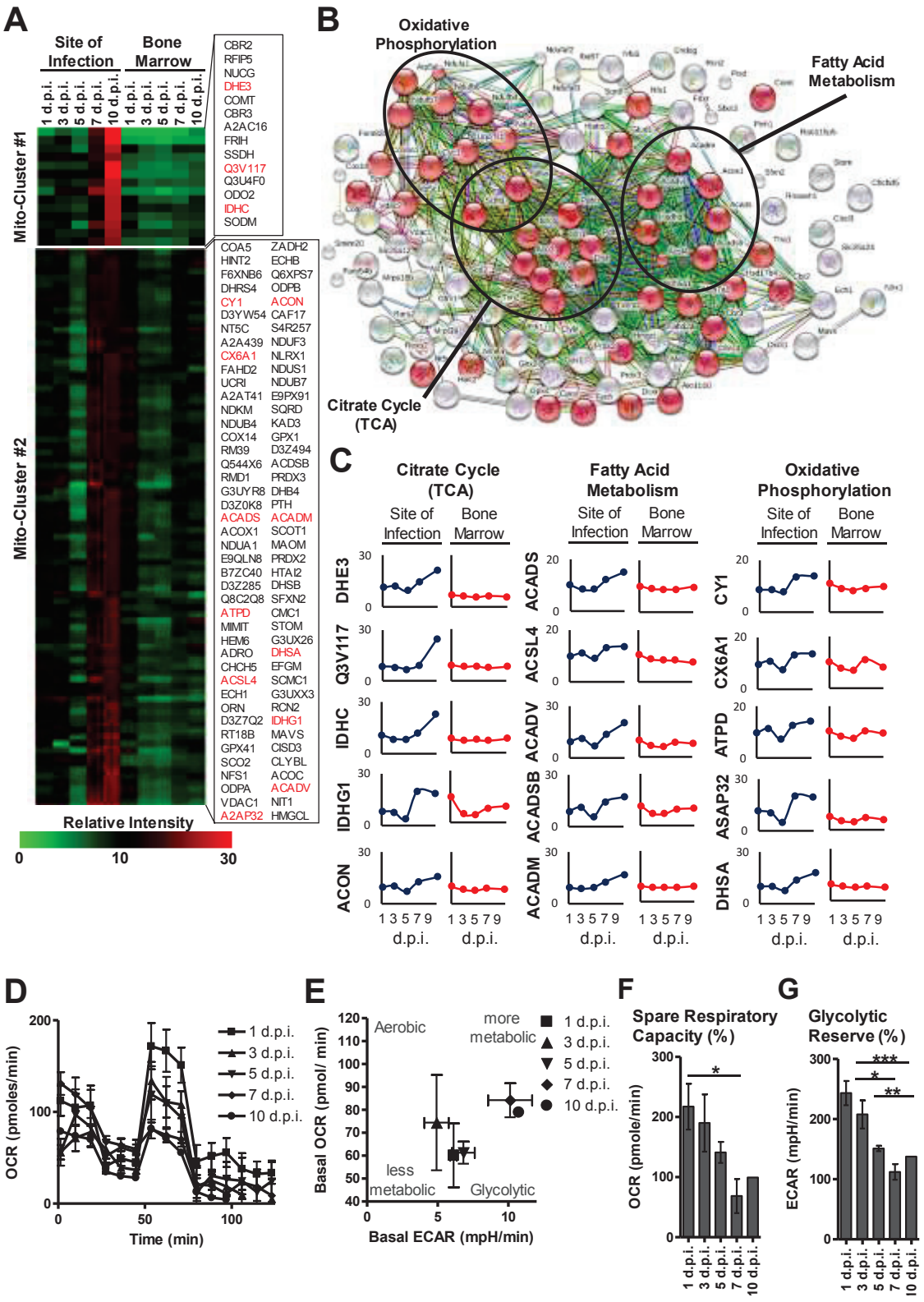

Figure 5.6. *Temporal Metabolic Reprogramming of Inflammatory CD11b^{+} Ly6G^{-} Ly6C$^{high-low}$ Cells.* (A) Comparison of the total proteomic dataset with MitoCarta2.0 dataset to

generate clusters *via* k-means clustering and Euclidean distance analysis. Selected 2 of 10 clusters are illustrated *via* heat map with indicated protein IDs. (B) String Network analysis of Mito-cluster #1 and 2 illustrating metabolic pathway-associated proteins in red and encircled are the identified proteins associated with the indicated KEGG pathway and their interactions. (C) Individual protein profiles (also highlighted in red in [A]) pertaining to the indicated KEGG pathways. (D) OCR of isolated cells for each collection point. Basal OCR and ECAR graphically represented (E) and summarized for the spare respiratory capacity (%) (F) and glycolytic reserve (%) (G). Graphs in D-G are data represented as mean +/- SEM and collected from n=1-4 each with a pooled population from 5-10 mice. One-way ANOVA with Bonferroni post-test (F and G) with 95% confidence interval were used for statistical analysis, and p values of <0.05 were considered significant. Asterisks were used to signify p values as follows: *$p \leq 0.05$; **$p \leq 0.01$; ***$p \leq 0.001$.

5.3.5 Virus-driven CD11b^{+} Ly6G^{-} Ly6C^{high} Cells Acquire M2-like Macrophage Characteristics

It has been hypothesized that immature myeloid cells give rise to antigen-presenting cells (APCs), especially those of monocytic lineage[407]. Our data suggest that the virus-driven CD11b^{+} Ly6G^{-} Ly6C$^{high-low}$ cells undergo temporal transformation and acquire molecular signatures of APCs. Hence, we next investigated whether these myeloid cells differentiate into any specific subtype of APCs. The QTiPs data (Fig 5.7A) identified an increasing trend for proteins (CCL24, ARG1, Alox15, Stab1, and TGF-β) characteristic of M2-macrophages, between 1-10 d.p.i. in SOI-isolated myeloid cells. In contrast, M1-macrophage-associated proteins (IRF5, MMP9, and IRF1) showed the opposing trend (Fig 5.7B). In support of this, flow cytometry analysis of inflammatory CD11b^{+} Ly6G^{-} Ly6C$^{high-low}$ cells further identified contrasting kinetics for the surface expression of M2-macrophage marker CD206 (increased over time; Fig 5.7C) and M1-macrophage marker CCR2 (decreased over time; Fig 5.7D). In line with our metabolic bioenergetics data, these results reveal the transition of inflammatory CD11b^{+} Ly6G^{-} Ly6C$^{high-low}$ cells into M2-like macrophages around 7-10 d.p.i..

To further strengthen our hypothesis that the inflammatory CD11b^{+} Ly6G^{-} Ly6C$^{high-low}$ cells acquire M2-like macrophage characteristics, we performed qPCR on SOI- and BM-isolated CD11b^{+} Ly6G^{-} Ly6C$^{high-low}$ cells. First, we analyzed the expression of key transcription factors *Irf4* and *Irf5* known to be involved in M2- vs. M1-macrophage polarization, respectively[408-410]. As shown in Figure 5.7E-F, SOI-isolated myeloid cells showed contrasting profiles of *Irf4* and *Irf5* between 1-10 d.p.i.; the levels of M2-macrophage transcription factor *Irf4* increased over time while *Irf5* decreased over time. Furthermore, using a list of M2- and M1-macrophage markers[411, 412], we showed that M2-

associated marker *Ccl17* followed a similar trend as *Irf4* (Fig 5.7G), while additional M2-associated genes (*Ym1*, *Cd206*, and *Il4*) displayed mostly non-significant changes (Supplementary Fig 5.7A). Importantly, the expression of M1-associated markers (*Cd86*, *Il-1β, Cd68, Socs1, Tnfα, Ifnγ*) showed an opposing trend throughout infection with decreasing expression from 1-10 d.p.i. (Fig 5.7H). Analysis of M2- and M1-associated genes in the BM-isolated cells showed little significant variation (Supplementary Fig 5.7B-C, respectively). These results, in combination with QTiPs analysis, conclusively demonstrate that the virus-driven CD11b^{+} Ly6G^{-} Ly6C$^{high\text{-}low}$ cells undergo a phenotypic and functional transition at the SOI and acquire the characteristics of M2 macrophages.

5.4 DISCUSSION

Myeloid cells and their descendants, including monocytes, dendritic cells, macrophages, or MDSCs, play pivotal roles in both innate and adaptive immunity during infections. With regards to viral infections, newly recruited Ly6C^{high} monocytes have been implicated in viral clearance following infection by West Nile virus, vaccinia virus, murine cytomegalovirus, and influenza virus[413-415]. These studies demonstrate that viral-driven myeloid cells readily interact with other innate (NK cells) and adaptive cells (virus-specific CD8^{+} T cells)[254, 415], and contribute towards viral clearance as well as disease pathology through direct or indirect mechanisms. For instance, inflammatory myeloid cells recruited following mouse hepatitis virus (MHV) contribute towards virus clearance through a CCR2-depedent mechanism[416]. Further, influenza-mediated CD11b^{+} Ly6G^{-} Ly6C^{high} cell recruitment is a major contributor to excessive collateral damage within the lungs, and the absence of such recruitment compromises viral clearance and decreases the CD8^{+} T cell

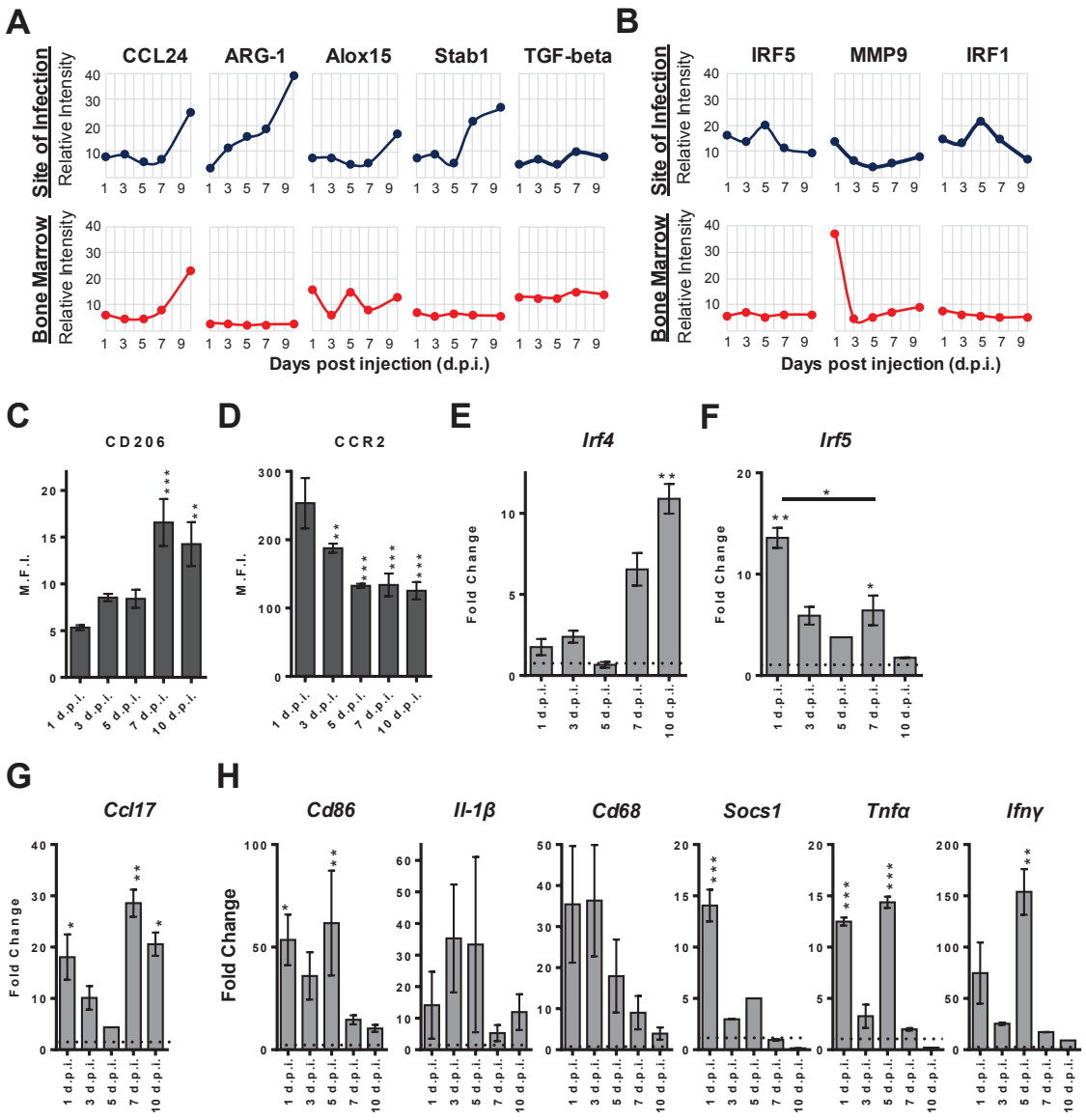

Figure 5.7. *Late Stage Reovirus-driven CD11b^{+} Ly6G^{-} Ly6C^{+} Cells Acquire M2-like Macrophage Characteristics.* (A and B) Individual protein profiles of M2- and M1-macrophage associated proteins, respectively, from total proteomic dataset shown in Figure 5.1B. Flow cytometry analysis of CD206 (C) and CCR2 (D) surface expression on CD11b^{+} Ly6G^{-} Ly6C$^{high\text{-}low}$ cells. QPCR analysis of isolated CD11b^{+} Ly6G^{-} Ly6C$^{high\text{-}low}$ cells for *Irf4* (E), *Irf5* (F), *Ccl17* (G) and M1-macrophage associated genes (H). Flow cytometry analysis for CD206 (C) and CCR2 (D) represent mean +/- SEM with n=3-5 mice. QPCR analysis in (E and F) are from a pooled population of 5-10 mice, n=2, ran in duplicate, normalized to *Gapdh*, and compared to 1 d.p.i. BM sample (indicated by the dotted line) to obtain the fold change. One-way ANOVA with Bonferroni post-test (C-H) with 95% confidence interval were used for statistical analysis, and *p* values of <0.05 were considered

significant. Asterisks were used to signify *p* values as follows: *$p \leq 0.05$; **$p \leq 0.01$; ***$p \leq 0.001$.

frequency[254]. In congruence with these reports, our data demonstrate that the recruitment of reovirus-driven CD11b^{+} Ly6G^{-} Ly6C^{high} inflammatory cells is CCR2-dependent (Fig 5.4D), and that their presence at the SOI positively correlates with viral clearance (Fig 5.4E). Interestingly, at the SOI, intracellular virus is found within cells with or without CD11b^{+} Ly6G^{-} Ly6C^{high} phenotype (Fig 5.4E), suggesting the involvement of other immune cells in anti-viral immune reactivities. Thus, it could be concluded that virus-driven CD11b^{+} Ly6G^{-} Ly6C^{high} inflammatory cells, in combination with other immune constituents, contribute towards virus clearance.

Here, we provide the first comprehensive temporospatial quantitative proteomic analysis of inflammatory CD11b^{+} Ly6G^{-} Ly6C$^{high-low}$ cells, directly isolated from their *in situ* microenvironment. Notably, our QTiPs approach accounts for host environmental factors, such as cytokines, metabolic changes, and immune infiltrating/resident cells, at the SOI. In combination with detailed biological validation, the QTiPs data show that reovirus-driven CD11b^{+} Ly6G^{-} Ly6C$^{high-low}$ cells have differential roles throughout the course of infection. Newly recruited CD11b^{+} Ly6G^{-} Ly6C^{high} cells mount a robust immune response and aid in viral clearance during the early phase of infection (1-5 d.p.i.); while during late phase infection (7 and 10 d.p.i.), these cells undergo a metabolic shift, acquire enhanced antigen presentation capacity, and gain M2-like macrophage characteristics.

Quantitative multiplexed-proteomic approaches (e.g., label-free, tags, or stable isotope labelling) represent an unbiased strategy to observe global proteomic changes and answer key biological questions. With respect to immunological studies, label-free quantitation has been the predominant means to investigate proteomic discrepancies of *ex vivo*

expanded/cultured or transformed cell lines (e.g., cytotoxic T lymphocytes[417], dendritic cells and/or macrophages[418-420]), and primary-isolated cells such as dendritic cell subsets[421], MDSCs[422], and human T cells[423]. Unlike such label-free approaches, tandem mass tag (TMT) reagents now facilitate simultaneous analysis of 10 proteomes. Employing TMT in our QTiPs approach enabled accurate and deep proteomic coverage of *in vivo* proteomic profiles of isolated CD11b^{+} Ly6G^{-} Ly6C$^{high\text{-}low}$ cells. The temporal nature of the dataset revealed a secondary phase of anti-viral/wound damage response at 5 d.p.i., indicative of increased type I and II IFN-associated proteins (e.g., IFI5A, IRF5, IRG1, and Q9DCE9 – an IFN-gamma induced GTPase). IFI5A, in particular, has been shown to be a transcriptional regulatory factor induced during myeloid cell development[424] and may have implications in CD11b^{+} Ly6G^{-} Ly6C$^{high\text{-}low}$ cell differentiation at 5-10 d.p.i.. Furthermore, late stage variations illustrated in cluster #4 and 5 or Mito-cluster #1 and 2 correlate with increased antigen presentation/processing and metabolic shift, respectively. Such temporal fluctuations in the proteomes highlight the advantages of utilizing an approach that monitors the *in vivo* dynamics of an immune cell population. Our QTiPs approach provides a global, timely, and in-depth platform facilitating the capture of immune cell transitions while accounting for the interplay between cytokines and immune cells throughout the course of infection.

Considering the current contentious nomenclature and phenotypic categorization around myeloid cells and its derivative subpopulations[411], we identified virus-driven murine myeloid cells simply by their factual phenotype (based on CD11b, Ly6G, and Ly6C surface expression). To this end, we viewed these myeloid cells as a newly recruited cell population at the SOI, and then analyzed their transition into existing paradigm subpopulations in

terms of surface marker, gene expression, protein, and metabolic profiles. Our temporal analysis unearthed that SOI-associated CD11b^{+} Ly6G^{-} Ly6C^{high} cells undergo a time-dependent decrease in Ly6C expression and display increased MHC-II expression and wound healing characteristics at 7-10 d.p.i., suggesting maturation/differentiation during the later stages of infection. Upon further dissection, we observed that M2-macrophage-associated proteins and transcripts increase at 7-10 d.p.i. as opposed to pro-inflammatory/M1-macrophage-associated markers that are upregulated during the early stages of infection. Similar to myeloid cells, there is a growing appreciation for the plasticity of the distinction between M1 versus M2-like macrophages. It is now acknowledged that macrophages rather demonstrate a spectrum of the phenotypic, functional and physiological features of M1 and M2 classes, and thus often display these features in a context-dependent manner. It should be noted that many of the M1 or M2-associated features have been originally discovered in the context of macrophages that were generated using defined *in vitro* growth conditions, such as through the supplementation of GM-CSF or M-CSF. Thus, it is possible that cells differentiated in the context of the complex *in vivo* milieu hosting a myriad of soluble and cellular interacting partners bear a differential pattern of M1 and M2 markers that is observed compared to the *in vitro* generated macrophages. In our analysis, virus-driven CD11b^{+} Ly6G^{-} Ly6C^{high} cells show several M2-associated markers during the later phases of infection; however, at the same time, these cells failed to show any congruent trends in *Il4*, *Ym1*, and *Cd206* gene expression that have been described to be associated with M2 phenotype. Based on these finding, we surmise that macrophages generated in a complex *in vivo* microenvironment differ from those generated *in vitro* using defined growth conditions and should be considered as such with a special consideration for their microenvironmental context.

The metabolic signature of myeloid cells, particularly macrophages, is a major hallmark to distinguish contrasting M1- vs. M2-macrophage phenotypes[425]. In comparison to this existing paradigm and our own experiments with *ex vivo* generated/cultured M1- and M2-like macrophages (Supplementary Fig 5.7D-E)[425], we observed that $CD11b^{+}$ $Ly6G^{-}$ $Ly6C^{high\text{-}low}$ cells became more metabolically active during the later stages of infection, as indicated by increasing basal OCR and basal ECAR (Fig 5.6D-E). Such metabolic shift could be indicative of the necessity to require energy for newly acquired endocytic, antigen presentation, and/or M2-like functionality. In the context of currently reported metabolic profiles assigned to M1- (low basal OCR, high basal ECAR, and low spare respiratory capacity) and M2- (high OCR, low basal ECAR, and high spare respiratory capacity) macrophages, the infection-driven $CD11b^{+}$ $Ly6G^{-}$ $Ly6C^{high\text{-}low}$ cells demonstrate a dynamic metabolic signature in transition between M1- and M2-like macrophages, in line with the proteomic signature elucidated through QTiPs. This analysis further confirms the highly plastic nature of the myeloid cell-macrophage transition, and in line with recent evidence[426, 427] specifically using lipopolysaccharide/TLR4 stimulation versus IL-4-stimulated BM-derived macrophages, further supports the hypothesis that *in vitro*-generated macrophages do not completely recapitulate all metabolic and functional characteristics of *in vivo*-isolated cells.

In conclusion, QTiPs analysis comprehensively captures the temporospatial transition of inflammatory $CD11b^{+}$ $Ly6G^{-}$ $Ly6C^{high\text{-}low}$ cells following reovirus infection. These data contain a plethora of information on native, as well as infection-driven, myeloid cells that reside in the BM or at the SOI, and are a resource for future hypothesis testing in regard to myeloid-specific differentiation, anti-viral response, and metabolic alteration. The data also

have implications for the therapeutic management of myeloid cells in the context of anti-viral immune responses, vaccine development, cancer immunotherapies, and especially oncolytic virus therapies – which are known to drive myeloid cell recruitment to the tumor microenvironment following administration[2]. Our data also demonstrate that the QTiPs approach can be applied further to precisely capture the complex, dynamic, and temporal nature of other types of immune cells collected from their *in situ* microenvironment.

5.5 ACKNOWLEDGEMENTS

This work was supported by grants from the Canadian Institutes of Health Research (CIHR) and Terry Fox Research Institute (TFRI) to SAG and PWKL. DC, YK, and TS are supported by the CIHR. PM and BK are supported through the Cancer Research Training Program (CRTP) of BHCRI. DC was supported previously by CRTP from BHCRI, and the Nova Scotia Health Research Foundation (NSHRF). Nova Scotia Graduate Scholarships fund both NH and PK. Work by JAP was funded in part by an NIH/NIDDK grant K01 DK098285. MPW was supported by a Welcome Trust Senior Fellowship (108070/Z/15/Z). We acknowledge Devanand Pinto and Ken Chisholm (National Research Council), as well as Alejandro Cohen at the Dalhousie Proteomics Core Facility, and Derek Rowter, and Renee Raudonis at Dalhousie Flow cytometry suites.

5.6 CONFLICT OF INTEREST

None to declare

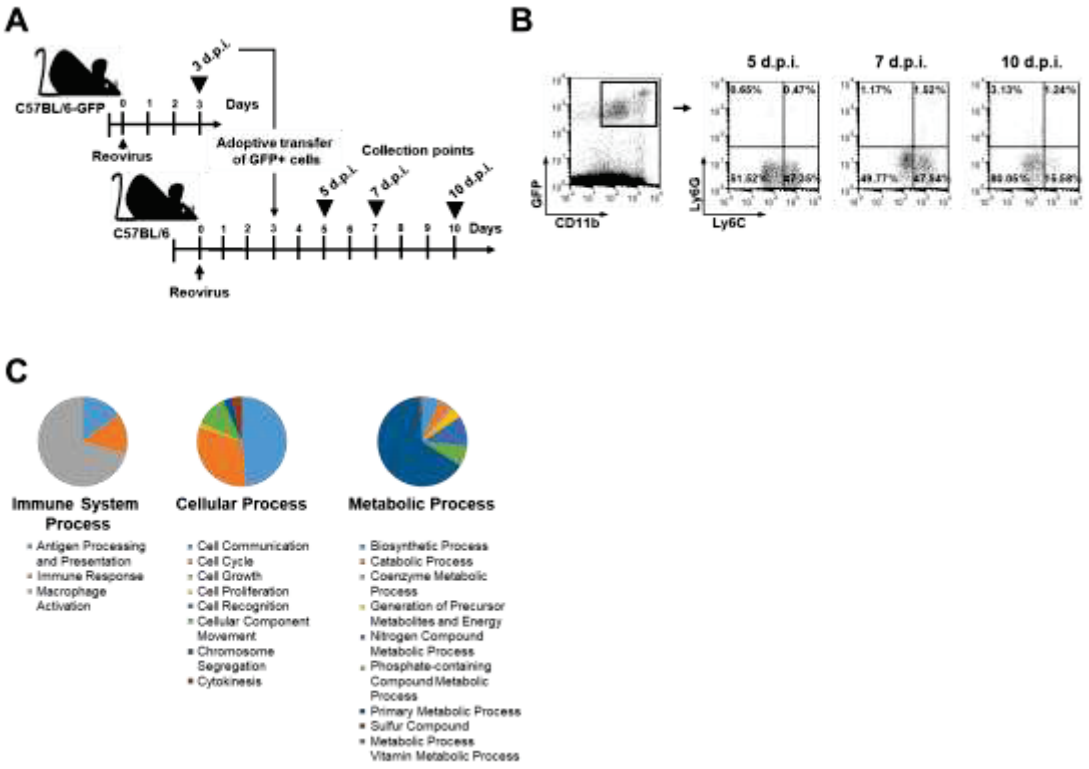

Supplementary Figure 5.1. *Ly6C Surface Expression Loss Throughout the Course of Infection and GO-annotation Analysis.* (A) Schematic layout of the GFP-adoptive transfer experiment to monitor the loss of Ly6C expression. (B) Representative dot-plots of adoptively transferred GFP^+ $CD11b^+$ $Ly6G^-$ $Ly6C^{high\text{-}low}$ cells at 5, 7, and 10 d.p.i.. Gating strategy was $CD11b^+$ GFP^+ cells followed by Ly6G and Ly6C markers. (C) GO-annotation analysis and breakdown of indicated BPs (immune system process, cellular process, metabolic process).

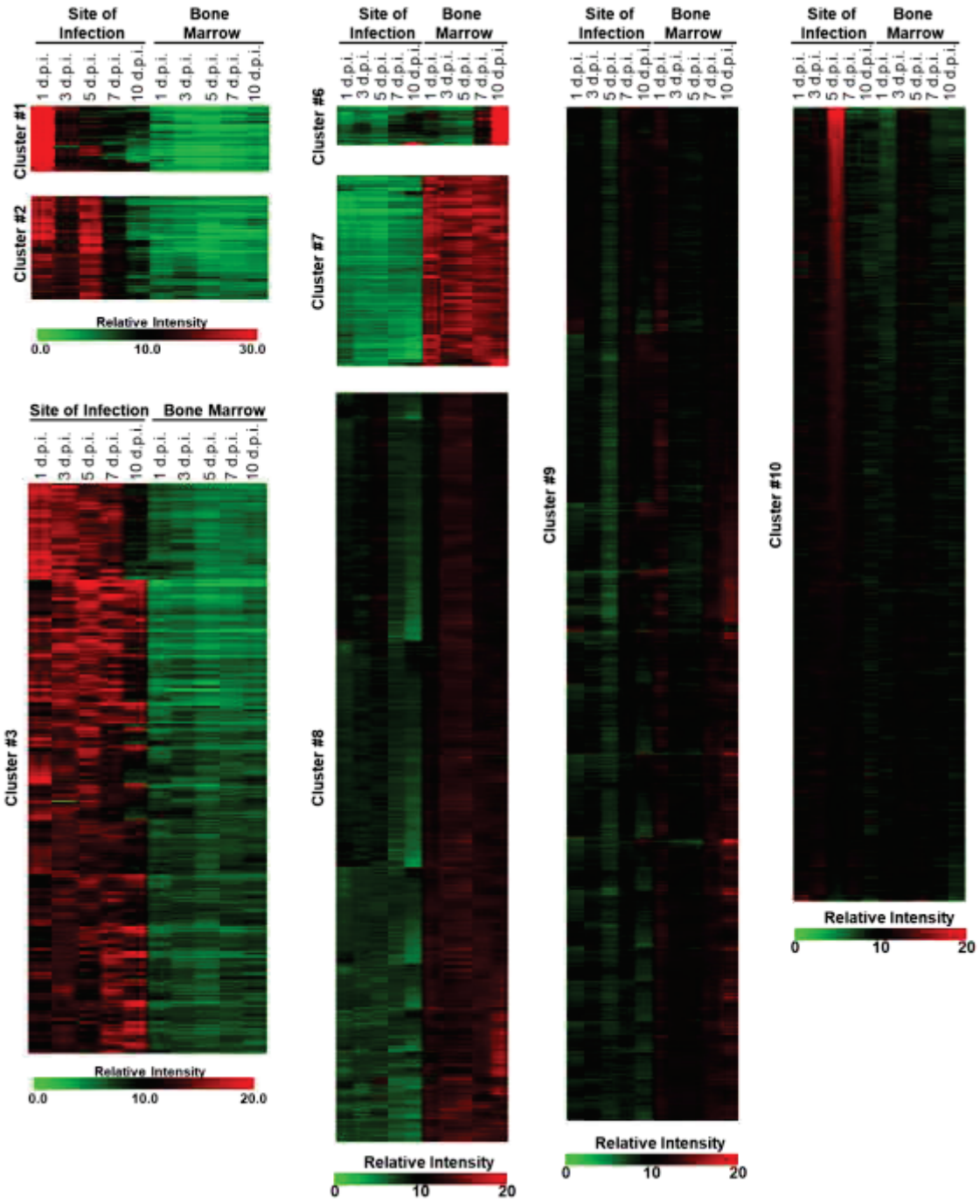

Supplementary Figure 5.2. *Heat map Representation for Clusters #1-3 and 6-10.* Clusters were generated *via* k-means clustering and Euclidean distance analysis of the total proteomic analysis of isolated $CD11b^{+}$ $Ly6G^{-}$ $Ly6C^{high\text{-}low}$ cells.

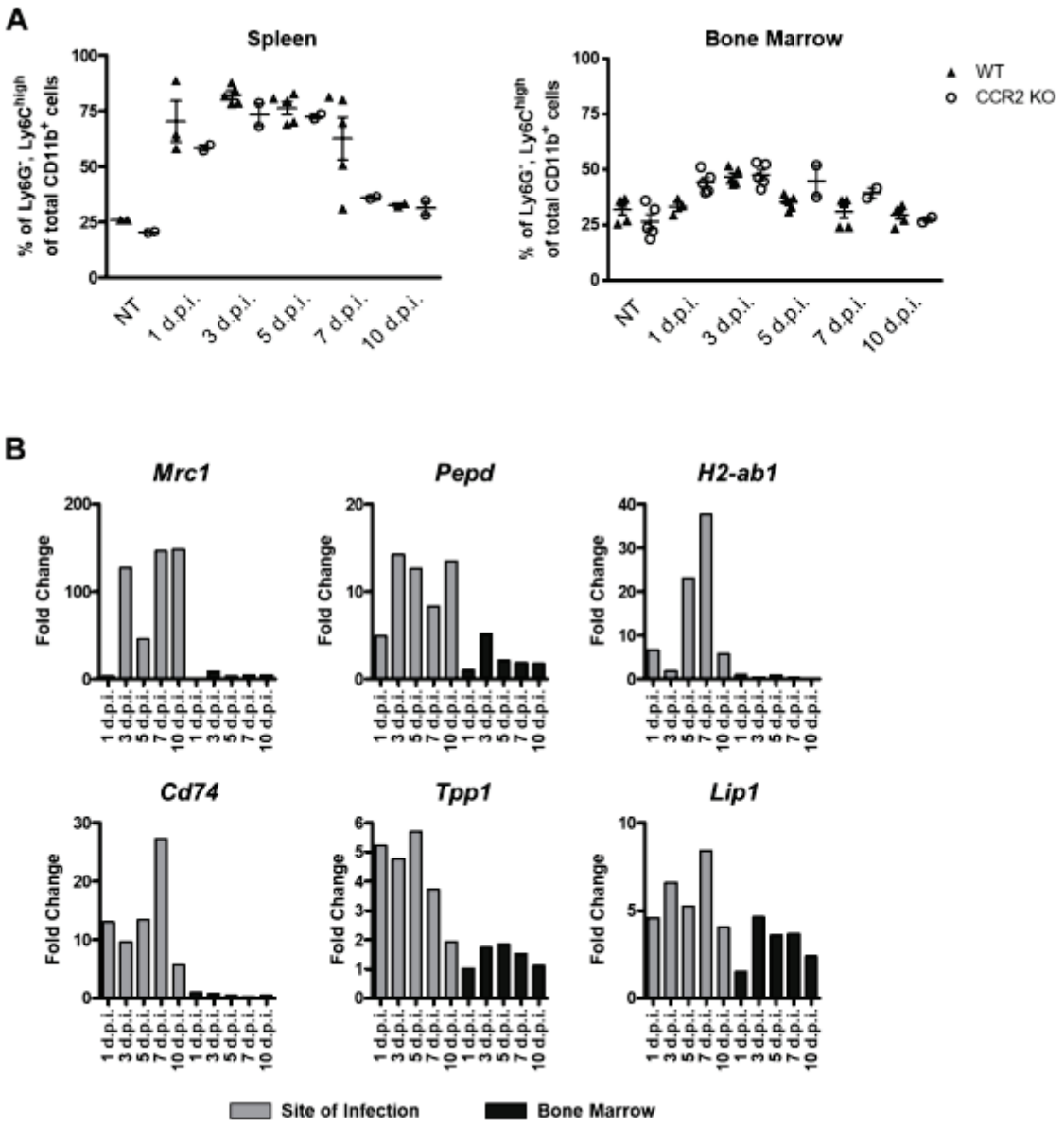

Supplementary Figure 5.3. *Frequency/Kinetic Analysis of WT Versus CCR2 KO Mice for CD11b^{+} Ly6G^{-} Ly6C$^{high\text{-}low}$ Cells and Gene Specific qPCR Validation for Cluster #1-3.* (A) Frequency analysis of CD11b^{+} Ly6G^{-} Ly6C$^{high\text{-}low}$ myeloid cells from the spleen and BM of reovirus-injected mice throughout the course of infection. Graphs are representative of n=30 wild type C57BL/6 mice and n=3-8 CCR2 KO mice per collection point post injection. (B) Fold change of the indicated genes were validated in isolated fractions from both the SOI (gray bars) and BM (black bars) at the indicated d.p.i.. Bars are the representative mean of n=2 of pooled populations of 5-10 mice per collection time point for both SOI- and BM-isolated cells.

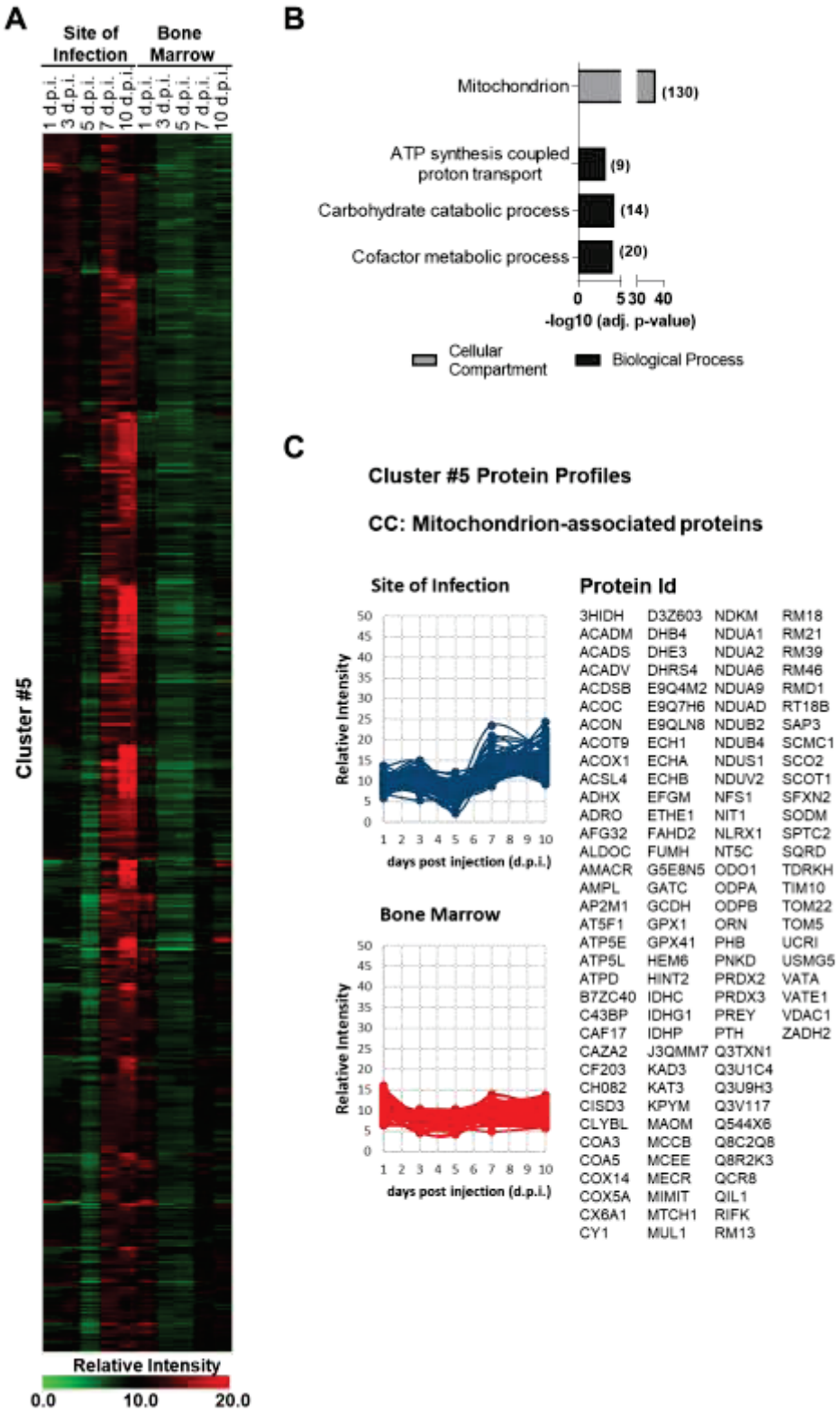

Supplementary Figure 5.4. *Cluster #5 Analysis of Mitochondrion-associated Proteins from the Total CD11b^{+} Ly6G^{-} Ly6C$^{high\text{-}low}$ Cells Proteomic Dataset.* (A) Heat map

representation of cluster #5 generated *via* k-means clustering and Euclidean distance analysis. (B) GO-annotation analysis of BP and cellular compartment (CC), using DAVID bioinformatics, summarized in bar graph, illustrating the -log10 [adjusted (adj.) *p*-value], and number of identified targets per GO-Term (in brackets). (C) Individual protein profiles of mitochondrion-associated proteins, determined by GO-annotation analysis of CC, using DAVID bioinformatics, of cluster #5 in both the SOI and BM.

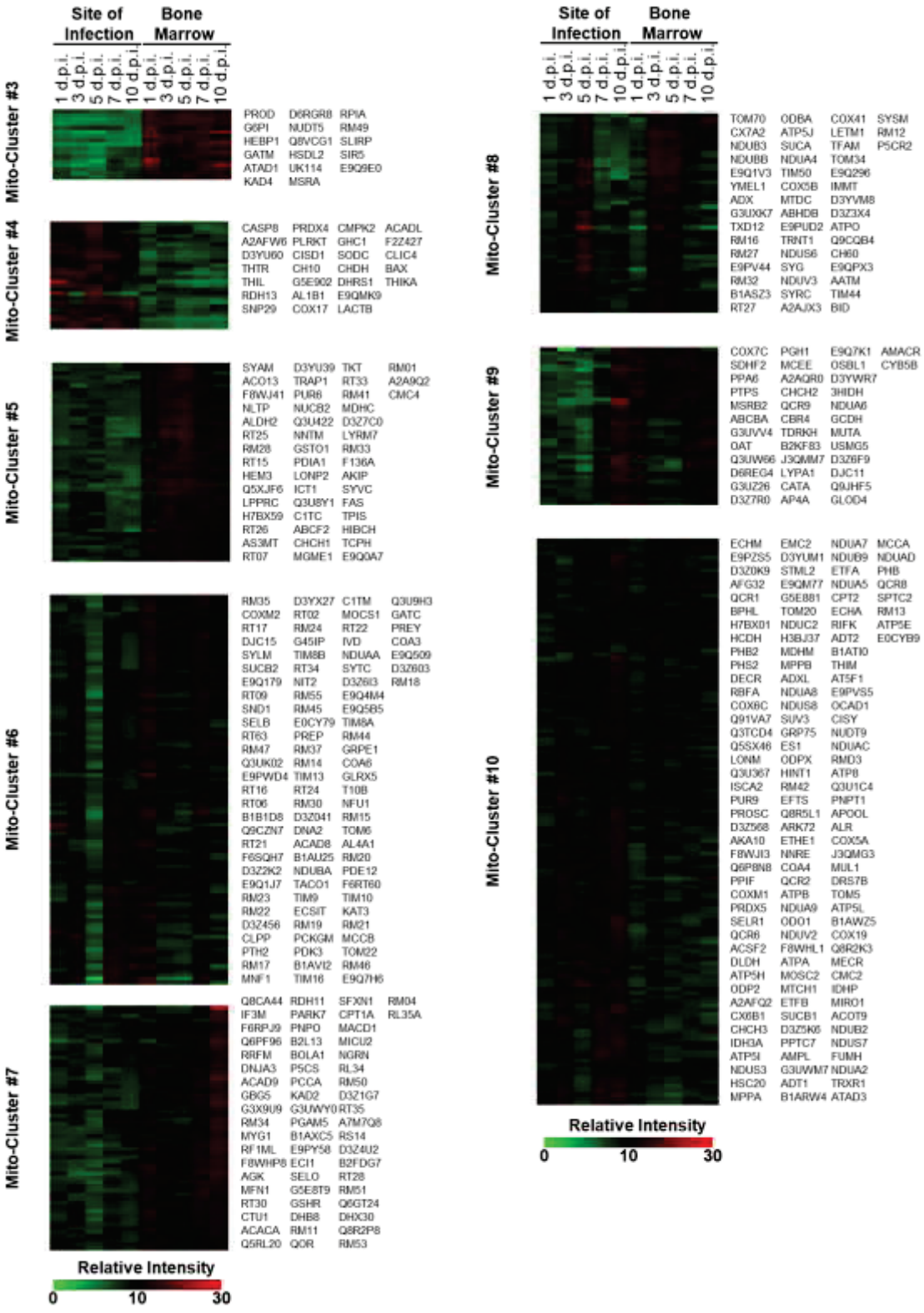

Supplementary Figure 5.5. *Additional Mito-Clusters #3-10 from Mitochondrial Localized Proteins.* Mito-clusters were generated *via* k-means clustering and Euclidean distance

analysis of only mitochondrial localized proteins (MitoCarta2.0 dataset comparison) and represented by heat maps. Individual protein identifications for each cluster are to the right of the heat map.

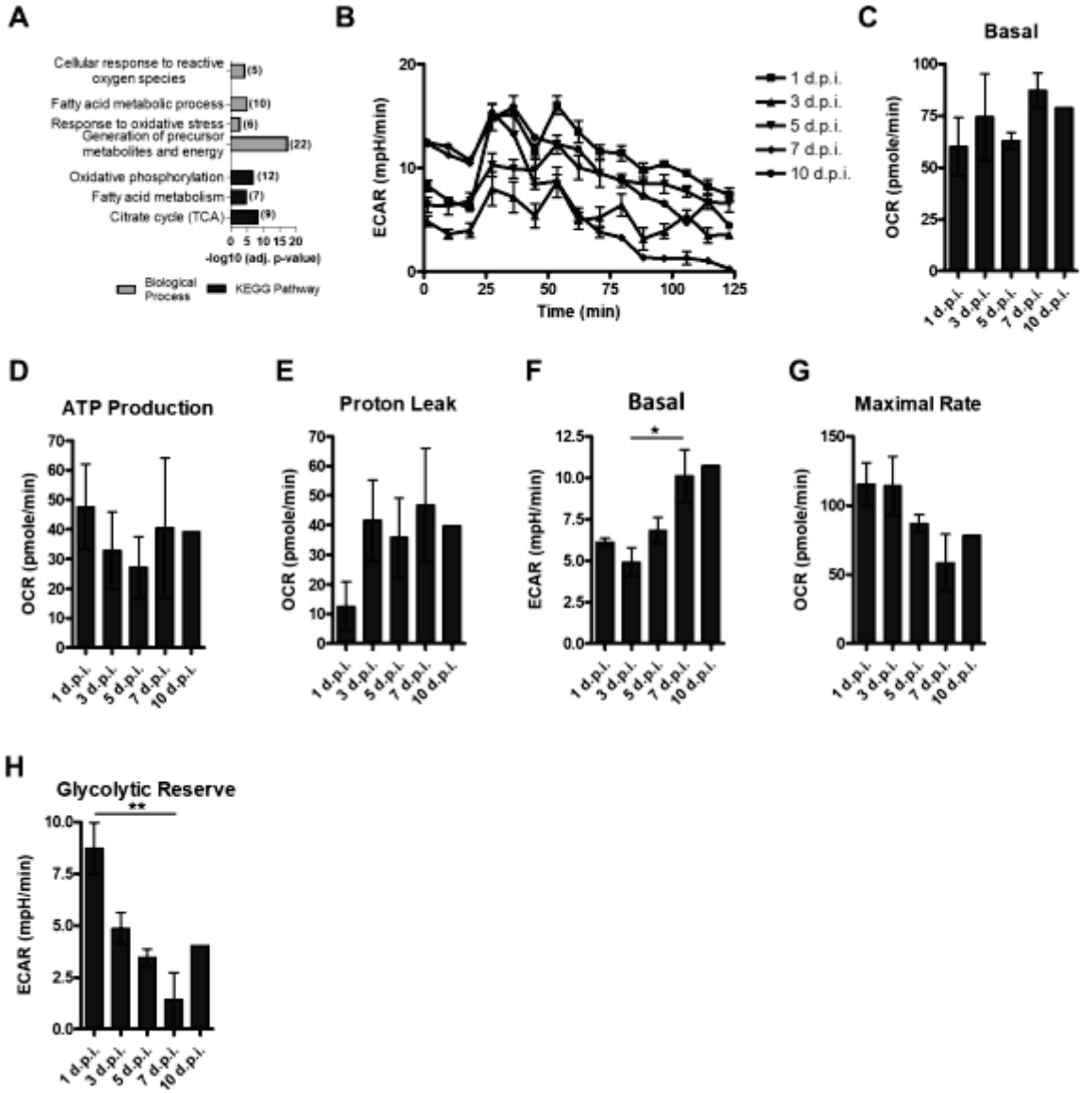

Supplementary Figure 5.6. *Assessment of the CD11b^{+} Ly6G^{-} Ly6C$^{high\text{-}low}$ Myeloid Cells' Metabolic Activity.* (A) GO-annotation analysis of BP and KEGG pathway, using DAVID bioinformatics, summarized in bar graph, illustrating the -log10 [adjusted (adj.) *p*-value], and number of identified targets per GO-Term (in brackets). ECAR and OCR were determined by a Seahorse XF24 analyser after subsequent additions of oligomycin (1 μM, at 25 min), FCCP (1.5 μM, at 50 min), rotenone (1 μM, at 75 min), and antimycin A (1 μM, at 100 min) to 5x10^{5} flow cytometry-isolated CD11b^{+} Ly6G^{-} Ly6C$^{high\text{-}low}$ cells from SOI 1, 3, 5, 7, or 10 days post infection (d.p.i) of reovirus. (B) ECAR analysis determined by Seahorse XF24 analyser. (C) Basal OCR, (D) ATP production, € proton leak, (F) basal ECAR, (G) maximal rate, and (H) glycolytic reserve were all calculated from the raw data acquired from the Seahorse XF24 analyser of isolated cells. Line graphs and bar graphs are represented as mean +/- SEM and collected from n=1-4 each with a pooled population from

5-10 mice. One-way ANOVA with Bonferroni post-test (B, C, D, and F) with 95% confidence interval were used for statistical analysis, and p values of <0.05 were considered significant. Asterisks were used to signify p values as follows: *$p \leq 0.05$; **$p \leq 0.01$.

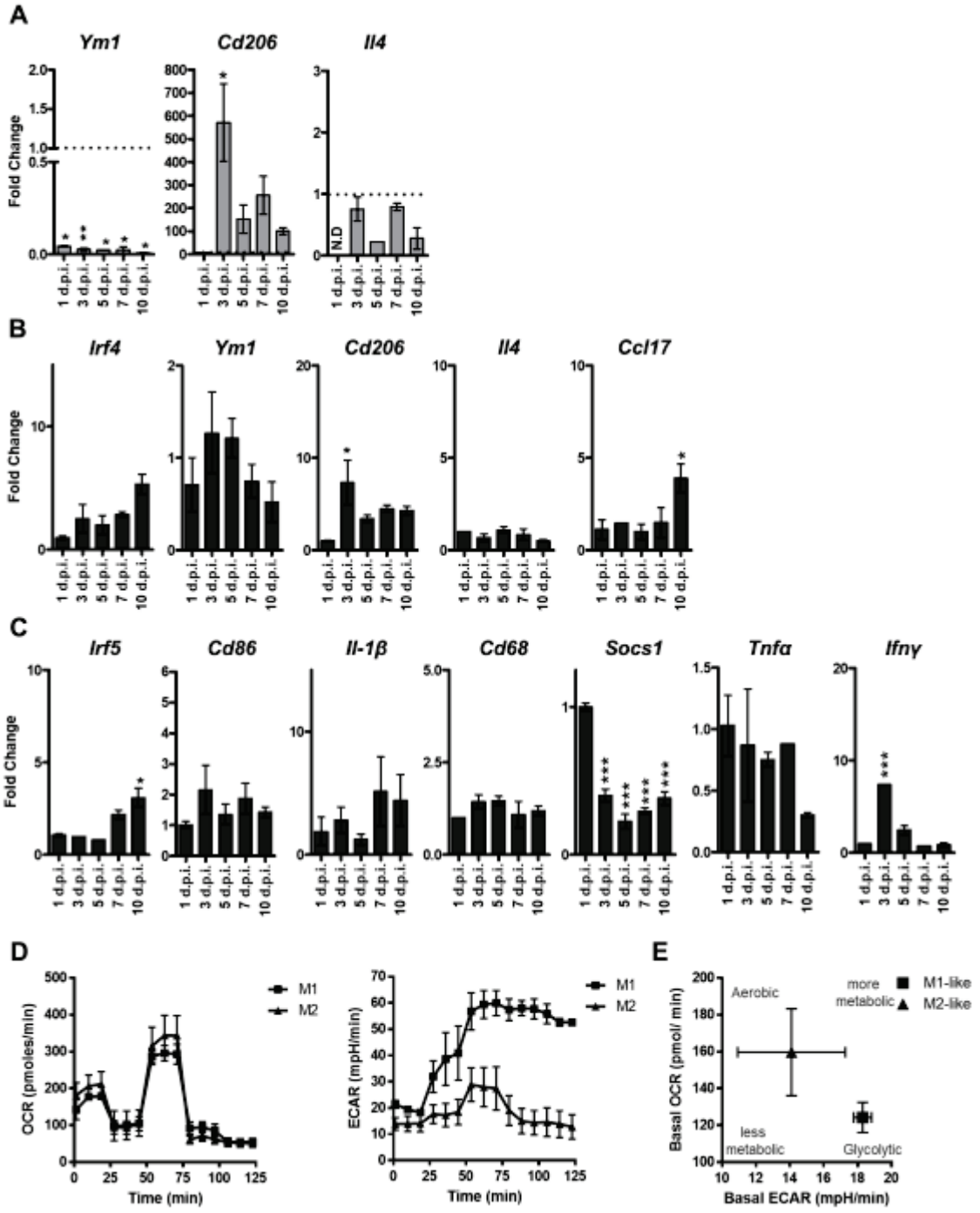

Supplementary Figure 5.7. *M1- Versus M2-like Macrophage Phenotyping.* (A) QPCR of SOI-isolated CD11b^{+} Ly6G^{-} Ly6C$^{high\text{-}low}$ cells for M2-macrophage associated markers. QPCR of BM-isolated CD11b^{+} Ly6G^{-} Ly6C$^{high\text{-}low}$ cells for M2- (B) and M1-macrophage (C) associated genes. QPCR analysis was from a pooled population of 5-10 mice, n=2, and ran in duplicate and normalized to *Gapdh* and compared to 1 d.p.i. BM sample (also represented as a dotted line in SOI graphic representations). (D) Seahorse XF24 analysis to

determine the OCR and ECAR of BM-derived M1- and M2-macrophages. (E) Graphic representation of basal OCR and basal ECAR of M1- and M2-like macrophages. Graphs are representative of mean +/- SEM with n=3. One-way ANOVA with Bonferroni post-test with 95% confidence interval were used for statistical analysis, and p values of <0.05 were considered significant. Asterisks were used to signify p values as follows: *$p \leq 0.05$; **$p \leq 0.01$; ***$p \leq 0.001$.

CHAPTER 6: CONCLUSION

Here, we show that reovirus drives the selective chemotaxis and accumulation of $CD11b^{+}Gr1^{+}$ $Ly6C^{high}$ (further elucidated as $CD11b^{+}$ $Ly6G^{-}$ $Ly6C^{high}$) MMCs immediately following its administration in naïve or tumor-bearing animals. In the context of the MOSE (ID8) ovarian peritoneal carcinomatosis mouse model, this MMC accumulation increases tumor-associated immunosuppression by enhancing local immunosuppressive cytokine concentrations and *via* cell-mediated immunosuppression[2, 6]. Furthermore, the inhibition of such MMC accumulation with gemcitabine during reovirus-based OV therapy accelerates tumor-specific $CD8^{+}$ T cell response development and prolongs survival[4, 5]. Contrary to such immunosuppressive characteristics within the TME, reovirus-driven MMCs, in non-tumor-bearing hosts, possess anti-viral/pro-inflammatory properties, aid in viral clearance, acquire enhanced antigen presentation capabilities, and undergo a phenotypic transformation into M2-like macrophages at a later stage of infection (after 10 days)[3]. These contrasting characteristics highlight the plasticity of MMCs and suggest that environmental cues are pivotal in the functionality and phenotype of infiltrating myeloid cells. Furthermore, the pliable nature of MMCs could provide a means to "tailor" such immune cells during cancer immunotherapies to achieve optimal clinical benefits (Fig 6.1).

The following sections will highlight how my research has contributed to the existing literature on the therapeutic and biological aspects of MMCs, as well as in the development of a total *in vivo* and temporal proteomics platform. In the end, I will put forward future directions for the understanding of therapy-driven myeloid cells in the context of cancer immunotherapies.

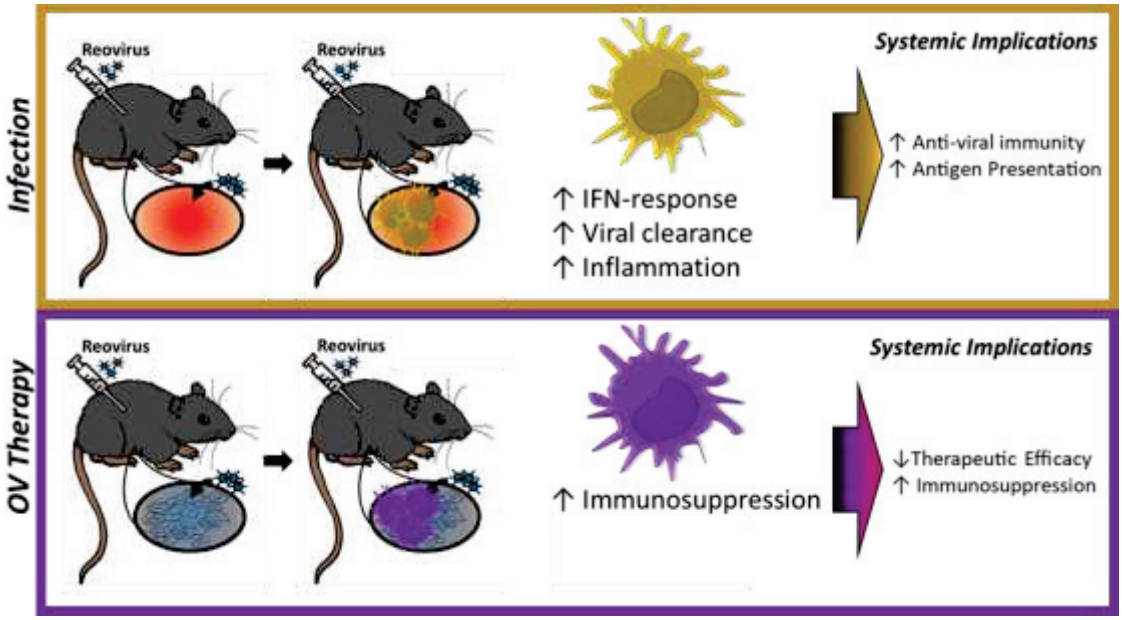

Figure 6.1. *Contrasting cellular phenotypes of reovirus-driven MMCs in the presence versus absence of a TME.* Reovirus-driven MMCs, in the absence of TME (infection), naturally possess pro-inflammatory/anti-viral properties and are precursors for antigen-presenting cells. Contrary to this phenotype, reovirus-driven MMCs which infiltrate and accumulate within an established TME have a highly immunosuppressive phenotype following virus administration. Such accumulation, within the TME, transiently mediates increased tumor associated immunosuppression. Depletion of these MMCs accelerated the development of anti-tumor immunity and improved therapeutic efficacy of reovirus-based OV therapy. These results suggest that the TME skews the possible anti-tumor properties of reovirus-driven MMCs to an immunosuppressive cellular state.

6.1 MY CONTRIBUTIONS TO THE LITERATURE

6.1.1 The Role of MMCs in the Context of OV Therapies

OV therapy represents a promising avenue for cancer immunotherapies as it indirectly generates a potent anti-tumor immune response while simultaneously killing cancer cells through the process of oncolysis. As numerous OVs are currently undergoing clinical trials and with the recent FDA approval for T-VEC, there is a need to devise complementary interventions to enhance the therapeutic effectiveness of OV therapies. While the direct oncolytic properties of OVs have previously been the major focus, it is now appreciated that harnessing the immunological repercussions of OV therapy holds the key to enhancing therapeutic effectiveness. As OVs possess natural immunostimulatory properties, it is of particular interest for treatment of "cold" tumors, which are often absent of an anti-tumor immune response. Similar to other cancer immunotherapeutic approaches, such as cancer vaccines, checkpoint inhibitor blockade, and cytokine supplementation, much of OV-based research has focused on augmenting pro-inflammation, and innate and adaptive immune cell recruitment and function in the TME. For example, the use of GM-CSF, commonly utilized to generate DCs *in vitro*, has been shown to expand T cell-activating DCs and potentiate anti-tumor immunity *in vivo*. As such, the use of GM-CSF supplementation/expression or GM-CSF expanded cells has successfully been implemented in the clinics with cancer vaccines (e.g., sipuleucel-T and STINGVAX)[375, 428] and OVs (e.g., T-VEC, reovirus, measles virus)[87, 119, 429]. Furthermore, treatments like prime and boost OV approaches and selective TLR signaling pathways are being used with the goal to avoid OV-specific immunity and promote $CD8^+$ T cell mediated anti-tumor immunity, respectively. Lastly, checkpoint inhibitor blockade has been introduced into

clinics to prevent T cell exhaustion, commonly associated with "hot" TMEs. Thus, complementing OV therapy with checkpoint inhibitor blockade has shown promise to potentiate the adaptive anti-tumor immune response[99, 117, 118, 122]. Not surprisingly, enhancing innate and adaptive immune cell activation and recruitment has become a prime focus with regards to OV therapy and research.

Although a few selected immunotherapeutic approaches have shown clinical benefit, they do not address if therapy-driven myeloid cells are conducive for the generation of an anti-tumor immune response. For example, GM-CSF, used in many immunotherapies with the goal of generating DCs, has also been shown to additionally promote BM-derived TAM progenitors and MDSCs, and elevate tumor-associated immunosuppression through the upregulation of IL-4α on MDSCs[430, 431]. Interestingly, targeting the production of GM-CSF has shown to reduce monocyte and neutrophil-like cell recruitment and hindered tumor progression[430]. Moreover, we and others have illustrated that OVs have the potential to mediate the recruitment and accumulation of immunosuppressive myeloid cells. Studies by Fortin *et al.* have illustrated that vaccinia virus-driven myeloid cells (both granulocytic and monocytic cells) hamper both NK- and T cell-mediated response, respectively[274, 432]. Similar recruitment of immunosuppressive myeloid cells has also been observed with vaccination approaches or adjuvant stimulation[352, 433, 434]. Importantly, pre-clinical and clinical findings have clearly illustrated that the accumulation of these immunosuppressive cells during tumor progression correlates with worse prognosis. However, not much is known regarding the therapy-driven immunosuppressive myeloid cells. Thus, in addition to driving a potent anti-tumor immune response, controlling therapy-induced myeloid cells

should be considered while devising strategies aimed at optimizing the efficacy of cancer immunotherapies.

6.1.2 Importance of Therapeutic Manipulation of Tumor-associated Myeloid Cells

The modulation of immunosuppressive myeloid cells using chemotherapeutics (e.g., gemcitabine and 5-FU) has been utilized in numerous combination therapies as they have been shown to selectively deplete MDSCs[279-281]. As gemcitabine and 5-FU are commonly used chemotherapeutic agents in clinics, they are practical choices for combination therapy in clinical trials. Unlike previous findings with gemcitabine-mediated MDSC depletion[280, 281], the concurrent gemcitabine and reovirus treatment hampered the virus-driven accumulation of MDSCs, and did not induce increased apoptosis in tumor-associated MDSCs[4, 5]. In addition to chemotherapeutics, small molecules, such as sunitinib[283], antibodies[435], and disrupting CCL2-CCR2 and M-CSF-M-CSFR signaling have all been shown to reduce tumor-associated myeloid cells and limit disease progression. Functional inhibition of MDSCs is also being pursued with the use of multiple factors such as phosphodiesterase type 5 (PDE-5)[285] or cyclooxygenase-2 (COX-2) inhibitors[286]. In particular, COX-2 inhibitors alter the TME by reducing MDSC-chemotactic factor CCL2 and by upregulating T cell-associated chemokine CXCL10[286]. Thus, depletion/inhibition of MDSCs can effectively manipulate the TME and suppress tumor progression.

It is important to note that MDSC depletion/inhibition approaches could impart adverse side effects during therapy. For instance, vemurafenib, an FDA approved BRAF inhibitor, which also has anti-MDSC properties[436], effectively blocks the mitogen-activated protein kinase (MAPK) signaling pathway and reduces tumor growth in BRAF(V600E) tumors. Additionally, interrupting CCL2 blockade can result in a sudden influx of monocytes from

the BM, which promotes metastasis and accelerates death in mice[437]. Furthermore, in our study utilizing the combination of reovirus and gemcitabine, we also demonstrated that gemcitabine directly affected reovirus replication *in vitro*. These findings suggest that although a combination approach that depletes tumor-associated MDSCs could further potentiate anti-tumor immunity, it could also induce adverse side effects. Thus, a critical analysis of the positive and negative effects of MDSC modulation should be considered to understand its clinical applicability.

The second approach of "tailoring" or manipulating myeloid cell populations is becoming a popular means to skew the phenotype/functionality of tumor-associated myeloid cells into pro-inflammatory/anti-tumor immune cells. To date, numerous studies have revealed potential targets by investigating striking differences in signaling pathways[268, 275, 311, 438], metabolism[439, 440], and epigenetic profiles[316] between pro-inflammatory/anti-tumor myeloid cells/macrophages and wound healing/pro-tumor M2-like macrophages. For instance, MerTK, a receptor tyrosine kinase of the TYRO3/AXL/MerTK family (TAM receptors) which limits TLR-induced pro-inflammatory signaling and responsiveness[438], is commonly overexpressed on tumor-associated $CD11b^+$ cells. Importantly, the inhibition of MerTK signaling displayed a reduction of wound healing cytokines, enhanced acute inflammatory cytokine expression, and increased intratumoral $CD8^+$ T cell infiltration[311]. In addition, macrophage PI3Kγ signaling inhibits NFκB activation and promotes immunosuppression and tumor growth[275]. Importantly, inhibition of PI3Kγ drove a more pro-inflammatory myeloid cell phenotype leading to increased anti-tumor treatment efficacy in the context of checkpoint blockade therapy[268]. Such studies suggest that

strategies which selectively skew myeloid cell functionality can exploit their anti-tumor potential.

In the context of OV therapy, it is important to consider that modulation of these immunosuppressive MMCs could have negative consequences towards reovirus replication. On one hand, gemcitabine could hamper OV replication directly; on the other hand, tailoring therapy-driven myeloid cells to have more pro-inflammatory properties could heighten anti-tumor and anti-viral immunities. As we have illustrated in our reovirus infection model, infection-driven MMCs display beneficial pro-inflammatory properties and IFN responsiveness; however, the presence of these MMCs accelerates virus clearance. Although both approaches could hamper OV replication, based on the role of anti-tumor immunity in the context of OV therapy, we hypothesize that the latter approach could be more clinically beneficial as it will harness the anti-tumor properties of infiltrating myeloid cells and further aid the generation of an effective anti-tumor immunity.

6.1.3 QTiPs, an Unbiased In Vivo Approach to Understand Total Proteome Dynamics of Immune Cells

Large scale "omics" science, whether genomics, transcriptomics, or proteomics, has transformed our ability to study cellular and molecular systems with unlimited potential. With respect to immunology, transcriptome analysis has proven to be a powerful tool to dissect immune cell identity, functionality, and tissue-specific profiles. However, RNA expression is not always indicative of protein expression or function. For example, C-type lectin Langerin, in mice, is homogeneously expressed at the RNA level but is differentially expressed at the protein level among different subsets of classical DCs and mouse cell lines[441]. Consequently, transcriptome analysis alone may not be sufficient to recognize different immune cell subsets, phenotypes, or functionalities. To this end, we turned to

mass spectrometry analysis to understand the global proteomic changes in specific immune cell populations. Recent technological advancements in mass spectrometry now allow quantification of upwards of 10,000 proteins from patient tissue samples, temporally monitor proteomic changes following viral infection, or investigate total post-translational modification changes regarding different treatments, organs/tissues, or stresses[394, 442]. With respect to immunological studies, total proteomic analysis has contributed to the understanding of a wide range of cells from a single comparative *in vivo* "snapshot" or *ex vivo* experimentations (e.g., stimulation or expanded immune cells)[443]. However, until our study, the temporal and spatial *in vivo* dynamics of proteomes within immune cell populations has been relatively unexplored.

Our QTiPs approach provides a means to monitor how the proteome of a specific immune cell subset changes over time. In our model, we examined the total proteome changes within virus-driven myeloid cells throughout the course of reovirus infection. We were able to decipher how these myeloid cells originally respond to reovirus infection and later transition into M2-like macrophages. With respect to immunotherapy, such an approach can be instrumental in understanding various stages of T cell exhaustion or how therapy alters the cellular signaling of various therapy-associated immune cells. As a result of time-dependent *in vivo* collections of specific immune cells, this approach accounts for the interplay between the isolated immune cell and host, something that lacks in much of the current proteomics platforms, especially focused on understanding the direct effect of pathogens on primary or derived immune cells. Our data elucidate the importance of such immune cell-host interactions as reovirus-driven MMCs undergo a temporal IFN responsiveness transition at different stages post infection (1 *versus* 5 days post infection)

(Fig 5.3 and Supplementary Fig 5.3). Such cellular responsiveness, due to environmental stimuli, suggests that direct *in vivo* analysis of immune cells is critical in the understanding of immune cell phenotype and functionality. Especially with increasing interests in cancer immunotherapeutic approaches, such an *in vivo* platform provides a more in-depth approach to dissecting the proteome of infiltrating and resident immune cells in the TME.

Although a quantitative proteomic approach provides an effective method to unbiasedly investigate global proteomic discrepancies, there is a limitation to this platform as well like all "omics" approaches. First, approximately 50 μg of protein or ~$1.5x10^7$ isolated cells seemed to be sufficient for a quantitative total proteome coverage of these primary isolated immune cells. For cancer cell lines, such an amount of protein is easily attainable. However, for immune cell populations especially those obtained from primary sources (i.e., human or mouse tissues), it has practical limitations. Thus, low frequency populations of immune cells from patient biopsies are not suitable for the current state of this total proteomic approach. Interestingly, and not known to us at the time of our platform development, advancements in sample preparation methodologies, specifically Single-Pot Solid-Phase-enhanced Sample preparation (SP3), could be utilized to obtain thorough total proteomic coverage on significantly less starting material. This paramagnetic bead technology allows for a single tube sample preparation with the compatibility to use harsh sample solubilization (providing more in-depth protein extraction) and quantitative labelling (TMT or reductive demethylation). Most importantly, Hughes *et al*. illustrated the use of only 5,000 HeLa cells of starting material with no significant loss in proteome coverage as compared to 50,000 HeLa cells in a single shot on the MS[444]. Thus, the implementation of

such an ultrasensitive sample preparation could potentially be utilized in combination with cellular sorting to obtain sufficient proteome coverage of low frequency cell populations.

6.2 FUTURE DIRECTIONS

As described above, reovirus-driven MMCs have contrasting behaviours and plasticity which is dependent on environmental cues. Current evidence suggests that CCR2-recruited monocytes/MDSCs progressively infiltrate the TME during tumor development. Notably, these studies have examined the role and phenotype of these infiltrating immune cells in the context of tumor progression and over a long period of time. With respect to reovirus-based OV therapy, we will need to first question whether such pathways or other mediators rapidly (within 24 hours) alter the behavior of therapy-driven and tumor-infiltrating MMCs. We feel that our QTiPs platform provides a mean to capture detailed temporal discrepancies between virus-driven MMCs in the presence or absence of the TME. This QTiPs analysis could further identify whether common or alternatively activated signaling pathways drive such clashing MMC phenotypes. Such findings could be beneficial in finding novel therapeutic targets immediately responsible for skewing myeloid cell phenotypes. Furthermore, knowledge gained from these investigations could be applied to other OV therapies or other cancer immunotherapies to achieve better patient outcomes.

6.3 CLOSING COMMENTS

MMCs are being appreciated as one of the major orchestrators in the development of innate and adaptive immune responses. Furthermore, the plasticity of such immune cells allows these cells to harness a plethora of functions. With respect to cancer progression and therapy, these cells commonly have been shown to be negatively correlated with survival.

In the context of reovirus OV therapy, the inhibition of reovirus-driven MMC recruitment in the TME (using gemcitabine) accelerates the development of anti-tumor T cell immunity and enhances therapeutic efficacy. Our findings on the characterization of these reovirus-driven MMCs in the context of infection and therapy suggest that strategic approaches simultaneously minimizing their suppressive activities and promoting their stimulatory phenotype could hold the key to achieve maximum benefits of reovirus-based cancer immunotherapy.

With increasing appreciation for cancer immunotherapies, it is also pivotal to monitor and investigate possible adverse effects induced by OVs. To date, autoimmunity is recognized as a major adverse effect of common cancer immunotherapies (e.g., anti-CTLA-4, anti-PD-1, and adoptive T cell therapy)[445, 446]. Furthermore, it is well established that infections can trigger the development of autoimmune responses *via* molecular mimicry, epitope spreading, bystander activation, and cryptic antigens[447]. To date, various OVs (e.g., reovirus, VSV, and HSV-1) have been shown to induce immune-related adverse events, such as glomerulonephritis, vasculitis, pneumonitis, psoriasis, vitiligo, cholangitis, and type-1 diabetes[87, 218, 448-451]. Although the incidence of certain immune-related adverse events has been correlated with prolonged survival[452-454], it is important for future studies to minimize such adverse events especially with combination approaches that implement multiple cancer immunotherapies. A study by Bridle *et al.* has demonstrated that the implementation of HDAC inhibition, *via* HDAC inhibitor (MS-275), was successful in abrogating the development of VSV-mediated vitiligo in melanoma-bearing C57BL/6 mice while enhancing secondary immune responses[449]. Although Bridle *et al.* illustrated that MS-275 suppressed the primary innate immune response, this study illustrates that

pharmacological strategies could be utilized to enhance anti-tumor immunity while simultaneously preventing immune-related adverse events. With increasing implementation of both monotherapies and combination therapies tailored to mediate a conducive anti-tumor immunity, it is important to additionally investigate preventative measures for long term immune-related adverse events following cancer immunotherapies.

REFERENCES

1. Gujar, S. *et al*. Multifaceted therapeutic targeting of ovarian peritoneal carcinomatosis through virus-induced immunomodulation. *Mol. Ther.* **21**, 338-347 (2013).

2. Clements, D. R. *et al*. Newly Recruited CD11b+, GR-1+, Ly6Chigh Myeloid Cells Augment Tumor-Associated Immunosuppression Immediately following the Therapeutic Administration of Oncolytic Reovirus. *J. Immunol.* **194**, 4397-4412 (2015).

3. Clements, D. R. *et al*. Quantitative Temporal in Vivo Proteomics Deciphers the Transition of Virus-Driven Myeloid Cells into M2 Macrophages. *J. Proteome Res.* **16**, 3391-3406 (2017).

4. Gujar, S. A., Clements, D. & Lee, P. W. Two is better than one: Complementing oncolytic virotherapy with gemcitabine to potentiate antitumor immune responses. *Oncoimmunology* **3**, e27622 (2014).

5. Gujar, S. A. *et al*. Gemcitabine enhances the efficacy of reovirus-based oncotherapy through anti-tumour immunological mechanisms. *Br. J. Cancer* **110**, 83-93 (2014).

6. Clements, D. R., Kim, Y., Gujar, S. A. & Lee, P. W. All that glitters is not gold: the need to consider desirable and undesirable immune aspects of oncolytic virus therapy. *Oncoimmunology* **5**, e1057674 (2015).

7. Murphy, K. M., Mowat, A. & Janeway, C. in *Janeway's immunobiology* (Garland Science, London [u.a.], 2012).

8. Xagorari, A. & Chlichlia, K. Toll-Like Receptors and Viruses: Induction of Innate Antiviral Immune Responses. *Open Microbiology Journal* **2**, 49-59 (2007).

9. Thompson, M. R., Kaminski, J. J., Kurt-Jones, E. A. & Fitzgerald, K. A. Pattern recognition receptors and the innate immune response to viral infection. *Viruses* **3**, 920-940 (2011).

10. Kato, H. *et al*. Length-dependent recognition of double-stranded ribonucleic acids by retinoic acid-inducible gene-I and melanoma differentiation-associated gene 5. *J. Exp. Med.* **205**, 1601-1610 (2008).

11. Maitra, R. *et al*. Toll like receptor 3 as an immunotherapeutic target for KRAS mutated colorectal cancer. *Oncotarget* **8**, 35138-35153 (2017).

12. Rojas, J. J. *et al*. Manipulating TLR Signaling Increases the Anti-tumor T Cell Response Induced by Viral Cancer Therapies. *Cell. Rep.* **15**, 264-273 (2016).

13. Shi, C. & Pamer, E. G. Monocyte recruitment during infection and inflammation. *Nat. Rev. Immunol.* **11**, 762-774 (2011).

14. Naumenko, V., Turk, M., Jenne, C. N. & Kim, S. Neutrophils in viral infection. *Cell Tissue Res.* (2018).

15. Dock, G. The influence of complicating diseases upon leukemia *Am J Med Sci* **127**, 563-592 (1904).

16. Pelner, L., Fowler, G. A. & Nauts, H. C. Effects of concurrent infections and their toxins on the course of leukemia. *Acta Med. Scand. Suppl.* **338**, 1-47 (1958).

17. Koprowski, H. & Norton, T. W. Interference between certain neurotropic viruses and transplantable mouse tumors. *Cancer* **3**, 874-885 (1950).

18. Moore, A. E. Effect of inoculation of the viruses of influenza A and herpes simplex on the growth of transplantable tumors in mice. *Cancer* **2**, 516-524 (1949).

19. Moore, A. E. & O'Connor, S. Further studies on the destructive effect of the virus of Russian Far East encephalitis on the transplantable mouse sarcoma 180. *Cancer* **3**, 886-890 (1950).

20. Moore, A. E. Inhibition of growth of five transplantable mouse tumors by the virus of Russian Far East encephalitis. *Cancer* **4**, 375-382 (1951).

21. Moore, A. E. The destructive effect of the virus of Russian Far East encephalitis on the transplantable mouse sarcoma 180. *Cancer* **2**, 525-534 (1949).

22. Southam, C. M. & Moore, A. E. Clinical studies of viruses as antineoplastic agents with particular reference to Egypt 101 virus. *Cancer* **5**, 1025-1034 (1952).

23. Southam, C. M., Bronstein, B. & Webber, L. F. Effect of West Nile and Ilheus viruses on mouse leukemias. *Cancer Res.* **11**, 669-675 (1951).

24. Bluming, A. Z. & Ziegler, J. L. Regression of Burkitt's lymphoma in association with measles infection. *Lancet* **2**, 105-106 (1971).

25. Pasquinucci, G. Possible effect of measles on leukaemia. *Lancet* **1**, 136 (1971).

26. Pack, G. T. Note on the experimental use of rabies vaccine for melanomatosis. *AMA Arch. Derm Syphilol* **62**, 694-695 (1950).

27. Asada, T. Treatment of human cancer with mumps virus. *Cancer* **34**, 1907-1928 (1974).

28. Berge, T. O., Banks, I. S. & Tigertt, W. D. Attenuation of Venezuelan equine encephalomyelitis virus by in vitro cultivation in guinea-pig heart cells. *Am J Epidemiol* **73**, 209-218 (1961).

29. Tigertt, W. D. *et al*. The virus of Venezuelan equine encephalomyelitis as an antineoplastic agent in man. *Cancer* **15**, 628-632 (1962).

30. Coffey, M. C., Strong, J. E., Forsyth, P. A. & Lee, P. W. Reovirus therapy of tumors with activated Ras pathway. *Science* **282**, 1332-1334 (1998).

31. Koromilas, A. E., Roy, S., Barber, G. N., Katze, M. G. & Sonenberg, N. Malignant transformation by a mutant of the IFN-inducible dsRNA-dependent protein kinase. *Science* **257**, 1685-1689 (1992).

32. Bello, M. J. *et al*. Molecular analysis of genomic abnormalities in human gliomas. *Cancer Genet. Cytogenet.* **73**, 122-129 (1994).

33. Sun, W. H. *et al*. Interferon-alpha resistance in a cutaneous T-cell lymphoma cell line is associated with lack of STAT1 expression. *Blood* **91**, 570-576 (1998).

34. Wong, L. H. *et al*. Interferon-resistant human melanoma cells are deficient in ISGF3 components, STAT1, STAT2, and p48-ISGF3gamma. *J. Biol. Chem.* **272**, 28779-28785 (1997).

35. Stojdl, D. F. *et al*. Exploiting tumor-specific defects in the interferon pathway with a previously unknown oncolytic virus. *Nat. Med.* **6**, 821-825 (2000).

36. Shmulevitz, M., Marcato, P. & Lee, P. W. Activated Ras signaling significantly enhances reovirus replication and spread. *Cancer Gene Ther.* **17**, 69-70 (2010).

37. Pikor, L. A., Bell, J. C. & Diallo, J. S. Oncolytic Viruses: Exploiting Cancer's Deal with the Devil. *Trends Cancer.* **1**, 266-277 (2015).

38. Li, S. *et al*. The tumor suppressor PTEN has a critical role in antiviral innate immunity. *Nat. Immunol.* **17**, 241-249 (2016).

39. Mansour, M., Palese, P. & Zamarin, D. Oncolytic specificity of Newcastle disease virus is mediated by selectivity for apoptosis-resistant cells. *J. Virol.* **85**, 6015-6023 (2011).

40. Stojdl, D. F. *et al*. VSV strains with defects in their ability to shutdown innate immunity are potent systemic anti-cancer agents. *Cancer. Cell.* **4**, 263-275 (2003).

41. Farassati, F., Yang, A. D. & Lee, P. W. Oncogenes in Ras signalling pathway dictate host-cell permissiveness to herpes simplex virus 1. *Nat. Cell Biol.* **3**, 745-750 (2001).

42. Shmulevitz, M., Pan, L. Z., Garant, K., Pan, D. & Lee, P. W. Oncogenic Ras promotes reovirus spread by suppressing IFN-beta production through negative regulation of RIG-I signaling. *Cancer Res.* **70**, 4912-4921 (2010).

43. Chou, J., Chen, J. J., Gross, M. & Roizman, B. Association of a M(r) 90,000 phosphoprotein with protein kinase PKR in cells exhibiting enhanced phosphorylation of translation initiation factor eIF-2 alpha and premature shutoff of protein synthesis after infection with gamma 134.5- mutants of herpes simplex virus 1. *Proc. Natl. Acad. Sci. U. S. A.* **92**, 10516-10520 (1995).

44. Wilden, H., Fournier, P., Zawatzky, R. & Schirrmacher, V. Expression of RIG-I, IRF3, IFN-beta and IRF7 determines resistance or susceptibility of cells to infection by Newcastle Disease Virus. *Int. J. Oncol.* **34**, 971-982 (2009).

45. Bergmann, M. *et al*. A genetically engineered influenza A virus with ras-dependent oncolytic properties. *Cancer Res.* **61**, 8188-8193 (2001).

46. Wang, F. *et al*. Disruption of Erk-dependent type I interferon induction breaks the myxoma virus species barrier. *Nat. Immunol.* **5**, 1266-1274 (2004).

47. Rojas, M., Arias, C. F. & López, S. Protein kinase R is responsible for the phosphorylation of eIF2alpha in rotavirus infection. *J. Virol.* **84**, 10457-10466 (2010).

48. Williams, B. R. PKR; a sentinel kinase for cellular stress. *Oncogene* **18**, 6112-6120 (1999).

49. Sarinella, F., Calistri, A., Sette, P., Palu, G. & Parolin, C. Oncolysis of pancreatic tumour cells by a gamma34.5-deleted HSV-1 does not rely upon Ras-activation, but on the PI 3-kinase pathway. *Gene Ther.* **13**, 1080-1087 (2006).

50. Dobbelstein, M. Replicating adenoviruses in cancer therapy. *Curr. Top. Microbiol. Immunol.* **273**, 291-334 (2004).

51. Guo, P. *et al*. ICAM-1 as a molecular target for triple negative breast cancer. *Proc. Natl. Acad. Sci. U. S. A.* **111**, 14710-14715 (2014).

52. Au, G. G., Lincz, L. F., Enno, A. & Shafren, D. R. Oncolytic Coxsackievirus A21 as a novel therapy for multiple myeloma. *Br. J. Haematol.* **137**, 133-141 (2007).

53. Shafren, D. R. *et al*. Systemic therapy of malignant human melanoma tumors by a common cold-producing enterovirus, coxsackievirus a21. *Clin. Cancer Res.* **10**, 53-60 (2004).

54. Delpeut, S., Sisson, G., Black, K. M. & Richardson, C. D. Measles Virus Enters Breast and Colon Cancer Cell Lines through a PVRL4-Mediated Macropinocytosis Pathway. *J. Virol.* **91** (2017).

55. Noyce, R. S. & Richardson, C. D. Nectin 4 is the epithelial cell receptor for measles virus. *Trends in Microbiology* **20**, 429-439 (2012).

56. Dörig, R. E., Marcil, A., Chopra, A. & Richardson, C. D. The human CD46 molecule is a receptor for measles virus (Edmonston strain). *Cell* **75**, 295-305 (1993).

57. Delpeut, S., Noyce, R. S. & Richardson, C. D. The tumor-associated marker, PVRL4 (nectin-4), is the epithelial receptor for morbilliviruses. *Viruses* **6**, 2268-2286 (2014).

58. Noyce, R. S. *et al*. Tumor cell marker PVRL4 (nectin 4) is an epithelial cell receptor for measles virus. *PLoS Pathog.* **7**, e1002240 (2011).

59. Anderson, B. D., Nakamura, T., Russell, S. J. & Peng, K. High CD46 receptor density determines preferential killing of tumor cells by oncolytic measles virus. *Cancer Res.* **64**, 4919-4926 (2004).

60. Hsu, E. C., Iorio, C., Sarangi, F., Khine, A. A. & Richardson, C. D. CDw150(SLAM) is a receptor for a lymphotropic strain of measles virus and may account for the immunosuppressive properties of this virus. *Virology* **279**, 9-21 (2001).

61. Tatsuo, H., Ono, N., Tanaka, K. & Yanagi, Y. SLAM (CDw150) is a cellular receptor for measles virus. *Nature* **406**, 893-897 (2000).

62. Shafren, D. R., Sylvester, D., Johansson, E. S., Campbell, I. G. & Barry, R. D. Oncolysis of human ovarian cancers by echovirus type 1. *Int. J. Cancer* **115**, 320-328 (2005).

63. Morizono, K. *et al*. Lentiviral vector retargeting to P-glycoprotein on metastatic melanoma through intravenous injection. *Nat. Med.* **11**, 346-352 (2005).

64. Hammond, A. L. *et al*. Single-chain antibody displayed on a recombinant measles virus confers entry through the tumor-associated carcinoembryonic antigen. *J. Virol.* **75**, 2087-2096 (2001).

65. Kim, K. H. *et al*. A phase I clinical trial of Ad5/3-Δ24, a novel serotype-chimeric, infectivity-enhanced, conditionally-replicative adenovirus (CRAd), in patients with recurrent ovarian cancer. *Gynecol. Oncol.* **130**, 518-524 (2013).

66. Liapis, H., Adler, L. M., Wick, M. R. & Rader, J. S. Expression of alpha(v)beta3 integrin is less frequent in ovarian epithelial tumors of low malignant potential in contrast to ovarian carcinomas. *Hum. Pathol.* **28**, 443-449 (1997).

67. You, Z. *et al*. Coxsackievirus-adenovirus receptor expression in ovarian cancer cell lines is associated with increased adenovirus transduction efficiency and transgene expression. *Cancer Gene Ther.* **8**, 168-175 (2001).

68. Schirrmacher, V. & Fournier, P. Newcastle disease virus: a promising vector for viral therapy, immune therapy, and gene therapy of cancer. *Methods Mol. Biol.* **542**, 565-605 (2009).

69. Aref, S., Bailey, K. & Fielding, A. Measles to the Rescue: A Review of Oncolytic Measles Virus. *Viruses* **8**, E294 (2016).

70. Msaouel, P., Iankov, I. D., Dispenzieri, A. & Galanis, E. Attenuated oncolytic measles virus strains as cancer therapeutics. *Curr. Pharm. Biotechnol.* **13**, 1732-1741 (2012).

71. Russell, S. J. & Peng, K. W. Measles virus for cancer therapy. *Curr. Top. Microbiol. Immunol.* **330**, 213-241 (2009).

72. Mota, H. C. Infantile Hodgkin's disease: remission after measles. *Br Med J* **2**, 421 (1973).

73. Taqi, A. M., Abdurrahman, M. B., Yakubu, A. M. & Fleming, A. F. Regression of Hodgkin's disease after measles. *Lancet* **1**, 1112 (1981).

74. Ziegler, J. L. Spontaneous remission in Burkitt's lymphoma. *Natl Cancer Inst Monogr* **44**, 61-65 (1976).

75. Zygiert, Z. Hodgkin's disease: remissions after measles. *Lancet* **1**, 593 (1971).

76. Barber, G. N. VSV-tumor selective replication and protein translation. *Oncogene* **24**, 7710-7719 (2005).

77. Kirn, D. H. & Thorne, S. H. Targeted and armed oncolytic poxviruses: a novel multi-mechanistic therapeutic class for cancer. *Nat. Rev. Cancer.* **9**, 64-71 (2009).

78. Goetz, C. & Gromeier, M. Preparing an oncolytic poliovirus recombinant for clinical application against glioblastoma multiforme. *Cytokine Growth Factor Rev.* **21**, 197-203 (2010).

79. Kaur, B., Chiocca, E. A. & Cripe, T. P. Oncolytic HSV-1 virotherapy: clinical experience and opportunities for progress. *Curr. Pharm. Biotechnol.* **13**, 1842-1851 (2012).

80. Ko, D., Hawkins, L. & Yu, D. C. Development of transcriptionally regulated oncolytic adenoviruses. *Oncogene* **24**, 7763-7774 (2005).

81. Kaneda, Y. & Saga, K. Oncolytic Sendai virus-based virotherapy for cancer: recent advances. *Oncolytic Virotherapy* **2015**, 141-147 (2015).

82. Brun, J. *et al*. Identification of genetically modified Maraba virus as an oncolytic rhabdovirus. *Mol. Ther.* **18**, 1440-1449 (2010).

83. Pol, J. G. *et al*. Maraba virus as a potent oncolytic vaccine vector. *Mol. Ther.* **22**, 420-429 (2014).

84. Miyamoto, S. *et al*. Coxsackievirus B3 is an oncolytic virus with immunostimulatory properties that is active against lung adenocarcinoma. *Cancer Res.* **72**, 2609-2621 (2012).

85. Garber, K. China approves world's first oncolytic virus therapy for cancer treatment. *J. Natl. Cancer Inst.* **98**, 298-300 (2006).

86. Rehman, H., Silk, A. W., Kane, M. P. & Kaufman, H. L. Into the clinic: Talimogene laherparepvec (T-VEC), a first-in-class intratumoral oncolytic viral therapy. *Journal for immunotherapy of cancer* **4**, 53 (2016).

87. Andtbacka, R. H. I. *et al*. Talimogene Laherparepvec Improves Durable Response Rate in Patients With Advanced Melanoma. *J. Clin. Oncol.* **33**, 2780-2788 (2015).

88. Donnelly, O. G. *et al*. Measles virus causes immunogenic cell death in human melanoma. *Gene Ther.* **20**, 7-15 (2013).

89. Diaconu, I. *et al*. Immune response is an important aspect of the antitumor effect produced by a CD40L-encoding oncolytic adenovirus. *Cancer Res.* **72**, 2327-2338 (2012).

90. Workenhe, S. T. & Mossman, K. L. Oncolytic Virotherapy and Immunogenic Cancer Cell Death: Sharpening the Sword for Improved Cancer Treatment Strategies. *Molecular Therapy* **22**, 251-256 (2014).

91. Ferguson, T., Green, D. R., Kroemer, G. & Zitvogel, L. Immunogenic and tolerogenic cell death. *Nature Reviews Immunology* **9**, 353-363 (2009).

92. Angelova, A. L. *et al*. Complementary induction of immunogenic cell death by oncolytic parvovirus H-1PV and gemcitabine in pancreatic cancer. *J. Virol.* **88**, 5263-5276 (2014).

93. Huang, B., Sikorski, R., Kirn, D. H. & Thorne, S. H. Synergistic anti-tumor effects between oncolytic vaccinia virus and paclitaxel are mediated by the IFN response and HMGB1. *Gene Ther.* **18**, 164-172 (2011).

94. Workenhe, S. T. *et al*. Immunogenic HSV-mediated oncolysis shapes the antitumor immune response and contributes to therapeutic efficacy. *Mol. Ther.* **22**, 123-131 (2014).

95. Heinrich, B. *et al*. Immunogenicity of oncolytic vaccinia viruses JX-GFP and TG6002 in a human melanoma in vitro model: studying immunogenic cell death, dendritic cell

maturation and interaction with cytotoxic T lymphocytes. *OncoTargets and Therapy* **10**, 2389-2401 (2017).

96. Richards, C. H., Mohammed, Z., Qayyum, T., Horgan, P. G. & McMillan, D. C. The prognostic value of histological tumor necrosis in solid organ malignant disease: a systematic review. *Future Oncol* **7**, 1223-1235 (2011).

97. Hou, J., Greten, T. F. & Xia, Q. Immunosuppressive cell death in cancer. *Nat. Rev. Immunol.* **17**, 401 (2017).

98. Gujar, S. A., Marcato, P., Pan, D. & Lee, P. W. Reovirus virotherapy overrides tumor antigen presentation evasion and promotes protective antitumor immunity. *Mol. Cancer. Ther.* **9**, 2924-2933 (2010).

99. Lichty, B. D., Breitbach, C. J., Stojdl, D. F. & Bell, J. C. Going viral with cancer immunotherapy. *Nat. Rev. Cancer.* **14**, 559-567 (2014).

100. Chahroudi, A. *et al*. Vaccinia virus tropism for primary hematolymphoid cells is determined by restricted expression of a unique virus receptor. *J. Virol.* **79**, 10397-10407 (2005).

101. Gujar, S. A. & Lee, P. W. Oncolytic virus-mediated reversal of impaired tumor antigen presentation. *Front. Oncol.* **4**, 77 (2014).

102. Prestwich, R. J. *et al*. Reciprocal human dendritic cell-natural killer cell interactions induce antitumor activity following tumor cell infection by oncolytic reovirus. *J. Immunol.* **183**, 4312-4321 (2009).

103. Clements, D., Helson, E., Gujar, S. A. & Lee, P. W. K. Reovirus in cancer therapy: an evidence-based review. *Oncolytic Virotherapy* **2014:3**, 69-82 (2014).

104. Gujar, S., Pol, J. G., Kim, Y., Lee, P. W. & Kroemer, G. Antitumor Benefits of Antiviral Immunity: An Underappreciated Aspect of Oncolytic Virotherapies. *Trends in Immunology*.

105. Gujar, S. A., Pan, D. A., Marcato, P., Garant, K. A. & Lee, P. W. Oncolytic virus-initiated protective immunity against prostate cancer. *Mol. Ther.* **19**, 797-804 (2011).

106. Koks, C. A. *et al*. Newcastle disease virotherapy induces long-term survival and tumor-specific immune memory in orthotopic glioma through the induction of immunogenic cell death. *Int. J. Cancer* **136**, 313 (2015).

107. Diaz, R. M. *et al*. Oncolytic immunovirotherapy for melanoma using vesicular stomatitis virus. *Cancer Res.* **67**, 2840-2848 (2007).

108. Hou, W., Sampath, P., Rojas, J. J. & Thorne, S. H. Oncolytic Virus-Mediated Targeting of PGE2 in the Tumor Alters the Immune Status and Sensitizes Established and Resistant Tumors to Immunotherapy. *Cancer Cell* **30**, 108-119 (2016).

109. Arulanandam, R. *et al*. VEGF-Mediated Induction of PRD1-BF1/Blimp1 Expression Sensitizes Tumor Vasculature to Oncolytic Virus Infection. *Cancer Cell* **28**, 210-224 (2015).

110. Ikeda, Y. *et al*. A novel antiangiogenic effect for telomerase-specific virotherapy through host immune system. *J. Immunol.* **182**, 1763-1769 (2009).

111. Benencia, F. *et al*. Oncolytic HSV exerts direct antiangiogenic activity in ovarian carcinoma. *Hum. Gene Ther.* **16**, 765-778 (2005).

112. Saito, Y. *et al*. Oncolytic replication-competent adenovirus suppresses tumor angiogenesis through preserved E1A region. *Cancer Gene Ther.* **13**, 242-252 (2006).

113. Breitbach, C. J. *et al*. Targeted inflammation during oncolytic virus therapy severely compromises tumor blood flow. *Mol. Ther.* **15**, 1686-1693 (2007).

114. Breitbach, C. J. *et al*. Targeting tumor vasculature with an oncolytic virus. *Mol. Ther.* **19**, 886-894 (2011).

115. Ilkow, C. S. *et al*. Reciprocal cellular cross-talk within the tumor microenvironment promotes oncolytic virus activity. *Nat. Med.* (2015).

116. Kottke, T. *et al*. Antiangiogenic cancer therapy combined with oncolytic virotherapy leads to regression of established tumors in mice. *J. Clin. Invest.* **120**, 1551-1560 (2010).

117. Rajani, K. *et al*. Combination Therapy With Reovirus and Anti-PD-1 Blockade Controls Tumor Growth Through Innate and Adaptive Immune Responses. *Mol. Ther.* **24**, 166-174 (2016).

118. Bourgeois-Daigneault, M. *et al*. Neoadjuvant oncolytic virotherapy before surgery sensitizes triple-negative breast cancer to immune checkpoint therapy. *Sci Transl Med* **10** (2018).

119. Ilett, E. *et al*. Prime-boost using separate oncolytic viruses in combination with checkpoint blockade improves anti-tumour therapy. *Gene Ther.* **24**, 21-30 (2017).

120. Zamarin, D. *et al*. Localized oncolytic virotherapy overcomes systemic tumor resistance to immune checkpoint blockade immunotherapy. *Sci Transl Med* **6**, 226ra32 (2014).

121. Shen, W., Patnaik, M. M., Ruiz, A., Russell, S. J. & Peng, K. Immunovirotherapy with vesicular stomatitis virus and PD-L1 blockade enhances therapeutic outcome in murine acute myeloid leukemia. *Blood* **127**, 1449-1458 (2016).

122. Liu, Z., Ravindranathan, R., Kalinski, P., Guo, Z. S. & Bartlett, D. L. Rational combination of oncolytic vaccinia virus and PD-L1 blockade works synergistically to enhance therapeutic efficacy. *Nat Commun* **8**, 14754 (2017).

123. Bouziat, R. *et al*. Reovirus infection triggers inflammatory responses to dietary antigens and development of celiac disease. *Science* **356**, 44-50 (2017).

124. Hata, Y. *et al*. Efficacy of oncolytic reovirus against human breast cancer cells. *Oncol. Rep.* **19**, 1395-1398 (2008).

125. Hirasawa, K. *et al*. Oncolytic reovirus against ovarian and colon cancer. *Cancer Res.* **62**, 1696-1701 (2002).

126. Norman, K. L. *et al*. Reovirus oncolysis of human breast cancer. *Hum. Gene Ther.* **13**, 641-652 (2002).

127. Yang, W. Q. *et al*. Reovirus as an experimental therapeutic for brain and leptomeningeal metastases from breast cancer. *Gene Ther.* **11**, 1579-1589 (2004).

128. Pan, D. *et al*. Stabilisation of p53 enhances reovirus-induced apoptosis and virus spread through p53-dependent NF-kappaB activation. *Br. J. Cancer* **105**, 1012-1022 (2011).

129. Pan, D. *et al*. Activation of p53 by chemotherapeutic agents enhances reovirus oncolysis. *PLoS One* **8**, e54006 (2013).

130. Wilcox, M. E. *et al*. Reovirus as an oncolytic agent against experimental human malignant gliomas. *J. Natl. Cancer Inst.* **93**, 903-912 (2001).

131. Roulstone, V. *et al*. Synergistic cytotoxicity of oncolytic reovirus in combination with cisplatin-paclitaxel doublet chemotherapy. *Gene Ther.* **20**, 521-528 (2013).

132. Pandha, H. S. *et al*. Synergistic effects of oncolytic reovirus and cisplatin chemotherapy in murine malignant melanoma. *Clin. Cancer Res.* **15**, 6158-6166 (2009).

133. Heinemann, L. *et al*. Synergistic effects of oncolytic reovirus and docetaxel chemotherapy in prostate cancer. *BMC Cancer* **11**, 221 (2011).

134. Kilani, R. T. *et al*. Selective reovirus killing of bladder cancer in a co-culture spheroid model. *Virus Res.* **93**, 1-12 (2003).

135. Sei, S. *et al*. Synergistic antitumor activity of oncolytic reovirus and chemotherapeutic agents in non-small cell lung cancer cells. *Mol. Cancer.* **8**, 47 (2009).

136. Alain, T. *et al*. Reovirus therapy of lymphoid malignancies. *Blood* **100**, 4146-4153 (2002).

137. Hashiro, G., Loh, P. C. & Yau, J. T. The preferential cytotoxicity of reovirus for certain transformed cell lines. *Arch. Virol.* **54**, 307-315 (1977).

138. Duncan, M. R., Stanish, S. M. & Cox, D. C. Differential sensitivity of normal and transformed human cells to reovirus infection. *J. Virol.* **28**, 444-449 (1978).

139. Marcato, P., Shmulevitz, M., Pan, D., Stoltz, D. & Lee, P. W. Ras transformation mediates reovirus oncolysis by enhancing virus uncoating, particle infectivity, and apoptosis-dependent release. *Mol. Ther.* **15**, 1522-1530 (2007).

140. Marcato, P., Shmulevitz, M. & Lee, P. W. Connecting reovirus oncolysis and Ras signaling. *Cell. Cycle* **4**, 556-559 (2005).

141. Marcato, P., Dean, C. A., Giacomantonio, C. A. & Lee, P. W. Oncolytic reovirus effectively targets breast cancer stem cells. *Mol. Ther.* **17**, 972-979 (2009).

142. Thirukkumaran, C. M. *et al*. Oncolytic viral therapy for prostate cancer: efficacy of reovirus as a biological therapeutic. *Cancer Res.* **70**, 2435-2444 (2010).

143. Morris, D. G. *et al*. REO-001: A phase I trial of percutaneous intralesional administration of reovirus type 3 dearing (Reolysin(R)) in patients with advanced solid tumors. *Invest. New Drugs* **31**, 696-706 (2013).

144. Forsyth, P. *et al*. A phase I trial of intratumoral administration of reovirus in patients with histologically confirmed recurrent malignant gliomas. *Mol. Ther.* **16**, 627-632 (2008).

145. Kicielinski, K. P. *et al*. Phase I Clinical Trial of Intratumoral Reovirus Infusion for the Treatment of Recurrent Malignant Gliomas in Adults. *Mol. Ther.* (2014).

146. Galanis, E. *et al*. Phase II trial of intravenous administration of Reolysin((R)) (Reovirus Serotype-3-dearing Strain) in patients with metastatic melanoma. *Mol. Ther.* **20**, 1998-2003 (2012).

147. Mita, A. et al. *Phase II Study of Intravenous REOLYSIN (Wild-type reovirus) in the Treatment of Patients with Bone and Soft Tissue Sarcomas Metastatic to the Lung [abstact] Abstract number: 10524* (2009 ASCO Annual Meeting.

148. Prestwich, R. J. *et al*. Immune-mediated antitumor activity of reovirus is required for therapy and is independent of direct viral oncolysis and replication. *Clin. Cancer Res.* **15**, 4374-4381 (2009).

149. Errington, F. *et al*. Inflammatory tumour cell killing by oncolytic reovirus for the treatment of melanoma. *Gene Ther.* **15**, 1257-1270 (2008).

150. Prestwich, R. J. *et al*. Tumor infection by oncolytic reovirus primes adaptive antitumor immunity. *Clin. Cancer Res.* **14**, 7358-7366 (2008).

151. Errington, F. *et al*. Reovirus activates human dendritic cells to promote innate antitumor immunity. *J. Immunol.* **180**, 6018-6026 (2008).

152. Ilett, E. *et al*. Cytokine conditioning enhances systemic delivery and therapy of an oncolytic virus. *Mol. Ther.* **22**, 1851-1863 (2014).

153. Morin, M. J., Warner, A. & Fields, B. N. Reovirus infection in rat lungs as a model to study the pathogenesis of viral pneumonia. *J. Virol.* **70**, 541-548 (1996).

154. Twigger, K. *et al*. Enhanced in vitro and in vivo cytotoxicity of combined reovirus and radiotherapy. *Clin. Cancer Res.* **14**, 912-923 (2008).

155. Harrington, K. J. *et al*. Two-stage phase I dose-escalation study of intratumoral reovirus type 3 dearing and palliative radiotherapy in patients with advanced cancers. *Clin. Cancer Res.* **16**, 3067-3077 (2010).

156. http://www.oncolyticsbiotech.com/English/news/press-release-details/2009/Oncolytics-Biotech-Inc-Announces-Positive-Results-of-UK-Phase-II-REOLYSIN-and-Radiation-Combination-Clinical-Trial.

157. Noonan, A. M. *et al*. Randomized Phase 2 Trial of the Oncolytic Virus Pelareorep (Reolysin) in Upfront Treatment of Metastatic Pancreatic Adenocarcinoma. *Mol. Ther.* **24**, 1150-1158 (2016).

158. Mahalingam, D. *et al*. A phase II study of REOLYSIN(R) (pelareorep) in combination with carboplatin and paclitaxel for patients with advanced malignant melanoma. *Cancer Chemother. Pharmacol.* **79**, 697-703 (2017).

159. Villalona-Calero, M. A. *et al*. Oncolytic reovirus in combination with chemotherapy in metastatic or recurrent non-small cell lung cancer patients with KRAS-activated tumors. *Cancer* **122**, 875-883 (2016).

160. Cohn, D. E. *et al*. Randomized phase IIB evaluation of weekly paclitaxel versus weekly paclitaxel with oncolytic reovirus (Reolysin(R)) in recurrent ovarian, tubal, or peritoneal cancer: An NRG Oncology/Gynecologic Oncology Group study. *Gynecol. Oncol.* **146**, 477-483 (2017).

161. Morris, D., Tu, D., Tehfe, M., Nicholas, G., Goffin, J., Gregg, R., Shepherd, F., Murray, N., Wierzbicki, R., Lee, C., Kuruvilla, S., Keith, B., Ahmed, A., Blais, N., Goss, G., Korpanty, G., Sederias, J., Laurie, S., Seymour, L. & Bradbury, P. A Randomized Phase II study of Reolysin in Patients with Previously Treated Advanced or Metatstatic Non Small Cell Lung Cancer (NSCLC) receiving Standard Salvage Chemotherapy – Canadian Cancer Trials Group IND 211. *J Clin Oncol* **34** (2016).

162. Farren, M. R. *et al*. Systemic Immune Activity Predicts Overall Survival in Treatment-Naive Patients with Metastatic Pancreatic Cancer. *Clin. Cancer Res.* **22**, 2565-2574 (2016).

163. Samson, A. *et al*. Intravenous delivery of oncolytic reovirus to brain tumor patients immunologically primes for subsequent checkpoint blockade. *Sci Transl Med* **10** (2018).

164. Mahalingam, D., Fountzilas, C., Moseley, J., Noronha, N., Cheetham, K., Dzugalo, A., Nuovo, G., Gutierrez, A. & Arora, S. A study of REOLYSIN in combination with pembrolizumab and chemotherapy in patients (pts) with relapsed metastatic adenocarcinoma of the pancreas (MAP). *J Clin Oncol* **35** (2017).

165. Fisher, K. Striking out at disseminated metastases: the systemic delivery of oncolytic viruses. *Curr. Opin. Mol. Ther.* **8**, 301-313 (2006).

166. Ferguson, M. S., Lemoine, N. R. & Wang, Y. Systemic delivery of oncolytic viruses: hopes and hurdles. *Adv. Virol.* **2012**, 805629 (2012).

167. Roy, D. & Bell, J. Cell carriers for oncolytic viruses; current challenges and future directions. *Oncolytic Virotherapy* **2013:2**, 47-56 (2013).

168. Eisenstein, S., Chen, S. H. & Pan, P. Y. Immune cells: more than simple carriers for systemic delivery of oncolytic viruses. *Oncolytic Virother* **3**, 83-91 (2014).

169. Eisenstein, S. *et al*. Myeloid-derived suppressor cells as a vehicle for tumor-specific oncolytic viral therapy. *Cancer Res.* **73**, 5003-5015 (2013).

170. Jennings, V. A. *et al*. Lymphokine-activated killer and dendritic cell carriage enhances oncolytic reovirus therapy for ovarian cancer by overcoming antibody neutralization in ascites. *Int. J. Cancer* **134**, 1091-1101 (2014).

171. Adair, R. A. *et al*. Cell carriage, delivery, and selective replication of an oncolytic virus in tumor in patients. *Sci. Transl. Med.* **4**, 138ra77 (2012).

172. Gollamudi, R. *et al*. Intravenous administration of Reolysin, a live replication competent RNA virus is safe in patients with advanced solid tumors. *Invest. New Drugs* **28**, 641-649 (2010).

173. Vidal, L. *et al*. A phase I study of intravenous oncolytic reovirus type 3 Dearing in patients with advanced cancer. *Clin. Cancer Res.* **14**, 7127-7137 (2008).

174. Lolkema, M. P. *et al*. A phase I study of the combination of intravenous reovirus type 3 Dearing and gemcitabine in patients with advanced cancer. *Clin. Cancer Res.* **17**, 581-588 (2011).

175. Comins, C. *et al*. REO-10: a phase I study of intravenous reovirus and docetaxel in patients with advanced cancer. *Clin. Cancer Res.* **16**, 5564-5572 (2010).

176. Karapanagiotou, E. M. *et al*. Phase I/II trial of carboplatin and paclitaxel chemotherapy in combination with intravenous oncolytic reovirus in patients with advanced malignancies. *Clin. Cancer Res.* **18**, 2080-2089 (2012).

177. Ilett, E. J. *et al*. Internalization of oncolytic reovirus by human dendritic cell carriers protects the virus from neutralization. *Clin. Cancer Res.* **17**, 2767-2776 (2011).

178. Aitken, A. S. *et al*. Brief Communication; A Heterologous Oncolytic Bacteria-Virus Prime-Boost Approach for Anticancer Vaccination in Mice. *J. Immunother.* (2017).

179. Hanahan, D. & Weinberg, R. A. Hallmarks of cancer: the next generation. *Cell* **144**, 646-674 (2011).

180. Kitamura, T., Qian, B. Z. & Pollard, J. W. Immune cell promotion of metastasis. *Nat. Rev. Immunol.* **15**, 73-86 (2015).

181. Schreiber, R. D., Old, L. J. & Smyth, M. J. Cancer immunoediting: integrating immunity's roles in cancer suppression and promotion. *Science* **331**, 1565-1570 (2011).

182. Dunn, G. P., Bruce, A. T., Ikeda, H., Old, L. J. & Schreiber, R. D. Cancer immunoediting: from immunosurveillance to tumor escape. *Nat. Immunol.* **3**, 991-998 (2002).

183. Schreiber, R. D., Old, L. J. & Smyth, M. J. Cancer immunoediting: integrating immunity's roles in cancer suppression and promotion. *Science* **331**, 1565-1570 (2011).

184. MacKie, R. M., Reid, R. & Junor, B. Fatal melanoma transferred in a donated kidney 16 years after melanoma surgery. *N. Engl. J. Med.* **348**, 567-568 (2003).

185. Myron Kauffman, H. *et al*. Transplant tumor registry: donor related malignancies. *Transplantation* **74**, 358-362 (2002).

186. Koebel, C. M. *et al*. Adaptive immunity maintains occult cancer in an equilibrium state. *Nature* **450**, 903-907 (2007).

187. Gajewski, T. F., Schreiber, H. & Fu, Y. X. Innate and adaptive immune cells in the tumor microenvironment. *Nat. Immunol.* **14**, 1014-1022 (2013).

188. Pardoll, D. M. The blockade of immune checkpoints in cancer immunotherapy. *Nat. Rev. Cancer.* **12**, 252-264 (2012).

189. Pardoll, D. M. Immunology beats cancer: a blueprint for successful translation. *Nat. Immunol.* **13**, 1129-1132 (2012).

190. Gabrilovich, D. I., Ostrand-Rosenberg, S. & Bronte, V. Coordinated regulation of myeloid cells by tumours. *Nat. Rev. Immunol.* **12**, 253-268 (2012).

191. Ashkenazi, E. *et al*. A selective impairment of the IL-2 system in lymphocytes of patients with glioblastomas: increased level of soluble IL-2R and reduced protein tyrosine phosphorylation. *Neuroimmunomodulation* **4**, 49-56 (1997).

192. Chen, Y. *et al*. Study on T lymphocyte recognition of tumor antigens on autologous CML cells. *Zhonghua Xue Ye Xue Za Zhi* **18**, 638-641 (1997).

193. Rosen, H. R. *et al*. Activated lymphocytes from breast cancer patients express the characteristics of type 2 helper cells--a possible role for breast cancer-associated p43. *Cancer Lett.* **127**, 129-134 (1998).

194. Elsasser-Beile, U. *et al*. Th1 and Th2 cytokine response patterns in leukocyte cultures of patients with urinary bladder, renal cell and prostate carcinomas. *Tumour Biol.* **19**, 470-476 (1998).

195. Lanitis, E., Irving, M. & Coukos, G. Targeting the tumor vasculature to enhance T cell activity. *Curr. Opin. Immunol.* **33C**, 55-63 (2015).

196. Palazon, A. *et al*. Agonist anti-CD137 mAb act on tumor endothelial cells to enhance recruitment of activated T lymphocytes. *Cancer Res.* **71**, 801-811 (2011).

197. Sata, M. & Walsh, K. TNFalpha regulation of Fas ligand expression on the vascular endothelium modulates leukocyte extravasation. *Nat. Med.* **4**, 415-420 (1998).

198. Motz, G. T. *et al*. Tumor endothelium FasL establishes a selective immune barrier promoting tolerance in tumors. *Nat. Med.* **20**, 607-615 (2014).

199. Palazon, A., Aragones, J., Morales-Kastresana, A., de Landazuri, M. O. & Melero, I. Molecular pathways: hypoxia response in immune cells fighting or promoting cancer. *Clin. Cancer Res.* **18**, 1207-1213 (2012).

200. Ksiazkiewicz, M. *et al*. Importance of CCL2-CCR2A/2B signaling for monocyte migration into spheroids of breast cancer-derived fibroblasts. *Immunobiology* **215**, 737-747 (2010).

201. Qian, B. Z. *et al*. CCL2 recruits inflammatory monocytes to facilitate breast-tumour metastasis. *Nature* **475**, 222-225 (2011).

202. Liao, D., Luo, Y., Markowitz, D., Xiang, R. & Reisfeld, R. A. Cancer associated fibroblasts promote tumor growth and metastasis by modulating the tumor immune microenvironment in a 4T1 murine breast cancer model. *PLoS One* **4**, e7965 (2009).

203. Feig, C. *et al*. The pancreas cancer microenvironment. *Clin. Cancer Res.* **18**, 4266-4276 (2012).

204. Whatcott, C. J., Posner, R. G., Von Hoff, D. D. & Han, H. in *Pancreatic Cancer and Tumor Microenvironment* (eds Grippo, P. J. & Munshi, H. G.) (Transworld Research Network, Trivandrum (India), 2012).

205. Sarvaria, A., Madrigal, J. A. & Saudemont, A. B cell regulation in cancer and anti-tumor immunity. *Cell. Mol. Immunol.* **14**, 662-674 (2017).

206. Fehervari, Z. & Sakaguchi, S. CD4+ Tregs and immune control. *J. Clin. Invest.* **114**, 1209-1217 (2004).

207. Onishi, Y., Fehervari, Z., Yamaguchi, T. & Sakaguchi, S. Foxp3+ natural regulatory T cells preferentially form aggregates on dendritic cells in vitro and actively inhibit their maturation. *Proc. Natl. Acad. Sci. U. S. A.* **105**, 10113-10118 (2008).

208. Chinen, T. *et al*. An essential role for the IL-2 receptor in T sub(reg) cell function. *Nature Immunology* **17**, 1322-1333 (2016).

209. Parker, K. H., Beury, D. W. & Ostrand-Rosenberg, S. Myeloid-Derived Suppressor Cells: Critical Cells Driving Immune Suppression in the Tumor Microenvironment. *Adv. Cancer Res.* **128**, 95-139 (2015).

210. Eruslanov, E. B. *et al*. Tumor-associated neutrophils stimulate T cell responses in early-stage human lung cancer. *J. Clin. Invest.* **124**, 5466-5480 (2014).

211. Fridlender, Z. G. *et al*. Polarization of tumor-associated neutrophil phenotype by TGF-beta: "N1" versus "N2" TAN. *Cancer Cell* **16**, 183-194 (2009).

212. Mills, A. *et al*. Indoleamine 2,3-dioxygenase in endometrial cancer: a targetable mechanism of immune resistance in mismatch repair-deficient and intact endometrial carcinomas. *Mod. Pathol.* (2018).

213. Chang, C. *et al*. Metabolic Competition in the Tumor Microenvironment Is a Driver of Cancer Progression. *Cell* **162**, 1229-1241 (2015).

214. Chiu, H. *et al*. Pre-existing Fas ligand (FasL) in cancer cells elicits tumor-specific protective immunity, but delayed induction of FasL expression after inoculation facilitates tumor formation. *Mol. Carcinog.* **52**, 705-714 (2013).

215. Kantoff, P. W. *et al*. Sipuleucel-T immunotherapy for castration-resistant prostate cancer. *N. Engl. J. Med.* **363**, 411-422 (2010).

216. Hodi, F. S. *et al*. Improved survival with ipilimumab in patients with metastatic melanoma. *N. Engl. J. Med.* **363**, 711-723 (2010).

217. Hamid, O. *et al*. Safety and tumor responses with lambrolizumab (anti-PD-1) in melanoma. *N. Engl. J. Med.* **369**, 134-144 (2013).

218. Greig, S. L. Talimogene Laherparepvec: First Global Approval. *Drugs* **76**, 147-154 (2016).

219. Peterson, A. C., Harlin, H. & Gajewski, T. F. Immunization with Melan-A peptide-pulsed peripheral blood mononuclear cells plus recombinant human interleukin-12 induces clinical activity and T-cell responses in advanced melanoma. *J. Clin. Oncol.* **21**, 2342-2348 (2003).

220. Fourcade, J. *et al*. Immunization with analog peptide in combination with CpG and montanide expands tumor antigen-specific CD8+ T cells in melanoma patients. *J. Immunother.* **31**, 781-791 (2008).

221. Adams, S. *et al*. Immunization of malignant melanoma patients with full-length NY-ESO-1 protein using TLR7 agonist imiquimod as vaccine adjuvant. *J. Immunol.* **181**, 776-784 (2008).

222. Gabrilovich, D. I. & Nagaraj, S. Myeloid-derived suppressor cells as regulators of the immune system. *Nat. Rev. Immunol.* **9**, 162-174 (2009).

223. Solito, S. *et al*. A human promyelocytic-like population is responsible for the immune suppression mediated by myeloid-derived suppressor cells. *Blood* **118**, 2254-2265 (2011).

224. Nagaraj, S., Schrum, A. G., Cho, H. I., Celis, E. & Gabrilovich, D. I. Mechanism of T cell tolerance induced by myeloid-derived suppressor cells. *J. Immunol.* **184**, 3106-3116 (2010).

225. Elkabets, M. *et al*. IL-1beta regulates a novel myeloid-derived suppressor cell subset that impairs NK cell development and function. *Eur. J. Immunol.* **40**, 3347-3357 (2010).

226. Sakuishi, K., Jayaraman, P., Behar, S. M., Anderson, A. C. & Kuchroo, V. K. Emerging Tim-3 functions in antimicrobial and tumor immunity. *Trends Immunol.* **32**, 345-349 (2011).

227. Noman, M. Z. *et al*. PD-L1 is a novel direct target of HIF-1alpha, and its blockade under hypoxia enhanced MDSC-mediated T cell activation. *J. Exp. Med.* **211**, 781-790 (2014).

228. Kuang, D. M. *et al*. Activated monocytes in peritumoral stroma of hepatocellular carcinoma foster immune privilege and disease progression through PD-L1. *J. Exp. Med.* **206**, 1327-1337 (2009).

229. Zhao, Q. *et al*. Activated CD69+ T cells foster immune privilege by regulating IDO expression in tumor-associated macrophages. *J. Immunol.* **188**, 1117-1124 (2012).

230. Sica, A. & Mantovani, A. Macrophage plasticity and polarization: in vivo veritas. *J. Clin. Invest.* **122**, 787-795 (2012).

231. Hagemann, T. *et al*. Ovarian cancer cells polarize macrophages toward a tumor-associated phenotype. *J. Immunol.* **176**, 5023-5032 (2006).

232. Chen, C. *et al*. Induced expression of B7-H4 on the surface of lung cancer cell by the tumor-associated macrophages: a potential mechanism of immune escape. *Cancer Lett.* **317**, 99-105 (2012).

233. Chen, C. *et al*. Induced expression of B7-H3 on the lung cancer cells and macrophages suppresses T-cell mediating anti-tumor immune response. *Exp. Cell Res.* **319**, 96-102 (2013).

234. Chang, C. I., Liao, J. C. & Kuo, L. Macrophage arginase promotes tumor cell growth and suppresses nitric oxide-mediated tumor cytotoxicity. *Cancer Res.* **61**, 1100-1106 (2001).

235. Chen, W., Liang, X., Peterson, A. J., Munn, D. H. & Blazar, B. R. The indoleamine 2,3-dioxygenase pathway is essential for human plasmacytoid dendritic cell-induced adaptive T regulatory cell generation. *J. Immunol.* **181**, 5396-5404 (2008).

236. Demoulin, S., Herfs, M., Delvenne, P. & Hubert, P. Tumor microenvironment converts plasmacytoid dendritic cells into immunosuppressive/tolerogenic cells: insight into the molecular mechanisms. *J. Leukoc. Biol.* **93**, 343-352 (2013).

237. Sisirak, V. *et al*. Impaired IFN-alpha production by plasmacytoid dendritic cells favors regulatory T-cell expansion that may contribute to breast cancer progression. *Cancer Res.* **72**, 5188-5197 (2012).

238. Predina, J. *et al*. Changes in the local tumor microenvironment in recurrent cancers may explain the failure of vaccines after surgery. *Proc. Natl. Acad. Sci. U. S. A.* **110**, 415 (2013).

239. Galdiero, M. R. *et al*. Tumor associated macrophages and neutrophils in cancer. *Immunobiology* **218**, 1402-1410 (2013).

240. Josefowicz, S. Z., Lu, L. F. & Rudensky, A. Y. Regulatory T cells: mechanisms of differentiation and function. *Annu. Rev. Immunol.* **30**, 531-564 (2012).

241. Gattinoni, L. *et al*. Removal of homeostatic cytokine sinks by lymphodepletion enhances the efficacy of adoptively transferred tumor-specific CD8+ T cells. *J. Exp. Med.* **202**, 907-912 (2005).

242. Qureshi, O. S. *et al*. Trans-endocytosis of CD80 and CD86: a molecular basis for the cell-extrinsic function of CTLA-4. *Science* **332**, 600-603 (2011).

243. Liang, B. *et al*. Regulatory T cells inhibit dendritic cells by lymphocyte activation gene-3 engagement of MHC class II. *J. Immunol.* **180**, 5916-5926 (2008).

244. He, Y. *et al*. The roles of regulatory B cells in cancer. *J. Immunol. Res.* **2014**, 215471 (2014).

245. Ch'ng, S., Wallis, R. A., Yuan, L., Davis, P. F. & Tan, S. T. Mast cells and cutaneous malignancies. *Mod. Pathol.* **19**, 149-159 (2006).

246. Feig, C. *et al*. Targeting CXCL12 from FAP-expressing carcinoma-associated fibroblasts synergizes with anti-PD-L1 immunotherapy in pancreatic cancer. *Proc. Natl. Acad. Sci. U. S. A.* **110**, 20212-20217 (2013).

247. Ochs, K. *et al*. Immature mesenchymal stem cell-like pericytes as mediators of immunosuppression in human malignant glioma. *J. Neuroimmunol.* **265**, 106-116 (2013).

248. Xiong, H. *et al*. Innate Lymphocyte/Ly6C(hi) Monocyte Crosstalk Promotes Klebsiella Pneumoniae Clearance. *Cell* **165**, 679-689 (2016).

249. Whitfield-Larry, F., Felton, J., Buse, J. & Su, M. A. Myeloid-derived suppressor cells are increased in frequency but not maximally suppressive in peripheral blood of Type 1 Diabetes Mellitus patients. *Clin. Immunol.* **153**, 156-164 (2014).

250. Kloepper, J. *et al*. Ang-2/VEGF bispecific antibody reprograms macrophages and resident microglia to anti-tumor phenotype and prolongs glioblastoma survival. *Proc. Natl. Acad. Sci. U. S. A.* **113**, 4476-4481 (2016).

251. Kumar, V. *et al*. CD45 Phosphatase Inhibits STAT3 Transcription Factor Activity in Myeloid Cells and Promotes Tumor-Associated Macrophage Differentiation. *Immunity* **44**, 303-315 (2016).

252. Kumar, V., Patel, S., Tcyganov, E. & Gabrilovich, D. I. The Nature of Myeloid-Derived Suppressor Cells in the Tumor Microenvironment. *Trends Immunol.* **37**, 208-220 (2016).

253. Serbina, N. V. & Pamer, E. G. Monocyte emigration from bone marrow during bacterial infection requires signals mediated by chemokine receptor CCR2. *Nat. Immunol.* **7**, 311-317 (2006).

254. Aldridge, J. R.,Jr *et al*. TNF/iNOS-producing dendritic cells are the necessary evil of lethal influenza virus infection. *Proc. Natl. Acad. Sci. U. S. A.* **106**, 5306-5311 (2009).

255. Ersland, K., Wuthrich, M. & Klein, B. S. Dynamic interplay among monocyte-derived, dermal, and resident lymph node dendritic cells during the generation of vaccine immunity to fungi. *Cell. Host Microbe* **7**, 474-487 (2010).

256. Varol, C. *et al*. Intestinal lamina propria dendritic cell subsets have different origin and functions. *Immunity* **31**, 502-512 (2009).

257. Cheong, C. *et al*. Microbial stimulation fully differentiates monocytes to DC-SIGN/CD209(+) dendritic cells for immune T cell areas. *Cell* **143**, 416-429 (2010).

258. Gabitass, R. F., Annels, N. E., Stocken, D. D., Pandha, H. A. & Middleton, G. W. Elevated myeloid-derived suppressor cells in pancreatic, esophageal and gastric cancer are an independent prognostic factor and are associated with significant elevation of the Th2 cytokine interleukin-13. *Cancer Immunol. Immunother.* **60**, 1419-1430 (2011).

259. Dumitru, C. A., Moses, K., Trellakis, S., Lang, S. & Brandau, S. Neutrophils and granulocytic myeloid-derived suppressor cells: immunophenotyping, cell biology and clinical relevance in human oncology. *Cancer Immunol. Immunother.* **61**, 1155-1167 (2012).

260. Bronte, V. *et al*. Recommendations for myeloid-derived suppressor cell nomenclature and characterization standards. *Nat. Commun.* **7**, 12150 (2016).

261. Sica, A. & Bronte, V. Altered macrophage differentiation and immune dysfunction in tumor development. *J. Clin. Invest.* **117**, 1155-1166 (2007).

262. Gallina, G. *et al*. Tumors induce a subset of inflammatory monocytes with immunosuppressive activity on CD8+ T cells. *J. Clin. Invest.* **116**, 2777-2790 (2006).

263. Greten, T. F., Manns, M. P. & Korangy, F. Myeloid derived suppressor cells in human diseases. *Int. Immunopharmacol.* **11**, 802-807 (2011).

264. Kusmartsev, S. *et al*. Reversal of myeloid cell-mediated immunosuppression in patients with metastatic renal cell carcinoma. *Clin. Cancer Res.* **14**, 8270-8278 (2008).

265. Obermajer, N., Muthuswamy, R., Odunsi, K., Edwards, R. P. & Kalinski, P. PGE2-Induced CXCL12 Production and CXCR4 Expression Controls the Accumulation of Human MDSCs in Ovarian Cancer Environment. *Cancer Research* **71**, 7463-7470 (2011).

266. Srivastava, M. K., Sinha, P., Clements, V. K., Rodriguez, P. & Ostrand-Rosenberg, S. Myeloid-derived suppressor cells inhibit T-cell activation by depleting cystine and cysteine. *Cancer Res.* **70**, 68-77 (2010).

267. Hanson, E. M., Clements, V. K., Sinha, P., Ilkovitch, D. & Ostrand-Rosenberg, S. Myeloid-derived suppressor cells down-regulate L-selectin expression on CD4+ and CD8+ T cells. *J. Immunol.* **183**, 937-944 (2009).

268. De Henau, O. *et al*. Overcoming resistance to checkpoint blockade therapy by targeting PI3Kgamma in myeloid cells. *Nature* **539**, 443-447 (2016).

269. Highfill, S. L. *et al*. Disruption of CXCR2-mediated MDSC tumor trafficking enhances anti-PD1 efficacy. *Sci. Transl. Med.* **6**, 237ra67 (2014).

270. Meyer, C. *et al*. Frequencies of circulating MDSC correlate with clinical outcome of melanoma patients treated with ipilimumab. *Cancer Immunol. Immunother.* **63**, 247-257 (2014).

271. Bjoern, J. *et al*. Immunological correlates of treatment and response in stage IV malignant melanoma patients treated with Ipilimumab. *Oncoimmunology* **5**, e1100788 (2015).

272. Holmgaard, R. B., Zamarin, D., Lesokhin, A., Merghoub, T. & Wolchok, J. D. Targeting myeloid-derived suppressor cells with colony stimulating factor-1 receptor blockade can reverse immune resistance to immunotherapy in indoleamine 2,3-dioxygenase-expressing tumors. *EBioMedicine* **6**, 50-58 (2016).

273. Long, A. H. *et al*. Reduction of MDSCs with All-trans Retinoic Acid Improves CAR Therapy Efficacy for Sarcomas. *Cancer. Immunol. Res.* **4**, 869-880 (2016).

274. Fortin, C., Huang, X. & Yang, Y. NK cell response to vaccinia virus is regulated by myeloid-derived suppressor cells. *J. Immunol.* **189**, 1843-1849 (2012).

275. Kaneda, M. M. *et al*. PI3Kgamma is a molecular switch that controls immune suppression. *Nature* **539**, 437-442 (2016).

276. Mirza, N. *et al*. All-trans-retinoic acid improves differentiation of myeloid cells and immune response in cancer patients. *Cancer Res.* **66**, 9299-9307 (2006).

277. Gabrilovich, D. I., Velders, M. P., Sotomayor, E. M. & Kast, W. M. Mechanism of immune dysfunction in cancer mediated by immature Gr-1+ myeloid cells. *J. Immunol.* **166**, 5398-5406 (2001).

278. Lu, L. *et al*. All-trans retinoic acid promotes TGF-beta-induced Tregs via histone modification but not DNA demethylation on Foxp3 gene locus. *PLoS One* **6**, e24590 (2011).

279. Vincent, J. *et al*. 5-Fluorouracil selectively kills tumor-associated myeloid-derived suppressor cells resulting in enhanced T cell-dependent antitumor immunity. *Cancer Res.* **70**, 3052-3061 (2010).

280. Le, H. K. *et al*. Gemcitabine directly inhibits myeloid derived suppressor cells in BALB/c mice bearing 4T1 mammary carcinoma and augments expansion of T cells from tumor-bearing mice. *Int. Immunopharmacol.* **9**, 900-909 (2009).

281. Suzuki, E., Kapoor, V., Jassar, A. S., Kaiser, L. R. & Albelda, S. M. Gemcitabine selectively eliminates splenic Gr-1+/CD11b+ myeloid suppressor cells in tumor-bearing animals and enhances antitumor immune activity. *Clin. Cancer Res.* **11**, 6713-6721 (2005).

282. Adotevi, O. *et al*. A decrease of regulatory T cells correlates with overall survival after sunitinib-based antiangiogenic therapy in metastatic renal cancer patients. *J. Immunother.* **33**, 991-998 (2010).

283. Ko, J. S. *et al*. Sunitinib mediates reversal of myeloid-derived suppressor cell accumulation in renal cell carcinoma patients. *Clin. Cancer Res.* **15**, 2148-2157 (2009).

284. Finke, J. H. *et al*. Sunitinib reverses type-1 immune suppression and decreases T-regulatory cells in renal cell carcinoma patients. *Clin. Cancer Res.* **14**, 6674-6682 (2008).

285. Noonan, K. A., Ghosh, N., Rudraraju, L., Bui, M. & Borrello, I. Targeting immune suppression with PDE5 inhibition in end-stage multiple myeloma. *Cancer. Immunol. Res.* **2**, 725-731 (2014).

286. Fujita, M. *et al*. COX-2 blockade suppresses gliomagenesis by inhibiting myeloid-derived suppressor cells. *Cancer Res.* **71**, 2664-2674 (2011).

287. Mantovani, A. & Sica, A. Macrophages, innate immunity and cancer: balance, tolerance, and diversity. *Curr. Opin. Immunol.* **22**, 231-237 (2010).

288. Qian, B. Z. & Pollard, J. W. Macrophage diversity enhances tumor progression and metastasis. *Cell* **141**, 39-51 (2010).

289. Zheng, Y. *et al*. Macrophages are an abundant component of myeloma microenvironment and protect myeloma cells from chemotherapy drug-induced apoptosis. *Blood* **114**, 3625-3628 (2009).

290. Jha, A. K. *et al*. Network integration of parallel metabolic and transcriptional data reveals metabolic modules that regulate macrophage polarization. *Immunity* **42**, 419-430 (2015).

291. Franklin, R. A. *et al*. The cellular and molecular origin of tumor-associated macrophages. *Science* **344**, 921-925 (2014).

292. Engblom, C., Pfirschke, C. & Pittet, M. J. The role of myeloid cells in cancer therapies. *Nat. Rev. Cancer.* **16**, 447-462 (2016).

293. Wertel, I. *et al*. Macrophage-derived chemokine CCL22 and regulatory T cells in ovarian cancer patients. *Tumour Biol.* (2015).

294. Kubota, Y. *et al*. M-CSF inhibition selectively targets pathological angiogenesis and lymphangiogenesis. *J. Exp. Med.* **206**, 1089-1102 (2009).

295. Lin, E. Y., Nguyen, A. V., Russell, R. G. & Pollard, J. W. Colony-stimulating factor 1 promotes progression of mammary tumors to malignancy. *J. Exp. Med.* **193**, 727-740 (2001).

296. Richardsen, E., Uglehus, R. D., Johnsen, S. H. & Busund, L. T. Macrophage-colony stimulating factor (CSF1) predicts breast cancer progression and mortality. *Anticancer Res.* **35**, 865-874 (2015).

297. Ueno, T. *et al*. Significance of macrophage chemoattractant protein-1 in macrophage recruitment, angiogenesis, and survival in human breast cancer. *Clin. Cancer Res.* **6**, 3282-3289 (2000).

298. Groblewska, M. *et al*. Serum levels of granulocyte colony-stimulating factor (G-CSF) and macrophage colony-stimulating factor (M-CSF) in pancreatic cancer patients. *Clin. Chem. Lab. Med.* **45**, 30-34 (2007).

299. Mroczko, B. *et al*. Serum macrophage-colony stimulating factor levels in colorectal cancer patients correlate with lymph node metastasis and poor prognosis. *Clin. Chim. Acta* **380**, 208-212 (2007).

300. Zhu, X. D. *et al*. High expression of macrophage colony-stimulating factor in peritumoral liver tissue is associated with poor survival after curative resection of hepatocellular carcinoma. *J. Clin. Oncol.* **26**, 2707-2716 (2008).

301. Smith, H. O. *et al*. The role of colony-stimulating factor 1 and its receptor in the etiopathogenesis of endometrial adenocarcinoma. *Clin. Cancer Res.* **1**, 313-325 (1995).

302. Zheng, Y. *et al*. PSGL-1/selectin and ICAM-1/CD18 interactions are involved in macrophage-induced drug resistance in myeloma. *Leukemia* **27**, 702-710 (2013).

303. Hughes, R. *et al*. Perivascular M2 Macrophages Stimulate Tumor Relapse after Chemotherapy. *Cancer Res.* **75**, 3479-3491 (2015).

304. Arlauckas, S. P. *et al*. In vivo imaging reveals a tumor-associated macrophage-mediated resistance pathway in anti-PD-1 therapy. *Sci. Transl. Med.* **9**, 10.1126/scitranslmed.aal3604 (2017).

305. Zhu, Y. *et al*. CSF1/CSF1R blockade reprograms tumor-infiltrating macrophages and improves response to T-cell checkpoint immunotherapy in pancreatic cancer models. *Cancer Res.* **74**, 5057-5069 (2014).

306. Ries, C. H. *et al*. Targeting tumor-associated macrophages with anti-CSF-1R antibody reveals a strategy for cancer therapy. *Cancer Cell* **25**, 846-859 (2014).

307. Mitchem, J. B. *et al*. Targeting tumor-infiltrating macrophages decreases tumor-initiating cells, relieves immunosuppression, and improves chemotherapeutic responses. *Cancer Res.* **73**, 1128-1141 (2013).

308. Strachan, D. C. *et al*. CSF1R inhibition delays cervical and mammary tumor growth in murine models by attenuating the turnover of tumor-associated macrophages and enhancing infiltration by CD8+ T cells. *Oncoimmunology* **2**, e26968 (2013).

309. Cortez-Retamozo, V. *et al*. Origins of tumor-associated macrophages and neutrophils. *Proc. Natl. Acad. Sci. U. S. A.* **109**, 2491-2496 (2012).

310. Leuschner, F. *et al*. Therapeutic siRNA silencing in inflammatory monocytes in mice. *Nat. Biotechnol.* **29**, 1005-1010 (2011).

311. Cook, R. S. *et al*. MerTK inhibition in tumor leukocytes decreases tumor growth and metastasis. *Journal of Clinical Investigation* **123**, 3231 (2013).

312. Graham, D. K., DeRyckere, D., Davies, K. D. & Earp, H. S. The TAM family: phosphatidylserine sensing receptor tyrosine kinases gone awry in cancer. *Nature reviews. Cancer* **14**, 769 (2014).

313. Wang, H. *et al*. Histone deacetylase inhibitor LAQ824 augments inflammatory responses in macrophages through transcriptional regulation of IL-10. *J. Immunol.* **186**, 3986-3996 (2011).

314. Chen, X. *et al*. Requirement for the histone deacetylase Hdac3 for the inflammatory gene expression program in macrophages. *Proc. Natl. Acad. Sci. U. S. A.* **109**, 2865 (2012).

315. Nicodeme, E. *et al*. Suppression of inflammation by a synthetic histone mimic. *Nature* **468**, 1119-1123 (2010).

316. Ivashkiv, L. B. Epigenetic regulation of macrophage polarization and function. *Trends Immunol.* **34**, 216-223 (2013).

317. Gabrilovich, D. Mechanisms and functional significance of tumour-induced dendritic-cell defects. *Nat. Rev. Immunol.* **4**, 941-952 (2004).

318. Woo, S. R., Corrales, L. & Gajewski, T. F. Innate Immune Recognition of Cancer. *Annu. Rev. Immunol.* (2015).

319. Esaki, S., Goshima, F., Kimura, H., Murakami, S. & Nishiyama, Y. Enhanced antitumoral activity of oncolytic herpes simplex virus with gemcitabine using colorectal tumor models. *Int. J. Cancer* **132**, 1592-1601 (2013).

320. Eisenberg, D. P. *et al*. 5-Fluorouracil and Gemcitabine Potentiate the Efficacy of Oncolytic Herpes Viral Gene Therapy in the Treatment of Pancreatic Cancer. *J Gastrointest Surg* **9**, 1068-1079 (2005).

321. Binz, E. *et al*. Chemovirotherapy of Pancreatic Adenocarcinoma by Combining Oncolytic Vaccinia Virus GLV-1h68 with nab-Paclitaxel Plus Gemcitabine. *Mol Ther Oncolytics* **6**, 10-21 (2017).

322. Jung, K. H. *et al*. Oncolytic adenovirus expressing relaxin (YDC002) enhances therapeutic efficacy of gemcitabine against pancreatic cancer. *Cancer Lett.* **396**, 155-166 (2017).

323. Maliandi, M. V. *et al*. AduPARE1A and gemcitabine combined treatment trigger synergistic antitumor effects in pancreatic cancer through NF-κB mediated uPAR activation. *Mol. Cancer* **14**, 146 (2015).

324. Bhattacharyya, M., Francis, J., Eddouadi, A., Lemoine, N. R. & Halldén, G. An oncolytic adenovirus defective in pRb-binding (dl922-947) can efficiently eliminate pancreatic cancer cells and tumors in vivo in combination with 5-FU or gemcitabine. *Cancer Gene Ther.* **18**, 734-743 (2011).

325. Jha, B. K., Dong, B., Nguyen, C. T., Polyakova, I. & Silverman, R. H. Suppression of antiviral innate immunity by sunitinib enhances oncolytic virotherapy. *Mol. Ther.* **21**, 1749-1757 (2013).

326. Walker, J. D., Sehgal, I. & Kousoulas, K. G. Oncolytic Herpes Simplex Virus 1 Encoding 15-Prostaglandin Dehydrogenase Mitigates Immune Suppression and Reduces Ectopic Primary and Metastatic Breast Cancer in Mice. *J. Virol.* **85**, 7363-7371 (2011).

327. Prestwich, R. J., Ilett, E. J., Steele, L. & Errington, F. The importance of the immune system in reovirus therapy. *Clin. Oncol. (R. Coll. Radiol)* **20**, 769 (2008).

328. Roby, K. F. *et al*. Development of a syngeneic mouse model for events related to ovarian cancer. *Carcinogenesis* **21**, 585-591 (2000).

329. Gujar, S. A. & Michalak, T. I. Flow cytometric quantification of T cell proliferation and division kinetics in woodchuck model of hepatitis B. *Immunol. Invest.* **34**, 215-236 (2005).

330. Livak, K. J. & Schmittgen, T. D. Analysis of relative gene expression data using real-time quantitative PCR and the 2(-Delta Delta C(T)) Method. *Methods* **25**, 402-408 (2001).

331. Murphy, J. P., Stepanova, E., Everley, R. A., Paulo, J. A. & Gygi, S. P. Comprehensive Temporal Protein Dynamics during the Diauxic Shift in Saccharomyces cerevisiae. *Mol. Cell. Proteomics* **14**, 2454-2465 (2015).

332. Rappsilber, J., Ishihama, Y. & Mann, M. Stop and go extraction tips for matrix-assisted laser desorption/ionization, nanoelectrospray, and LC/MS sample pretreatment in proteomics. *Anal. Chem.* **75**, 663-670 (2003).

333. Ashburner, M. *et al*. Gene ontology: tool for the unification of biology. The Gene Ontology Consortium. *Nat. Genet.* **25**, 25-29 (2000).

334. Gene Ontology Consortium. Gene Ontology Consortium: going forward. *Nucleic Acids Res.* **43**, 1049 (2015).

335. Saeed, A. I. *et al*. TM4: a free, open-source system for microarray data management and analysis. *BioTechniques* **34**, 374-378 (2003).

336. Vizcaino, J. A. *et al*. ProteomeXchange provides globally coordinated proteomics data submission and dissemination. *Nat. Biotechnol.* **32**, 223-226 (2014).

337. Vizcaino, J. A. *et al*. 2016 update of the PRIDE database and its related tools. *Nucleic Acids Res.* **44**, 447 (2016).

338. Couzin-Frankel, J. Breakthrough of the year 2013. Cancer immunotherapy. *Science* **342**, 1432-1433 (2013).

339. Sato, E. *et al*. Intraepithelial CD8+ tumor-infiltrating lymphocytes and a high CD8+/regulatory T cell ratio are associated with favorable prognosis in ovarian cancer. *Proc. Natl. Acad. Sci. U. S. A.* **102**, 18538-18543 (2005).

340. Liu, B. *et al*. Ovarian cancer immunotherapy: opportunities, progresses and challenges. *J. Hematol. Oncol.* **3**, 7 (2010).

341. Zhang, L. *et al*. Intratumoral T cells, recurrence, and survival in epithelial ovarian cancer. *N. Engl. J. Med.* **348**, 203-213 (2003).

342. Leach, D. R., Krummel, M. F. & Allison, J. P. Enhancement of antitumor immunity by CTLA-4 blockade. *Science* **271**, 1734-1736 (1996).

343. Mellman, I., Coukos, G. & Dranoff, G. Cancer immunotherapy comes of age. *Nature* **480**, 480-489 (2011).

344. Maitra, R., Ghalib, M. H. & Goel, S. Reovirus: a targeted therapeutic--progress and potential. *Mol. Cancer. Res.* **10**, 1514-1525 (2012).

345. Schouppe, E., De Baetselier, P., Van Ginderachter, J. A. & Sarukhan, A. Instruction of myeloid cells by the tumor microenvironment: Open questions on the dynamics and plasticity of different tumor-associated myeloid cell populations. *Oncoimmunology* **1**, 1135-1145 (2012).

346. Nagaraj, S., Youn, J. I. & Gabrilovich, D. I. Reciprocal relationship between myeloid-derived suppressor cells and T cells. *J. Immunol.* **191**, 17-23 (2013).

347. Serafini, P. Myeloid derived suppressor cells in physiological and pathological conditions: the good, the bad, and the ugly. *Immunol. Res.* **57**, 172-184 (2013).

348. Ostrand-Rosenberg, S. Myeloid-derived suppressor cells: more mechanisms for inhibiting antitumor immunity. *Cancer Immunol. Immunother.* **59**, 1593-1600 (2010).

349. Sinha, P., Clements, V. K., Bunt, S. K., Albelda, S. M. & Ostrand-Rosenberg, S. Cross-talk between myeloid-derived suppressor cells and macrophages subverts tumor immunity toward a type 2 response. *J. Immunol.* **179**, 977-983 (2007).

350. Sinha, P., Clements, V. K. & Ostrand-Rosenberg, S. Interleukin-13-regulated M2 macrophages in combination with myeloid suppressor cells block immune surveillance against metastasis. *Cancer Res.* **65**, 11743-11751 (2005).

351. Van Ginderachter, J. A., Beschin, A., De Baetselier, P. & Raes, G. Myeloid-derived suppressor cells in parasitic infections. *Eur. J. Immunol.* **40**, 2976-2985 (2010).

352. Martino, A. *et al*. Mycobacterium bovis bacillus Calmette-Guerin vaccination mobilizes innate myeloid-derived suppressor cells restraining in vivo T cell priming via IL-1R-dependent nitric oxide production. *J. Immunol.* **184**, 2038-2047 (2010).

353. Bowen, J. L. & Olson, J. K. Innate immune CD11b+Gr-1+ cells, suppressor cells, affect the immune response during Theiler's virus-induced demyelinating disease. *J. Immunol.* **183**, 6971-6980 (2009).

354. De Santo, C. *et al*. Invariant NKT cells reduce the immunosuppressive activity of influenza A virus-induced myeloid-derived suppressor cells in mice and humans. *J. Clin. Invest.* **118**, 4036-4048 (2008).

355. Zhu, J., Huang, X. & Yang, Y. Myeloid-derived suppressor cells regulate natural killer cell response to adenovirus-mediated gene transfer. *J. Virol.* **86**, 13689-13696 (2012).

356. Ribechini, E., Leenen, P. J. & Lutz, M. B. Gr-1 antibody induces STAT signaling, macrophage marker expression and abrogation of myeloid-derived suppressor cell activity in BM cells. *Eur. J. Immunol.* **39**, 3538-3551 (2009).

357. Ostrand-Rosenberg, S. & Sinha, P. Myeloid-derived suppressor cells: linking inflammation and cancer. *J. Immunol.* **182**, 4499-4506 (2009).

358. Ahmed, N. & Stenvers, K. L. Getting to know ovarian cancer ascites: opportunities for targeted therapy-based translational research. *Front. Oncol.* **3**, 256 (2013).

359. Norris, B. A. *et al*. Chronic but not acute virus infection induces sustained expansion of myeloid suppressor cell numbers that inhibit viral-specific T cell immunity. *Immunity* **38**, 309-321 (2013).

360. Goh, C., Narayanan, S. & Hahn, Y. S. Myeloid-derived suppressor cells: the dark knight or the joker in viral infections? *Immunol. Rev.* **255**, 210-221 (2013).

361. Goni, O., Alcaide, P. & Fresno, M. Immunosuppression during acute Trypanosoma cruzi infection: involvement of Ly6G (Gr1(+))CD11b(+)immature myeloid suppressor cells. *Int. Immunol.* **14**, 1125-1134 (2002).

362. Young, M. R., Newby, M. & Wepsic, H. T. Hematopoiesis and suppressor bone marrow cells in mice bearing large metastatic Lewis lung carcinoma tumors. *Cancer Res.* **47**, 100-105 (1987).

363. Buessow, S. C., Paul, R. D. & Lopez, D. M. Influence of mammary tumor progression on phenotype and function of spleen and in situ lymphocytes in mice. *J. Natl. Cancer Inst.* **73**, 249-255 (1984).

364. Seung, L. P., Rowley, D. A., Dubey, P. & Schreiber, H. Synergy between T-cell immunity and inhibition of paracrine stimulation causes tumor rejection. *Proc. Natl. Acad. Sci. U. S. A.* **92**, 6254-6258 (1995).

365. Tacke, R. S. *et al*. Myeloid suppressor cells induced by hepatitis C virus suppress T-cell responses through the production of reactive oxygen species. *Hepatology* **55**, 343-353 (2012).

366. Qin, A. *et al*. Expansion of monocytic myeloid-derived suppressor cells dampens T cell function in HIV-1-seropositive individuals. *J. Virol.* **87**, 1477-1490 (2013).

367. du Plessis, N. *et al*. Increased frequency of myeloid-derived suppressor cells during active tuberculosis and after recent mycobacterium tuberculosis infection suppresses T-cell function. *Am. J. Respir. Crit. Care Med.* **188**, 724-732 (2013).

368. Giordanengo, L. *et al*. Cruzipain, a major Trypanosoma cruzi antigen, conditions the host immune response in favor of parasite. *Eur. J. Immunol.* **32**, 1003-1011 (2002).

369. Zhu, B. *et al*. CD11b+Ly-6C(hi) suppressive monocytes in experimental autoimmune encephalomyelitis. *J. Immunol.* **179**, 5228-5237 (2007).

370. Shehata, M. *et al*. Human leukocyte antigen class I expression is an independent prognostic factor in advanced ovarian cancer resistant to first-line platinum chemotherapy. *Br. J. Cancer* **101**, 1321-1328 (2009).

371. Vitale, M. *et al*. HLA class I antigen down-regulation in primary ovary carcinoma lesions: association with disease stage. *Clin. Cancer Res.* **11**, 67-72 (2005).

372. Han, L. Y. *et al*. HLA class I antigen processing machinery component expression and intratumoral T-Cell infiltrate as independent prognostic markers in ovarian carcinoma. *Clin. Cancer Res.* **14**, 3372-3379 (2008).

373. Li, M. O., Wan, Y. Y., Sanjabi, S., Robertson, A. K. & Flavell, R. A. Transforming growth factor-beta regulation of immune responses. *Annu. Rev. Immunol.* **24**, 99-146 (2006).

374. Salazar-Onfray, F. Interleukin-10: a cytokine used by tumors to escape immunosurveillance. *Med. Oncol.* **16**, 86-94 (1999).

375. Antonarakis, E. S. & Drake, C. G. Current status of immunological therapies for prostate cancer. *Curr Opin Urol* **20**, 241-246 (2010).

376. Drake, C. G. & Antonarakis, E. S. Update: immunological strategies for prostate cancer. *Curr Urol Rep* **11**, 202-207 (2010).

377. Kim, J. *et al*. Phase II clinical trial of induction chemotherapy with fixed dose rate gemcitabine and cisplatin followed by concurrent chemoradiotherapy with capecitabine for locally advanced pancreatic cancer. *Cancer Chemother. Pharmacol.* **70**, 381-389 (2012).

378. Bellmunt, J. *et al*. Randomized phase III study comparing paclitaxel/cisplatin/gemcitabine and gemcitabine/cisplatin in patients with locally advanced or metastatic urothelial cancer without prior systemic therapy: EORTC Intergroup Study 30987. *J. Clin. Oncol.* **30**, 1107-1113 (2012).

379. Pérol, M. *et al*. Randomized, phase III study of gemcitabine or erlotinib maintenance therapy versus observation, with predefined second-line treatment, after cisplatin-gemcitabine induction chemotherapy in advanced non-small-cell lung cancer. *J. Clin. Oncol.* **30**, 3516-3524 (2012).

380. Hendrickson, A. E. W. *et al*. A phase II study of gemcitabine in combination with tanespimycin in advanced epithelial ovarian and primary peritoneal carcinoma. *Gynecol. Oncol.* **124**, 210-215 (2012).

381. Garcia, A. A. *et al*. Phase II study of gemcitabine and docetaxel in recurrent platinum resistant ovarian cancer. *Cancer Invest.* **30**, 295-299 (2012).

382. Hansen, S. W. Gemcitabine in the treatment of ovarian cancer. *Int. J. Gynecol. Cancer* **11 Suppl 1**, 39-41 (2001).

383. Suzuki, E., Sun, J., Kapoor, V., Jassar, A. S. & Albelda, S. M. Gemcitabine has significant immunomodulatory activity in murine tumor models independent of its cytotoxic effects. *Cancer Biol. Ther.* **6**, 880-885 (2007).

384. Lechner, M. G., Liebertz, D. J. & Epstein, A. L. Characterization of cytokine-induced myeloid-derived suppressor cells from normal human peripheral blood mononuclear cells. *J. Immunol.* **185**, 2273-2284 (2010).

385. Vanneman, M. & Dranoff, G. Combining immunotherapy and targeted therapies in cancer treatment. *Nat. Rev. Cancer* **12**, 237-251 (2012).

386. Bunt, S. K., Sinha, P., Clements, V. K., Leips, J. & Ostrand-Rosenberg, S. Inflammation induces myeloid-derived suppressor cells that facilitate tumor progression. *J. Immunol.* **176**, 284-290 (2006).

387. Hirasawa, K. *et al*. Systemic reovirus therapy of metastatic cancer in immune-competent mice. *Cancer Res.* **63**, 348-353 (2003).

388. Verollet, C. *et al*. HIV-1 reprograms the migration of macrophages. *Blood* **125**, 1611-1622 (2015).

389. Koffel, R. *et al*. Monocytic cell differentiation from band-stage neutrophils under inflammatory conditions via MKK6 activation. *Blood* **124**, 2713-2724 (2014).

390. Azzaoui, I. *et al*. T-cell defect in diffuse large B-cell lymphomas involves expansion of myeloid-derived suppressor cells. *Blood* **128**, 1081-1092 (2016).

391. Zirlik, K. MDSCs: the final frontier of the microenvironment in CLL? *Blood* **124**, 666-668 (2014).

392. Peters, W., Dupuis, M. & Charo, I. F. A mechanism for the impaired IFN-gamma production in C-C chemokine receptor 2 (CCR2) knockout mice: role of CCR2 in linking the innate and adaptive immune responses. *J. Immunol.* **165**, 7072-7077 (2000).

393. McAlister, G. C. *et al*. Increasing the multiplexing capacity of TMTs using reporter ion isotopologues with isobaric masses. *Anal. Chem.* **84**, 7469-7478 (2012).

394. Weekes, M. P. *et al*. Quantitative temporal viromics: an approach to investigate host-pathogen interaction. *Cell* **157**, 1460-1472 (2014).

395. Ting, L., Rad, R., Gygi, S. P. & Haas, W. MS3 eliminates ratio distortion in isobaric multiplexed quantitative proteomics. *Nat. Methods* **8**, 937-940 (2011).

396. McAlister, G. C. *et al*. MultiNotch MS3 enables accurate, sensitive, and multiplexed detection of differential expression across cancer cell line proteomes. *Anal. Chem.* **86**, 7150-7158 (2014).

397. Yang, W. Q. *et al*. Efficacy and safety evaluation of human reovirus type 3 in immunocompetent animals: racine and nonhuman primates. *Clin. Cancer Res.* **10**, 8561-8576 (2004).

398. Huang da, W., Sherman, B. T. & Lempicki, R. A. Bioinformatics enrichment tools: paths toward the comprehensive functional analysis of large gene lists. *Nucleic Acids Res.* **37**, 1-13 (2009).

399. Huang da, W., Sherman, B. T. & Lempicki, R. A. Systematic and integrative analysis of large gene lists using DAVID bioinformatics resources. *Nat. Protoc.* **4**, 44-57 (2009).

400. Rusinova, I. *et al*. Interferome v2.0: an updated database of annotated interferon-regulated genes. *Nucleic Acids Res.* **41**, 1040 (2013).

401. Peng, K. W. *et al*. Tumor-associated macrophages infiltrate plasmacytomas and can serve as cell carriers for oncolytic measles virotherapy of disseminated myeloma. *Am. J. Hematol.* **84**, 401-407 (2009).

402. Muthana, M. *et al*. Macrophage delivery of an oncolytic virus abolishes tumor regrowth and metastasis after chemotherapy or irradiation. *Cancer Res.* **73**, 490-495 (2013).

403. Zhang, T. *et al*. Lysosomal cathepsin B plays an important role in antigen processing, while cathepsin D is involved in degradation of the invariant chain inovalbumin-immunized mice. *Immunology* **100**, 13-20 (2000).

404. Calvo, S. E., Clauser, K. R. & Mootha, V. K. MitoCarta2.0: an updated inventory of mammalian mitochondrial proteins. *Nucleic Acids Res.* **44**, 1251 (2016).

405. Pagliarini, D. J. *et al*. A mitochondrial protein compendium elucidates complex I disease biology. *Cell* **134**, 112-123 (2008).

406. Szklarczyk, D. *et al*. STRING v10: protein-protein interaction networks, integrated over the tree of life. *Nucleic Acids Res.* **43**, 447 (2015).

407. Zigmond, E. *et al*. Ly6C hi monocytes in the inflamed colon give rise to proinflammatory effector cells and migratory antigen-presenting cells. *Immunity* **37**, 1076-1090 (2012).

408. Satoh, T. *et al*. The Jmjd3-Irf4 axis regulates M2 macrophage polarization and host responses against helminth infection. *Nat. Immunol.* **11**, 936-944 (2010).

409. Krausgruber, T. *et al*. IRF5 promotes inflammatory macrophage polarization and TH1-TH17 responses. *Nat. Immunol.* **12**, 231-238 (2011).

410. Weiss, M., Blazek, K., Byrne, A. J., Perocheau, D. P. & Udalova, I. A. IRF5 is a specific marker of inflammatory macrophages in vivo. *Mediators Inflamm.* **2013**, 245804 (2013).

411. Murray, P. J. *et al*. Macrophage activation and polarization: nomenclature and experimental guidelines. *Immunity* **41**, 14-20 (2014).

412. Kobayashi, K. *et al*. Minocycline selectively inhibits M1 polarization of microglia. *Cell. Death Dis.* **4**, e525 (2013).

413. Barbalat, R., Lau, L., Locksley, R. M. & Barton, G. M. Toll-like receptor 2 on inflammatory monocytes induces type I interferon in response to viral but not bacterial ligands. *Nat. Immunol.* **10**, 1200-1207 (2009).

414. Lim, J. K. *et al*. Chemokine receptor Ccr2 is critical for monocyte accumulation and survival in West Nile virus encephalitis. *J. Immunol.* **186**, 471-478 (2011).

415. Salazar-Mather, T. P., Orange, J. S. & Biron, C. A. Early murine cytomegalovirus (MCMV) infection induces liver natural killer (NK) cell inflammation and protection through macrophage inflammatory protein 1alpha (MIP-1alpha)-dependent pathways. *J. Exp. Med.* **187**, 1-14 (1998).

416. Held, K. S., Chen, B. P., Kuziel, W. A., Rollins, B. J. & Lane, T. E. Differential roles of CCL2 and CCR2 in host defense to coronavirus infection. *Virology* **329**, 251-260 (2004).

417. Hukelmann, J. L. *et al*. The cytotoxic T cell proteome and its shaping by the kinase mTOR. *Nat. Immunol.* **17**, 104-112 (2016).

418. Na, Y. R. *et al*. Proteomic Analysis Reveals Distinct Metabolic Differences Between Granulocyte-Macrophage Colony Stimulating Factor (GM-CSF) and Macrophage Colony Stimulating Factor (M-CSF) Grown Macrophages Derived from Murine Bone Marrow Cells. *Mol. Cell. Proteomics* **14**, 2722-2732 (2015).

419. Becker, L. *et al*. Unique proteomic signatures distinguish macrophages and dendritic cells. *PLoS One* **7**, e33297 (2012).

420. Guo, M. *et al*. High-resolution quantitative proteome analysis reveals substantial differences between phagosomes of RAW 264.7 and bone marrow derived macrophages. *Proteomics* **15**, 3169-3174 (2015).

421. Luber, C. A. *et al*. Quantitative proteomics reveals subset-specific viral recognition in dendritic cells. *Immunity* **32**, 279-289 (2010).

422. Boutte, A. M., McDonald, W. H., Shyr, Y., Yang, L. & Lin, P. C. Characterization of the MDSC proteome associated with metastatic murine mammary tumors using label-free mass spectrometry and shotgun proteomics. *PLoS One* **6**, e22446 (2011).

423. Mitchell, C. J. *et al*. A multi-omic analysis of human naive CD4+ T cells. *BMC Syst. Biol.* **9**, 4 (2015).

424. Weiler, S. R. *et al*. D3: a gene induced during myeloid cell differentiation of Linlo c-Kit+ Sca-1(+) progenitor cells. *Blood* **93**, 527-536 (1999).

425. Tavakoli, S., Zamora, D., Ullevig, S. & Asmis, R. Bioenergetic profiles diverge during macrophage polarization: implications for the interpretation of 18F-FDG PET imaging of atherosclerosis. *J. Nucl. Med.* **54**, 1661-1667 (2013).

426. Lachmandas, E. *et al*. Microbial stimulation of different Toll-like receptor signalling pathways induces diverse metabolic programmes in human monocytes. *Nat. Microbiol.* **2**, 16246 (2016).

427. Stienstra, R., Netea-Maier, R. T., Riksen, N. P., Joosten, L. A. B. & Netea, M. G. Specific and Complex Reprogramming of Cellular Metabolism in Myeloid Cells during Innate Immune Responses. *Cell. Metab.* **26**, 142-156 (2017).

428. Fu, J. *et al*. STING agonist formulated cancer vaccines can cure established tumors resistant to PD-1 blockade. *Sci Transl Med* **7**, 283ra52 (2015).

429. Grossardt, C. *et al*. Granulocyte-macrophage colony-stimulating factor-armed oncolytic measles virus is an effective therapeutic cancer vaccine. *Hum. Gene Ther.* **24**, 644-654 (2013).

430. Bayne, L. J. *et al*. Tumor-derived granulocyte-macrophage colony-stimulating factor regulates myeloid inflammation and T cell immunity in pancreatic cancer. *Cancer. Cell.* **21**, 822-835 (2012).

431. Kohanbash, G. *et al*. GM-CSF promotes the immunosuppressive activity of glioma-infiltrating myeloid cells through interleukin-4 receptor-α. *Cancer Res.* **73**, 6413-6423 (2013).

432. Fortin, C., Yang, Y. & Huang, X. Monocytic myeloid-derived suppressor cells regulate T-cell responses against vaccinia virus. *Eur. J. Immunol.* **47**, 1022-1031 (2017).

433. Morecki, S. *et al*. CpG-induced myeloid CD11b+Gr-1+ cells efficiently suppress T cell-mediated immunoreactivity and graft-versus-host disease in a murine model of allogeneic cell therapy. *Biol. Blood Marrow Transplant.* **14**, 973-984 (2008).

434. Fernández, A. *et al*. Inhibition of tumor-induced myeloid-derived suppressor cell function by a nanoparticulated adjuvant. *J. Immunol.* **186**, 264-274 (2011).

435. Srivastava, M. K. *et al*. Myeloid suppressor cell depletion augments antitumor activity in lung cancer. *PLoS ONE* **7**, e40677 (2012).

436. Schilling, B. *et al*. Vemurafenib reverses immunosuppression by myeloid derived suppressor cells. *Int. J. Cancer* **133**, 1653-1663 (2013).

437. Bonapace, L. *et al*. Cessation of CCL2 inhibition accelerates breast cancer metastasis by promoting angiogenesis. *Nature* **515**, 130-133 (2014).

438. Rothlin, C. V., Ghosh, S., Zuniga, E. I., Oldstone, M. B. A. & Lemke, G. TAM receptors are pleiotropic inhibitors of the innate immune response. *Cell* **131**, 1124-1136 (2007).

439. Al-Khami, A. A., Rodriguez, P. C. & Ochoa, A. C. Metabolic reprogramming of myeloid-derived suppressor cells (MDSC) in cancer. *Oncoimmunology* **5**, e1200771 (2016).

440. Stienstra, R., Netea-Maier, R. T., Riksen, N. P., Joosten, L. A. B. & Netea, M. G. Specific and Complex Reprogramming of Cellular Metabolism in Myeloid Cells during Innate Immune Responses. *Cell Metabolism* **26**, 142-156 (2017).

441. Idoyaga, J. *et al*. Specialized role of migratory dendritic cells in peripheral tolerance induction. *J. Clin. Invest.* **123**, 844-854 (2013).

442. Tyanova, S. *et al*. Proteomic maps of breast cancer subtypes. *Nat. Commun.* **7**, 10259 (2016).

443. Ron-Harel, N. *et al*. Mitochondrial Biogenesis and Proteome Remodeling Promote One-Carbon Metabolism for T Cell Activation. *Cell Metab.* **24**, 104-117 (2016).

444. Hughes, C. S. *et al*. Ultrasensitive proteome analysis using paramagnetic bead technology. *Molecular Systems Biology* **10**, 757 (2014).

445. June, C. H., Warshauer, J. T. & Bluestone, J. A. Is autoimmunity the Achilles' heel of cancer immunotherapy? *Nat. Med.* **23**, 540-547 (2017).

446. Chalan, P. *et al*. Thyroid dysfunctions secondary to cancer immunotherapy. *J. Endocrinol. Invest.* (2017).

447. Ercolini, A. M. & Miller, S. D. The role of infections in autoimmune disease. *Clin. Exp. Immunol.* **155**, 1-15 (2009).

448. Harrington, K. J. *et al*. Efficacy and safety of talimogene laherparepvec versus granulocyte-macrophage colony-stimulating factor in patients with stage IIIB/C and IVM1a melanoma: subanalysis of the Phase III OPTiM trial. *Onco Targets Ther* **9**, 7081-7093 (2016).

449. Bridle, B. W. *et al*. HDAC inhibition suppresses primary immune responses, enhances secondary immune responses, and abrogates autoimmunity during tumor immunotherapy. *Mol. Ther.* **21**, 887-894 (2013).

450. Notkins, A. L., Yoon, J., Onodera, T. & Jenson, A. B. Virus-induced diabetes mellitus: infection of mice with variants of encephalomyocarditis virus, coxsackievirus B4, and reovirus type 3. *Adv. Exp. Med. Biol.* **119**, 137-146 (1979).

451. Onodera, T., Jenson, A. B., Yoon, J. W. & Notkins, A. L. Virus-induced diabetes mellitus: reovirus infection of pancreatic beta cells in mice. *Science* **201**, 529-531 (1978).

452. Freeman-Keller, M. *et al*. Nivolumab in Resected and Unresectable Metastatic Melanoma: Characteristics of Immune-Related Adverse Events and Association with Outcomes. *Clin. Cancer Res.* **22**, 886-894 (2016).

453. Nanda, N. K. & Sercarz, E. E. Induction of anti-self-immunity to cure cancer. *Cell* **82**, 13-17 (1995).

454. Overwijk, W. W. & Restifo, N. P. Autoimmunity and the immunotherapy of cancer: targeting the "self" to destroy the "other". *Crit. Rev. Immunol.* **20**, 433-450 (2000).

APPENDIX A- COPYRIGHT PERMISSIONS

November 22, 2017

Derek Clements
Dalhousie University
5850 College Street
Halifax, Nova Scotia, B3H 4R2
Canada

Email: derek.clements@dal.ca

Dear Dr. Clements,

The American Association of Immunologists, Inc., grants permission to use the entire article, "Newly Recruited CD11b+, GR-1+, Ly6Chigh Myeloid Cells Augment Tumor-Associated Immunosuppression Immediately following the Therapeutic Administration of Oncolytic Reovirus," published in *The Journal of Immunology*, vol. 194, pp. 4397-4412, 2015, in your *Ph.D. thesis*, contingent on the following conditions:

1. That you give proper credit to the authors and to *The Journal of Immunology*, including in your citation the volume, date, and page numbers.

2. That you include the statement:

   Copyright 2015. The American Association of Immunologists, Inc.

3. That permission is granted for one-time use only for print and electronic format. Permission must be requested separately for future editions, revisions, derivative works, and promotional pieces. Reproduction of any content, other than Figures and Figure Legends, from *The Journal of Immunology* is permitted in English only.

Thank you for your interest in *The Journal of Immunology*.

Sincerely,

Kaylene J. Kenyon, Ph.D.
Publication Director
The Journal of Immunology

THE AMERICAN ASSOCIATION OF IMMUNOLOGISTS
1451 Rockville Pike, Suite #650, Rockville, MD 20852 | Phone 301.634.7197 | Fax 301.634.7829 | infoji@aai.org | www.jimmunol.org

RightsLink®

Home | Account Info | Help

Title:	Gemcitabine enhances the efficacy of reovirus-based oncotherapy through anti-tumour immunological mechanisms
Author:	S A Gujar, D Clements, R Dielschneider, E Helson, P Marcato et al.
Publication:	British Journal of Cancer
Publisher:	Nature Publishing Group
Date:	Nov 26, 2013

Logged in as:
Derek Clements
Dalhousie University

LOGOUT

Creative Commons

The request you have made is considered to be non-commercial/educational. As the article you have requested has been distributed under a Creative Commons license (Attribution-Noncommercial), you may reuse this material for non-commercial/educational purposes without obtaining additional permission from Nature Publishing Group, providing that the author and the original source of publication are fully acknowledged(please see the article itself for the license version number). You may reuse this material without obtaining permission from Nature Publishing Group, providing that the author and the original source of publication are fully acknowledged, as per the terms of the license. For license terms, please see http://creativecommons.org/

BACK | CLOSE WINDOW

Click here if you have difficulty reading this email >>

Dr. Derek Clements,

Your permission requested is granted and there is no fee for this reuse. In your planned reuse, you must cite the ACS article as the source, add this direct link <http://pubs.acs.org/doi/abs/10.1021%2Facs.jproteome.7b00425>, and include a notice to readers that further permissions related to the material excerpted should be directed to the ACS.

If you need further assistance, please let me know.

Regards,

Jawwad Saeed

ACS Customer Services & Information

https://help.acs.org

Your help request has been resolved. If you have further issues regarding this matter, please let us know by responding to this email. Please note that this request will auto-close in 14 days. If you need to contact us after 14 days regarding this matter please submit a new help request and refer to this help request number.